Dipl.-Ing. Patrick P. Pichler, BSc.

Numerical Analysis of the Influence of Initial Hydraulic Boundary Conditions on the Infiltration Behaviour and Stability of Unsaturated Soil Slopes

DOCTORAL THESIS

to achieve the university degree of

Doktor der technischen Wissenschaften

submitted to

Graz University of Technology

Supervisor

Ao.Univ.-Prof. Dipl.-Ing. Dr.techn. Helmut F. Schweiger, MSc.

Institute of Soil Mechanics, Foundation Engineering and Computational Geotechnics
Graz University of Technology

Prof. Paolo Simonini, MSc., PhD.

Department of Civil, Environmental and Architectural Engineering
University of Padova

Univ.-Prof. Dipl.-Ing. Dr. techn. Robert Hofmann

Institut für Infrastruktur, Arbeitsbereich für Geotechnik und Tunnelbau
Universität Innsbruck

Graz, June 2019

Affidavit

I declare that I have authored this thesis independently, that I have not used other than the declared sources/resources, and that I have explicitly indicated all material which has been quoted either literally or by content from the sources used. The text document uploaded to TUGRAZonline is identical to the present doctoral thesis.

....

Date Signature

Acknowledgements

This dissertation would not have been possible without the great support and advice of Ao.Univ.-Prof. Dipl.-Ing. Dr.techn. Helmut F. Schweiger. I greatly enjoyed working with him in the Computational Geotechnics Group at Graz University of Technology. Thank you Helmut for sharing your broad knowledge about soil mechanics and giving me the opportunity to attend many informative conferences and workshops.

I am grateful to Prof. Paolo Simonini of University of Padova and Univ.-Prof. Robert Hofmann of University of Innsbruck for reviewing this thesis.

I would also like to thank Univ.-Prof. Dipl.-Ing. Dr.techn. Roman Marte, Head of the Institute of Soil Mechanics, Foundation Engineering and Computational Geotechnics for making the research facilities available to me. Thank you Roman for all personal advices and professional discussions at our institute meetings.

I would like to thank all colleagues at the Institute of Soil Mechanics, Foundation Engineering and Computational Geotechnics in Graz for the pleasant working atmosphere and all the meaningful discussions. In particular, I would like to thank Franz Tschuchnigg, Matthias Rebhan, Christopher Krammer, Laurin Hauser, Simon Oberhollenzer and the colleagues from the laboratory. Special thanks to my former colleague Georg Ausweger, with whom I was not only allowed to attend interesting international conferences, but also had fruitful discussions, which were not always limited to the subject of my research activities.

I gratefully acknowledge Mag. Dr. Gernot Klammler (Joanneum Research) for providing me with data, without which this thesis would not have been possible.

I am deeply grateful to my mother, who have enabled my education and motivated and supported me all my life.

Last but not least, I would like to thank my amazing wife Nina for her understanding, patience and outstanding support these past years. Thank you for your unconditional love and encouraging words even in difficult situations in life. Thanks also to my wonderful son Valentin, who often welcomed me at home with a broad smile on his face.

Graz, June 2019 Patrick P. Pichler

Kurzfassung

Numerische Analyse des Einflusses initialer hydraulischer Randbedingungen auf das Infiltrationsverhalten und die Stabilität von teilgesättigten Böschungen

Niederschlag und damit einhergehende Veränderungen im Porenwasserdruckprofil können einen großen Einfluss auf die Instabilität von Böschungen aufweisen. Die hydraulischen Bodeneigenschaften bestimmen die relative Durchlässigkeit, die Intensität und Dauer von Niederschlagsereignissen definieren die aktuelle Infiltrationsrate und die daraus folgenden Auswirkungen auf den Porenwasserdruckverlauf sowie auf die Sicherheit. Im Hinblick auf das Infiltrationsverhalten spielen die initialen Porenwasserdrücke im Bodenkörper (gegeben durch die Lage des Grundwasserspiegels bzw. durch den darüber liegenden Saugspannungsverlauf) eine bedeutende Rolle und beeinflussen alle nachfolgenden Resultate maßgebend.

Im Rahmen dieser Arbeit werden die theoretischen Grundlagen, sowie die speziellen physikalischen Eigenschaften, die Grundwasserströmung, hydraulische Modelle und ausgewählte Techniken zur Bestimmung von Saugspannungen in teilgesättigten Böden beschrieben. Im Rahmen mehrerer Vorstudien werden die aufgetretenen Unzulänglichkeiten präsentiert.

Das Hauptziel der vorliegenden Arbeit ist die Quantifizierung des Einflusses der initialen hydraulischen Randbedingungen im Hinblick auf Veränderungen im Saugspannungsverlauf während Niederschlagsereignissen unter Verwendung von "Echtzeit" Lysimeterdaten, um sowohl die Wasserretentionskurve, als auch das initiale Profil der Porenwasserdrücke im Boden zu kalibrieren. Die verwendeten Wasserretentionskurven werden mathematisch durch das weitverbreitete und größtenteils akzeptierte van Genuchten-Modell beschrieben. Aus numerischen Gleichgewichtsgründen führt die alleinige Verwendung des Ausgangsgrundwasserspiegels zu einem – unrealistisch erscheinenden – linearen Anstieg der negativen Porenwasserdrücke (Saugspannungen) über dem Grundwasserspiegel. Um dies im numerischen Modell zu umgehen, werden Lysimeterdaten zur Kalibrierung des Saugspannungsprofils herangezogen. In Rahmen eines numerischen Säulentests wird nachgewiesen, dass die im Feld gemessenen Saugspannungsverläufe numerisch nachgebildet werden können.

Die Wichtigkeit einer sorgfältigen Auswahl der hydraulischen Randbedingungen und deren Einfluss auf weitere Berechnungsergebnisse werden an einer "Benchmark-Böschung" aufgezeigt. Der Einfluss unterschiedlicher möglicher Parameterveränderungen, im Rahmen der numerischen phi-c-Reduktion auf die Sicherheit der Böschung, wird dargestellt.

Eine numerische Untersuchung im Hinblick auf den Einfluss mehrerer unterschiedlicher hydraulischer Randbedingungen wie veränderbarer Wasserretentionskurven, gesättigter Durchlässigkeiten und die Diskretisierung des aufgebrachten Niederschlagsdatensatzes auf den Sicherheitsfaktor einer Massenbewegung, schließen diese Arbeit ab.

Abstract

Numerical analysis of the influence of initial hydraulic boundary conditions on the infiltration behaviour and stability of unsaturated soil slopes

Precipitation, and the associated changes in the pore water pressure profile that it causes, often plays a major role in the instability of slopes. The hydraulic properties of the soil determine its relative permeability, and the intensity and duration of rainfall events define the actual infiltration rate into the slope and its impacts on the pore water pressure profile and the factor of safety (FoS) of the slope. With respect to the infiltration behaviour during a rainfall event, the initial pore water pressures in the soil body (e.g. location of the groundwater-level, suction profile above the groundwater-level) play a major role and influence all following results significantly.

Within this thesis, a theoretical background is first presented by defining and describing the distinctive physical properties of unsaturated soils, and how water flows through it, as well as hydraulic models and selected techniques for suction measurement of unsaturated soils. Then several preliminary studies of these soils which have been performed and their associated shortcomings are presented.

The main objective of this presented thesis is to quantify the influence of various initial hydraulic boundary conditions with respect to the changes in suction during rainfall events after specified times of infiltration or evapotranspiration by using “real time” Lysimeter-data to calibrate the Soil Water Characteristic Curve (SWCC) of a soil and the starting pore water pressure profile in a slope. In order to describe the SWCC mathematically, the commonly used and widely accepted van Genuchten (vG) model was used in all the numerical analyses. In the models, the use of initial groundwater-levels would lead to a linearly increasing negative pore water pressure above the groundwater-level due to reasons of numerical equilibrium, which may not be realistic. To overcome this issue, Lysimeter-data are used to calibrate the suction profiles in the numerical model. The general capability to numerically reproduce measured suction values is demonstrated in a numerical column test. The importance of a careful choice of hydraulic boundary conditions in numerical modelling and its influence on further results is illustrated by means of a benchmark slope. The effects of several numerical ways of executing a phi-c-reduction with a finite element code on the factors of safety of the slope stability are demonstrated. A numerical investigation concerning the influence of different hydraulic conditions, such as changing SWCCs, saturated permeabilities and discretisation of the applied net-precipitation dataset, on the FoS of a slow moving landslide completes this thesis.

Table of contents

List of symbols and abbreviations

The symbols used in this thesis are listed in alphabetic order. Additional explanation is provided in the text at first appearance.

Small letters

c'	[kPa]	effective cohesion
g	[m³/kg s²]	gravitational constant
g_a, g_l, g_n	[-]	van Genuchten parameters
h	[m]	pressure head
h_c	[m]	maximum height of the water column inside the tube
i_m	[m]	hydraulic gradient
k	[m/s]	hydraulic permeability
k_{ra}	[m/s]	relative permeability of air phase
k_{ref}	[m/s]	reference hydraulic permeability
k_{rel}	[m/s]	relative permeability
k_{rw}	[m/s]	relative permeability of water phase
k_{sat}	[-]	saturated permeability
k_x	[m/s]	saturated hydraulic permeability in horizontal direction
k_y	[m/s]	saturated hydraulic permeability in vertical direction
m	[kN]	sample mass
p'	[-]	effective mean stress
p_{air}	[kPa]	pore air pressure
p_{atm}	[kPa]	atmospheric air pressure
p_{excess}	[kPa]	excess pore water pressure
p_{fluid}	[kPa]	pore fluid pressure
q	[m/s]	specific discharge
q_x, q_y, q_z	[m/s]	fluxes in the x, y, z directions
r	[m]	radius
r_1, r_2	[m]	radii of curvature

s	[kPa]	suction
t	[min]	time
u_a	[kPa]	pore air pressure
u_v	[kPa]	partial pressure of pore water vapour
u_{vo}	[kPa]	saturation pressure of pore water
u_w	[kPa]	pore water pressure
z	[m]	distance

Capital letters

A	[m²]	surface area
C_{air}	[1/kPa]	air compressibility
C_{fluid}	[1/kPa]	pore fluid compressibility
C_{water}	[1/kPa]	pore water compressibility
E_{oed}	[kPa]	actual stiffness for primary oedometer loading
ET_0	[m]	evapotranspiration according to FAO-Penman-Monteith
ET_r	[m]	evapotranspiration (measured)
I_p	[-]	plasticity index
K	[m/s]	hydraulic conductivity
M	[kN]	total mass
M_a	[kN]	mass of free air
M_s	[kN]	mass of soil particles
M_w	[kN]	mass of water
P	[m]	precipitation
R_h	[%]	relative humidity
R_s	[m]	related curvature radius
R_u	[-]	universal gas constant
S	[%]	degree of saturation
S_e	[%]	effective degree of saturation
S_{res}	[%]	residual degree of saturation
S_{sat}	[%]	degree of saturation under saturated conditions
T	[°]	absolute temperature

T_s	[kPa]	surface tension of air-water interface
V	[kN/m³]	total volume
V_a	[kN/m³]	volume of free air
V_s	[kN/m³]	volume of soil particles
V_w	[kN/m³]	volume of water

Small Greek letters

α	[°]	slope angle
μ	[m²/s]	dynamic viscosity of the fluid
θ	[-]	volumetric water content
κ	[-]	fitting parameter
χ	[-]	effective stress parameter
κ_i	[m/s]	intrinsic permeability of the porous medium
ψ_{max}	[m]	run-off parameter
ψ_{min}	[m]	minimum pore pressure head for evapotranspiration
ϕ_p	[m]	pressure head
θ_{res}	[-]	volumetric water content at residual saturation
ϕ_s	[kPa]	osmotic suction
θ_{sat}	[-]	volumetric water content at full saturation
ω_v	[kN]	Molecular mass of water vapour
ρ_w	[kN/m³]	density of water
γ	[kN/m³]	unit weight of soil
γ_{sat}	[kN/m³]	bulk unit weight of soil below ground water table
γ_{unsat}	[kN/m³]	bulk unit weight of soil above ground water table
γ_w	[kN/m³]	unit weight of water
φ'	[°]	effective friction angle
ν'	[-]	effective Poisson's ratio
σ	[kPa]	stress / total stress
σ'	[kPa]	effective stress
σ_1	[kPa]	total major principal stress
σ_1'	[kPa]	effective major principal stress

σ_2'	[kPa]	effective intermediate principal stress
σ_3	[kPa]	total minor principal stress
σ_3'	[kPa]	effective minor principal stress
ψ	[m]	matric potential
ψ'	[°]	dilatancy angle

Abbreviations

AE	actual evaporation
AEV	air entry value
BC	boundary condition
C	HYPRES' "Coarse" SWCC
CC	climatic condition
FE	finite element
FoS	factor of safety
GEO	geometry
gw	groundwater
HAE	high air entry
HYPRES	Hydraulic Properties of European Soils
ICFEP	Imperial College Finite Element Program
MCC	Modified Cam Clay
MF	HYPRES' "Medium Fine" SWCC
model A	automatically generated initial pore water pressures
model M	manually defined initial pore water pressures
SSCC	Suction Stress Characteristic Curve
SWCC	Soil Water Characteristic Curve
TDR	Time-Domain Reflectometry
USDA	United States Department of Agriculture
VF	HYPRES' "Very Fine" SWCC
vG	van Genuchten

1 Introduction

1.1 Motivation

Precipitation, and the associated changes in the pore water pressure profile that it causes, often plays a major role in the instability of slopes. The initial factor of safety (FoS) of a slope with given soil properties is controlled by its geometry, the depth of the groundwater table and the corresponding initial pore water pressure profile in the unsaturated zone which is defined by the SWCC (e.g. Ni et al. 2018). The hydraulic properties of the soil determine the relative permeability, and the intensity and duration of rainfall events define the actual infiltration rate into the slope and its impacts on the pore water pressure profile. With respect to the infiltration behaviour during a rainfall event, the initial pore water pressures in the soil body (e.g. location of the groundwater level with corresponding suction profile above the groundwater level) play a major role. They also significantly influence the results in numerical analyses.

When numerical analyses are performed considering explicitly the unsaturated zone above the groundwater table, a linearly increasing negative pore water pressure above the groundwater-level will be the “default” condition due to equilibrium reasons in the calculations, which may not be realistic to the condition in the field.

A linearly increasing negative pore water pressure above the groundwater-level may lead to unrealistic high suction values with very low accompanying permeabilities at the ground surface, especially with deep-lying groundwater levels. This very low permeability at the surface results in very high calculated run-off rates with associated low infiltration rates in near-surface areas, which also affects the calculated water flow into and through deeper sectors of the soil. The representation of suction in the top layers influences the generated pore water pressure profile of the entire soil system and therefore may also affect the shear strength in deeper spheres of the calculated system.

The Lysimeter, a device which is typically used for agricultural research purposes, is able to provide data to calibrate the hydraulic conditions of soils in numerical analysis. This device is installed in the ground and continuously measures suction at specific depths of the soil body (Reszler & Fank 2016, Schuhmann et al. 2015). A local weather station provides information about the current precipitation, evapotranspiration and wind speed. In a study within this thesis, these data are used directly as input data in the numerical analysis, specifically to define the initial pore pressure profile of soil slopes where the problem of the aforementioned unrealistic automatically generated “default” pore water pressure condition can be overcome.

To analyse the simultaneous development of deformation and pore water pressures in the soil as a result of time-dependent changes of hydraulic boundary conditions, fully coupled flow-deformation analyses are required. These analyses were performed in this thesis employing two-dimensional finite element models utilizing the code PLAXIS 2D 2017 (Brinkgreve et al. 2017).

The main objective of this thesis is to compare the development of changes in suction due to climatic conditions, in which different initial suction profiles, either automatically generated or delivered from the Lysimeter, have been used. The question of which circumstances cause major differences in the results, when compared to the results from the modified suction profile based on measurement data, and when using solely the initial groundwater level to automatically generate the initial pore water pressure profile, should be answered within this contribution.

Since measurement data of the Lysimeter is available until a depth of 0.5 m, the numerical investigations presented here are well suited to model near surface suction profiles and shallow slope instabilities.

1.2 Scope and outline of thesis

The thesis is divided into two major parts. In the first part (chapters 2 and 3), an overview of the state of the art is presented and the theoretical background and the physical behaviour of unsaturated soils is explained for the subsequent numerical studies. The second part (chapter 3 to chapter 9) deals with several numerical analyses in order to answer the aforementioned questions.

Chapter 2 provides a short literature review related to the particular behaviour of unsaturated soils. Referring to the research question to be answered, the focus was put on infiltration behaviour into unsaturated soil slopes and on the associated effects on slope stability.

Chapter 3 defines the term “unsaturated soil” and describes its characteristics and physical particularities in a thorough manner. In traditional soil mechanics approaches, soils below the ground water table are considered to be two-phase mediums: solids and one fluid. However, the unsaturated soil mechanics approach assumes these soils to be a three- or four-phase system, in which the soil voids can be filled with both fluid and gas, in varying amounts. Besides the soil solids phase and the water and air phases, the air-water interface (i.e. contractile skin) is also often referred to as a separate phase and has to be considered in analyses. “Total soil suction” which is composed of the “matric suction” and the “osmotic suction” component, is described. Darcy’s law to describe the water flow in unsaturated soils is presented as soil suction strongly affects hydraulic permeability. After that, detailed descriptions of selected hydraulic models and the Soil Water Characteristic Curve (SWCC), which

represents the relationship between water content and suction for the soil, are presented. Finally, after presenting several techniques for suction measurement in the laboratory, the mechanical behaviour of unsaturated soils is presented and closes this chapter.

Chapter 4 highlights the most challenging aspects of numerically modelled infiltration into, and water flow through, unsaturated soils. Among other flow-related problems such as steady- and transient seepage analyses in unsaturated embankment dams, the calculation of recharge rates to aquifers and studies concerning water balance at the soil-atmosphere interface, certain types of unsaturated soils can also be used as cover-layers for underground waste storage and containment. Within this thesis, a practice-related numerical analysis of water flow through an unsaturated soil, which has been used as cover-layer for underground waste storage, was executed by means of a 1D-column test. The presented procedure could be used to prove that the strict requirements of allowed maximum quantities of water reaching the protective cover layer below are justified. In order to define the SWCCs necessary for the numerical analysis, a combination of three test procedures, “hanging water column”, “pressure plate extractor” and “evaporation method” had been performed in our laboratory to cover the whole suction range. The results of the analysis show, that under certain assumptions and when ensuring a maximum saturated hydraulic permeability of $1*10^{-8}$ m/s, the prescriptions of the authorities could be fulfilled.

In chapter 5, the influence of varying water flow characteristics, of associated changes of pore water pressures and of shear strength on the stability of simplified slope geometries with inhomogeneous soil, is analysed. The influence of different SWCCs on the factor of safety (FoS) of slopes is evaluated by means of fully coupled flow-deformation analyses. In order to quantify the slopes’ factor of safety during rainfall events after specified times of infiltration or evaporation, the phi-c-reduction method is applied.

Chapter 6 deals with the numerical back-calculation of data delivered by a Lysimeter, to calibrate the hydraulic conditions of soils in numerical analysis. (see chapter 5). The presented recalculation of Lysimeter-data in a numerical column-test utilizing PLAXIS 2D (Brinkgreve et al. 2017) deliveres very satisfactory results, and serve as a basis for the investigations in further chapters. The application of this procedure avoids the use of uncertain hydraulic input-parameters, which can significantly affect the infiltration behaviour.

The aim of chapter 7 is to investigate the infiltration behaviour due to rainfall on a slope geometry with variable boundary conditions. In the previous chapter 5, it was shown that the use of Lysimeter data as input is capable of reliably reproducing the change of suction profiles due to infiltration. The main goal of this chapter is to predict and determine when the manually (“model M”) and automatically (“model A”) generated pore water pressures match in the climatic

hydrograph. Generally, the determination of initial hydraulic boundary conditions within a slope is cost-intensive, hard to achieve or even impossible. Therefore, a study to quantify the influence of the initial hydraulic conditions is performed. The data delivered from the Lysimeter as described and used in the preliminary study in chapter 5 is also used in the benchmark slope calculations of this chapter, but serves only to qualitatively highlight the differences between ("model M") and ("model A") calculations for theoretical purposes.

Chapter 8 describes the study of a high intensity rainfall event, with a discharge of 30 mm/hour, being constantly applied for 72 hours onto a slope. The slope is modelled with simple, homogeneous or inhomogeneous, slope geometries. The effects of varying run-off conditions and the influence of an either open or closed flow boundary on the right side of the numerical model on the FoS of the slope are presented.

Chapter 9 is based on the very detailed work of Ausweger (2018), who investigated the influences of water level changes on the behaviour of a slow moving landslide in Austria. Within this chapter the resulting differences when alternative SWCCs, various saturated hydraulic permeabilities and more discretized rainfall datasets are used in the numerical analysis are summarized. Furthermore, the effects of heavy rainfall events, with up to 300 mm/day discharge (which recently has been happening more frequently in Austria), on the stability of this moving slope, are investigated. To investigate this, the aforementioned constant and high rainfall rate was either applied instead of, or directly after the original climatic hydrograph. This procedure allows for a quantification of antecedent rainfall effects on the factor of safety of this slope. Because, as previously mentioned, the initial condition before a heavy rainfall event takes place, plays a significant role in the instability of soil slopes.

Chapter 10 presents the conclusions of this thesis and gives some recommendations for further research and investigations. References are provided in chapter 10.

2 State of the art

A number of researchers described the process of rainfall infiltration into unsaturated soils and have evaluated major factors which control the instability of soil slopes under precipitation, of which a short summarizing overview of the points pertinant to this thesis is given in the following paragraphs:

Fourie (1996) discussed the failure mechanisms of shallow slope failures caused by water infiltration, which usually occur in regions with steep slopes consisting of residual soils, subjected to periods of prolonged and heavy rainfall. They found that the water infiltration leads to an ingress of a wetting front with a simultaneous decrease of soil suction until a critical depth is reached and slope failure occurs.

Ng & Shi (1998) utilized the finite element method to study the effects of several rainfall events on slope stability in partially saturated soils, especially considering the initial boundary and ground water table conditions on transient seepage. They found that the infiltration of rainfall leads to a decrease in matric suction, whereas the moisture content and hydraulic conductivity of the unsaturated soil increases. The stability of the slope is highly influenced by the intensity and duration of rainfall, the location of the initial ground water table and the hydraulic permeability of the soil.

Gasmo et al. (2000) utilized numerical models to study infiltration of rainfall into slopes, considering the rainfall intensity and the effects on the FoS of the slope. The quantification of the amount of infiltration occurring in a slope was described to be a difficult process, nonetheless, the numerical analysis showed qualitatively that the amount of infiltration was highest at the crest of the slope.

Cho & Lee (2001) examined the infiltration process of rainfall into a slope and its effect on the overall slope stability behaviour by utilizing the finite element method with coupled flow-deformation analysis. The distribution of pore water pressures, which affect the stress field, is controlled by the spatial variation of hydraulic permeability during the infiltration of rainfall. As the hydraulic permeability is a function of water content and matric suction, the hydraulic permeability itself showed an inhomogeneous distribution, even though the soil slope was homogeneous. However, using the smoothed stress field obtained from the finite element analysis, a FoS was still calculated. Furthermore, an optimization technique was used to determine a critical slip surface.

Cai & Ugai (2004) applied the finite element method in order to investigate the effects of the initial degree of saturation, the hydraulic characteristics, and the different boundary conditions of the soil, as well as the intensity and duration of rainfall on the water pressure in slopes. The shear-strength reduction technique was used to determine the FoS of slopes under rainfall. The results show that all

the parameters mentioned above influence the water pressure in slopes and thus, significantly influence the stability of slopes under rainfall infiltration. The FoS of slopes increased when the shear strength contributed by matric suction was taken into account, but the influence of the matric suction decreased and finally disappeared when the soil was saturated by the infiltration of rainfall.

Griffiths & Lu (2005) presented results of unsaturated slope stability using elasto-plastic finite element analysis in combination with an analytical solution for suction stresses above the water table. The results indicated that suction above the ground water table increases the FoS of a slope for a variety of different infiltration rates and soil types. They also found that the suction profile is governed by three parameters: the soil's pore size parameters, the saturated hydraulic conductivity of the soil and infiltration or evaporation rate.

Rahardjo et al. (2007) performed a series of parametric studies in order to investigate the relative effects of soil characteristics, geometry of the slope, and location of the initial water table on the instability of a homogeneous slope under rainfall events of varying intensity. The results showed that soil characteristics and the rainfall intensity are the primary factors controlling the instability of slopes due to rainfall, whereas the geometry of the slope and the location of the initial water table only played a secondary role. For a predefined rainfall duration, the threshold rainfall intensity which would yield the minimum global factor of safety could be determined. Additionally, this parametric study clearly showed that the significance of previous rainfall events on the instability depends on the permeability of the soil.

Oh & Vanapalli (2010) presented the results of stability analyses for a homogeneous compacted embankment under consideration of water infiltration. Several different practical scenarios, including long- and short-term analyses for both saturated and unsaturated conditions, were investigated. Rainfall infiltration into an initially unsaturated embankment was identified as the critical instability condition, however, it was recommended to analyse the embankment stability of all different scenarios discussed in their contribution.

Rahardjo et al. (2010) performed parametric studies in order to study the effects of groundwater table positions, the intensity of rainfall and of soil properties on the stability of slopes. The results of the parametric study were compared with numerical analyses of existing slopes consisting of residual soils or sedimentary formations in Singapore. The results showed large variations in the location of the groundwater table between dry and wet periods, showing the highest position in wet periods with associated low FoS for both formations. In this study, rainfall intensities higher than 22 mm/hour did not further decrease the factor of safety because the soil reached its capacity to receive water. The smallest FoS may not occur at the end of the rainfall event, but rather several hours after the rainfall

stops because rainwater did not reach the critical slip surface at the end of rainfall when low permeable soil were used.

Rahimi et al. (2010) executed a series of parametric studies to determine the effects of hydraulic soil properties on rainfall-induced slope failure. The results indicated that SWCC fitting parameters considerably influence the stability of poor drainage soil slopes, whereas the stability of well-drained soil slopes is not that sensitive to variations of these fitting parameters.

Valentino et al. (2011) presented a simplified empirical model, which allows for calculation of the degree of saturation of soils using readily available climate data on rainfall and air temperature. The model was tested with in situ measurements of soil water content collected at three different sites in Italy. The empirical model was used to generate soil water content to time series at different depths. In each depth where the degree of saturation was computed, a separate calibration was required. The model is generally suitable to simulate complete, multiple annual cycles of water content in different depths of shallow unsaturated soil layers. The complex mechanism of evapotranspiration could not be adequately described through the unique set of material parameters as used in the proposed formulation and is therefore not suitable for deep soil layers (more than 20 cm) of vegetated soils.

Zhang et al. (2011) provided an overview of existing research on slope stability analysis under rainfall infiltration and reviewed studies on infiltration with conceptual, analytical and numerical modelling. They discussed typical pore water pressure profiles and recent developments in slope stability analysis under rainfall conditions which utilize the limit equilbrium method and coupled hydro-mechanical models. In relation to rainfall-induced landslides, critical hydrological factors were presented.

Askarinejad (2013) studied the effects of perturbations of pore water pressures on the stability of unsaturated silty sand slopes and investigated mechanisms leading to shear deformations and possible rapid mass movements. In order to identify the triggering mechanisms of several shallow landslides which occurred in Ruedlingen (Switzerland) in 2002 as a consequence of rainfall events, two field test experiments where rainfall was applied artificially were carried out to failure. Moreover, the behaviour of the test slope prior to failure, induced by the artificial rainfall, was examined, using both analytical and numerical models methods. Askarinejad (2013) performed 2D- and 3D limit equilibrium models, as well as 2D- and 3D uncoupled hydro-mechanical finite element simulations.

In addition to the work of Askarinejad (2013), the contribution of Springman et al. (2013) focused on the measurements of water balance and suctions, together with natural meteorological inputs which are used to prepare a prediction of environmental effects on saturation-suction relationships and slope stability. A

two-year monitoring experiment on a slope in shallow weathered soils overlying sandstone bedrock in Switzerland was described. Tensiometers in combination with Time-Domain Reflectometry (TDR) probes were found to be appropriate for this kind of experiment, whereas the limited suction measurement range of maximum 80-100 kPa was described to be suboptimal. Changing permeabilities and the possible development of perched water tables were indicated by changes of infiltration characteristics in the diverse soil layers. Preferential flow paths in soil layers below the topsoil indicates of small-scale variability. The different soil layers in the slope with associated changes of permeability led to the possible development of perched water tables, indicated by changes of infiltration characteristics. Additionally, the results clearly indicate that there was a bi-seasonal response in the slope demonstrating a typical summer and a typical winter character, as observed through the respective precipitation events. The finite-element analyses used allowed for a quite well prediction of pore water pressures from the meteorological inputs. The FoS of the slope strongly depends on the saturation of the slope, whereby the smallest FoS was calculated after the wetter winter months.

Chirico et al. (2013) examined the role of vegetation on the stability of unsaturated and shallow soil slopes and discussed two major positive effects of vegetation on slope stability: Beside geo-mechanical effects (reinforcement of the soil by plant roots), also the soil-hydrological effects (increased suction affected by root water uptake) increase the stability of slopes. Those effects were investigated with an infinite slope model, showing that in case of a loamy-sand soil under Mediterranean climatic regimes, the geo-mechanical effect was more relevant than the soil-hydrological effect during the rainy season.

Tsiampousi et al. (2013) investigated the relationship between the factor of safety and time for an excavation performed in an unsaturated silty soil, employing finite element method and the Imperial College Finite Element Program (ICFEP) was used. Two types of analyses, either assuming unsaturated or fully saturated soil behaviour, have been performed considering a hypothetical boundary value problem. Contrary to what is generally accepted to be the case in fully saturated soils, the analyses results show that for unsaturated soils the FoS may increase with time. In the saturated analysis, the negative applied load from the excavation was transferred to the incompressible fluid and subsequently to the soil skeleton during swelling. Additionally, suction causes the effective stresses to increase when using the Modified Cam Clay (MCC) model in the saturated analysis. In unsaturated analysis, due to the presence of air within unsaturated soil pores the mixture of fluids was not incompressible. Additionally, in the numerical model adopted in the unsaturated analysis, suction causes the apparent cohesion to increase as a function of the degree of saturation. Independently of the value of k_{sat} used and the assumptions taken with regards to the increase of apparent cohesion with suction (as long as this was not zero), it could be shown that the long term FoS calculated for the saturated analysis was smaller than for

the unsaturated analysis. As this conclusion does not stand for short or intermediate-term conditions and is largely dependent on the value of k_{sat}, it is not possible to know in advance which one of the two types of analysis performed (saturated or unsaturated) will produce conservative results. Therefore it is advisable to perform unsaturated analysis in geotechnical practice.

Robinson et al. (2017) investigated the impact of extreme precipitation events under current and future climate scenarios on landslides using extreme precipitation estimates derived from the so-called stationary assumption. Future precipitation patterns were integrated into a series of fully coupled two-dimensional finite element simulations. The presented results indicate that using historical rainfall data may underestimate the effects on hydromechanical behaviour of future extreme rainfall events. The increasing rainfall intensities in the future climate may impact not only natural slopes, but also engineered slopes and earth retaining structures.

Senthilkumar et al. (2018) presented the investigation of a rainfall-induced landslide that occured in 2009 in the Marappalam area in India, which was triggered by a high-intensity and short rainfall event that occured after a prolonged low-intensity rainfall period. A transient seepage analysis utilizing the finite difference method was used to study the effects of rainfall infiltration into this unsaturated residual soil slope. The fluid–mechanical interaction of unsaturated soil was obtained using coupled fluid flow analysis and was carried out in two stages. The first stage with an extensive low-intensity rainfall event increased the soil moisture content and coefficient of permeability and therefore made the soil more permeable to future rainfall infiltration. In the second stage, a short-duration and high-intensity rainfall event followed, leading to a further increase in water content which then led, due to the advancement of the wetting front, to full saturation of the slope to the soil-rock interface. The increase in saturation accompanied by a reduction in matric suction, together with the subsequent development of positive pore water pressures led to a reduction in effective stresses and thus reduced the shear strength along the soil-rock interface, which then caused the landslide in Marappalam.

Siemens (2017) highlights the unsaturated soil's principles presenting application-driven examples in the areas of deformation behaviour as well as capillarity, flow and strength. More and more designs are asked to consider climate change effects to predict performance. The increasing computer capabilities to incorporate unsaturated relationships and the appreciation of unsaturated soils behaviour broadened unsaturated soil mechanics use in practice.

Wang et al. (2018) presented a simplified monitoring and warning system against rainfall-induced shallow slope failures. The introduced system, which allows measuring water contents at multiple depths in the field by using low-cost microelectromechanical system based sensor sticks, in combination with SWCCs

inferred from grain-size distributions allows deriving the FoS of infinite slopes. The development of this new system could circumvent the use of challenging and costly field and laboratory tests while providing a quantitative and real-time slope stability assessment. It must be mentioned, however, that the presented simplified procedure is ideal for monitoring soil slopes that do not involve serious risks. Soil slopes which possibly tend to failure require a more elaborated monitoring including rigorous laboratory tests in order to determine the necessary SWCCs and shear strength parameters.

This chapter shows that the particular behaviour of unsaturated soils and the possible benefits of accounting for unsaturated effects have been very well studied and presented in literature in recent times. Beside several back-calculations of slope failures and landslides, analytical and experimental investigations, especially the development of ever-improving and powerful computers led to a variety of numerical studies to simulate rainfall infiltration into unsaturated soil slopes and the associated effects on the FoS. The influence of various rainfall events on slopes with given geometrical and hydraulic properties, as well as the infiltration behaviour itself and the failure mechanism that it possibly causes is still subject of ongoing research but seem to be widely understood.

The possibly negative influence of unknown initial hydraulic conditions within a slope before a heavy rainfall event takes place, has not been investigated in full detail so far in literature. The initial suction profile within a slope has major influence on soils capability to take water (infiltration). The infiltration of water into soil slopes leads to changes in pore water pressures causing a decrease of effective stresses and thus reduces the shear strength of the slope. Due to equilibrium reasons in numerical analyses, a linearly increasing negative pore water pressure above the groundwater-level will be the “default” condition. Especially if the groundwater-level is very deep, this may lead to very high suction values at the ground surface in the calculations, which may not be realistic to field conditions. To overcome this issue of uncertainty, the so-called Lysimeter device, which is usually used for agricultural research purposes and is able to provide hydraulic data to calibrate the suction profile in numerical analysis, can be used. Main goal of this contribution was to quantify the development of changes in suction due to climatic conditions, in which different initial suction profiles have been used. The effects of either using (referred to Lysimeter-data) manually defined (“model M”) or (only related to the groundwater level) automatically generated (“model A”) initial pore water pressure profile on the FoS of different slope geometries during various climatic conditions, have been investigated. Additionally, the influence of antecedent precipitation before a major rainfall event takes place on the FoS has been investigated in this thesis.

3 Unsaturated soils

In traditional soil mechanics approaches, soils below the ground water table are considered to be two-phase media: solids and one fluid. The primary motivation for this simplified assumption is the easier characterisation of soils containing only one fluid phase (either water or air). In contrast, the unsaturated soil mechanics approach assumes these soils to be a three- or four-phase system, in which the soil voids (pores) can be filled with both water and gas (i.e. air), in varying amounts. In the unsaturated soil mechanics approach, the classical soil mechanics soils, where all soil voids (pores) are either completely filled with water or air, are integrated as special cases. The role of the unsaturated soil environment in the natural hydrological cycle is schematically illustrated in Fig. 1. The steady-state position of the water table is given by the overall topography of the system, the soil characteristics and the balance achieved among the natural mechanisms which either add or remove water to or from the subsoil. The scale of this hydrological cycle could be either local (e.g. limited to a specific building site) or extended to as large as the continental or even the global scale. The unsaturated zone forms the necessary transition between the atmosphere and deeper-lying saturated zones (Lu & Likos 2004). However, water moving (unsaturated flow) in this particular zone also plays a significant role to the overall stability of the slope and points up the need of unsaturated soil mechanics approaches, which can consider this aspect. This chapter highlights the general behaviour of unsaturated soils and the advantages of taking unsaturated soil's behaviour into account in engineering practice.

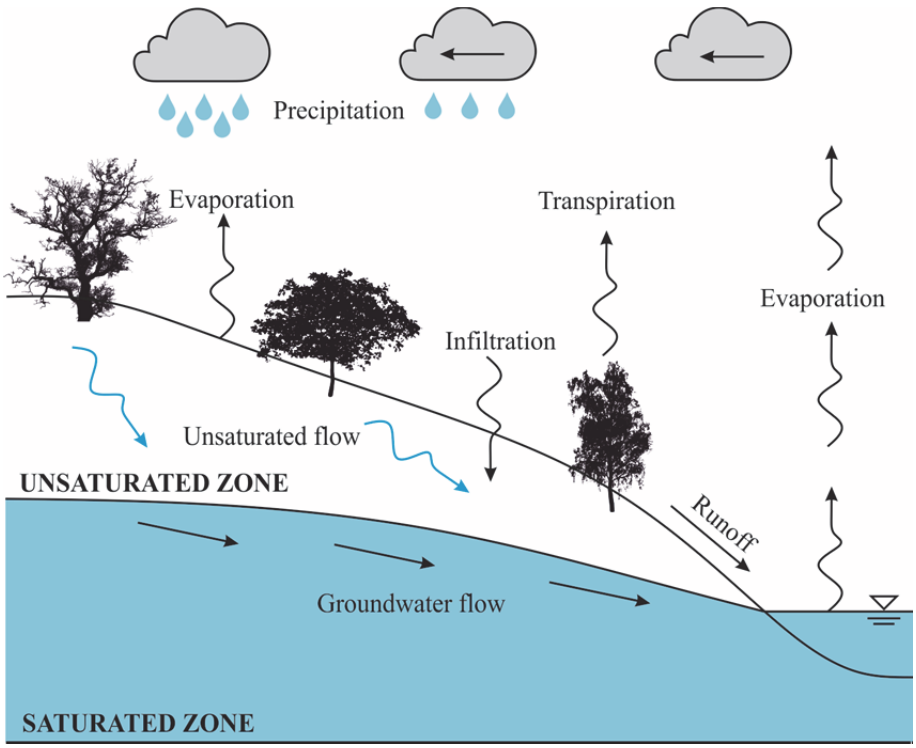

Fig. 1: Unsaturated soils in the hydrological cycle (after Lu & Likos 2004)

3.1 Definition and phase properties of unsaturated soils

An unsaturated soil is a soil with partial saturation which is neither completely full nor completely empty of water, but rather having both of at least some water and some air present. Accordingly, a partially saturated or unsaturated soil is a multiphase system and, depending on the definition used, consists of three or four phases. Besides the soil solids (particles) phase and the water and air phases, the air-water interface (i.e. contractile skin) is also often referred to as a separate phase. In terms of volume and mass properties, it is not necessary to separate the water in the contractile skin from the remaining water mass. However, in terms of stress state conditions, this fourth phase (which is described in more detail in the upcoming chapter 3.2.2) needs to be considered (Fredlund et al. 2012), and will be considered in this thesis. Fig. 2 illustrates the phase diagram for unsaturated soils.

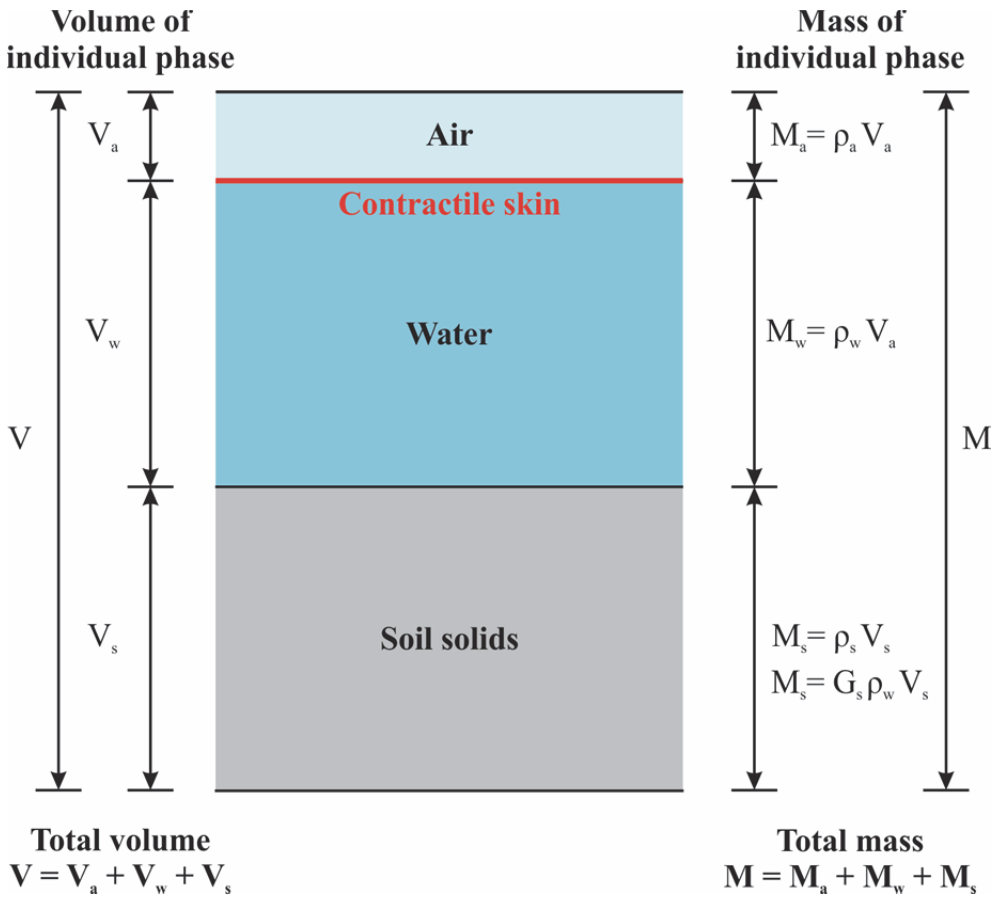

Fig. 2: Phase diagram for unsaturated soil (after Fredlund et al. 2012)

Numerous authors have discussed the difference between the various stages of saturation (e.g. Boutonnier 2010, Köhler & Montenegro 2005). For example, decreasing pore water pressures may lead to entrapped air bubbles within the

pore water phase, making it behave differently to a continuous water phase. In order to differentiate the various saturation stages, the characteristics of the air and water phases must be considered. The Soil Water Characteristic Curve (SWCC) is often used to show these characteristics for a particular soil. A soil is called fully saturated, when all the pores are filled with water and no air is present in the pore water, and is, in essence, incompressible. The presence of even a small amount of air, occurring as enclosed air bubbles, makes the pore fluid, as a whole, compressible. However, a soil can stay essentially saturated while the pore water pressure becomes negative in relation to the air phase. The area immediately above the groundwater table is referred to as the capillary zone and is characterized as being substantially saturated while having negative pore water pressures (Fredlund et al. 2012). The relative to the internal or external air pressure negative pore water pressures qualifies a soil to be unsaturated (see Fig. 3).

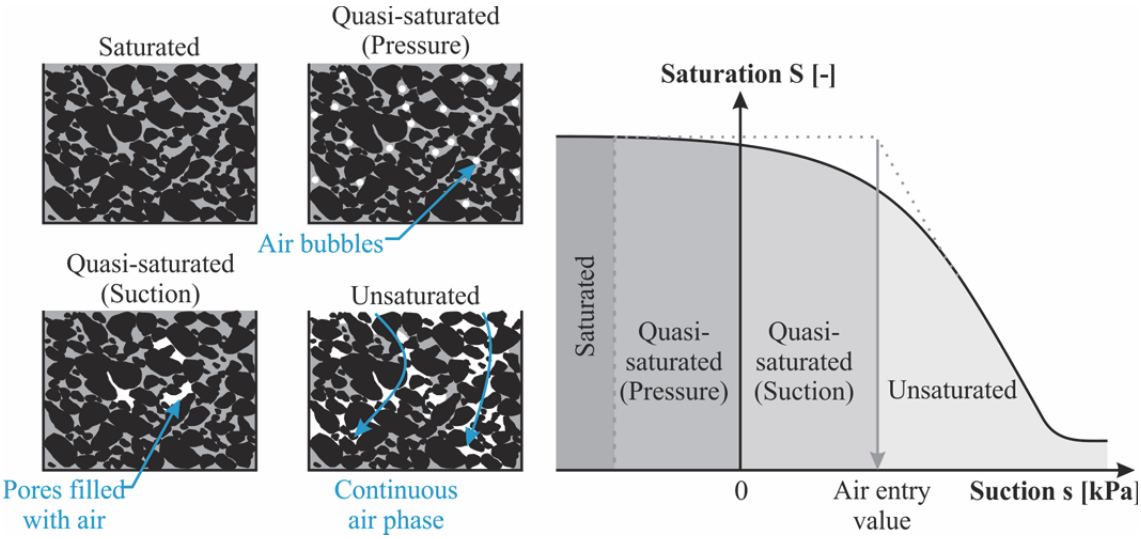

Fig. 3: Stages of saturation and exemplary SWCC ((Ausweger 2018), original work of Boutonnier 2010)

As the difference in pore water and pore air pressures becomes considerably larger, the application of particular theories and concepts to describe the unsaturated soil's behaviour is required. The first concept to consider is the air-water interface (contractile skin) that forms a fixed divider between the air and water phases and acts like a thin membrane interlaced throughout the voids of the soil (Fredlund et al. 2012). Terzaghi estimated the contractile skin to have a thickness of 10^{-6} mm, however, other studies since then suggest that the thickness of this interface might be in the order of 1.5 to 2 water molecules (~ 4.5-6 * 10^{-6} mm) in diameter (Townsend & Rice 1991)

It's commonly accepted that the contractile skin and its associated surface tension (pressure) are required to reach equilibrium in calculations, when there is a pressure difference between the air and the water phases. This special interface (contractile skin) thus plays a major role in really understanding unsaturated soil mechanics.

3.2 Soil suction

In general, the total soil suction quantifies the thermodynamic potential of the soil pore water relative to a reference point of free water. Soil suction ψ has a major impact on the behaviour of unsaturated soils and is composed of four components:

$$\psi_{total} = \psi_c + \psi_s + \psi_g + \psi_z \quad (1)$$

where the difference between pore air pressure u_a and the pore water pressure u_w u_a-u_w is denoted as matric suction ψ_c (or capillary pressure), osmotic suction ϕ_s is the result of a chemical imbalance between different salt concentrations in the pore water within the soil volume under consideration and an external nearby source of water, ψ_g is the gas pressure potential and ψ_z is the gravitational potential.

Suction can be defined as the capability of soil to absorb additional water, whether it is fully or partially saturated, and can be defined as the free energy state of soil water (Edlefsen & Anderson 1943). In order to determine the free energy state of soil water, the partial vapour pressure of the soil water can be used. This thermodynamic relationship between the partial vapour pressure and the soil suction can be written as (Richards 1965):

$$\psi = -\frac{R_u T \rho_w}{\omega_v} ln\left(\frac{u_v}{u_{vo}}\right) \quad (2)$$

where R_u is the universal gas constant, T is the absolute temperature, u_v the partial pressure of pore water vapour, u_{vo} is the saturation pressure of pore water over a flat surface of pure water at the same temperature, the term u_v/u_{vo} represents relative humidity R_h and ω_v is the molecular mass of water vapour.

Generally, most engineering problems involving unsaturated soils are the consequence of environmental changes which primarily affect the matric suction component. For example, the stability of unsaturated soil slopes may be affected by weather induced conditions such as excessive rainfall events with associated infiltration into the soil body that could reduce the (mainly matric) suction in the soil. There are situations, however, where the presence of salt within the soil water can lead to changes in osmotic suction and could have an effect on the mechanical behaviour of the soil (Alonso et al. 1987).

Fig. 4 illustrates the relatively small importance of changes in osmotic suction compared to changes in matric suction with varying water contents in glacial till. Except for small deviations, particularly in the range of higher water content, both the matric and total suction curves are almost congruent one to another (Krahn & Fredlund 1972).

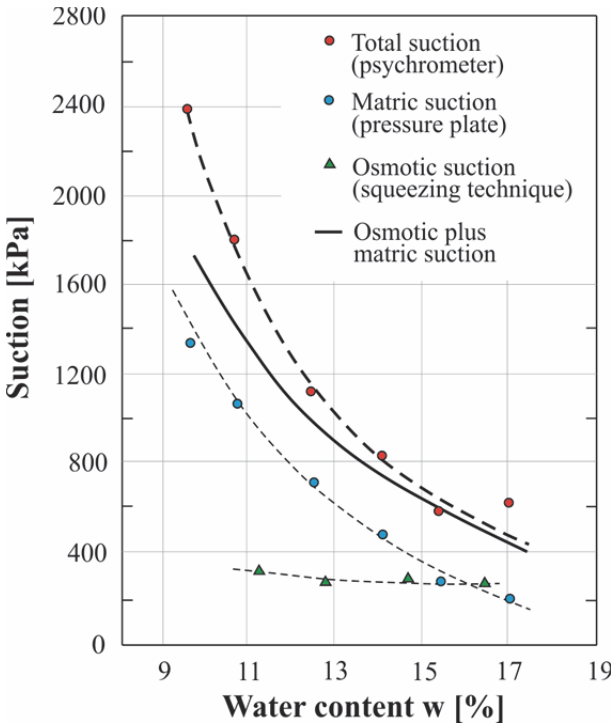

Fig. 4: Total, matric and osmotic suctions for glacial till (after Krahn & Fredlund 1972)

Thus, as long as no salts are additionally added to the soil and since matric suction changes usually correlate with the same changes in total suction, osmotic suction can essentially be neglected in geotechnical problems, and will be neglected within the framework of this thesis.

3.2.1 Capillary Phenomenon

The matric suction component of total suction is primarily a result of the capillary phenomenon and can play a major role in infiltration behaviour and hence the stability of soil slopes.

Within the laboratory setting, the height of the capillary rise in a tube is inversely related to the radius r of the tube and the related curvature radius $R_s = r / \cos \alpha$ of the air-water interface has a direct effect on the saturation – suction – relationship (represented by the SWCC, which will be further explained in chapter 3.4.1) in soils. Generally, the equivalent of tube radius in soils is the pore radius, where a smaller pore radius leads to a higher capillary rise, and increased suction.

A physical model of capillarity is demonstrated in Fig. 5 where a glass tube is placed into water under atmospheric pressure conditions. As a result of the

surface tension of the contractile skin and water's tendency to wet the surface of the glass tube (i.e. hygroscopic behaviour), water rises up inside the tube. The surface tension T_s acts around the circumference of the meniscus at an angle α to the vertical wall of the tube, which is also referred to as the contact angle. The size of the contact angle depends on the adhesive forces between the material of the tube (e.g. glass) and the molecules in the contractile skin. A rearrangement of the vertical force equilibrium equation (where p_w is the density of water and g is the gravitational constant) of the water in the tube gives the maximum height of the water column inside the tube, h_c:

$$h_c = \frac{2T_s}{\rho_w g R_s} \tag{3}$$

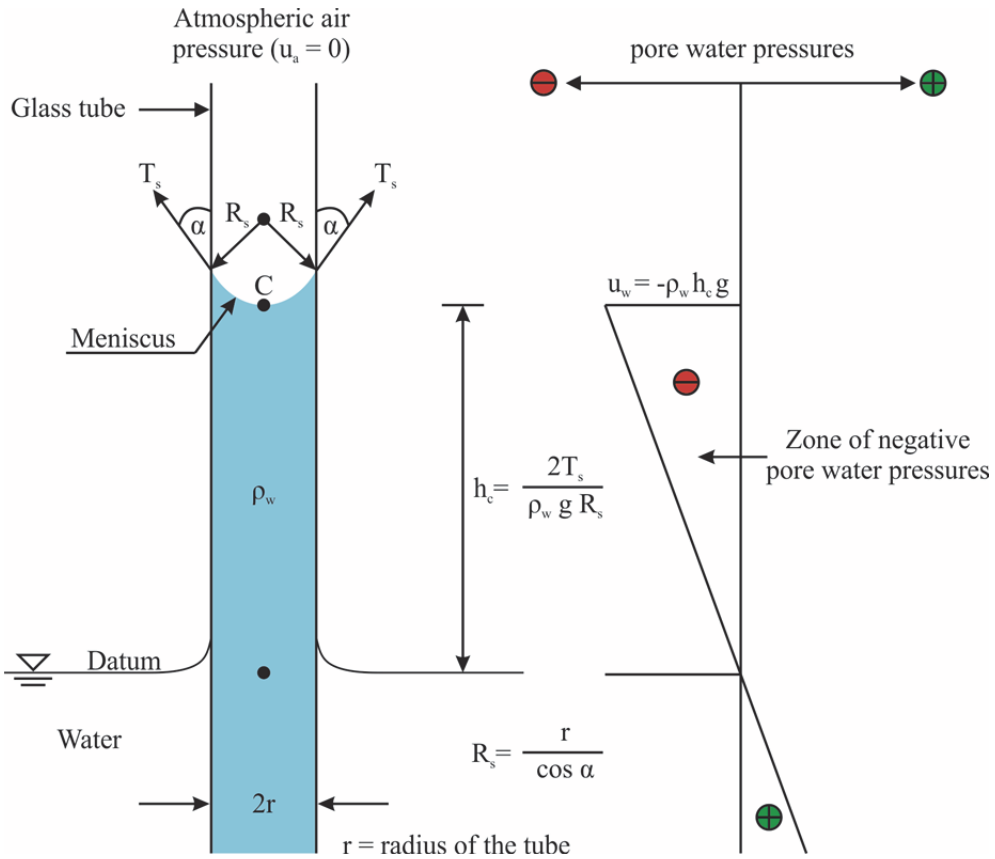

Fig. 5: Physical model of capillarity (after Fredlund et al. 2012)

Referring to the phenomenon of capillarity and equation 3, matric suction (u_a-u_w) can be expressed in terms of surface tension, as indicated in Fig. 5 (right), and is also known as Kelvin's capillary model equation:

$$u_a - u_w = \frac{2T_s}{R_s} \tag{4}$$

3.2.2 Contractile skin and surface tension

In order to understand the particular physical properties of unsaturated soil mechanics, one needs to know the general capillary phenomenon, as well as surface tension and the special characteristics of the air-water interface. Surface tension T_s occurs due to unbalanced molecular forces at the air-water interface which lead to a temperature dependent (Weast et al. 1981) "tensile pull" along the interface.

As indicated on the left side of Fig. 6, the water molecule situated within the water volume experiences equal and opposing forces in all directions, and thus there is no unbalanced force acting on it. In contrast, as the outside air pressure is higher than the inside water pressure ($u_a > u_w$), a water molecule inside the contractile skin experiences an unbalanced force in the direction of the interior of the water volume. In order for the contractile skin molecules to be in a force equilibrium, a tensile pull (Equation 4) is generated along this air-water interface which causes the contractile skin to bend into a curve. It is the contractile skin's surface tension that allows it to exert a tensile pull. As illustrated on the right side of Fig. 6, the air-water interface can also be considered as a three-dimensional surface, and the pressure difference at the air-water interface extended using the Young-Laplace function as shown in Equation 5.

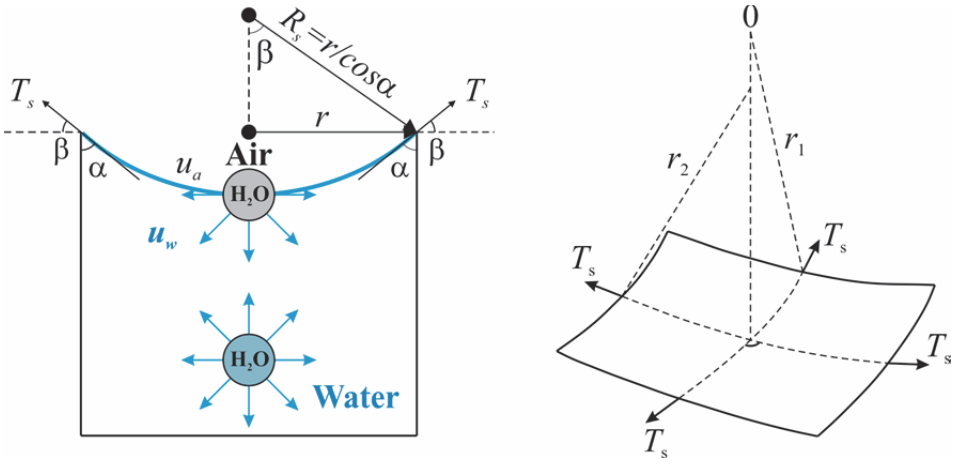

Fig. 6: Surface tension forces at curved two-dimensional air-water interface (left) and on three-dimensional warped membrane (right) (after Fredlund et al. 2012 (adapted))

In general, the geometry of the interface between any two fluids (liquid or gas) is governed by the equilibrium of forces acting on both sides of the interface. In a liquid-liquid system (e.g. oil drop on water) the interface geometry is characterized by the interfacial tension acting between the two liquids. In contrast, in a gas-liquid system, such as the air-water interface in partially saturated soils, the surface tension of the air face is insignificant. Thus in order to reach mechanical equilibrium and to govern the interface geometry, only three components are at play: air pressure, water pressure and the surface tension of the liquid (Lu & Likos 2004).

The air-water interface geometry in soils is also controlled by particles with various shapes, sizes and complex pore fabric, hence, a spherical shaped interface is rare. As an example, Fig. 7 shows a microscopic photograph of a meniscus between two sand grains.

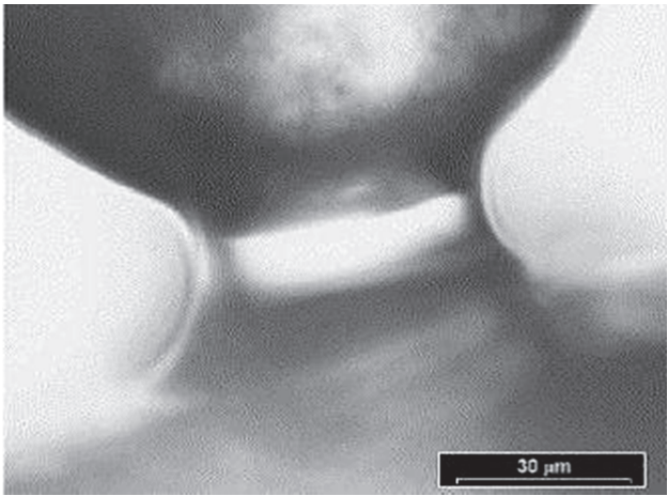

Fig. 7: Microscopic photograph of the menisci between two sand grains (van Mechelen 2004)

Consequently, in order to extend the simple capillary tube models to unsaturated soil mechanics, assumptions about the complex pore geometry must be made. Nearby soil particles are assumed to be two equal spherical soil particles, and the water volume in between delimited by two air-water interfaces. It is assumed that each interface can be simplified with the toroidal approximation. The geometry of this idealized air-water interface between two spherical soil grains can be defined by two radii of curvature r_1 and r_2 as indicated in Fig. 7.

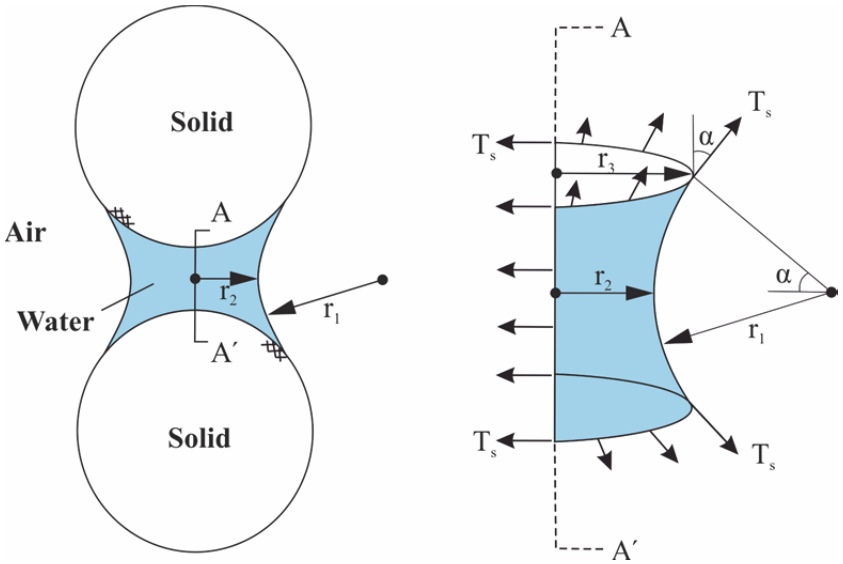

Fig. 8: Idealized geometry of an air-water interface in unsaturated soils: (left) two water menisci between two spherical soil particles (solids); and (right) a free- body diagram for a water meniscus (after Lu & Likos 2004)

Equation 5 presents a simple mathematical expression (the Young-Laplace equation) describing the pressure difference across the air-water-solid interface between idealized soil grains, putting together Equation 4 and the radii from Fig 7.

$$u_a - u_w = T_s \left(\frac{1}{r_1} - \frac{1}{r_2} \right) \tag{5}$$

As can be seen in Equation 5, the value of the matric suction u_a-u_w depends on the relative magnitudes of the radii r_1 and r_2 and can be either positive, negative or zero.

3.3 Water flow in unsaturated soil mechanics

The presence of air, which states the soil to be unsaturated, also affects the water flow in this unsaturated porous media. The rate of water flow through a porous medium is regulated by coefficient of permeability of the soil. As the amount of air increases and there is less cross-sectional area through which water can flow, the coefficient of permeability decreases (water can only flow that portion of the porous medium that consists of water). Consequently, the coefficient of permeability of a partially saturated soil strongly depends on the degree of saturation with associated changes of the stress state of the soil. In general, any changes in the stress state of an unsaturated soil affects the coefficient of permeability, however, changes beyond the air entry value, which is defined as the specific point in suction stress where air starts to enter the largest pores of the soil when suction increases, have the greatest effect. As the degree of saturation decreases with increasing suction, the cross-sectional area through which water can flow decreases, and therefore also the coefficient of permeability decreases.

Fig. 9 shows the conceptual SWCC *(1)* and hydraulic permeability curve *(2)* corresponding to the degree of saturation (*a-d*) for a rigid soil matrix of sand. The sketches at the bottom of Fig. 9 (*a-d*) illustrate schematically the distributions of pore water and pore air in a cross section of a rigid soil matrix throughout an incremental drainage process.

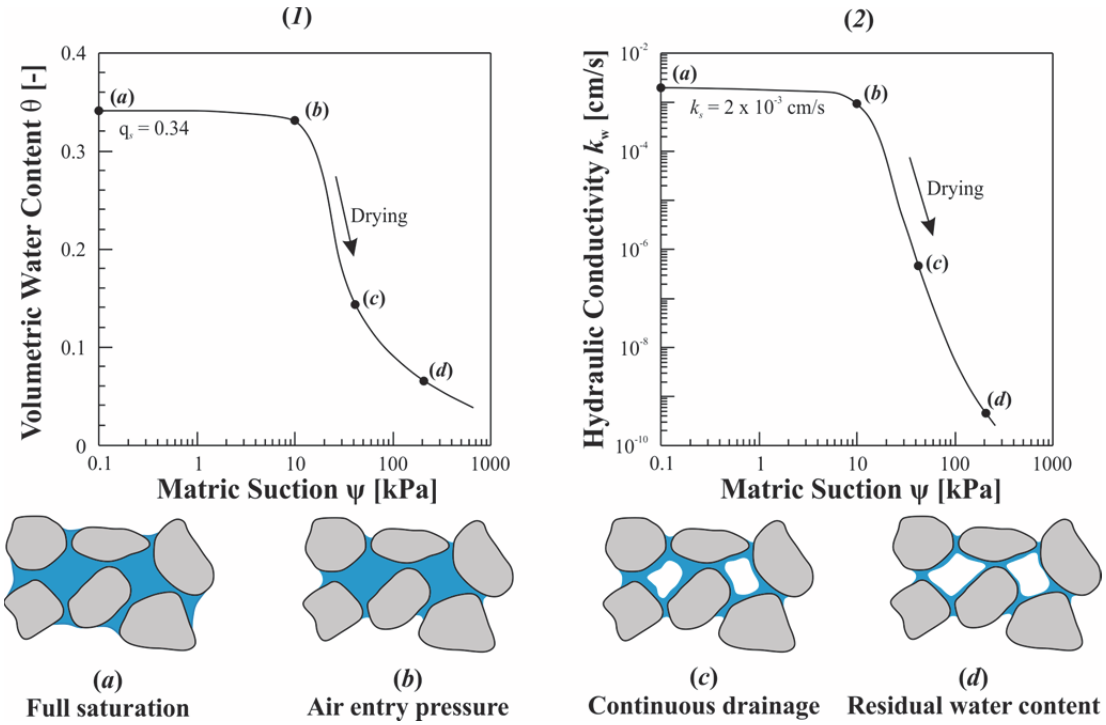

Fig. 9: Conceptual SWCC (left) and hydraulic conductivity curve (right) in relation to conditions of saturation (after Lu & Likos 2004)

Starting at condition *(a)* the soil matrix is fully saturated, consequently, matric suction is zero. During the first part of the drainage process, between point *(a)* and *(b)*, the soil sustains a limited amount of suction prior to desaturation, which starts at the air entry value *(b)*. From this point onwards in the drainage process, a further suction increase leads to continued drainage of the system. Drainage under increasing suction results in significant drops in both water content and hydraulic conductivity, however, only until point *(c)*. Increasing suction means that only smaller and more tortuous paths are available for the water to flow, which reduces the permeability of the soil significantly. The reduction in hydraulic permeability is initially quite steep because the first pores to empty are the most interconnected and largest and therefore the most conductive to water. At point *(d)*, the pore water exists predominantly in the form of disconnected menisci between the soil grains. The permeability at this point, which is near the residual water content, decreases effectively to zero and the pore water is then primarily transported through the vapour phase. Characteristic of many soils, the total change in the magnitude of hydraulic conductivity from point *(a)* to *(d)* can be over six orders of magnitude (Lu & Likos 2004).

As the pore voids in an unsaturated soil can be filled with both air and water phases at the same time, its hydraulic permeability strongly depends on the proportion of these phases. The relative permeability functions, which are defined as the ratio of permeability at a given saturation to the permeability in the saturated state for the air phase k_{ra} and water phase k_{rw} of an unsaturated sand sample, are illustrated in Fig. 10.

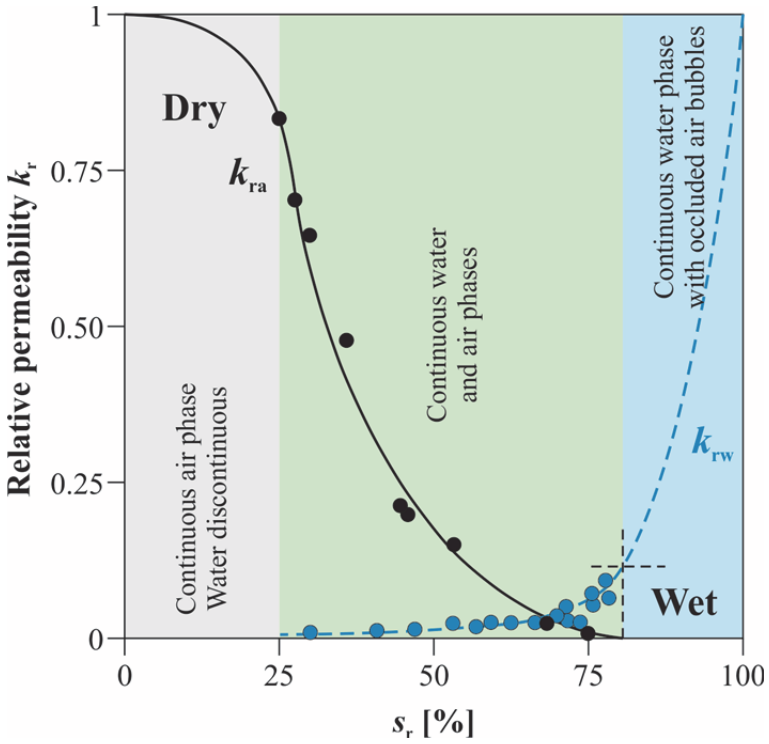

Fig. 10: Air and water relative permeability functions of an unsaturated sand sample (Delage 2015, adapted)

As shown in Fig. 10, the relative permeability depends on the degree of saturation S, indicated as a percentage. The “dry” range between zero percent and approximately 25 % saturation is characterized by a continuous air phase, and a discontinuous water phase. In the next graphical division (green), ranging between about 25 % and 80 % saturation, both the air and the water phase can be described as continuous. In the “wet” zone, with saturation higher than 80 %, only the water phase is continuous, but air can also be there in the form of occluded bubbles.

In the following sections, water flow through unsaturated soils will be theoretically described, using a number of concepts. To begin with, the concept of water flow through saturated soils has historically been described by geotechnical engineers in terms of hydraulic head gradient. Also in unsaturated soils, the flow of water can most appropriately be defined in terms of a hydraulic head gradient, consisting of both the pressure head gradient and the elevation head gradient of the water.

3.3.1 Continuity equation

Hydraulic conductivity regulates the rate of water flow through a porous medium. When performing steady-state or transient flow analysis of an incompressible fluid (e.g. water) through a porous medium such as soil, the coefficient of permeability of the soil is the main soil property required.

In order to describe transient fluid flow in unsaturated soils under isothermal conditions, the principle of mass conservation can be applied. This principle, which is also called the continuity principle, states that the rate of water loss or gain is equal to the net flow into and out of a given soil volume. The principle of flow through the elemental volume of soil is illustrated in Fig. 11.

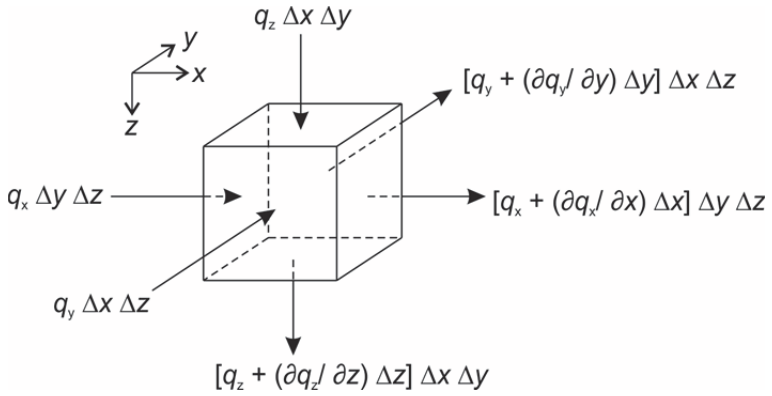

Fig. 11: Elemental volume of soil (after Lu & Likos 2004), original work of Richards (1931b) and Terzaghi (1943)

Therefore, under the assumption that there are no changes in water density, the governing equation of transient or unsteady fluid that flows through an elemental soil volume, (Fig. 11), either saturated or unsaturated, can be written as follows:

$$-\rho\left(\frac{\partial q_x}{\partial x}+\frac{\partial q_y}{\partial y}+\frac{\partial q_z}{\partial z}\right)=\frac{\partial(\rho\theta)}{\partial t} \tag{6}$$

where ρ is the density of water (kg/m³) and q_x, q_y, and q_z are fluxes in the x, y, and z directions, respectively (m/s).

3.3.2 Darcy's Law for unsaturated soil mechanics

In saturated soils, water flow is usually described using Darcy's law (1856), which states that the rate of water flow through a soil mass is proportional to the hydraulic head gradient of the water in that soil mass.

The equilibrium equation for groundwater flow can be expressed using the following equation:

$$\nabla p_w + \rho_w \underline{g} + \underline{\varphi} = 0 \tag{7}$$

where ∇p_w is referred to as the gradient of the pore water pressure which causes the groundwater flow, ρ_w is the unit weight of water, $\underline{g}$ is the vector of gravitational acceleration $(0, -g, 0)^T$ and $\underline{\varphi}$ is the vector of the friction force, per unit volume, between the flowing fluid and the soil skeleton (solid particles). This friction force depends linearly on the velocity of the fluid and acts in the opposite direction. This can be expressed by the following relation:

$$\underline{\varphi} = -\underline{\underline{m}}^{int} \underline{q} \tag{8}$$

where $\underline{q}$ is the velocity of the fluid (specific discharge) and $\underline{\underline{m}}$ can be written as:

$$\underline{\underline{m}}^{int} = \begin{vmatrix} \frac{\mu}{K_x} & 0 & 0 \\ 0 & \frac{\mu}{K_y} & 0 \\ 0 & 0 & \frac{\mu}{K_z} \end{vmatrix} \tag{9}$$

where μ is the dynamic viscosity of the fluid and κ_i is the intrinsic permeability of the porous medium. As hydrostatic conditions are assumed, the term $\rho_w \underline{g}$ (in Equation 7) is not affected by the gradient of the water pore pressure in the vertical direction. Combining Equation 7 and Equation 8 yields:

$$-\nabla p_w - \rho_w \underline{g} + \underline{\underline{m}}^{int} \underline{q} = \underline{0} \tag{10}$$

which can be either expressed as follows:

$$\underline{q} = \underline{\underline{k}}^{int} \left(\nabla p_w + p_w \underline{g} \right) \tag{11}$$

or

$$\underline{q} = \frac{1}{\underline{\underline{m}}^{int}} \left(\nabla p_w + p_w \, \underline{g} \right) \tag{12}$$

where $\underline{\underline{k}}^{int}$ is defined as:

$$\underline{\underline{k}}^{int} = \begin{vmatrix} \frac{K_x}{\mu} & 0 & 0 \\ 0 & \frac{K_y}{\mu} & 0 \\ 0 & 0 & \frac{K_z}{\mu} \end{vmatrix} \tag{13}$$

However, instead of requiring both intrinsic permeability and viscosity, the coefficient of permeability $\underline{\underline{k}}^{sat}$ (or hydraulic permeability) is commonly used in soil mechanics, and can be expressed as follows:

$$\underline{\underline{k}}^{sat} = \rho_w \, g \, \frac{\kappa_i}{\mu} \qquad i=x,y,z \tag{14}$$

or alternatively, it can be written as:

$$\underline{\underline{k}}^{sat} = \rho_w \, g \, \underline{\underline{k}}^{int} \tag{15}$$

A reshuffling of the terms leads to

$$\underline{\underline{k}}^{int} = \frac{\underline{\underline{k}}^{sat}}{\rho_w \, g} \tag{16}$$

where $\underline{\underline{k}}^{sat}$ represents the saturated permeability matrix, which is much simpler to determine than the matrix in Equation 13, and can be expressed as:

$$\underline{\underline{k}}^{sat} = \begin{vmatrix} {k_x}^{sat} & 0 & 0 \\ 0 & {k_y}^{sat} & 0 \\ 0 & 0 & {k_z}^{sat} \end{vmatrix} \tag{17}$$

Substituting Equation 16 into the k_{int} term of Equation 11 yields:

$$\underline{q} = \frac{k_{rel}}{\rho_w g} \underline{\underline{k}}^{sat} \left(\nabla p_w + \rho_w \underline{g} \right) \tag{18}$$

the basic form of Darcy's Law which defines water flow in a porous medium at full saturation.

However, the coefficient of permeability in an unsaturated state depends on the degree of saturation of the soil. Thus, for partially saturated soils the permeability can be written as:

$$\underline{\underline{k}} = k_{rel} \underline{\underline{k}}^{sat} \tag{19}$$

where k_{rel} *(S)* is defined as the ratio of the permeability at a given saturation to the permeability in saturated state.

Thus, to have a form of Darcy's Law which can be used for partially saturated soils, the coefficient of permeability in equation 18 needs to be modified from the saturated term by including k_{rel}, as shown in equation 19, resulting in the following:

$$\underline{q} = \frac{krel}{\rho_w g} \underline{\underline{k}}^{sat} \left(\nabla p_w + \rho_w \underline{g} \right) \tag{20}$$

3.3.3 Compressibility of pore fluid and pure water

There are certain loading cases in engineering practice (e.g. undrained loading) where the compressibility of the pore fluids affects the stress state of the soil. The magnitude of this induced changes in pore air and pore water pressures in the soil volume is highly dependent on the compressibility of the water-air mixture in the pores, which is derived from the compressibility of the individual water and air components, in consideration of their proportion of the total volume (Fredlund 1976).

Various authors have described the fundamental physical laws to determine the compressibility of an air-water mixture (e.g. Schuurmann 1966, Fredlund 1976). In general, the isothermal compressibility of a fluid can be written as (Fredlund et al. 2012):

$$C_{fluid} = -\frac{1}{V} \cdot \frac{dV}{dp_{fluid}} \tag{20}$$

where C_{fluid} is the compressibility of the fluid, V is its volume and dV is the volume change relating to a change in the pore fluid pressure dp_{fluid}.

Under the assumption of constant atmospheric air pressure p_{atm}, the compressibility of air C_{air} is inversely proportional to the absolute air pressure, which is defined as the sum of the air pressure in the soil p_{air} and the atmospheric air pressure p_{atm} (Fredlund et al. 2012):

$$C_{air} = \frac{1}{p_{air}+p_{atm}} \qquad (21)$$

According to Dorsey (1940), who presented measurement results of the compressibility of water, pure water is nearly incompressible (Fig. 12).

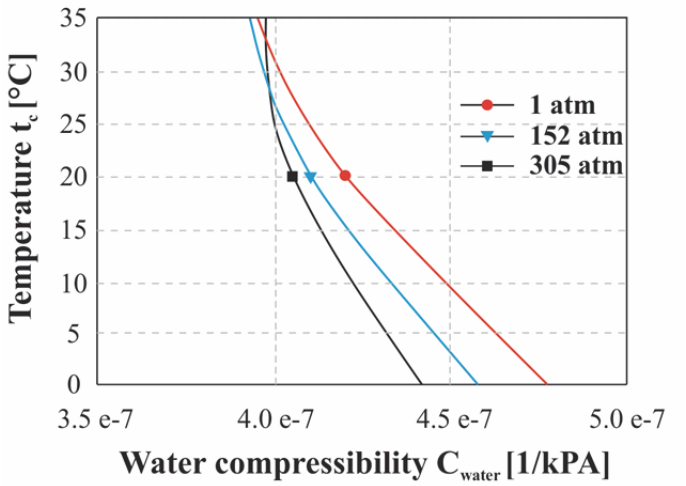

Fig. 12: Compressibility of pure water (after Fredlund et al. 2012)

According to Fredlund (1976), the compressibility of the air-water mixture can be derived from the compressibility of the individual constituents, considering their proportion of the total volume.

For standard applications in soil mechanics, the compressibility of water in soils is assumed to be incompressible.

3.4 Hydraulic models

The relationship between the water content and suction (or negative pore water pressure) of a soil can be described by the Soil Water Characteristic Curve (SWCC). There are several other terms used in the literature when referring to the relationship between the amount of water in the soil and soil suction as follows: suction-water content relationship, moisture retention curves, retention curves, water retention curves and more.

The term Soil Water Characteristic Curve has been selected as the preferred terminology for this thesis.

Water content is a measure of the amount of water in the soil pores and can be defined with numerous variables: gravimetric water content, volumetric water content, specific water volume or degree of saturation. Within the framework of this thesis, the water content is defined by means of either volumetric water content or degree of saturation only. Generally, SWCCs are s-shaped curves and plotted in a semi logarithmic scale (suction is plotted in logarithmic scale).

3.4.1 Soil Water Characteristic Curves

In general, the shape of SWCCs depends on several soil characteristics. In coarse-grained soils, the SWCC can be related to the grain size distribution. Due to the presence of smaller pores, well graded sands retain less water than poorly graded sands at the same suction levels. In fine-grained soils, the liquid limit and the plasticity index quantify the ability of the clay fraction to attract water (Delage 2002), and thus of the soil to retain water under suction. Finer grained, more plastic soils, which commonly contain a larger clay fraction, and are often denser soils, are able to retain larger water volumes than coarse-grained soils at same suction levels. The following Fig. 13 clearly illustrates the differences in the degree of saturation for various soil types at a same suction values (Barbour 1998), and shows that the curves have different shapes depending on whether the soil is coarse- or fine-grained. At the same amount of suction (in this case e.g. 1 MPa), the sand is almost dry (S = 10 %) while the degree of saturation of finer grained soils increases with plasticity (S = 15 %, 67 and 97 % for the “Botkin silt”, “Indian Head till” and “Regina clay”, respectively). The shapes show that in coarse-grained soils, it is capillarity that dictates the water held under suction, whereas in fine-grained soils, it is the larger plasticity index (I_p) and the clay-water interaction that holds the water.

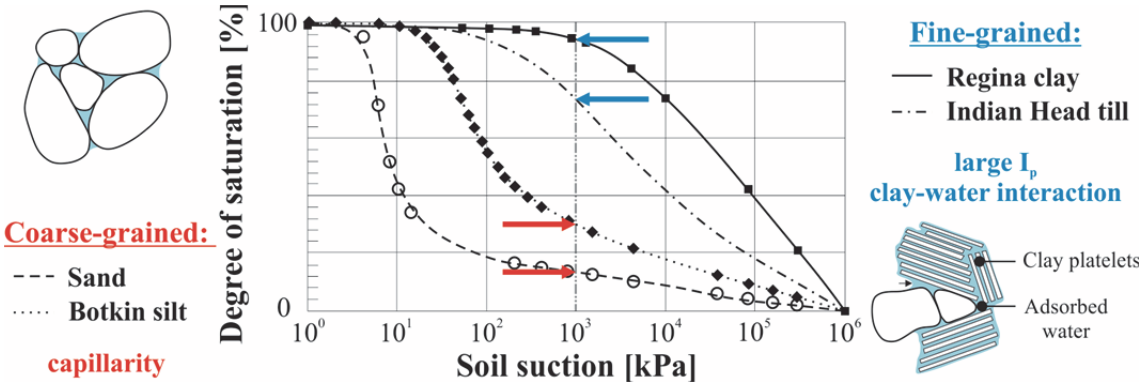

Fig. 13: Influence of soil type on the SWCC (Barbour 1998, adapted)

In order to best fit laboratory data into SWCCs, numerous empirical equations in closed-form have been proposed. Fredlund et al. (2012) presents an overview of the most important equations, appearing in the research literature, that mathematically describe SWCCs. In general, these equations can be classified either as two- or three-parameter equations and can be best fitted to laboratory data using a least-squares regression analysis (Fredlund & Xing 1994).

In those equations, there is always one variable which is related to the air entry value (AEV) of the soil and a second variable which is related to the rate at which soil desaturates. The third variable, which is only used in certain equations, allows for the description of the low suction range independently of the shape of the SWCC in higher suction ranges. The use of three-parameter equations increases the flexibility to fit the data to a curve in best-fitting analysis. It must be noted, however, that parameters in three-parameter equations are not fully independent of each other (e.g. van Genuchten equation, see section 2.4.3).

Once the SWCC has been determined, it can be used to predict further unsaturated soil properties such as the unsaturated coefficient of permeability and unsaturated shear strength (e.g. Fredlund et al. 1995, Fredlund et al. 2011). A method to analyse suction stress profiles based on the SWCC have been developed by Lu & Griffiths (2004). Furthermore, Lu & Likos (2006) introduced a suction stress characteristic curve (SSCC) in order to describe the stress state in partially saturated soils.

3.4.2 Hysteresis in the Soil Water Characteristic Curve

The relationship between the water content and suction in the soil is hysteretic. This means that the SWCCs of the wetting and drying paths are different and each SWCC equation can be best fitted to either the wetting (adsorption) or drying path (desorption). In general, the drying path shows higher suction values at a similar water content compared to the wetting path.

It must be noted, however, that there is no unique or single SWCC for any one kind of soil or even for one specific soil sample. As there exists an infinite number of intermediate curves, called wetting and drying scanning curves, the

aforementioned wetting and drying curves act solely as extreme boundaries of the SWCC (Fig. 14).

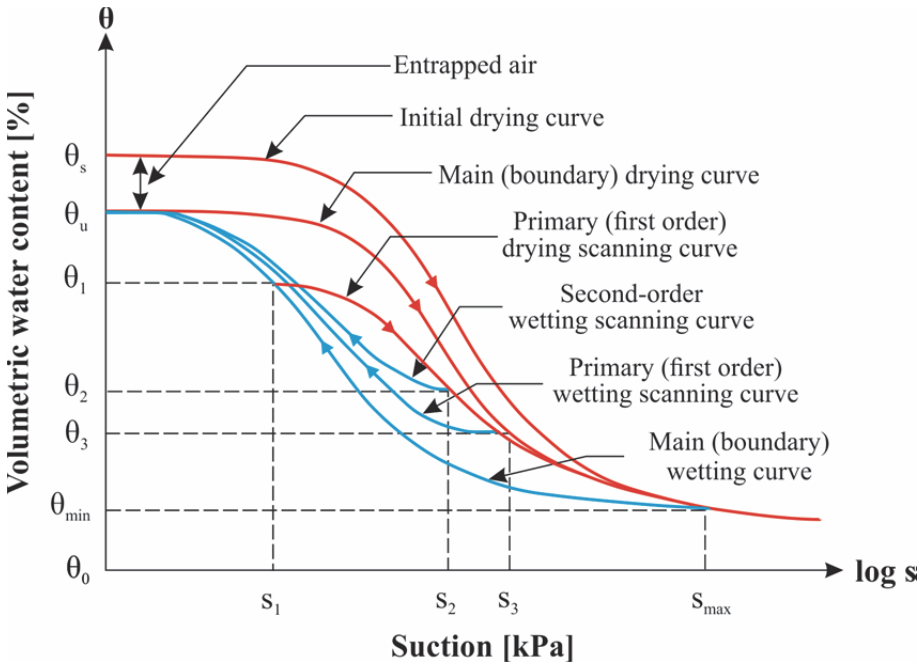

Fig. 14: Conceptual boundary and scanning curves used to define drying and wetting of unsaturated soils (after Pham et al. 2003a)

Fig. 14 also illustrates that due to the entrapment of occluded air bubbles, full saturation θ_s may not be reached during the wetting process. Furthermore, it is not possible to determine whether a soil is on the wetting or the drying path at the moment of sampling in the field. Since there can be a big difference between the two paths, it becomes necessary to distinguish their associated soil characteristics. The air entry value describes the minimum suction value that prevents air to enter the system and is inversely proportional to the maximum pore size of that soil. There are different air entry values for the same soil sample depending on whether it is on the wetting or drying path. Consequently, a judgement about the process (wetting or drying) that is to be simulated in a numerical model is necessary in most geotechnical engineering problems. There are some elaborate soil models available, which are able to consider this particular hysteretic behaviour (e.g. Pham et al. 2003a, Pham et al. 2003b). Nevertheless, in some cases, it may be more practical and appropriate to use an average of the wetting and drying SWCC to model the unsaturated soil behaviour in geotechnical engineering practice (Fredlund et al. 2012).

The water retention hysteresis of soils has been investigated by several researchers (e.g. Mualem 1984), who attributed their observations to several microscopic (particle size) properties and relative macroscopic scales. One explanation for this special hysteretic behaviour is commonly known as the “ink-bottle” effect (Childs 1969), which describes that the hysteretic behaviour is based on the non-uniform distribution of interconnected pores’ size and shape in the structure of the soil. This hypothesis can be schematically illustrated using

the analogy of a non-uniform capillary tube. The capillary rise during upwards flow (or wetting) is controlled by the larger radius of the tube, while the capillary height upon downward flow (drying) is governed by the smaller pore radius (Fig. 15).

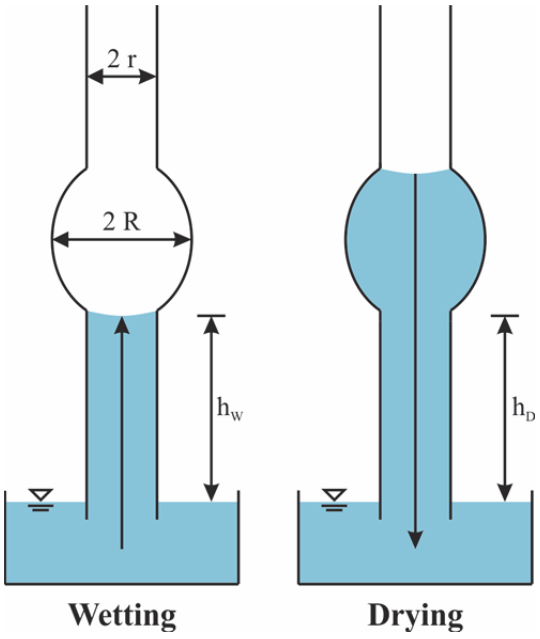

Fig. 15: The "ink-bottle" effect illustrated by a non-uniform capillary tube after (Childs 1969)

Hillel (1998) suggested another mechanism in order to explain the hysteretic behaviour in soil water retention. This mechanism is generally known as the contact angle or "raindrop" effect and is described as the difference in the liquid-solid contact angles for advancing and receding water menisci (Fig. 16).

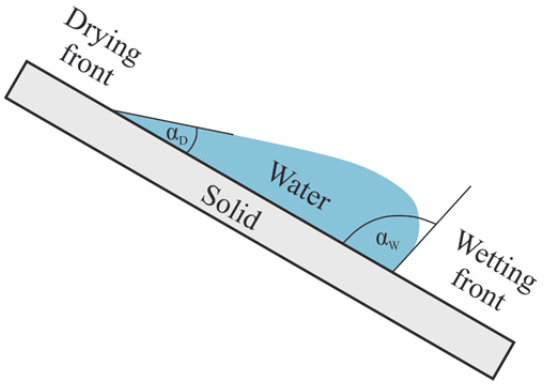

Fig. 16: "Raindrop" effect with differing soil-water contact angle during flow (after Hillel 1998)

3.4.3 Van Genuchten equations

There are numerous models available to describe the SWCC mathematically (see 3.4.1). In this thesis, solely the commonly used and widely accepted van Genuchten model (van Genuchten 1980) was used in the following numerical analyses. The van Genuchten function (Equation 23) is a three-parameter equation which relates the saturation to the pressure head ϕ_p (defined in Equation 22).

$$\phi_p = \frac{p_w}{\rho_w \, g} \tag{22}$$

$$S\left(\phi_p\right) = S_{res} + (S_{sat} - S_{res}) \left[1 + \left(g_a \left|\phi_p\right|\right)^{g_n}\right]^{g_c} \tag{23}$$

The shape of this function is dependent on the grain- and pore-size distribution and the mineralogy of the material. S_{res} is defined as residual saturation, which remains even at high suction levels, whereas S_{sat} is the degree of saturation under saturated conditions. As already described in previous chapters, there could be some air-bubbles in the water even at saturated conditions which causes S_{sat} generally to be less than one. There are three measurable curve fitting parameters in Equation 23: g_a is related to the air entry value of the soil, g_n is a function of the water extraction rate of the soil once the air entry value has been exceeded and g_c is a function of the residual water content, and therefore related to the shape of the curve in high suction ranges.

A more detailed explanation of each fitting parameter and their effects on the shape of the SWCC is given in literature (e.g. van Genuchten 1980, Galavi 2010, Rahimi et al. 2010) and exemplarily illustrated based on selected curves in the following chapter 3.4.5). In order to calculate the relative permeability $k_{rel}\,(S)$ of a soil (Equation 25) in relation to Mualem (1976) and van Genuchten (1980), first the effective degree of saturation S_e is obtained as follows:

$$S_e = \frac{S - S_{res}}{S_{sat} - S_{res}} \tag{24}$$

$$k_{rel}(S) = (S_e)^{gl} \left[1 - \left(1 - S_e^{\frac{g_n}{g_n - 1}}\right)^{\frac{g_n - 1}{g_n}}\right]^2 \tag{25}$$

where g_l is a material specific, empirical parameter.

The derivative of the degree of saturation with respect to the suction pore pressure can be written as:

$$\frac{\partial S(p_w)}{\partial p_w} = (S_{sat} - S_{res}) \left[\frac{1 - g_n}{g_n}\right] \left[g_n \left(\frac{g_a}{\gamma_w}\right)^{g_n} {p_w}^{(g_n - 1)}\right] \left[1 + \left(g_a \frac{p_w}{\gamma_w}\right)^{g_n}\right]^{\frac{1-2g_n}{g_n}} \qquad (26)$$

It must be noted, however, that there are several alternative equations for the SWCC (see overview in Fredlund et al. 2012) which could be employed, but they are not used within the framework of this thesis.

3.4.4 Datasets for Soil Water Characteristic Curves

To ensure the use of representative SWCCs in any kind of unsaturated soils analyses, or within the framework of specific projects, the SWCC for each soil should ideally be determined by fitting laboratory (and/or field) measurement data to the curve. It must be noted, however, that these laboratory tests are often time-consuming and cost-intensive. Regardless, they should always be the first choice. Within the framework of this thesis, selected laboratory tests have been used in order to determine SWCCs for the numerical quantification of water flow through unsaturated soils. The methodology of the performed laboratory tests is described in section 3.5.

For preliminary studies, or if the determination of SWCCs in the laboratory is not possible, there are several different SWCC data sets available. These datasets distinguish between varieties of different soil types, and in order to correctly model the flow in unsaturated soils for each particular problem, the most appropriate soil type should be used. As the focus of this thesis lies more on the overall quantification of the influences of several hydraulic parameters and boundary conditions (e.g. on the difference in results by using different SWCCs), than on the determination of SWCCs itself, these time-consuming and cost-intensive laboratory tests have only been performed for the numerical study described in chapter 4.

In all other numerical analyses in this thesis, two different well-known and widely accepted datasets, which are also implemented in PLAXIS 2D, have been used.

The HYPRES (**HY**draulic **PR**operties of **E**uropean **S**oils) series is an international soil classification system developed by Wösten et al. (1999). The following Tab. 1 lists the van Genuchten parameters for the HYPRES series.

Tab. 1: Van Genuchten parameters for HYPRES ("subsoil") series

Soil	**k_{sat}**	**g_a**	**g_n**	**g_l**
	[m/s]	**[1/m]**	**[-]**	**[-]**
Coarse	6.9 e-06	4.3	1.52	1.25
Medium	1.4 e-06	2.49	1.17	-0.74
Medium fine	4.6 e-07	0.82	1.22	0.5
Fine	9.8 e-07	1.98	1.09	-3.71
Very fine	9.5 e-07	1.68	1.07	0.0001
Organic	9.3 e-07	1.3	1.20	0.4

The SWCCs, the corresponding relative permeability curves either related to suction or to saturation for the HYPRES series using van Genuchten parameters, are illustrated in the following diagrams (Fig. 17 to Fig. 19). Fig. 17 shows the decrease in saturation with the therefore accompanying sharp drop in (relative) permeability, starting even after slight increase of suction as indicated in Fig. 18.

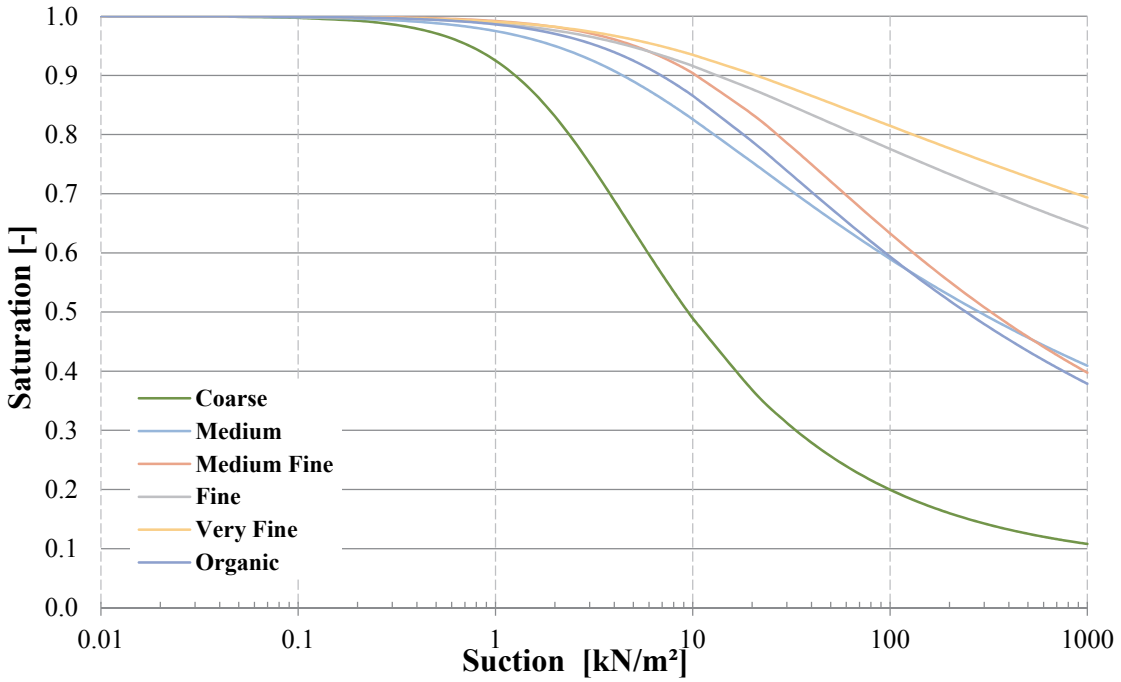

Fig. 17: SWCCs for the HYPRES series (mathematically described by the van Genuchten equation)

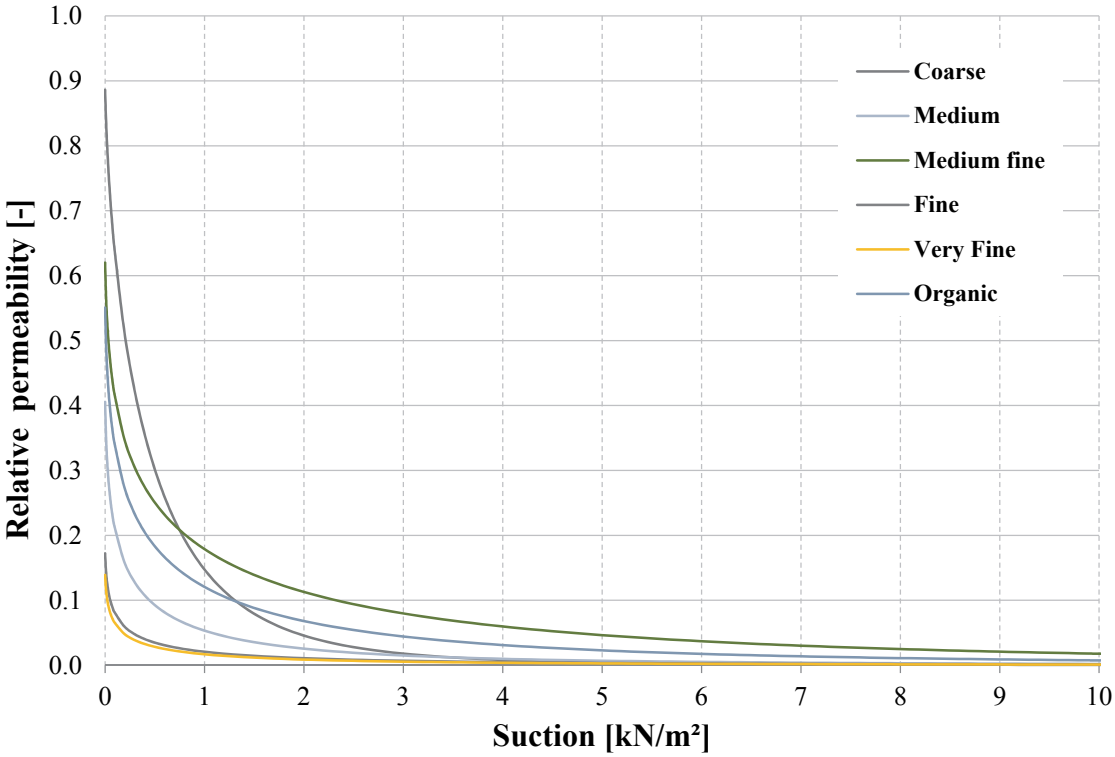

Fig. 18: Relationship between relative permeability and suction for HYPRES series (mathematically described by van Genuchten equations)

The relationship between relative permeability and saturation is given in Fig. 19. Even a small reduction in saturation causes a sharp decrease in relative permeability for all curves considered.

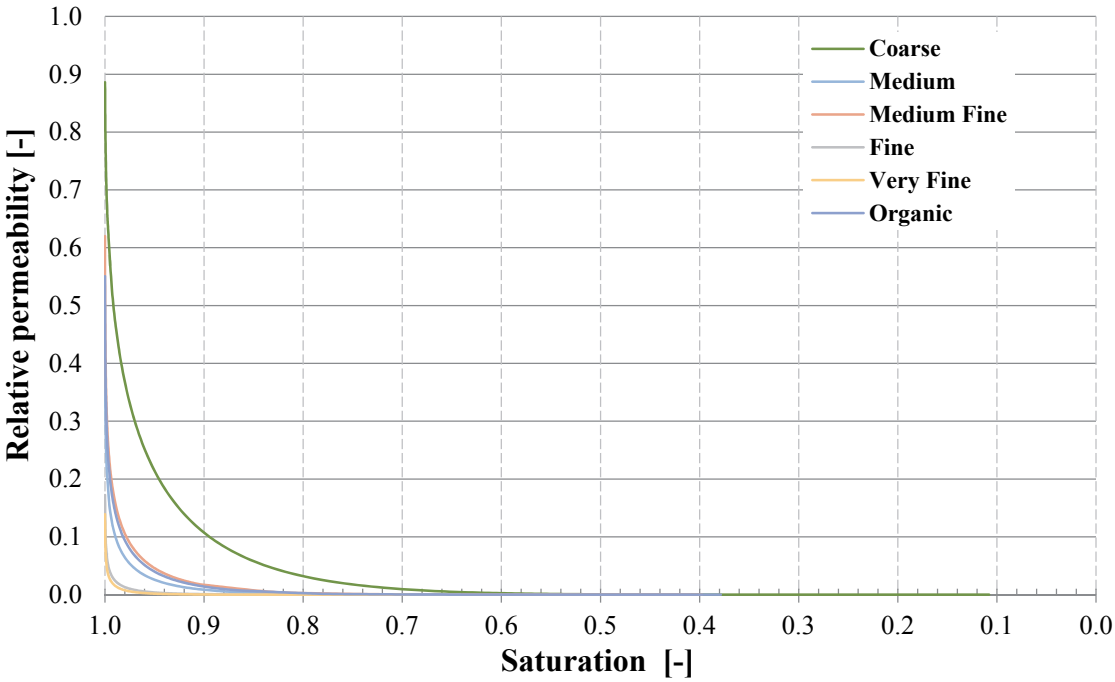

Fig. 19: Relationship between relative permeability and saturation for HYPRES series (mathematically described by van Genuchten equations)

The USDA (**U**nited **S**tates **D**epartment of **A**griculture) provides an alternative soil classification series, which was originally developed for agricultural purposes. The van Genuchten parameters for the USDA series are given in Tab. 2:

Tab. 2: Van Genuchten parameters for USDA series

Soil	k_{sat}	g_a	g_n	g_l
	[m/s]	**[1/m]**	**[-]**	**[-]**
Sand	8.3 e-05	14.50	2.68	0.50
Loamy Sand	4.1 e-05	12.40	2.28	0.50
Sandy Loam	1.2 e-05	7.50	1.89	0.50
Loam	2.9 e-06	3.60	1.56	0.50
Silt	6.9 e-06	1.60	1.37	0.50
Silty Loam	1.3 e-06	2.00	1.41	0.50
Sandy Clay Loam	3.6 e-06	5.90	1.48	0.50
Clayey Loam	7.2 e-06	1.90	1.31	0.50
Silty Clay Loam	1.9 e-06	1.00	1.23	0.50
Sandy Clay	3.3 e-06	2.70	1.23	0.50
Silty Clay	5.5 e-08	0.50	1.09	0.50
Clay	5.5 e-07	0.80	1.09	0.50

The SWCCs, the corresponding relative permeability curves either related to suction or to saturation for the HYPRES series using van Genuchten parameters, are illustrated in the following diagrams (Fig. 20 to Fig. 22).

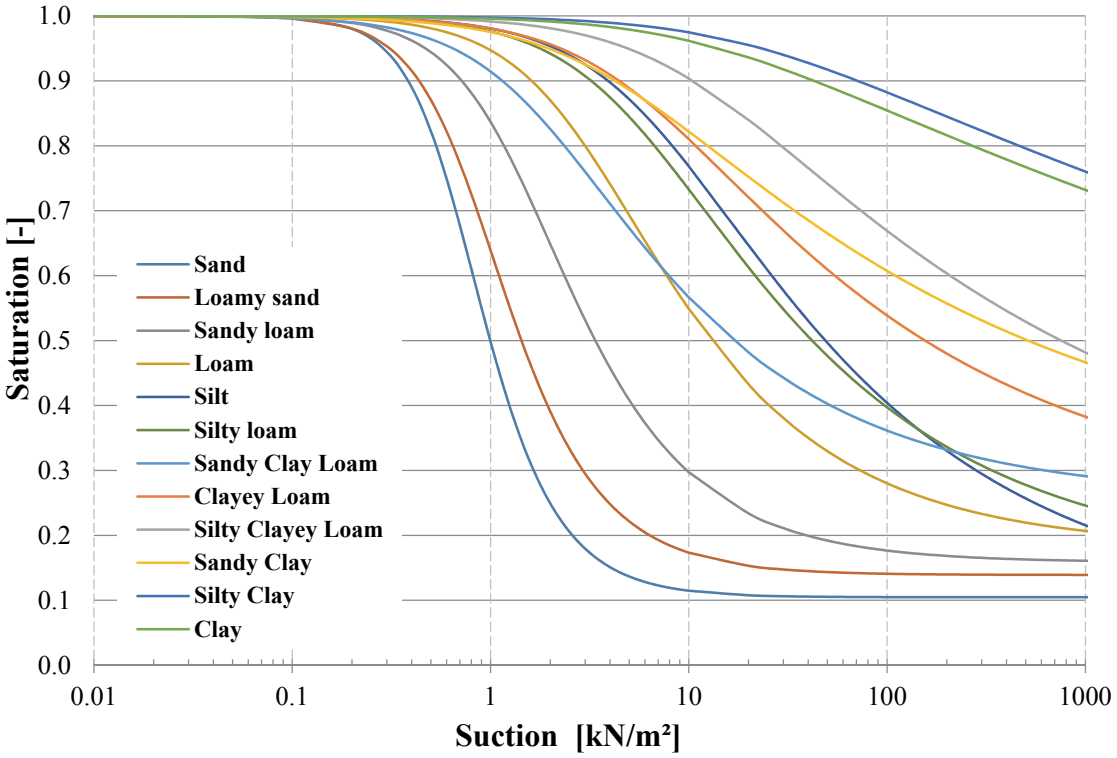

Fig. 20: SWCCs for the USDA series (mathematically described by van Genuchten equations)

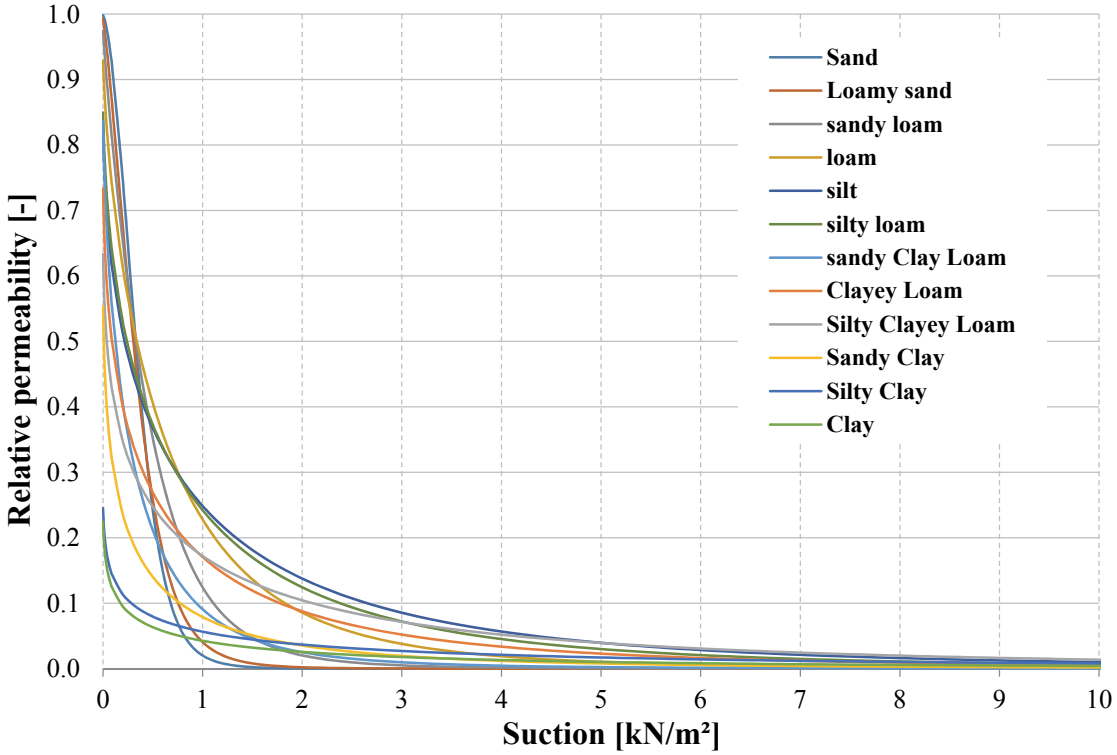

Fig. 21: Relationship between relative permeability and suction for USDA series (mathematically described by van Genuchten equations)

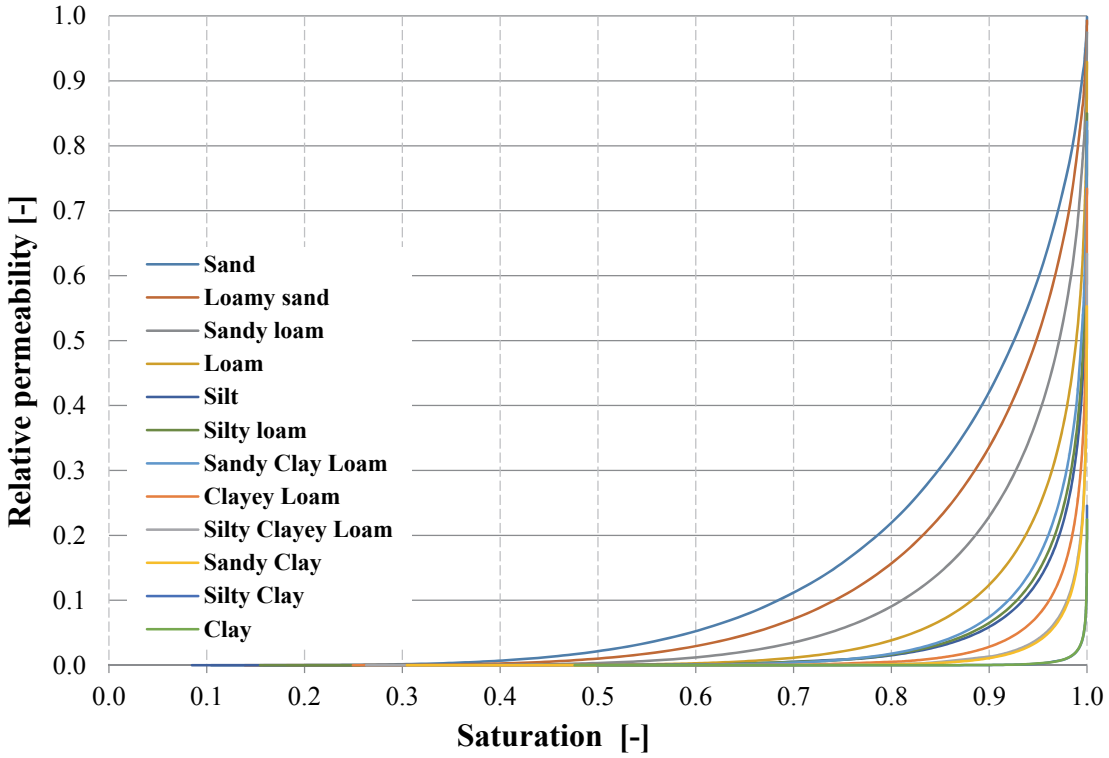

Fig. 22: Relationship between relative permeability and saturation for USDA series (mathematically described by van Genuchten equations)

3.4.5 Influence of the van Genuchten equation fitting parameters

This chapter illustrates exemplarily the influence of each van Genuchten fitting parameter on the shape of selected SWCCs out of the HYPRES and USDA databases, described in the previous chapter 3.4.4. In the following figures, the curve matching the originally used factor value (e.g. g_a = 0.82 for HYPRES' "Medium Fine" SWCC in Fig. 23) is always indicated with a thicker red line.

The influence of the g_a factor, which is related to the air entry value, on the shape of HYPRES' "MediumFine" SWCC is given in Fig. 23.

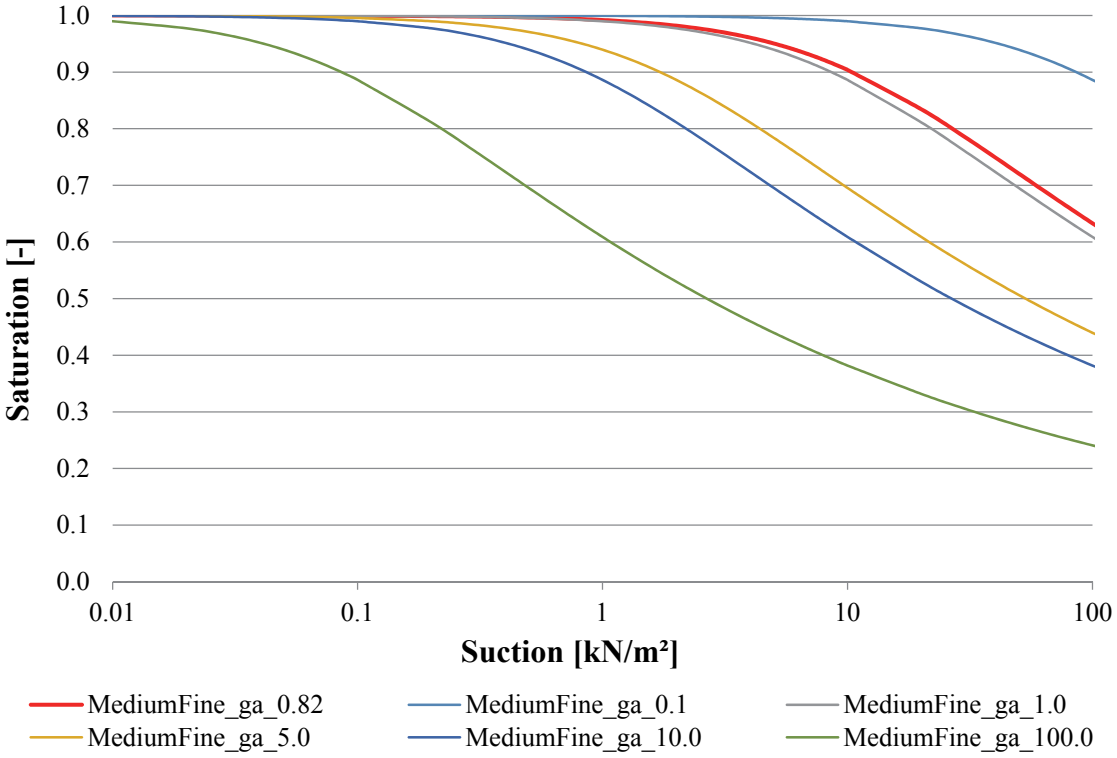

Fig. 23: Influence of g_a factor on the shape of HYPRES' "MediumFine" SWCC

Fig. 24 shows the influence of the g_n factor, which is generally related to the inclination of the curve after the air entry value is reached due to desaturation, on the shape of HYPRES' "MediumFine" SWCC.

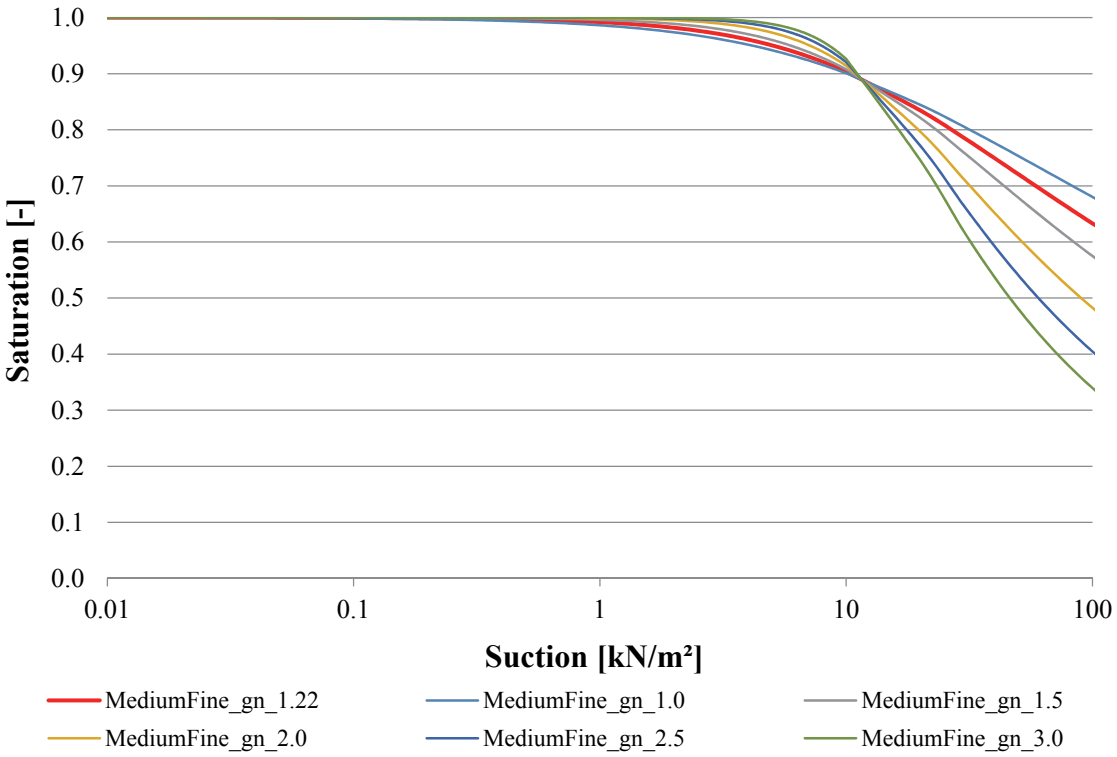

Fig. 24: Influence of g_n factor on the shape of HYPRES' "MediumFine" SWCC

Fig. 25 illustrates the influence of g_a factor on the shape of USDA's "Silt" SWCC. Again, the curve matching the originally used factor value, in the present case g_a = 1.6 for USDA's "Silt" SWCC, is indicated with a thicker red line.

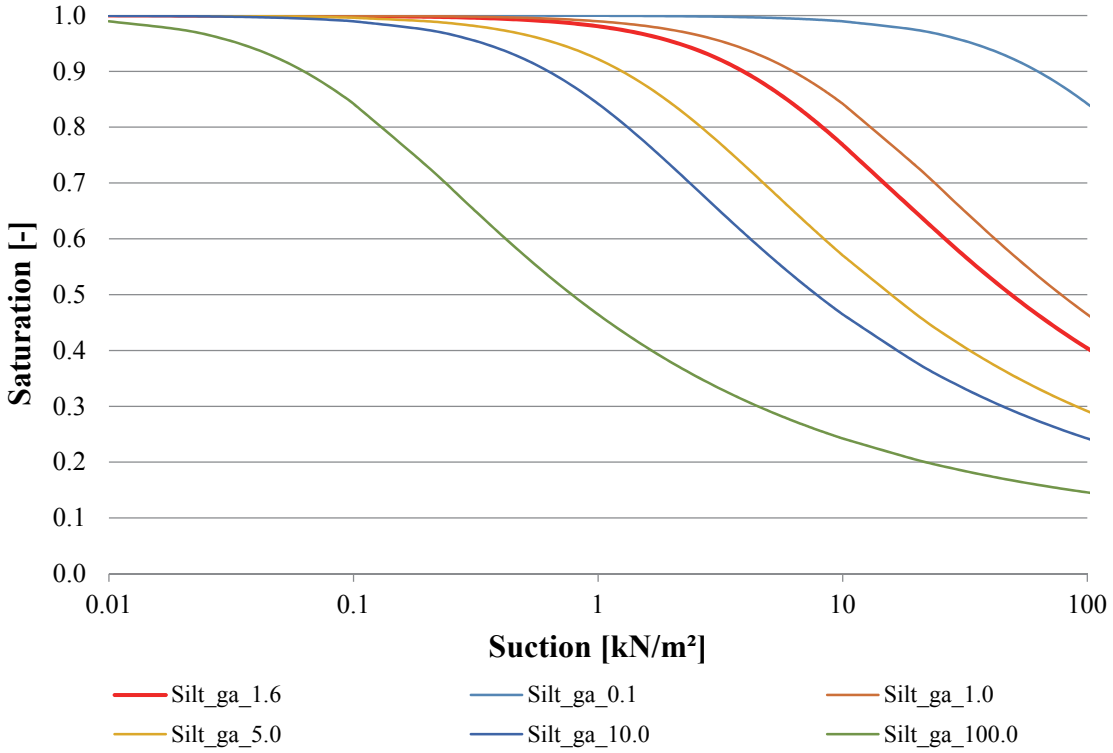

Fig. 25: Influence of g_a factor on the shape of USDA's "Silt" SWCC

Fig. 26 presents the influence of the g_n factor, on the shape of USDA's "Silt" SWCC.

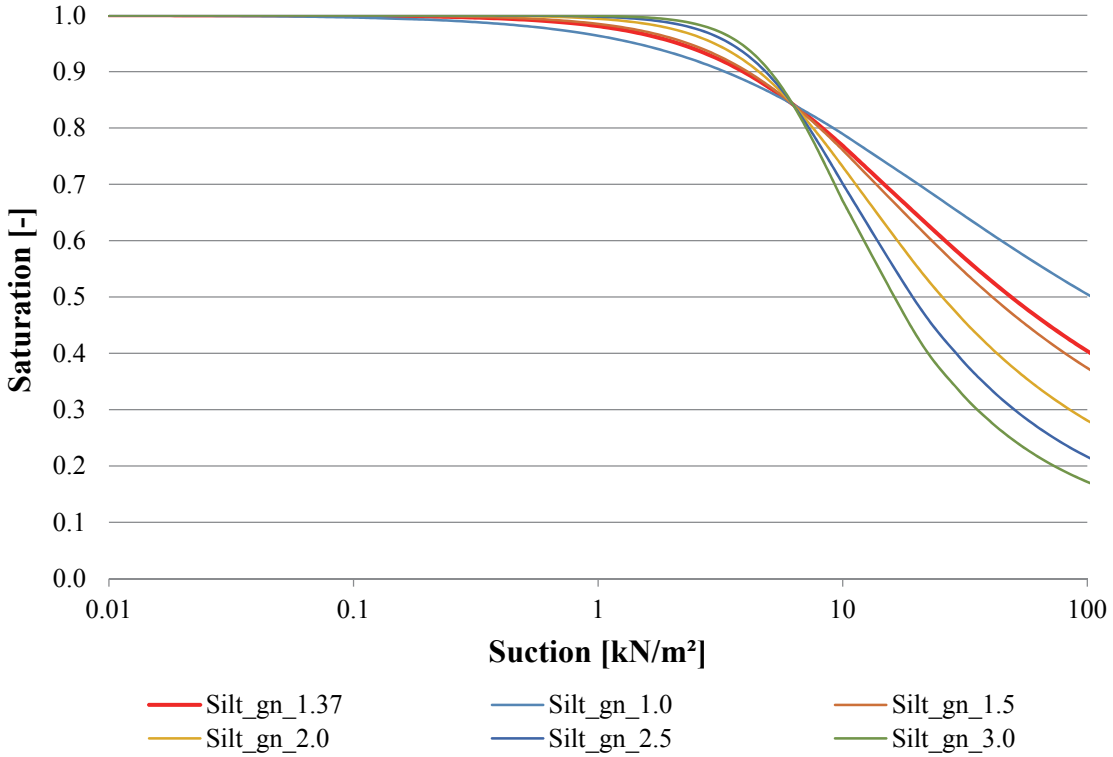

Fig. 26: Influence of g_n factor on the shape of USDA's "Silt" SWCC

The influence of the g_l parameter on the hydraulic permeability has been investigated by Mualem (1976) and van Genuchten (1980), both of whom suggested that $g_l = 0.5$ may be used with sufficient correctness. According to this recommendation, the USDA-series uses $g_l = 0.5$ for all available soil types, whereas in the HYPRES-series, the value is assumed to lie between -3.7124 and 2.5, depending on the material-type used (see Tab. 1 and Tab. 2).

Fig. 27 illustrates the impact of g_l on the shape of the unsaturated permeability curve when using HYPRES' "MediumFine" SWCC and various g_l-factor values.

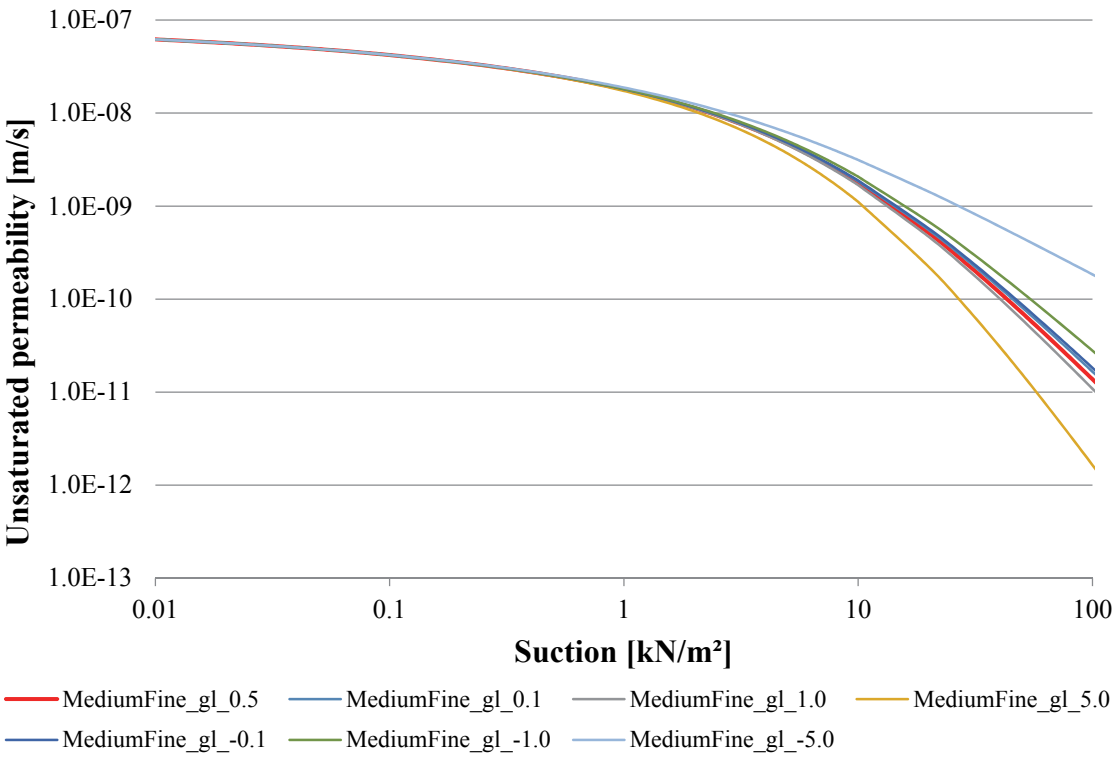

Fig. 27: Influence of g_l factor on unsaturated permeability using HYPRES' "MediumFine" SWCC

Fig. 28 illustrates the impact of g_l on the shape of the unsaturated permeability curve when using USDA's "silty clay" SWCC and various g_l-factor values.

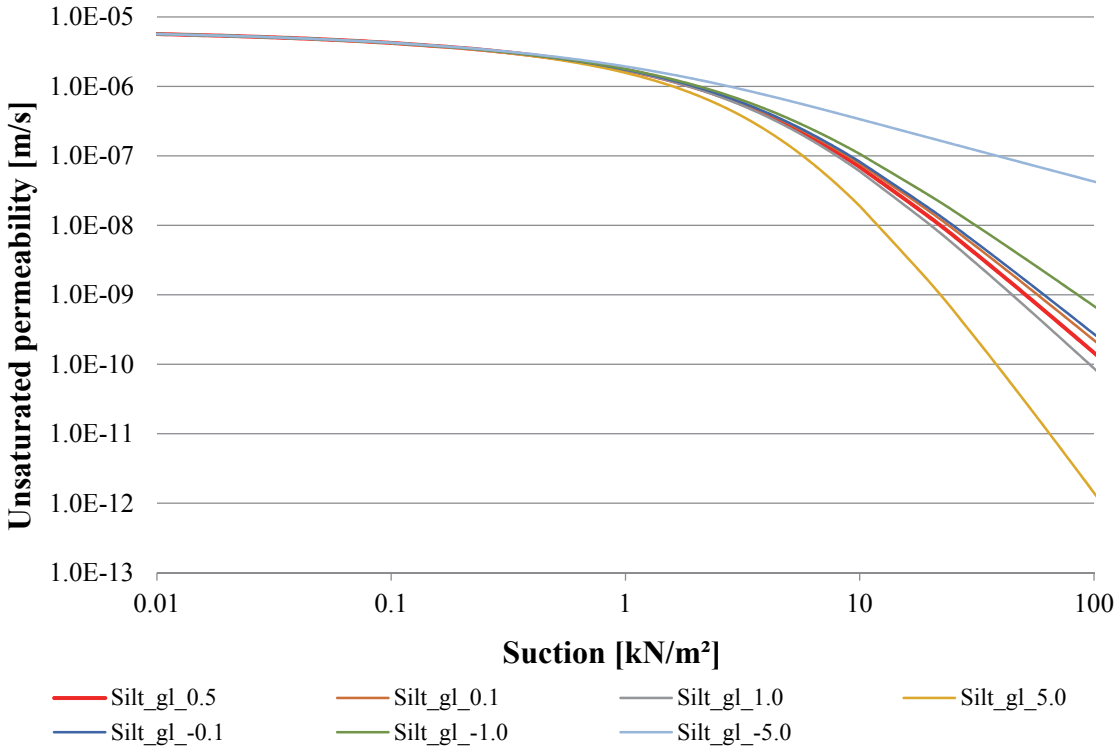

Fig. 28: Influence of g_l factor on unsaturated permeability using USDA's "Silt" SWCC

However, due to the inherent uncertainties in the determination of the saturated hydraulic permeability k_{sat}, the g_l parameter is generally negligible. Several researchers have worked on an improved prediction of the unsaturated hydraulic permeability with the Mualem – van Genuchten model (e.g. Schaap & Leij 2000).

It must be noted, however, that under certain circumstances, it only takes slight changes in the shape of the (relative) permeability curve to make the difference in whether a sensitive numerical calculation is feasible or not, especially if the saturated hydraulic permeability is very low.

3.5 Techniques for suction measurement

The techniques for measuring soil suction and determining corresponding SWCCs can be categorized as either laboratory or field methods and are distinguished by the type of suction (total or matric) that is measured. The currently available techniques generally differ by their complexity and suction measurement range.

For the execution of specific numerical analysis (see chapter 4) it was necessary to determine the SWCCs for specific soil samples in the laboratory. Within the framework of this thesis, only the techniques used to determine SWCCs are described in more detail. A more complete overview and comparison of various techniques with corresponding suction ranges is given in Lu & Likos (2004) and Fredlund et al. (2012).

3.5.1 Hanging water column

The well-known hanging water column technique is a simple and accurate method for applying (small) negative pore water pressure (suction) to the soil samples. A "hanging water column" is used to apply suction to initially fully saturated soil samples.

The "sandbox" (Eijkelkamp 2007), where sand is used to transfer the suction from the drainage system to the soil samples, can be used to apply a very limited range of pressures from zero (corresponding to full saturation) to -10 kPa. Fig. 29 shows an assembled sandbox with a PVC-pipe drainage system at the bottom of the box. A nylon filter cloth covers the fully saturated, fine, synthetic sand with which the experimental box is filled (Fig. 30). Before the experiment is started, the fully saturated soil samples in core rings are placed on top of the filter cloth in the box. In the next step, a specified suction pressure is determined and put in place by measuring the height difference between the adjustable "suction regulator" and the middle of the soil samples. Once the soil samples have reached water flow equilibrium at the set suction pressure, the samples are removed and weighed. To conclude the experiment, the water content of each sample is determined by drying it and then weighing it.

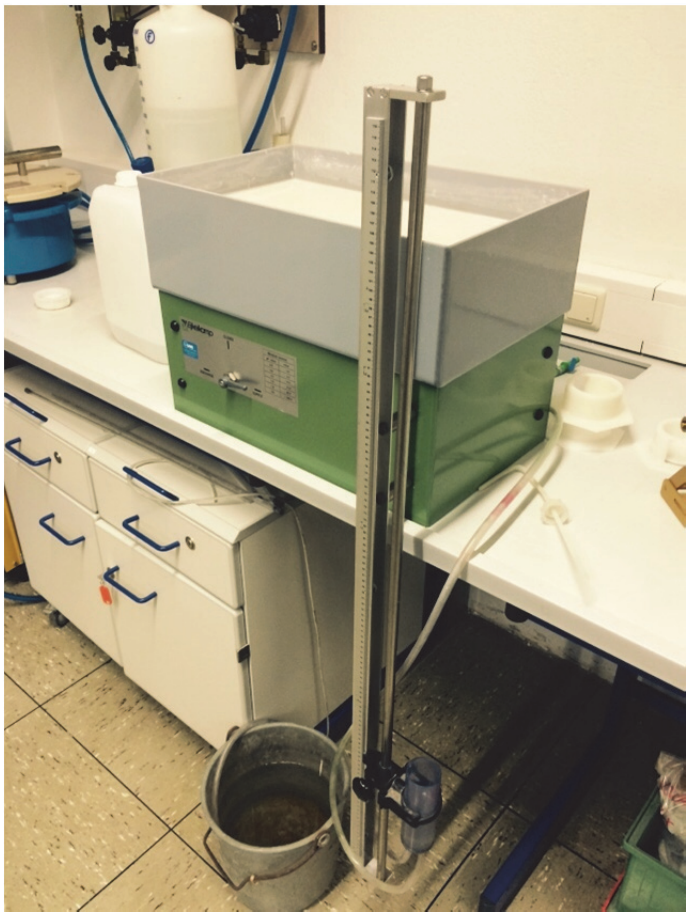

Fig. 29: Assembled sandbox system (Eijkelkamp 2007)

Fig. 30: Sandbox with soil samples (Eijkelkamp 2007)

3.5.2 Axis translation technique

In general, cavitation in free water under negative pressures of approx. 100 kPa leads to a discontinuous water phase in both soil and any measurement system trying to test suction, resulting in unreliable testing results. However, for many applications and soil types, control of the matric suction, as a variable, is required for a range much larger than 100 kPa (0 to -100 kPa). Therefore, alternatives to those testing methods are necessary if measurement and control of suction in a wider range are needed, and this is where the axis translation technique is used. The term "axis translation" refers to the practice of elevating pore air pressure u_a in a partially saturated soil, while retaining the pore water pressure u_w at a measurable reference value, typically atmospheric pressure (Lu & Likos 2004). The application of this technique allows control of the matric suction variable u_a-u_w over a range far greater than that dictated by the cavitation limit for water under negative pressure. The "axis" for matric suction is "translated" from the previously (non-testable) condition of negative water pressure and atmospheric air pressure to the condition of positive air pressure and atmospheric water pressure. In this way, the more easily controlled and measured positive air pressure enables matric suction to be accurately controlled in the testing setup. The axis translation is achieved by separating the water and air phases of the soil sample with the pores of a high-air entry (HAE) material such as a sintered ceramic plate. If the soil specimen is placed in good contact with the saturated HAE material, the system demonstrates good capability to maintain a water pressure of *(x)* kPa on one side and an air pressure of *(x+y)* kPa on the other side, without air passing through the HAE material. The *y* value is known as the "air entry value" or "air entry pressure" of the HAE material, which can be as high as 1,500 kPa for sintered ceramics or up to 10,000 kPa for extraordinary cellulose membranes. Fig. 31 illustrates the basic principle of the ceramic disc with soil particles in contact to the porous ceramic plate.

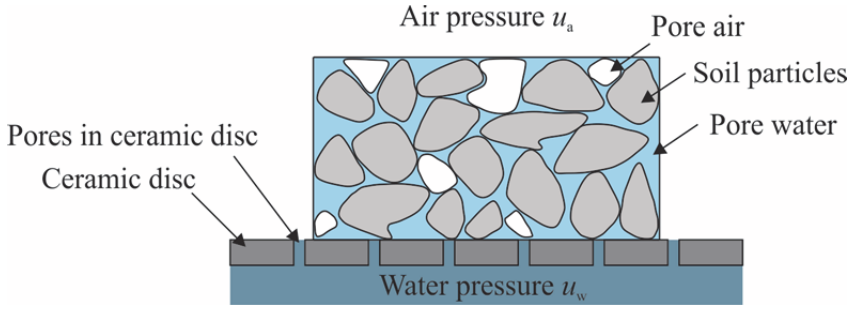

Fig. 31: Schematic cross section of the interface between the soil sample and the high-air entry disc (after Murray & Sivakumar 2010)

Pressure plate extractors can be viewed as a modification of the suction method presented by Richards (1941) and Gardner (1956), where liquid phase water is mobilized across the porous ceramic or membrane using positive pressures.

When equilibrium is reached, the moisture content is held by an equal, but negative force. A photographic picture of the (15 bar) pressure plate extractor (system Eijkelkamp 2009) is shown in Fig. 32.

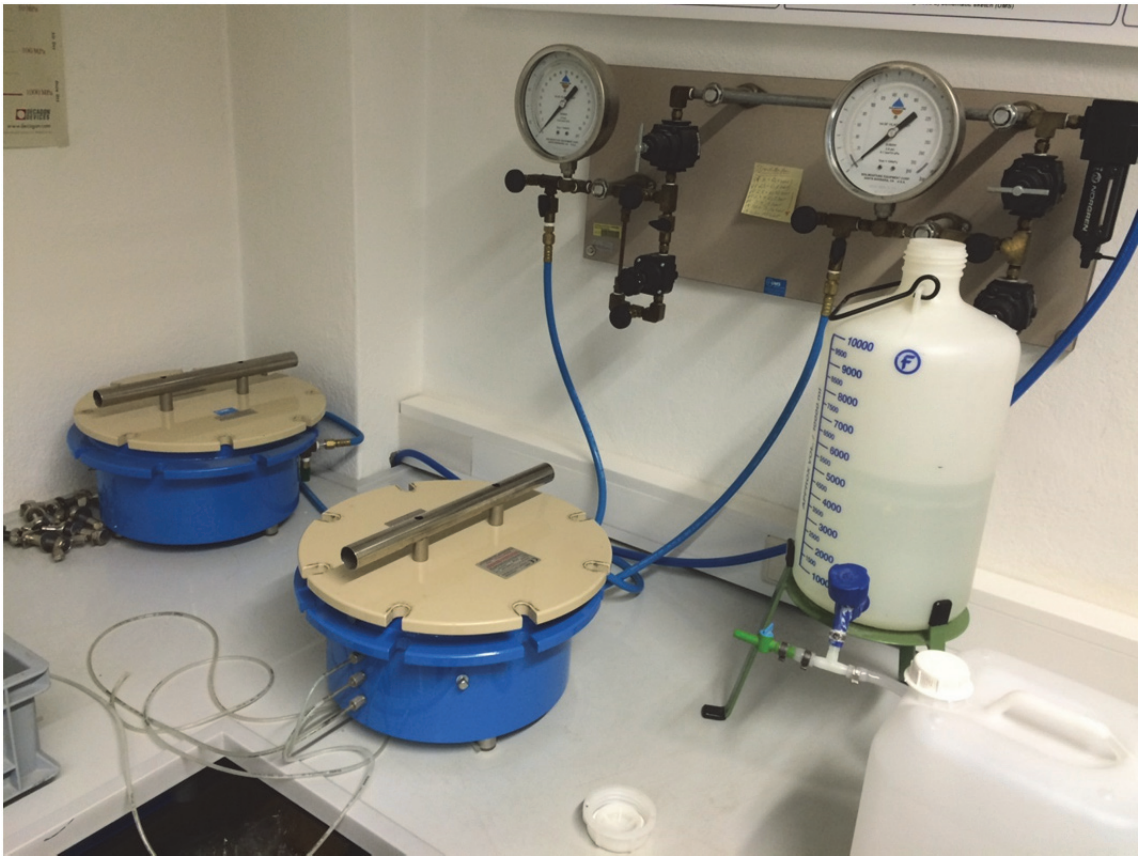

Fig. 32: Pressure plate extractor (Eijkelkamp 2009)

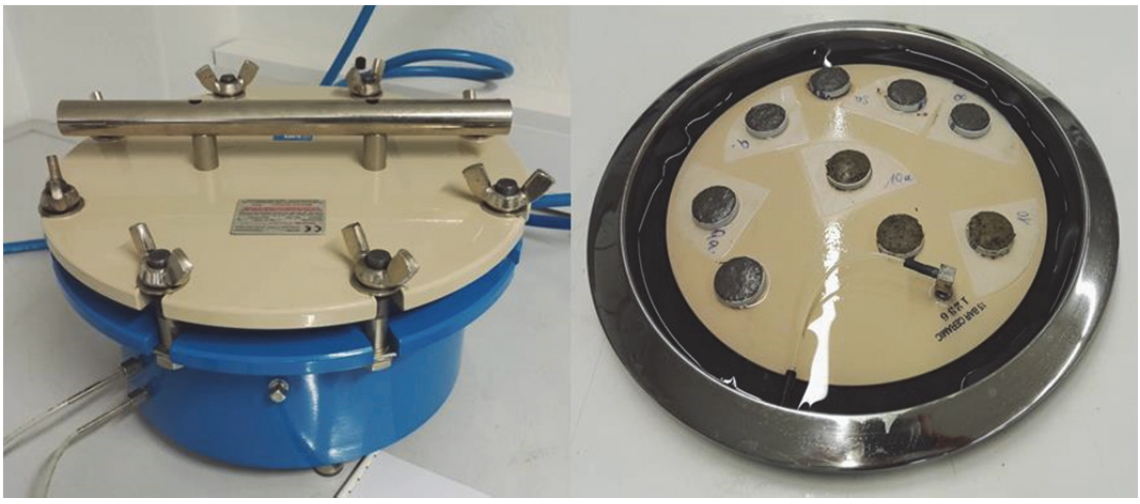

Fig. 33: Locked pressure plate extractor (left) and ceramic plate (right) (Eijkelkamp 2009)

In this modified system, the wetted porous ceramic plate is supported by a fine mesh screen and is additionally sealed by a rubber membrane backing. The saturation procedure of the soil samples, which are placed directly onto the ceramic plate, occurs on the plate itself. After locking the extractor lid to the extractor, the air pressure is increased to the required test value (0.1 to 1,500 kPa). Fig. 33 illustrates the "locked" system (left) and the 15 bar ceramic plate with numbered soil samples (right).

Once the air pressure inside the chamber exceeds the atmospheric pressure, the higher pressure inside the chamber forces excess water to flow through the plate's microscopic pores. As the pores are completely filled with water, they prevent the high pressure air from flowing out the chamber through the plate. Additionally, the surface tension at the air-water interface of each of the plate's pores supports the high pressure like a flexible rubber diaphragm. The increasing air pressure inside the extractor leads to decreasing radii of the air-water interfaces. Nonetheless, the water film will not break and consequently enable air to pass through the whole pressure range of the extractor.

At any specified air pressure inside the chamber, soil water flows from around each of the soil particles out through the ceramic plate until the effective curvature of the water films throughout the soil are equal to those at the pores in the ceramic plate. When this state of equilibrium is reached, the moisture flow stops. A new pressure increase in the extractor causes the soil moisture flow to restart until an equilibrium state is reached once again. When equilibrium is reached, there is an exact, but inverse relationship between the (positive) air pressure in the extractor and the (negative) soil suction. The volumetric (or gravimetric) water content for the sample which was in an equilibrium state can then be specified by weighing and drying in the oven.

A typical response of the air and water pressure in the pressure plate apparatus over time is illustrated in Fig. 34.

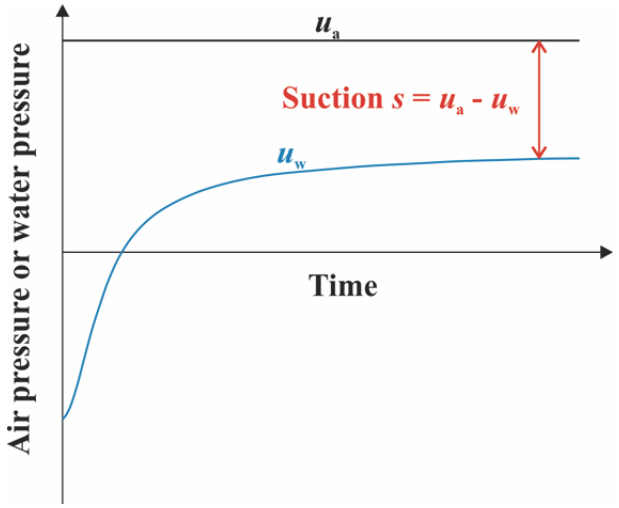

Fig. 34: Pressure-time response in pressure plate apparatus (after Murray & Sivakumar 2010)

Suction is the difference between the pore air pressure applied in the chamber and the pore water pressure in the drainage line (Murray & Sivakumar 2010).

3.5.3 Evaporation method

The evaporation method is a commonly used technique for the simultaneous measurement of the water retention curve and the hydraulic permeability of unsaturated soil samples (e.g. Wind 1966, Schindler et al. 2010). However, in general, all variants of the evaporation method suffer from the same limitation: the measurement ranges of tensiometers are typically 80 kPa on the dry end, which limits the determination of water retention curves to approximately 60 kPa.

As a development of the evaporation method, the commercial and fully automated measuring and evaluation system HYPROP© ("**HY**draulic **PROP**erty analyser") uses the air entry pressure of the tensiometer's ceramic cup as additionally defined tension value. This technique overcomes the usual restrictions in the tensiometer measurement range and consequently allows for the determination of the hydraulic functions (SWCC and hydraulic permeability) to a wider range, for example from zero to – 250 kPa, up to close to the wilting point of the soil sample. The general principle of this experimental setup is shown in Fig. 35.

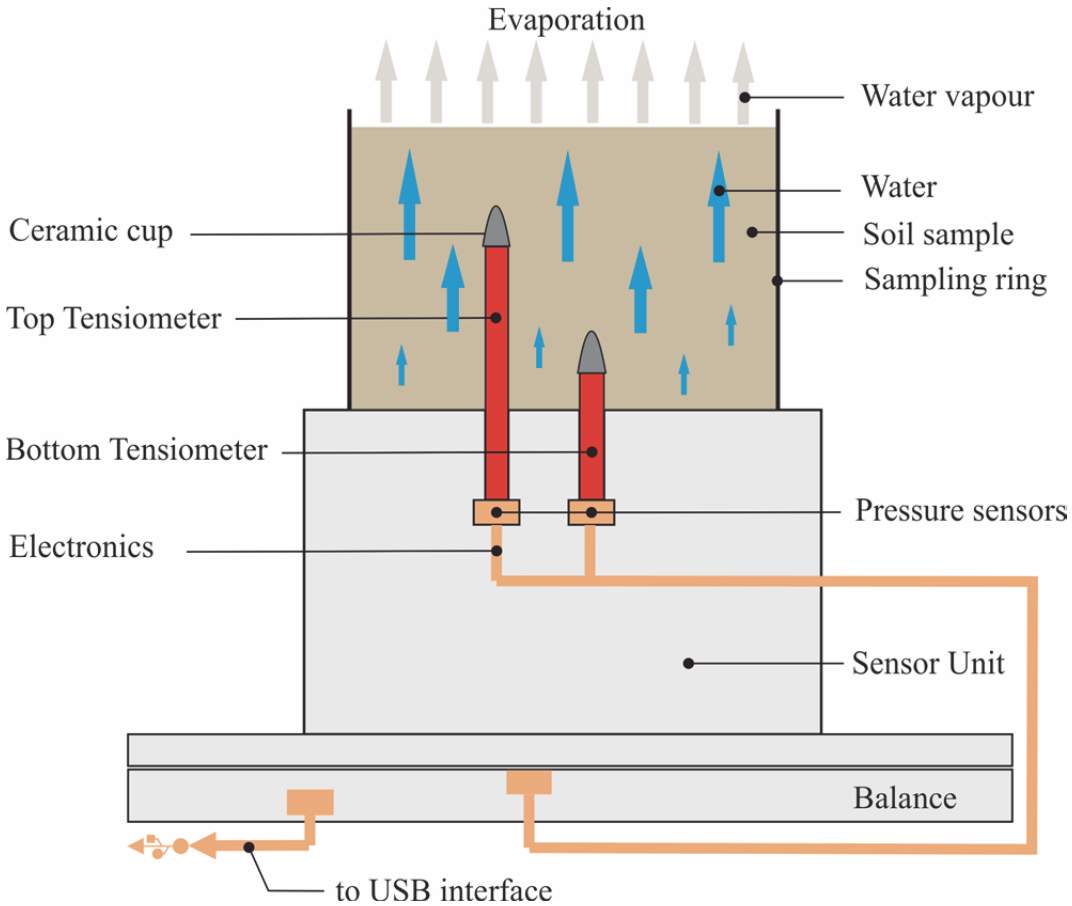

Fig. 35: Principle of the HYPROP© system (after UMS 2015)

The HYPROP© system is based on the method of Schindler (1980), which uses a simplified setup of WIND's test (Wind 1966), and records only the total soil samples masses m and tensions ψ (= absolute value of matric potential) at two height levels. This serves as the basis for quantifying the unsaturated permeability functions. The hydraulic gradient i_m is determined from the tension values and the distance between the tensiometers. From the soil water mass difference Δm per surface area A and time unit Δt, the flux density q is derived. The recording of water loss per volume of the core sample and mean tension in the sample at time t allows for the calculation of single stress points of the Soil Water Characteristic Curve. Consequently, the hydraulic conductivity K can be calculated as follows:

$$K(\overline{\psi}) = \frac{\Delta V}{2A\,\Delta t\,i_m} \tag{27}$$

where $\overline{\psi}$ is the mean tension, averaged over the upper and lower tensiometer and time interval, A represents the cross-sectional area of the soil sample, ΔV is the evaporated volume of the water, obtained by $\Delta V = \Delta m/\rho_w$ with loss of mass Δm per time interval Δt, ρ_w is the density of water, and i_m is the mean hydraulic gradient per interval, which is given by:

$$i_m = \frac{1}{2}\left(\frac{\psi_{t1,upper} - \psi_{t1,lower}}{\Delta z} + \frac{\psi_{t2,upper} - \psi_{t2,lower}}{\Delta z}\right) - 1 \tag{28}$$

with $\psi_{t,upper,lower}$ indicating upper and lower tensiometer values at times t_1 and t_2, and Δz as the vertical distance between the two tensiometer positions, respectively.

Equation 28 is valid when assuming that both flux and hydraulic gradient are approximately constant over time ("quasi-steady-state" conditions) and that there is a linear water content distribution across the entire sample height during the measuring time interval. Consequently, the flow through the measuring plane (located precisely at the mid height of the soil sample, between the positions of the two tensiometers), is determined to be half of the total evaporative water flow from the soil and derived from the mass loss of the sample. According to Schindler (1980) and Schindler & Müller (2006) this assumption is valid for sand, silt, loam, and peaty soils.

At the end of the experiment, the residual water content of the sample is derived by weighing the sample after it has been dried in the oven set to 105°C. Using the total water loss (residual plus evaporation) and the core sample volume, the initial water content is determined.

3.6 Shear strength in unsaturated soils

Similar to the principles of saturated soil mechanics (Terzaghi 1936) the mechanical behaviour of unsaturated soils is a function of changes in effective stresses (physically the stresses acting between the solid particles of a soil element). In saturated soil mechanics, the effective stresses are expressed as follows:

$$\sigma' = \sigma - u_w \tag{29}$$

where σ' is the effective stress, σ the total stress and u_w the pore water pressure.

However, the formulation of effective stresses under unsaturated conditions is much more complicated compared to the saturated condition. Due to the existence of (at least) three phases in unsaturated soils, there has not been found any single stress variable which allows for a description of all the aspects of mechanical behaviour of a given soil under partially saturated conditions (Jommi 2000).

Burland (1964) and others suggested that the mechanical response of unsaturated soils should be determined by considering matric suction and net stress. Bishop & Blight (1963) observed different mechanical reactions from an unsaturated soil element when they changed only net stress or only suction while keeping the other one constant. Alonso et al. (1990) used effective stress measurements to model the stress-strain-strength behaviour of unsaturated soils. Fredlund & Morgenstern (1977) recommended that any pair of the stress states σ-u_a, u_a-u_w, or σ-u_w can be used as a suitable framework for the constitutive modelling of partially saturated soils.

One of the most commonly used equations for effective stresses in unsaturated soils is proposed by Bishop (1959) and can be written as:

$$\sigma' = (\sigma - u_a) + \chi(u_a - u_w) \tag{30}$$

with σ as total stress, u_a as the pore air pressure, χ as effective stress parameter, which is generally linked to the degree of saturation S and u_w as the pore water pressure. The combined term σ-u_a is named as net normal stress, the term u_a-u_w as matric suction. The coefficient χ varies between 0 and 1 and reaches the value of 1 under fully saturated conditions, which leads Bishop's effective stress equation to reduce to Terzaghi's (saturated) effective stress formulation.

In order to evaluate effective stresses in unsaturated soils, the determination of χ and its dependency on the amount of water in the soil system is essential. The empirical link between χ and S is based on laboratory results from numerous researchers and plotted in Fig. 36 (Lu & Likos 2004).

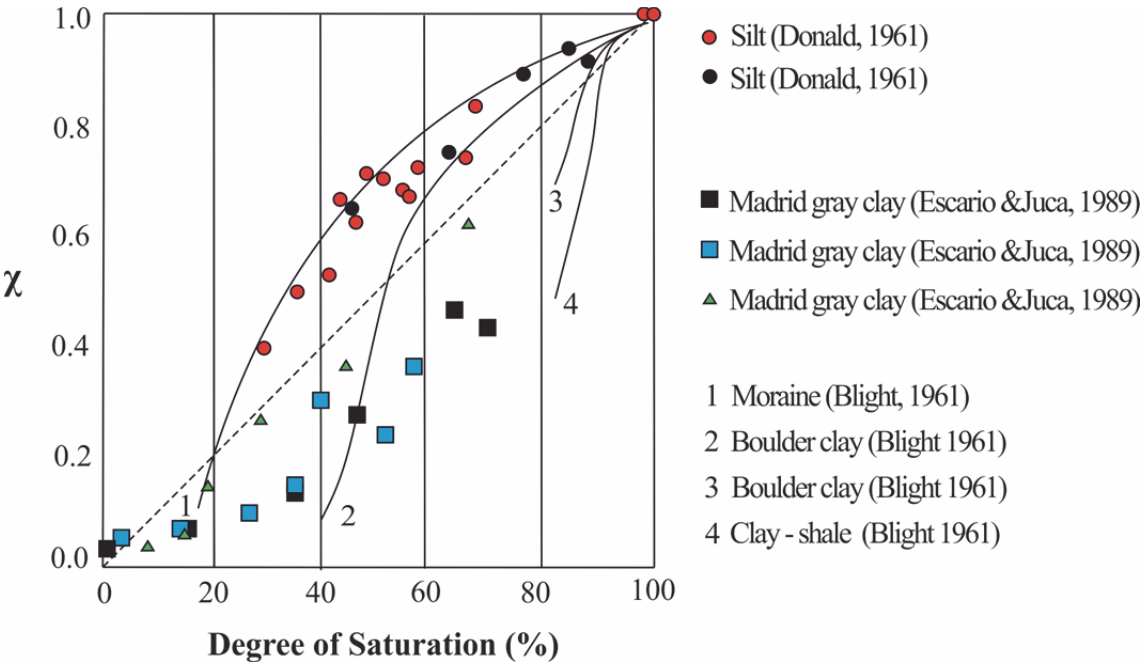

Fig. 36: Experimental data relationship between Bishop's effective stress parameter χ and degree of saturation (after Lu & Likos 2004)

In a direct shear test where the net total stress σ-u_a is known, the net effective stress can be determined from the shear stress in the state of failure. Hence, an indirect measurement of χ under controlled suction conditions is possible (at least in high suction ranges). Bishop (1959) followed this overall strategy and proposed a nonlinear form of χ, based on direct shear tests taken to failure state and thus developed his prevalently used effective stress equation (Equation 30).

In a typical triaxial test, the value of matric suction at failure could be used to indirectly specify the degree of saturation S by ways of the known soil water characteristic curve. Using this method, a one-to-one relationship between χ and S can be established (Lu & Likos 2004). However, especially in the low saturation range, the determination of the stress parameter- degree of saturation function is experimentally challenging.

Vanapalli & Fredlund (2000) examined the validity of numerous forms of χ as a function of S by using results of a series of direct shear tests of statically compacted mixtures of sand, silt and clay from Escario et al. (1989). For a matric suction range of 0 to 1500 kPa, they found that the following two equations showed a good fit to the experimental results:

$$\chi = S^{\kappa} = \left(\frac{\theta}{\theta_s}\right)^{\kappa} \tag{31}$$

$$\chi = \frac{S - S_{res}}{1 - S_{res}} = \frac{\theta - \theta_{res}}{\theta_{sat} - \theta_{res}} \tag{32}$$

where S is the degree of saturation, S_{res} the residual degree of saturation, θ the volumetric water content, θ_{sat} the volumetric water content at full saturation, θ_{res} the residual volumetric water content and κ a fitting parameter.

The nature of these different equations for χ in relation to several values of saturation S and to several values of the fitting parameter κ used in Vanapalli & Fredlund (2000) is depicted in Fig. 37.

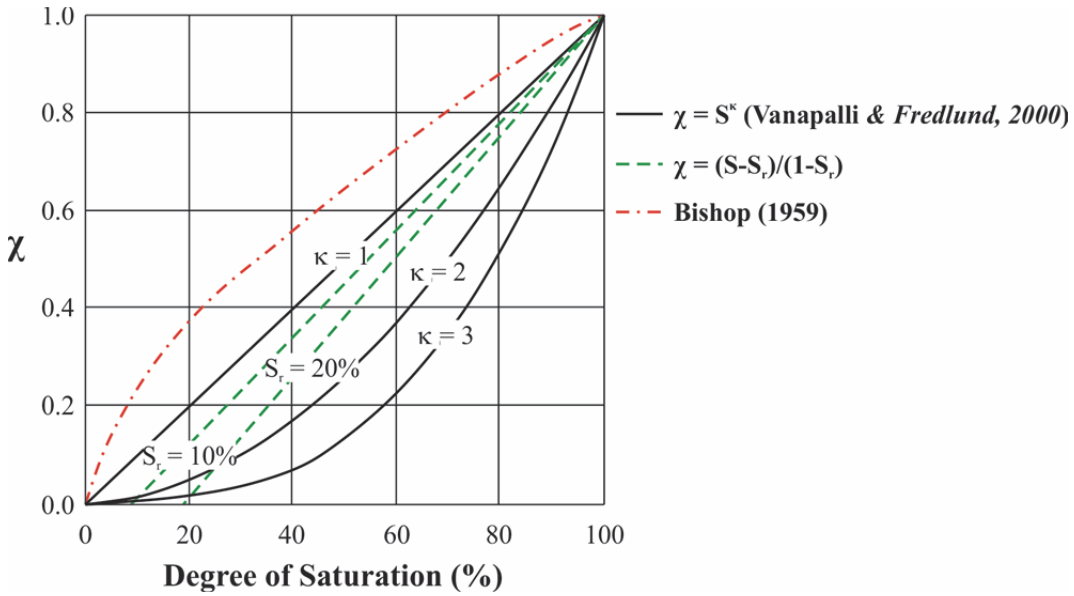

Fig. 37: Various forms for the effective stress parameter χ as a function of saturation (after Lu & Likos 2004)

The particular characteristics of χ, as well as its evaluation by experimental techniques are important and are still ongoing topics of research in unsaturated soil mechanics (e.g. Öberg & Sällfors 1997, Khalili & Khabbaz 1998, Jommi 2000, Nuth & Laloui 2008, Casini 2012).

3.7 Matric suction profiles

Several factors control the matric suction profile in unsaturated soils. The location of the groundwater level, the drainage conditions, the saturated hydraulic permeability of the soil, the SWCC used for the soil and environmental conditions such as precipitation and evaporation all affect the shape of the matric suction profile.

If the water that flows in and out of the soil body reaches equilibrium, then steady state conditions are reached. Equal values of unsaturated hydraulic conductivity and water infiltration lead to constant pore water pressures within the soil.

Fig. 38 shows two possible scenarios for matric suction development under different rainfall intensities. An infiltration intensity q which is smaller than the saturated hydraulic permeability k_{sat} of the unsaturated soil leads to decreasing, but still existing matric suction values (Fig. 38 left). In order to reduce the matric suction to zero, infiltration intensities equal or higher than the hydraulic permeability are necessary (Fig. 38 right).

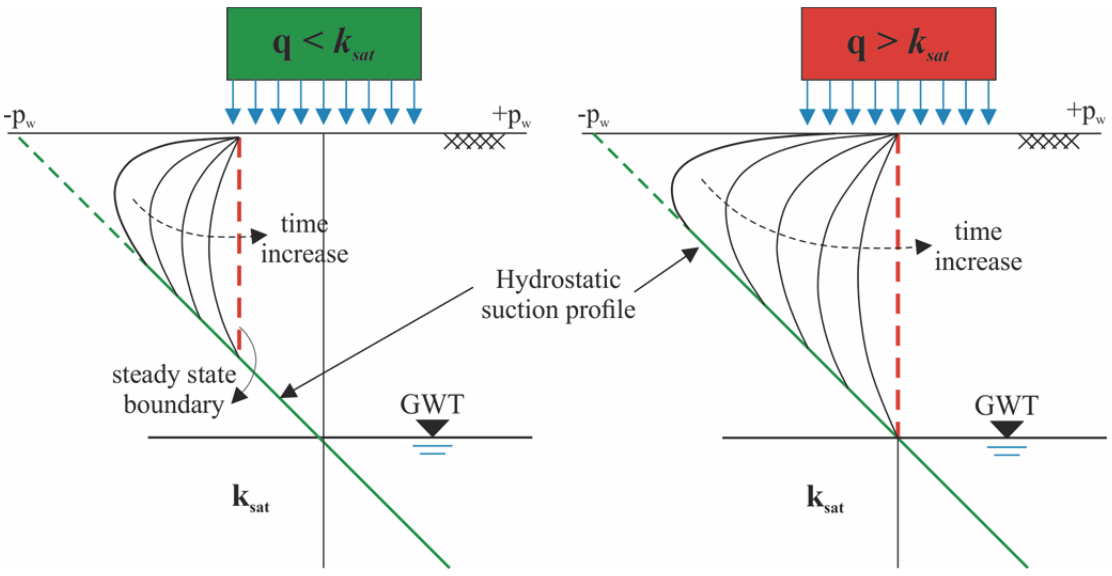

Fig. 38: Matric suction profiles during rainfall in dependence of infiltration intensity

Fig. 39 presents a conceptual illustration of saturated and unsaturated moisture and stress profiles (Lu & Likos 2004). In (*a top)*, it illustrates the example of a homogeneous sandy soil layer that is initially fully saturated from the top down to the interface between this soil and the bedrock layer. Then in (*a bottom)*, the example continues with a lower water level at the boundary to the bedrock layer. This change in water level would lead to a changing water content profile (*b*). Also, as the self-weight of the soil decreases due to the dewatering process, and considering an appropriate parameter χ, both the vertical total *(c)* and effective *(d)* stress profiles change from their initial linear distributions. Comparing the effective stress profiles under saturated or unsaturated conditions, as illustrated in this conceptual example, clearly shows the considerable increase of effective stress of the soil upon desaturation of the whole soil layer.

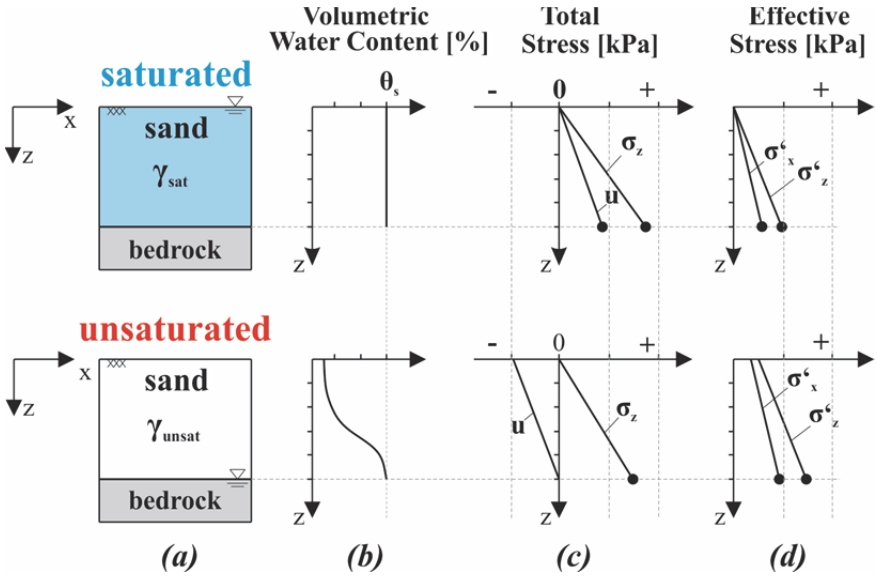

Fig. 39: Profiles of volumetric water content, total and effective stress in a sandy soil layer under saturated (top) and unsaturated (bottom) conditions (after Lu & Likos 2004)

3.7.1 Limit equilibrium method

The factor of safety of a slope can (among some other methods not considered within the framework of this thesis) either be evaluated by means of numerical methods like the finite element method or by means of traditional slip surface analysis (method of slices) according to the concept of limit equilibrium.

Due to their simplicity, limit equilibrium methods have been widely adopted and are still commonly used approaches in slope stability analysis. In contrast to finite element deformation analysis, these procedures give a global factor of safety for a particular slip surface, but assume no deformation prior to failure and cannot take the history of the slope into account (Cho & Lee 2001).

These methods are convincing by their simplicity and ability to evaluate the sensitivity of various input parameters on slope stability and the extensive experience that geotechnical engineers have acquired over the past decades in calculating safety factors with them.

In limit equilibrium methods, failure generally occurs through the sliding of a mass along a slip surface. The failing soil mass is divided into slices, where depending on the method or assumption used, different forces are acting between them. It should be noted that all the different limit equilibrium methods use the same definition of factor of safety, which is defined as the ratio of the shear strength of the soil to the shear stress required for equilibrium (Equation 33):

$$FoS = \frac{Shear\ strength\ of\ soil}{Shear\ stress\ required\ for\ equilibrium} \tag{33}$$

It is well accepted that rainfall infiltration can affect the safety factor of soil slopes. Limit equilibrium methods can be applied when the process of rainfall infiltration should be considered in slope stability analysis. In this case, predicted pore water pressures serve as input ground water conditions for the following safety analysis utilizing the limit equilibrium method (e.g. Ng & Shi 1998). It has to be mentioned, that the limit equilibrium is not capable to consider the transient infiltration process due to rainfall automatically. Therefore, this method only allows calculating the FoS for a certain point in time with pore water pressures as a consequence of infiltration processes which have been predicted from analytical equations, transient seepage analysis or numerical models.

3.7.2 Finite element method

Griffiths & Lane (1999) showed that the finite element method represents an accurate, adaptable and powerful alternative method for slope stability analysis, as it requires less a priori assumptions, especially concerning possible failure mechanisms. In the finite element method, the development of the failure mechanism takes place "naturally" as an outcome of the analysis.

The well-established phi-c-reduction technique can be applied in the finite element method. This approach commonly assumes a Mohr-Coloumb failure criterion and obtains the factor of safety by successively reducing the shear strength parameters $tan\varphi'$ and c' as well as the tensile strength of the soil until no equilibrium can be found in the calculations and failure of the soil structure occurs (Equation 34).

$$FoS = \frac{tan\varphi'_{input}}{tan\varphi'_{reduced}} = \frac{c'_{input}}{c'_{reduced}} \tag{34}$$

The angle of dilatancy ψ is generally not affected by the phi-c-reduction procedure. However, when the friction angle has reduced so much that it becomes equal to the defined dilatancy angle, any further reduction of the friction angle will lead to the same reduction of the dilatancy angle (Brinkgreve et al. 2017). In the finite element method, simple self-weight calculations, and the influence on the factor of safety of single construction stages of more complex slopes, or of the installation of particular support measures can be quantified at any step of the calculation. There is no need to make assumptions about the shape or location of the failure surface when performing safety calculations using the finite element method. Failure is found automatically as slope failure occurs naturally through the zones due to insufficient shear strength to resist shear stresses, not where it is assumed, which can be considered a big advantage when compared to limit equilibrium methods.

The general procedure to determine the FoS at a predefined point in time of the finite element analysis is then to execute a numerical phi-c-reduction after the corresponding phase of interest. In the present thesis, the (pore water pressure) condition at the after a rainfall event is determined by means of a numerical fully coupled flow-deformation analysis (then followed by a phi-c-reduction phase). As suction is an indissoluble part of the coupling between deformations, pore pressures and groundwater flow, a fully coupled flow-deformation analysis will always take suction into account. It must be noted, that the finite element code PLAXIS 2D (Brinkgreve et al. 2017) allows the user to take into account suction in either all or only selected calculation phases (more information is given in chapter 7.3.).

4 Practical example of water flow through unsaturated soils

4.1 Introduction

There are several types of flow-related engineering scenarios involving predominantly unsaturated soils (Lu & Likos 2004):

- Water balance at the soil-atmosphere interface
- Net recharge rates into aquifers (saturated zone)
- Steady and transient seepage in partially saturated embankment dams
- Design of final covers for containment and waste storage

It is obvious, that these engineering scenarios are also strongly related to numerous stress- and deformation related problems.

Particular types of unsaturated soils can be used as cover-layers for underground waste storage and containment and must meet regulatory requirements. Within this thesis, a practice-related numerical analysis of water flow through an unsaturated soil, which has been planned to be used as cover-layer for underground waste storage, was executed. The sketch in Fig. 40 represents the problem description by means of a cross-section. A (dense) covering layer (indicated in green) should be used to protect the material below (indicated in red) from water infiltration as a consequence of climatic conditions.

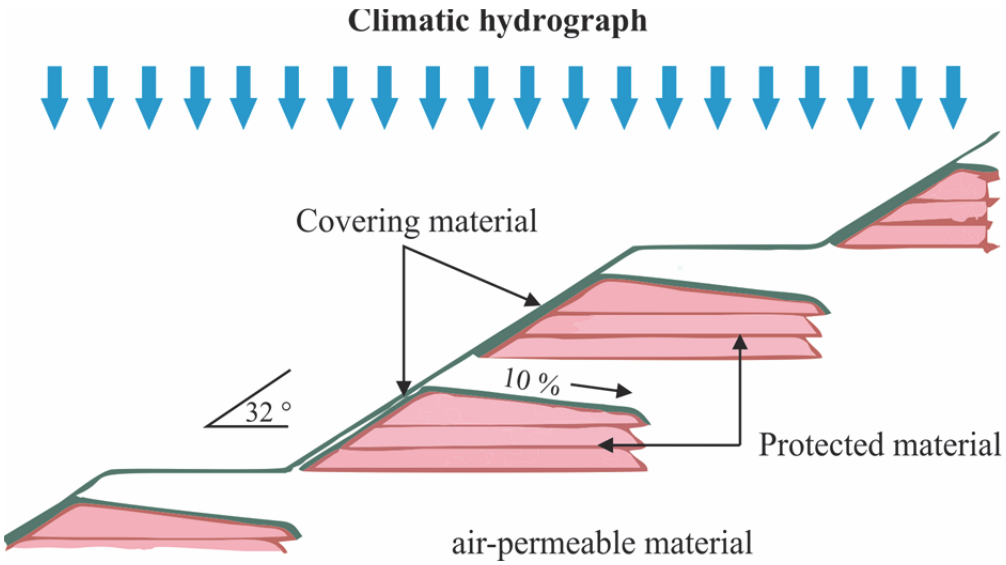

Fig. 40: Schematic illustration of the practical cover-layer example

In order to quantify the water reaching the protected layer below the covering layer, a numerical 1D-column test has been performed and is described in more detail in the following chapter 4.2.

4.2 Quantification of water flow through unsaturated soil layers

The numerical procedure presented here can be used in order to prove that the very strict requirement of allowed maximum quantities of water reaching the protected layer below is justified. The aim of this preliminary study is the quantification of water flowing through and reaching the lower boundary of the cover layer soil cluster at a certain real location, and for comparative purposes, three different soil types have been used:

- *Silty sand*
  3.2 % clay; 30.8 % silt; 64.5 % sand; 1.5 % gravel

- *50 % silty sand + 50 % compacted slate material*
  5.7 % clay; 20.9 % silt; 62.2 % sand; 11.2 % gravel

- *33,33 % silty sand + 66,67 % compacted slate material*
  8.5 % clay; 24.0 % silt; 55.2 % sand; 12.3 % gravel

The corresponding grain size distributions for each soil material are illustrated in the following figures (Fig. 42-Fig. 44). The adding of compacted slate material to the "pure" silty sand material leads to an increase in the clay and gravel fraction, and to a relative decrease in the silty fraction. Fig. 41 shows photographic pictures of the initial materials before they have been taken either in this form ("silty sand") or mixed together in a certain ratio.

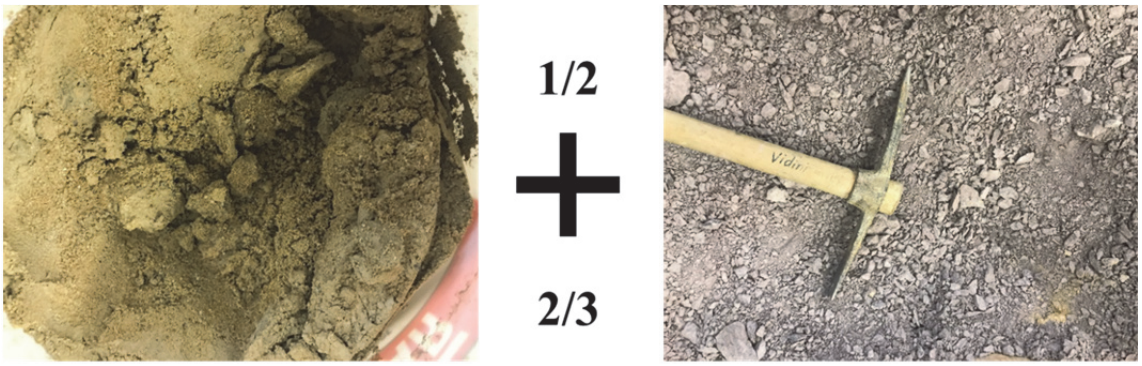

Fig. 41: (Left) "silty sand" (right) "compacted slate"

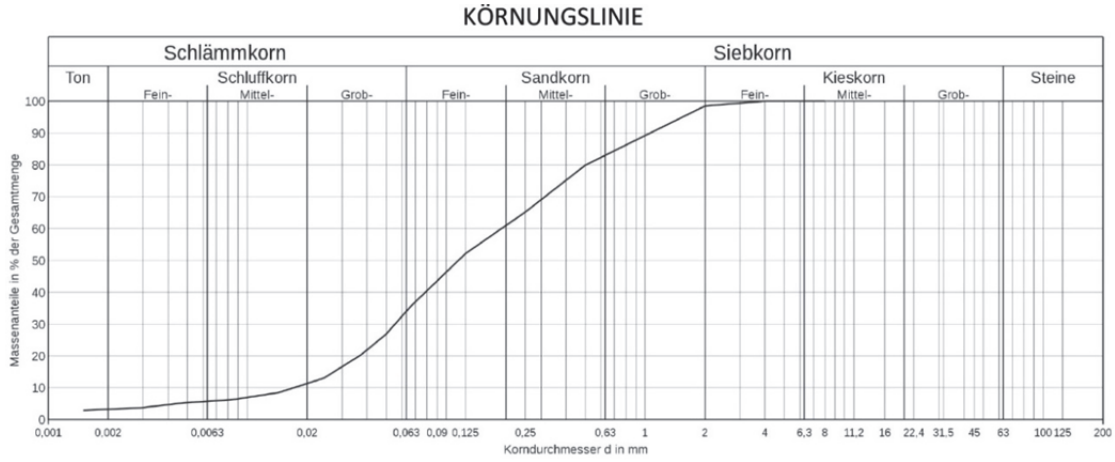

Lab.Nr.	Signatur	Anteile kleiner Ø [mm]	Ton	Schluff	Sand	Kies	Steine	Anteile größer Ø [mm]	Bodenart	D10	D30	D60	Cu	Cc
19764	——	-	3,2	30,8	64,5	1,5	-	-	cl'' sI Sa	0,0172mm	0,0553mm	0,1897mm	11,03	0,94

Fig. 42: Grain-size distribution “silty sand”

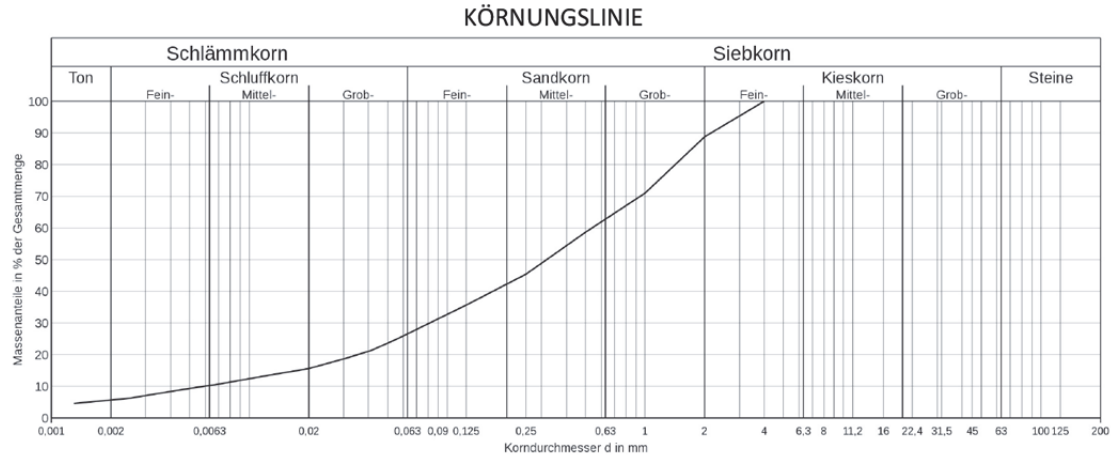

Lab.Nr.	Signatur	Anteile kleiner Ø [mm]	Ton	Schluff	Sand	Kies	Steine	Anteile größer Ø [mm]	Bodenart	D10	D30	D60	Cu	Cc
198261	——	-	5,7	20,9	62,2	11,2	-	-	cl' gr' si Sa	0,0059mm	0,0817mm	0,5396mm	91,46	2,10

Fig. 43: Grain-size distribution 50 % “silty sand” + 50 % “compacted slate material”

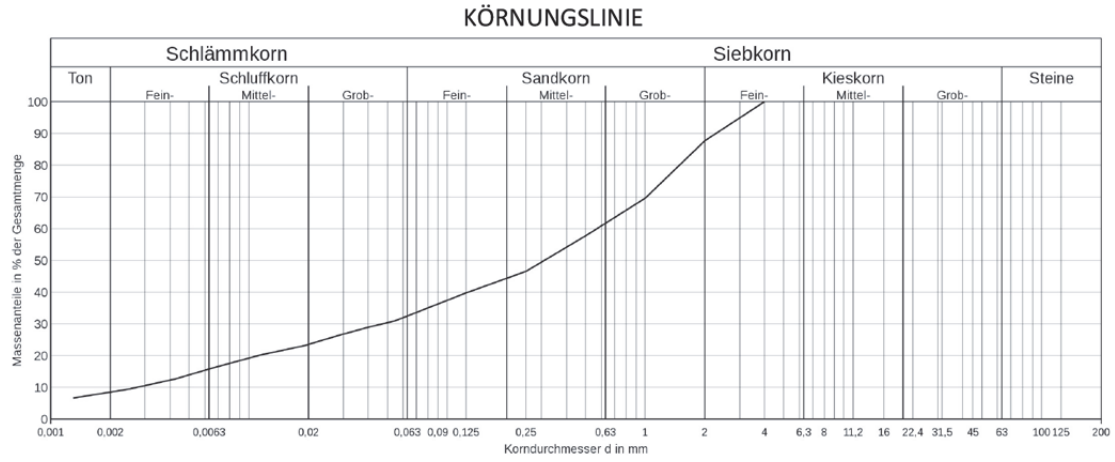

Lab.Nr.	Signatur	Anteile kleiner Ø [mm]	Ton	Schluff	Sand	Kies	Steine	Anteile größer Ø [mm]	Bodenart	D10	D30	D60	Cu	Cc
198251	——	-	8,5	24,0	55,2	12,3	-	-	cl' gr' si Sa	0,0027mm	0,0473mm	0,5712mm	211,56	1,45

Fig. 44: Grain-size distribution 33.3 % “silty sand” + 66.7 % “compacted slate material”

Besides standard laboratory test programs, the determination of SWCCs is of major importance for quantifying unsaturated soil flow. In order to define the SWCCs necessary for the numerical analysis, a combination of the test procedures “hanging water column” (3.5.1), “pressure plate extractor” (3.5.2) and “evaporation method” (3.5.3) have been used to cover the whole relevant suction range. Subsequently, the SWCC was fitted to the measured values and mathematically described by van Genuchten parameters. The corresponding SWCCs for each material used in the numerical analyses are presented in the following diagrams (Fig. 45 to Fig. 47).

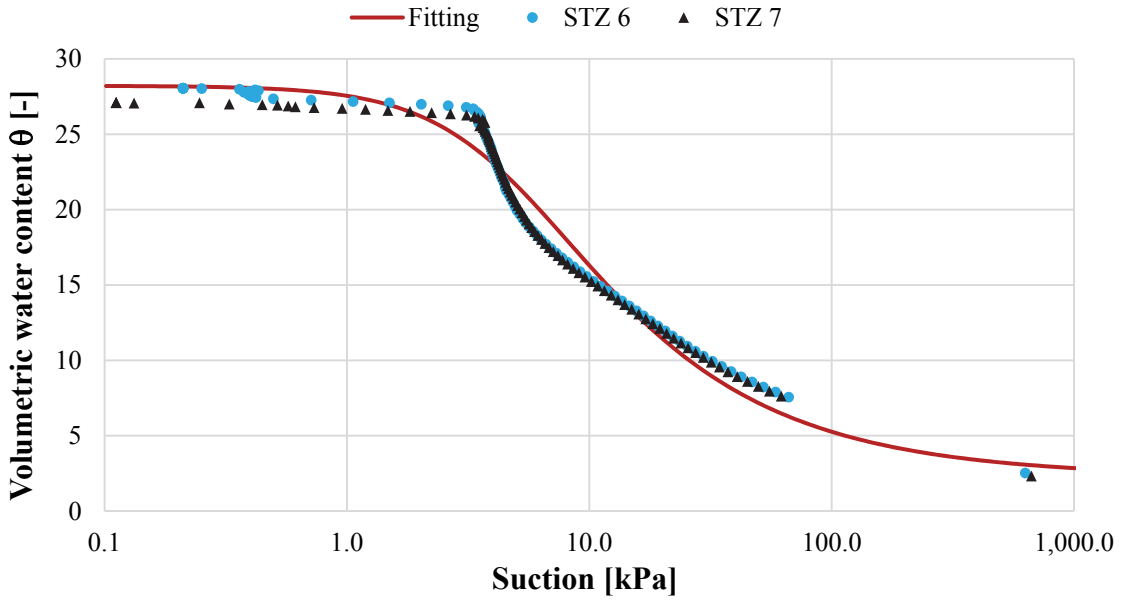

Fig. 45: SWCC for “silty sand”

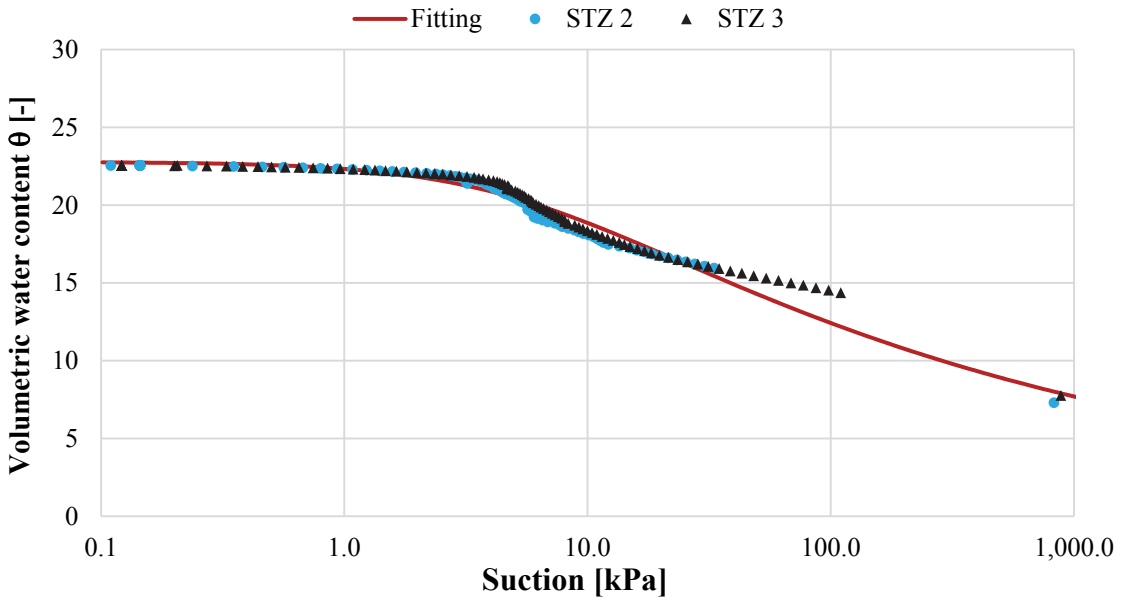

Fig. 46: SWCC for 50 % “silty sand” + 50 % “compacted slate material”

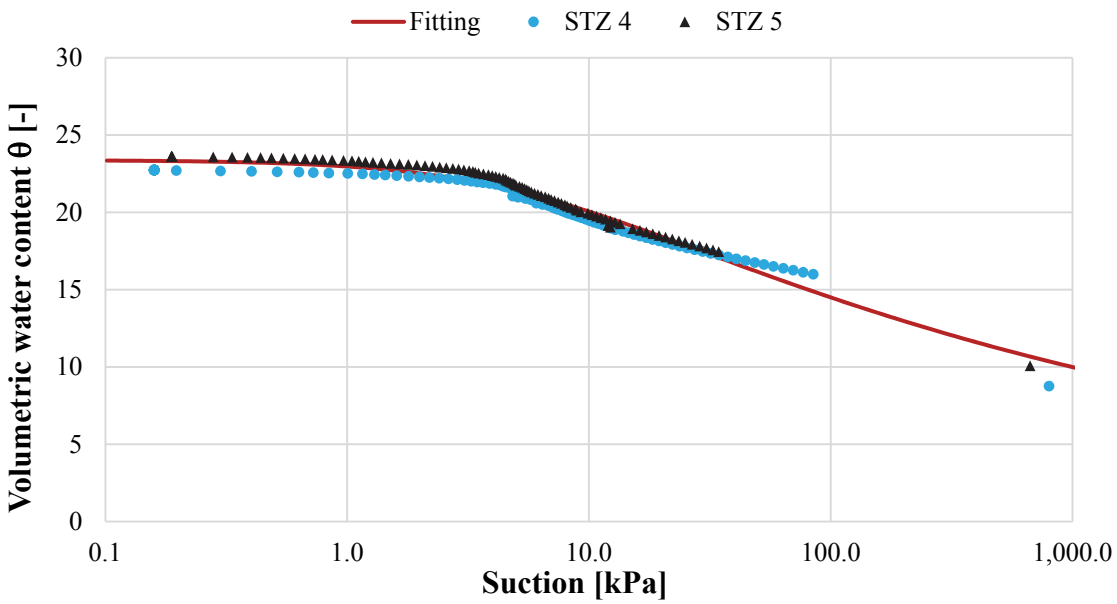

Fig. 47: SWCC for 33.3 % “silty sand” + 66.7 % “compacted slate material”

Fig. 48 illustrates the precipitation dataset over a period of one year with a total amount of precipitation of 1610 mm which was delivered from a rain gauge sensor. Since evaporation and evapotranspiration have not been measured on site where the soil material and general hydrological information comes from, the evapotranspiration part was assumed to be equal to 24 % of the total annual precipitation, as per the hydrological standard. The resulting 387 mm of evapotranspiration was divided into the 152 days with no recorded rainfall and was subsequently applied to those days by means of “negative precipitation”. The resulting climatic hydrograph used in this numerical study with an annual “net-precipitation” of 1223 mm is given in Fig. 49.

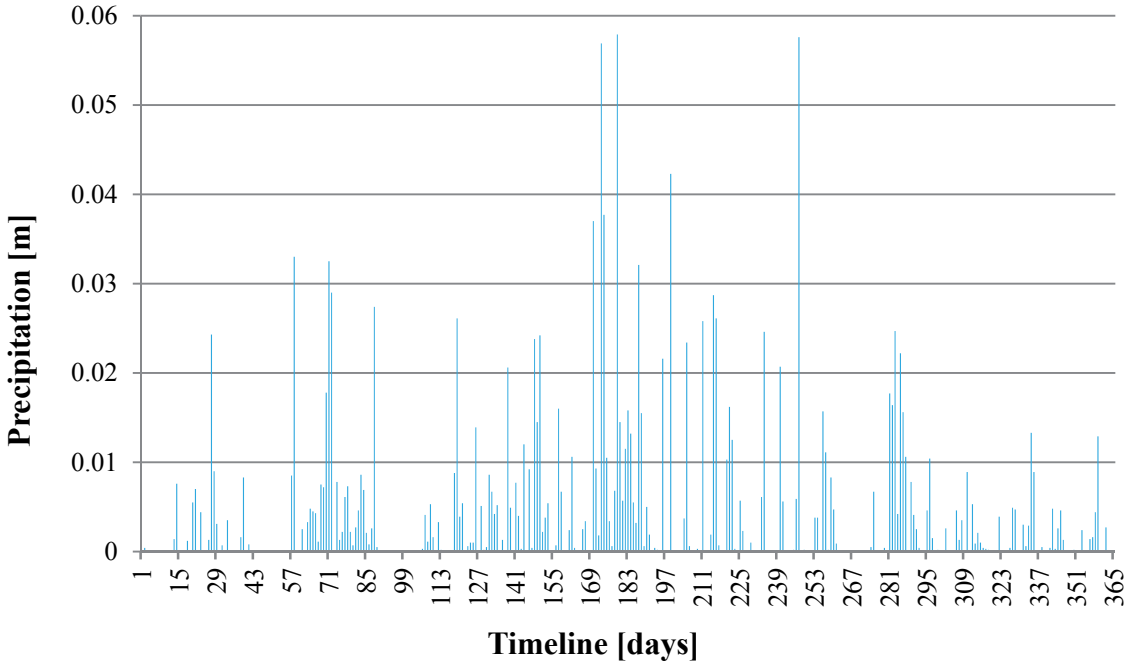

Fig. 48: Precipitation dataset for 365 days

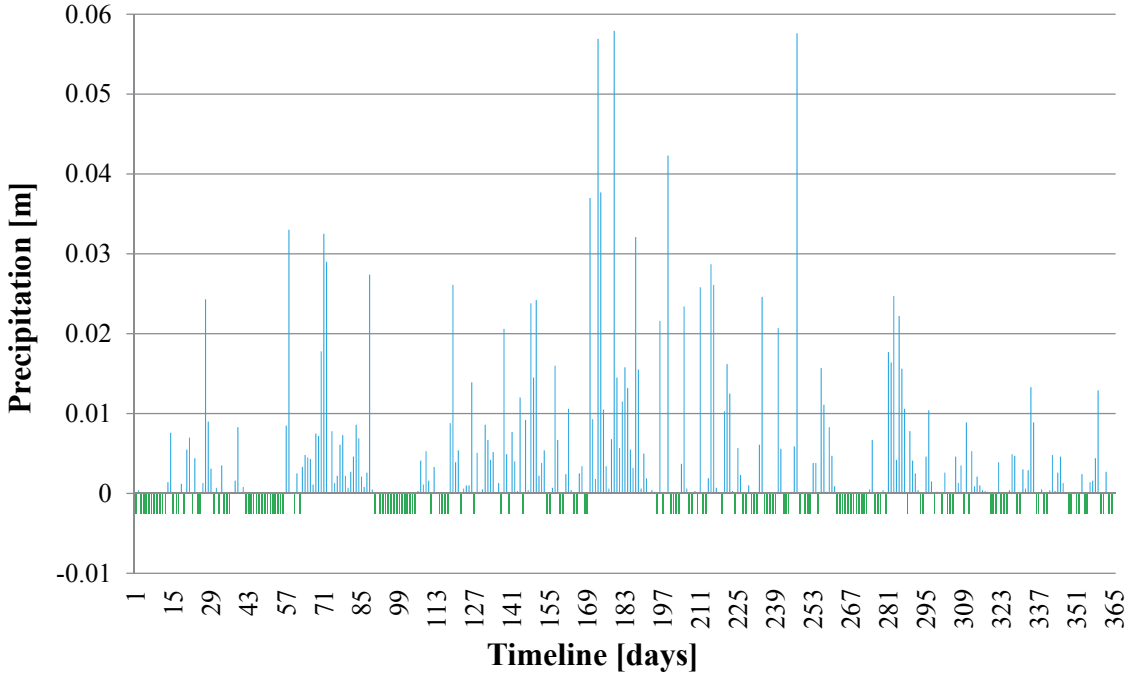

Fig. 49: Climatic hydrograph (considering evaporation) for 365 days

4.2.1 Numerical test procedure

In order to quantify the amount of water reaching through the cover soil layer to the protected material below, a simple numerical 1D-column test was performed. Due to the necessity of a very fine mesh size distribution in numerical flow calculations, the column had a width of 0.1 m and a height of 2.0 m. As the uncertainties of the input parameters are more influential than the geometric

simplifications, this approach is justified. Fig. 50 schematically describes the setup of the numerical analysis. To take into account the position of the groundwater table at the site, a "head" boundary condition was prescribed at the bottom boundary of the covering material and was kept constant during the entire analysis. To represent a worst-case scenario with a very high laying groundwater table, the "head" was defined to be -0.01 m related to the bottom boundary as indicated at the bottom of Fig. 50. Then, to reach numerical equilibrium, the linearly increasing suction above this "head" position leads to a suction value of 20.01 kPa at the ground surface. The 1-D model is characterised by closed-flow boundaries on both vertical borders. Water was allowed to flow in through the upper boundary condition, where the climatic hydrograph (Fig. 49) was applied. The run-off parameter ψ_{max} was defined to be 5 mm in this analysis. As the focus of this study lies on the verification of the amount of water reaching the bottom boundary, a fast "flow only" analysis, without taking the influence of water flow on stresses and deformations into account was deemed to be sufficient and was therefore executed in these analyses. The consideration of stiffness- and strength-parameters in a fully-coupled flow deformation analysis would have led to an enormous increase in calculation effort.

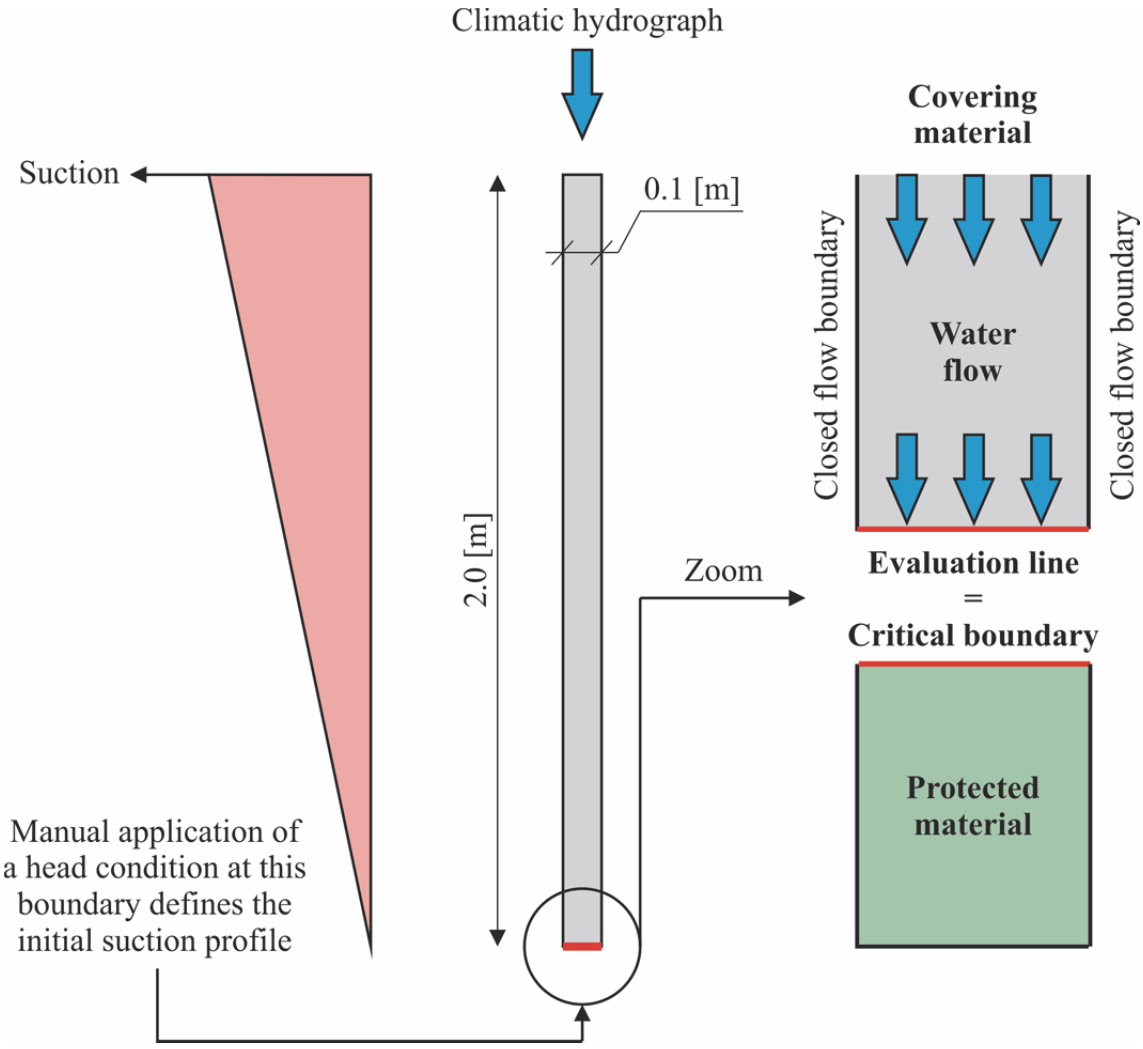

Fig. 50: Schematic description of the numerical test setup

4.2.2 Results

In the requirements for protective soil covers prescribed by the authorities, it is stated that only 10 % of the annual precipitation rate (reduced by 24 % of evapotranspiration) is allowed to reach the bottom boundary of the soil layer. Depending on the material and saturated hydraulic permeability used in this study, different amounts of water reach the protected layer below. Fig. 51 shows the applied climatic hydrograph (see also Fig. 49) along with the corresponding water flow through the bottom boundary of the numerical model assuming a saturated hydraulic permeability k_{sat} of $7*10^{-8}$ m/s. The results show that, regardless of the investigated material, it took at least 50 days for the water flowing through the column to reach the critical boundary. The use of this "higher" saturated permeability led to large amounts of water reaching the protected material, and the requirements of the authorities could not be met (see Tab. 3).

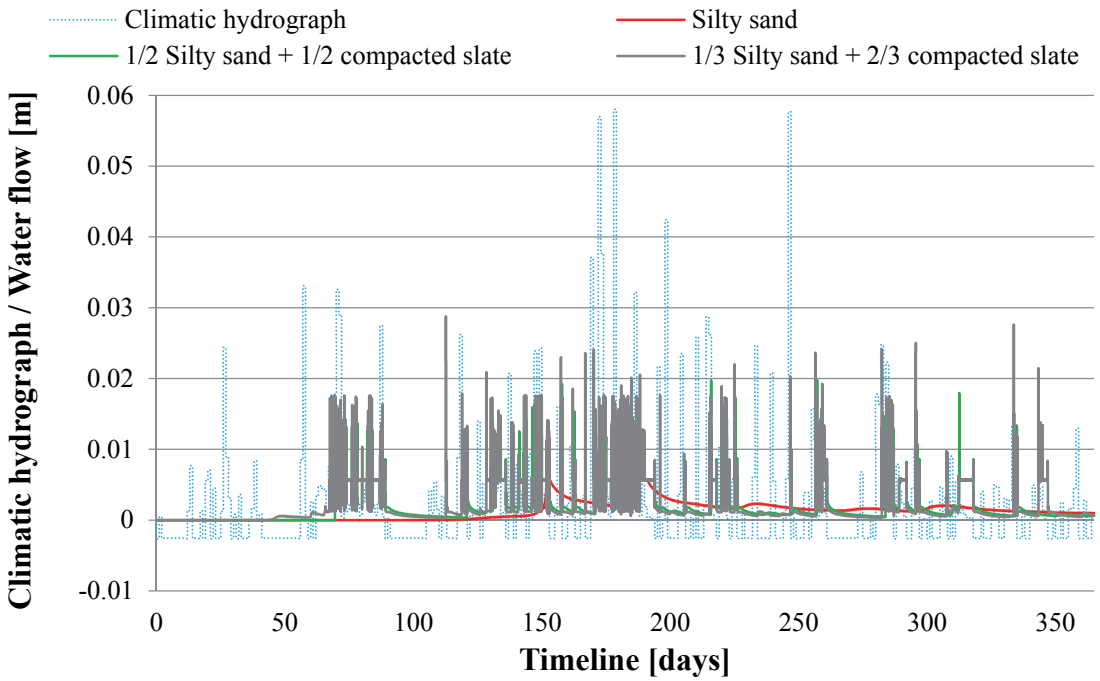

Fig. 51: Water flow through bottom model boundary for different soils; $k_{sat} = 7*10^{-8}$

The analysis using a lower saturated permeability of $1*10^{-8}$ m/s results in strongly decreasing amounts of water flowing through the bottom model boundary. As illustrated in Fig. 52, the "Silty sand" material demonstrated no water flow through, and the mixed materials only very low water rates reaching the crucial boundary, within the 365 days of the climatic hydrograph. Note that this figure does not overlay the results onto the climatic hydrograph as the flows are too small. As a result, the prescriptions of the authorities could be fulfilled independently of the investigated material.

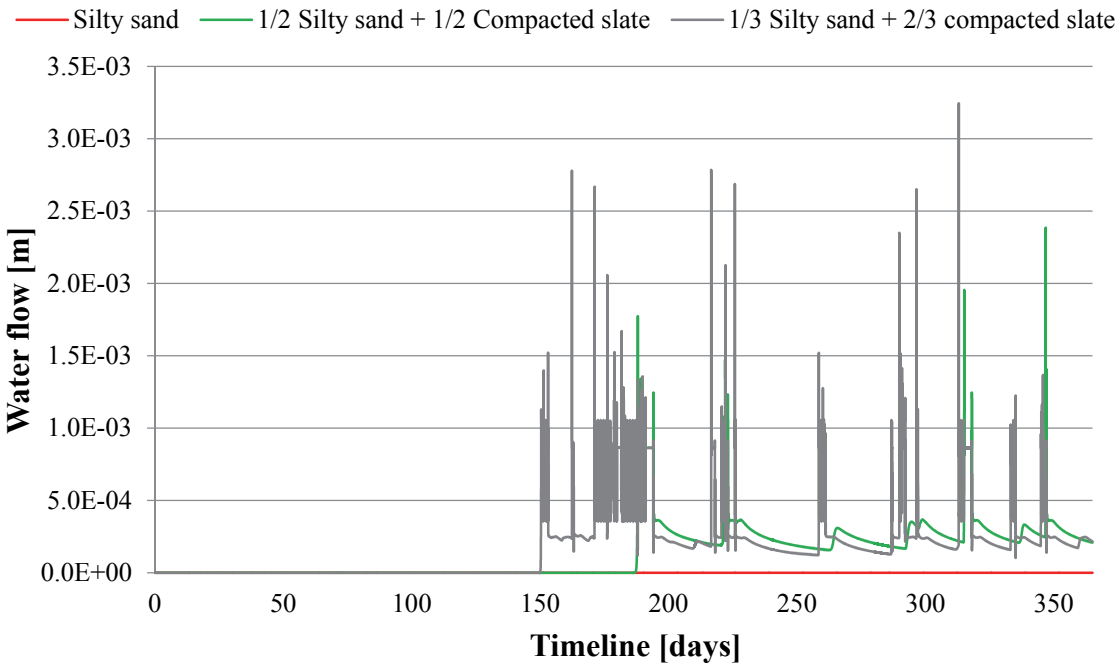

Fig. 52: Water flow through bottom model boundary for different soils; $k_{sat} = 1*10^{-8}$

Tab. 3 illustrates the calculated water flows for the three different material sets by using two variants of saturated hydraulic permeabilities. It must be mentioned that the percentage given in Tab. 3 is related to the net-precipitation.

Tab. 3: Water flow through bottom model boundary for different materials and saturated hydraulic permeabilities

Material	**$k_{sat} = 7*10^{-8}$ [m/s]**		**$k_{sat} = 1*10^{-8}$ [m/s]**	
	Water flow [m]	[%]	Water flow [m]	[%]
"Silty sand"	0.47	38	0	0
1/2 "Silty sand" + 1/2 "Compacted slate material"	0.72	58	0.07	6
1/3 "silty sand" + 2/3 "Compacted slate material"	0.69	56	0.05	4

4.3 Conclusions and outcomes of modelling water flow

The results show that under the assumption of a saturated permeability of $7*10^{-8}$ m/s, with corresponding water flows reaching the bottom boundary between 0.47 m for “Silty sand” (38 % of applied net-precipitation) and 0.72 m for the 50% “Silty sand” plus 50% “Compacted slate” mixture (58 % of applied net-precipitation), the requirements could not be met. Using a lower saturated permeability of $1*10^{-8}$ m/s decreases the amount of water reaching the critical boundary to less than 6 % of the applied net-precipitation, independently of the material used in the numerical calculations and therefore meets the requirements of the authorities.

It must be noted, however, that the results plotted in Tab. 3 are sensitive to even slight changes in the model boundary conditions. A minor material change with its accompanying deviations in for example, saturated permeability or the SWCC, could lead to big differences in the results. Additionally, it must be mentioned that the results reflect the situation after applying a yearlong climatic hydrograph only. The consideration of previous rainfall events or of longer climatic hydrographs would probably lead to higher water infiltration rates.

However, in reality, the soil surface would most likely be inclined and would produce more run-off than the flat surface used in these calculations and therefore would lead to less infiltration into the system. Regarding the amount of suction with its associated permeability at the ground surface, this analysis has assumed a very high lying groundwater level at the border between the examined and the protected material and therefore represents a worst-case scenario. According to the defined SWCC, a deeper groundwater level means higher suction and lower permeability at the top of the soil model, which leads to lower infiltration rates.

5 Numerical investigation of inhomogeneous soil slopes

The main objective of this chapter is to quantify the influence of varying climatic hydrographs, its associated changes of pore water pressures and shear strength on the stability of simplified slope geometries with inhomogeneous soil. In the context of this study, the influence of different SWCCs on the FoS of slopes stability is evaluated by means of fully coupled flow-deformation analyses employing the finite element method. To quantify the slopes' factor of safety during rainfall events after specified times of infiltration or evaporation, the strength reduction method was applied. In addition to various combinations of soil layers, the influence of a water-bearing, highly permeable soil layer between two less permeable soil layers (a situation which is often encountered in practice) on the factor of safety of the slope has been investigated. The analyses were performed employing two-dimensional finite element models utilizing the code PLAXIS 2D (Brinkgreve et al. 2017). The analyses performed and presented in this chapter served primarily as a simple benchmark to test the overall performance of the finite element code used in the numerical analyses.

5.1 Geometry and boundary conditions

The geometry of the slope and its boundary conditions are illustrated in Fig. 53. The height of the slope is 10 m and the slope angle α is 26.56° (the slope's horizontal to vertical is 2:1). The initial groundwater level was assumed to be inclined with the same angle as the boundary between the different soil layers. The left and the lower boundary were taken as closed flow boundaries, whereas water was able to flow through the upper and the right boundary of the model. The two-dimensional finite element mesh consists of 1300 15-noded elements.

In a first step, the influence of three different locations of the boundary between the upper and lower soil layer (geometries 1, 2, 3 at the left half of Fig. 53) was evaluated. In geometry 1 ("GEO 1"), the layer boundary runs through the toe of the slope, in geometry 3 ("GEO 3") the boundary lies at the same position as the initial groundwater level and geometry 2 ("GEO 3") lies exactly between them. Fig. 53 (right) shows the geometry of the slope for the case of a highly permeable sandy layer situated between the upper and the lower less permeable soil layers. The groundwater table is located at the boundary between the middle and the lower soil layer. All the other model properties of the "2-layered model" were kept the same for this 3-layer model.

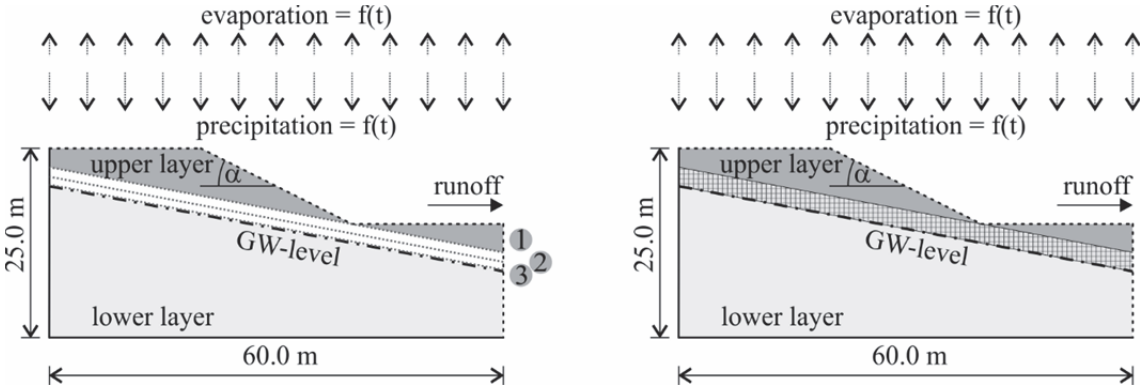

Fig. 53: Slope geometries with two (left) and three (right) different soil layers

5.2 Soil properties

As the purpose of this study is to evaluate the influence of hydraulic properties and rainfall intensity on the FoS of the slope, the strength and stiffness parameters are assumed to be the same for all soil layers (sand and silt) (Tab. 4). Only the hydraulic properties differ for the various layers.

Tab. 4: Soil parameters for Mohr-Coloumb model

Description	**Symbol**	**Value**	**Unit**
Unit weight	γ	20	[kN/m³]
Elasticity modulus	E’	7500	[kPa]
Effective Poissons’ ratio	ν’	0.35	[-]
Effective cohesion	c’	10	[kPa]
Effective friction angle	φ’	20	[°]

5.3 Hydraulic properties and climatic hydrographs

The influence of precipitation, evaporation and periods of no rainfall are analysed. Furthermore, various scenarios of applying the same amount of rain in different time periods were investigated. The rainfall intensities used in this study were adopted from the design rainfall with a return period of 20 years for Graz (Austria), which is around 120 mm /day (BMLFUW 2012).

Different scenarios to apply the same amount of rainfall within 24 hours have been investigated:

- Condition 1 (CC1):

  Constant precipitation during a predefined period with variable infiltration rates

  - 5 mm/ hour for 24 h = 120 mm/ day
  - 10 mm/ hour for 24 h = 240 mm/ day
  - 20 mm/ hour for 24 h = 480 mm/ day

- Condition 2 (CC2):

  Alternating phases of precipitation and periods without precipitation (Fig. 54 left).

Clarification: condition two means alternating periods with precipitation of 10 mm/hour and precipitation of 0 mm/hour, each with a duration of 3 hours (Fig. 54 right).

- Condition 3 (CC3):

  Alternating phases of precipitation and evaporation (Figure 5).

Note: For theoretical purposes in condition 1 only, and to make the study with constant precipitation even “more worst case”, this design rainfall had been increased to 240 mm /day and 480 mm /day, respectively. In order to quantify the differences between these climatic conditions, the total amount of precipitation (or precipitation minus evaporation) was then kept the same (120 mm /day) during the considered period (Fig. 54).

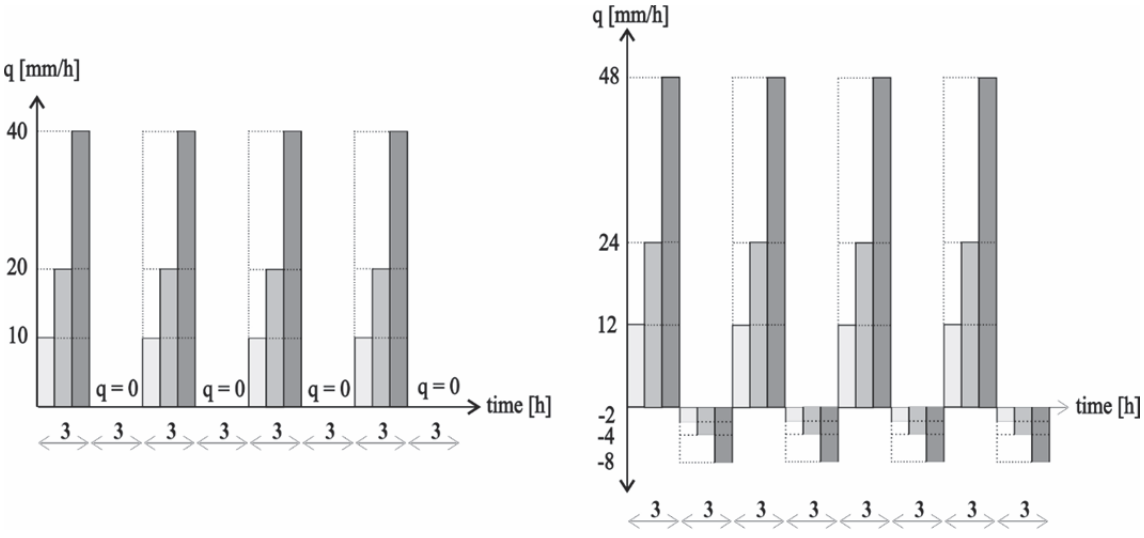

Fig. 54: Condition 2 (CC2) with alternating phases of precipitation and phases without precipitation (q=0) (left); Condition 3 (CC3) with alternating phases of precipitation and evaporation (right)

5.3.1 Soil Water Characteristic Curve

In this study, alternative hydraulic cases, one with a more permeable (sand) upper layer and a less permeable (silt) lower layer and vice versa, have been investigated. In this analysis, the van Genuchten function was used to describe the SWCC mathematically. The van Genuchten parameters necessary in this numerical analysis were taken from the USDA-Database for equivalent soils (see chapter 3.4.4) and are illustrated in Fig. 55. Thus the sand layer has a saturated hydraulic conductivity of $8.25*10^{-5}$ m/s, and the silt layer $1*10^{-6}$ m/s. For the case of the more permeable sandy middle soil layer between two less permeable silty layers (3-layered-model in Fig. 53 right), the SWCC for "sand" was also taken for the middle layer, but the saturated permeability was increased to $1.0*10^{-3}$ m/s. Tab. 5 lists the saturated hydraulic permeability and the van Genuchten curve-fitting parameters, which were used for this study.

Tab. 5: Saturated permeability and van Genuchten parameters of used USDA soils

Description	**k_{sat} [m/s]**	**g_a**	**g_n**	**g_l**
USDA Sand *reference*	8.25 e-5	14.5	2.68	0.5
USDA Sand *reference * 100*	8.25 e-3			
USDA Sand *middle layer*	1.00 e-3			
USDA Silt	1.00 e-6	1.6	1.37	0.5

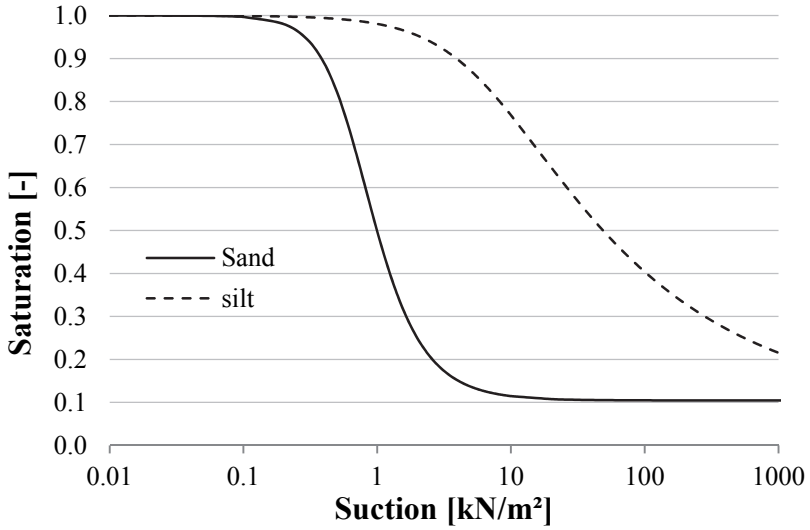

Fig. 55: SWCCs for sand and silt (USDA series)

5.3.2 Relative Permeability Curve

Fig. 56 shows the relative permeability functions, which depends on the degree of saturation, for “sand” and “silt” (USDA) which were used in this study. Due to the initial depth of the groundwater level being below the upper soil layer, as indicated in Fig. 53, the saturation of the upper soil layer is quite low. This, in combination with the chosen SWCC, led in this case independently of the used material, to very low values of unsaturated (relative) permeability.

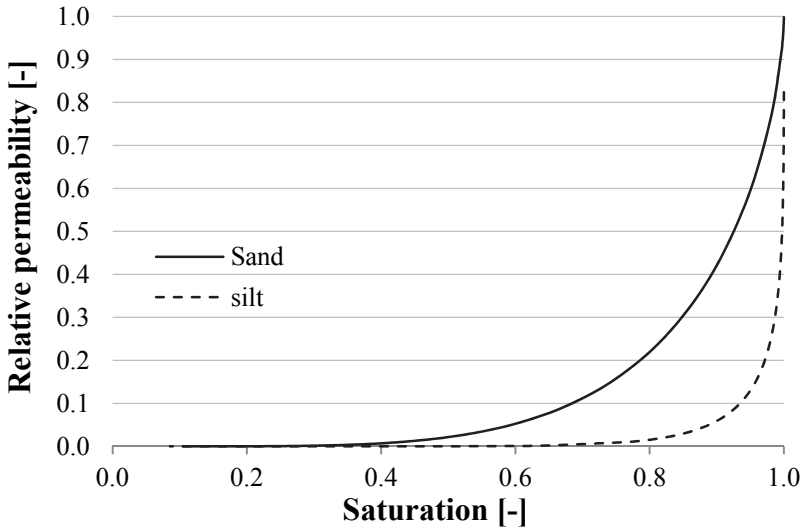

Fig. 56: Relative permeability depending on saturation for sand and silt (USDA series)

In practice the permeability of a soil in situ is a parameter associated with a high degree of uncertainties. Due to that, a comparative study with 2 orders higher permeability in the upper soil layer was done additionally (see 5.4.5).

5.4 Discussion of results

The influence of various factors, the different slope geometries ("GEO 1/2/3"), the permeability of the soil layers ("sand-silt" / "silt-sand"), the different hydraulic conditions ("CC 1/2/3"), the difference between the 2-layered and 3-layered models and the duration of applied rainfall events, have all been investigated. To quantify the slopes' factor of safety during rainfall events after specified times of infiltration or evaporation, the well-known strength reduction method was applied (Equation 34 in chapter 3.7.2). Fig. 57 exemplarily illustrates the failure mechanism by means of incremental deviatoric strains as a result of the phi-c-reduction after rainfall application.

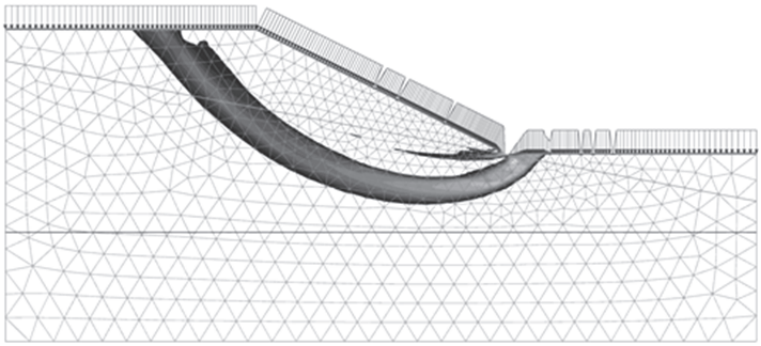

Fig. 57: Incremental deviatoric strains after strength reduction method (5 mm / hour, GEO1, CC1) after 24 hours

5.4.1 Influence of geometry changes of the soil layers

One major outcome of this study is that the configuration with a less permeable upper layer ("silt-sand" scenario) and climatic condition 1 (constant rainfall), independent of geometry (1/2/3), generally leads to an increasing FoS. This is due to the very low permeability of the silt in the upper soil layer resisting infiltration.

If the soil body is not able to take up the applied precipitation, run-off will take place. In PLAXIS, the ψ_{max} parameter controls the maximum allowable pore pressure head (relative to the elevation of the boundary to which it applies). When the groundwater head rises above this user-defined level ($y+\psi_{max}$), the infiltration discharge changes into the corresponding head in order to simulate run-off. In order to simulate a considerable amount of water which acts like an additional surcharge on the upper model boundary (e.g. ponding water), the ψ_{max} parameter was set to 0.1 m in the course of this study.

This situation is certainly not realistic from a practical point of view, because run-off would probably be faster than simulated here and inevitable cracks in the

soil would actually allow water to infiltrate in. However, this parameter setting was kept in this case in order to highlight the importance of correct boundary conditions. It must be noted for clarification that a ψ_{max} parameter defined to zero would simulate all run-off.

On the other hand, the results show a decreasing safety factor when the upper layer is the more permeable sand ("sand-silt" scenario). As the initial groundwater level is kept in the same location in all calculations, the initial factor of safety is given by the geometry of the model and the arrangement of the soil layers ("GEO 1-3"). Fig. 58 shows the development of the FoS for different configurations of the geometry, where only CC1 (with three discharge rates) was applied. Each line type has three lines as the CC1 scenario applies the total daily discharge in three rates (120/240/480 mm/day). It follows that the influence of the SWCC with its corresponding saturated permeability and how these are arranged ("sand-silt" or "silt-sand") is more significant than the characteristic of constantly applied rainfall events.

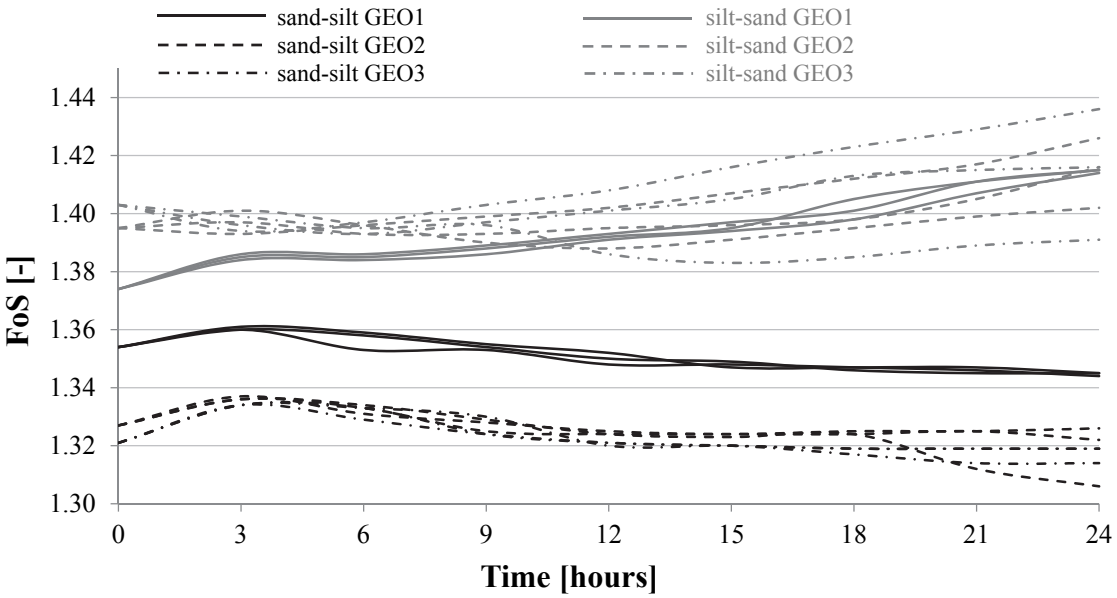

Fig. 58: Development of the FoS of GEO 1/2/3 over 1 day and with precipitation input CC 1 (three rates) applied.

5.4.2 Influence of hydraulic conditions

Changes in the climatic conditions, as tested with CC2 and CC3, do not show any significant differences in the development of FoS with time, as compared to climatic condition CC1, which uses a constant infiltration rate over 24 hours as described in 5.3. CC2 and CC3 led to alternate periods with increasing and decreasing FoS, respectively.

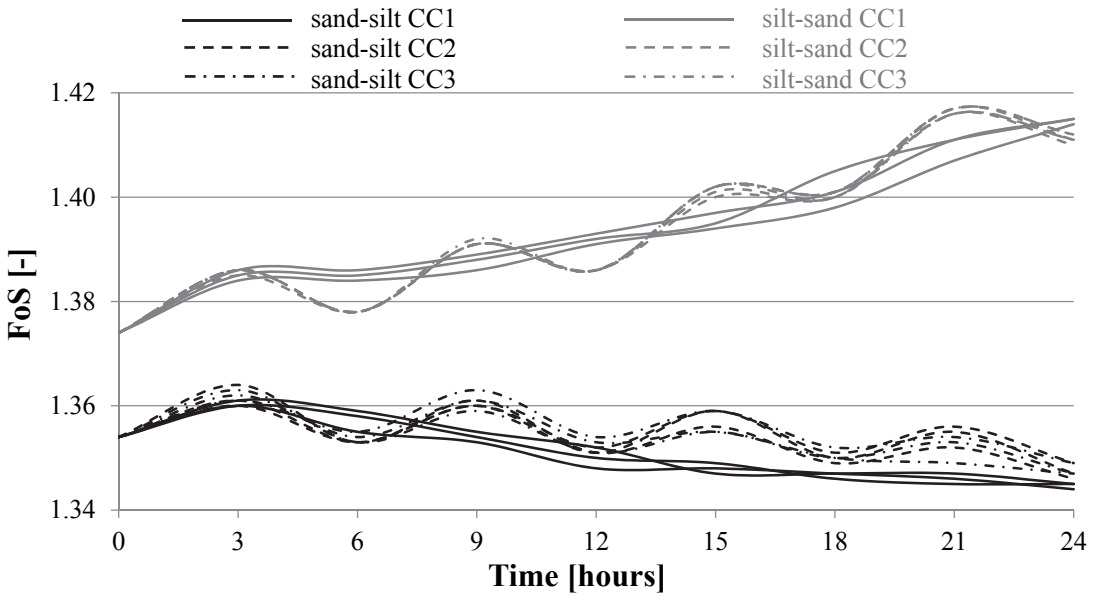

Fig. 59: Development of the FoS of GEO 1/2/3 over 1 day and with CC 1/2/3 applied

In the present study, the constellation with a less permeable upper layer (silt) was no longer investigated. Furthermore, due to the fact that changes in geometry ("GEO 1/2/3") led to qualitatively comparable results, only GEO 1 was taken into consideration in the following chapters of this preliminary study.

5.4.3 Comparison of 2-layered and 3-layered geometries

The boundary conditions for the 3-layered soil model (Fig. 53 right) with a highly permeable soil layer between the upper and the lower layers showed negligibly small changes in the FoS with time for an observation time of 24 hours (Fig. 60).

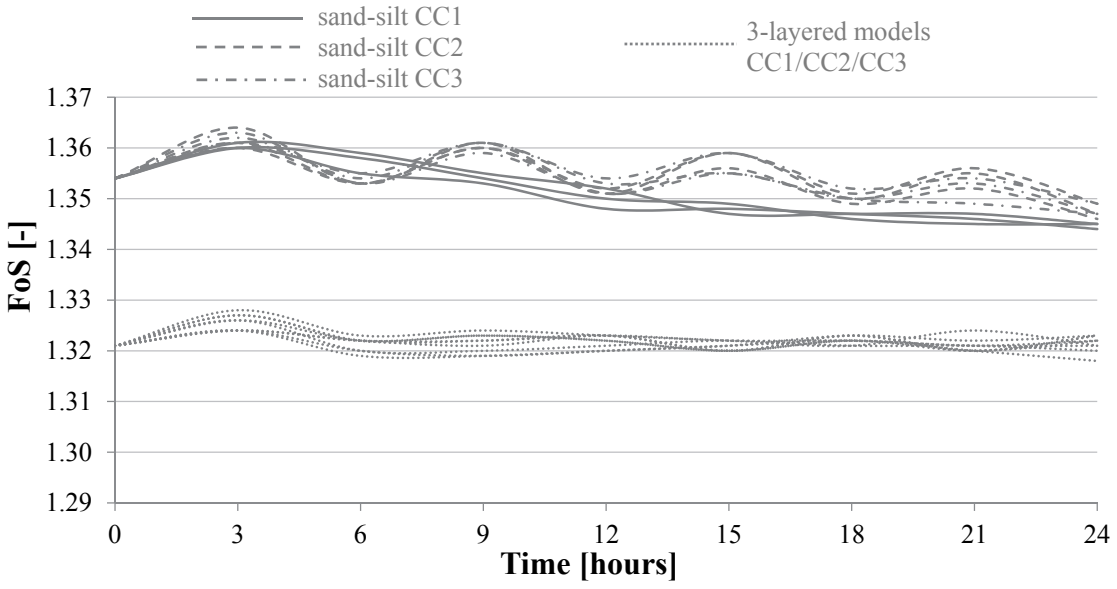

Fig. 60: Development of the FoS of the 2 layer geometry (GEO 1) and the geometry with 3 layers over 1 day and with CC 1/2/3 applied

5.4.4 Development of the FoS over a period of three days

As the FoS only slightly decreases when applying the total amount of rainfall over 24 hours, the influence of a three-day long lasting rainfall event (consequently with lower precipitation rates, as the total precipitation was kept constant) was examined.

The results show a decrease of the FoS for the two-layered model with a permeable upper layer ("sand"), where hydraulic condition CC1 with a constant precipitation of 6.67 mm/hour for three days (equivalent to 20 mm/ hour for 1 day) induced the largest decrease in safety with time (Fig. 61).

The investigated three-layered soil model showed again only negligible changes of the FoS with time and was therefore no longer investigated.

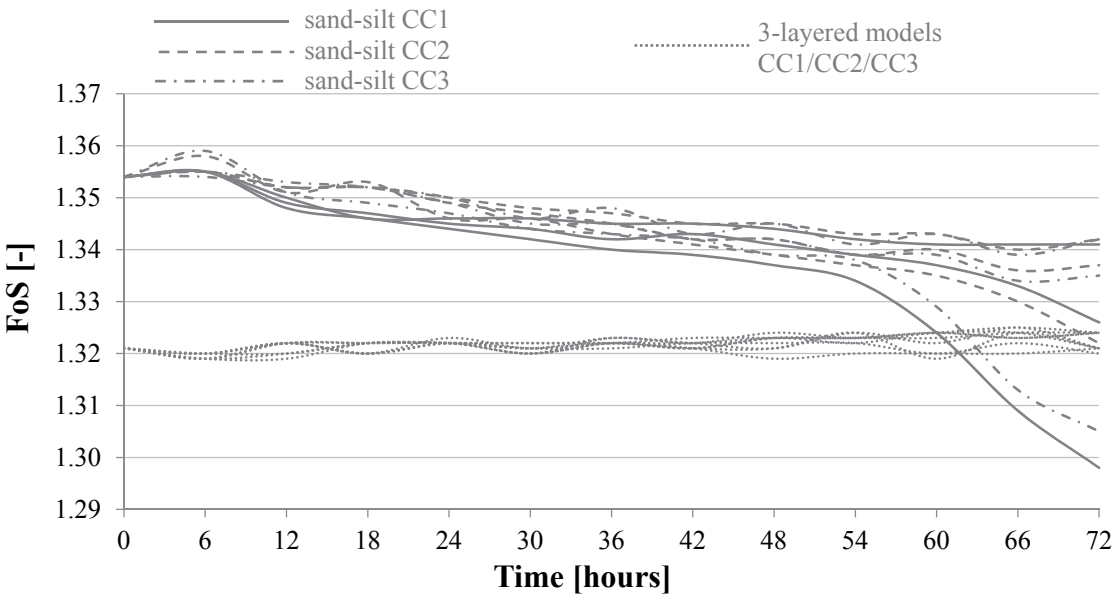

Fig. 61: Development of the FoS of the 2 layer geometry (GEO 1) and the geometry with 3 layers over 3 days with CC 1/2/3 applied

5.4.5 Development of the FoS over a period of three days and using a higher hydraulic permeability of the upper soil layer

Fig. 62 shows the development of the FoS of the two-layered geometry GEO 1 under different climatic conditions (CC 1/2/3) and where the permeability in the upper soil layer ("sand") was increased by two orders of magnitude. The main difference, as compared to the results presented thus far is that there is, due to the higher initial permeability, no increase in the factor of safety within the first period of precipitation (6 hours). However, the total decrease in the FoS after 72 hours is very small and comparable to the results from the sand with lower initial permeability (compare Fig. 61 and Fig. 62).

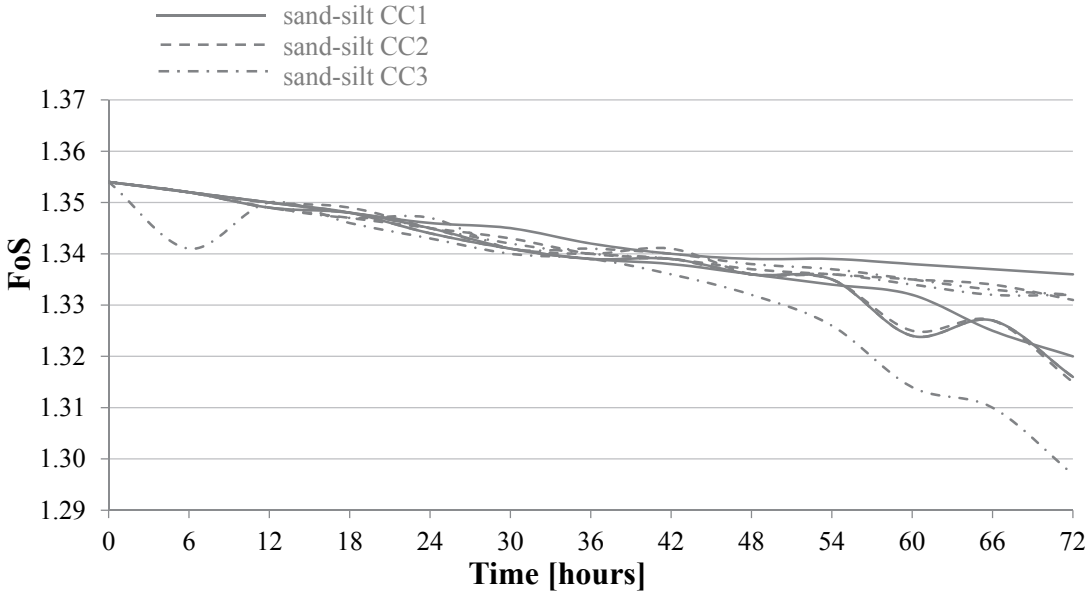

Fig. 62: Development of the FoS of the 2 layer geometry (GEO 1) over 3 days, with CC 1/2/3 applied and permeability in the upper soil layer (sand) increased by two orders of magnitude

5.5 Conclusions and outcomes of inhomogeneous soil slopes

In the study presented in this chapter, the changes in FoS of inhomogeneous soil slopes, which were subjected to different scenarios of rainfall, have been investigated.

For the investigated soil layer geometries, there are no significant differences in the factor of safety resulting from difference geometries (GEO 1/2/3, which define the boundary between the two soil layers). The lower saturated permeability of the silt led to an increase in the FoS if it was used as the upper soil layer, because a head, which acts like a surcharge, is built up at the ground surface. On the other hand, the factor of safety decreases when the upper soil layer has a higher saturated hydraulic conductivity, because water is able to infiltrate more easily.

Regarding the climatic conditions, there are only slight differences between the three conditions used in this study. The highest decrease in the slopes' safety was generally reached under Climatic Condition 1, when a constant value of precipitation, without any periods of evaporation, was applied. The total sum of applied precipitation was always kept the same (120/240/480 mm) and either applied over one or three days. As compared to the results of a one day precipitation period with higher precipitation rates, where only slight changes in the factor of safety occurred, the lower precipitation rate in the case of a three days period led, to a larger decrease in the FoS with time. The results also show, that under the conditions of this study, an increase of the upper soil layer's (sand) hydraulic conductivity does not change the FoS of the slope.

The high suction values at the ground surface (due to the initial location of the groundwater-level) led to very low infiltration rates into the slope model as a consequence of the applied climatic hydrograph in most of the analyses. This generally resulted in only minor changes in the FoS which may not be realistic and highlights the importance of a careful selection of hydraulic boundary conditions. The shortcomings associated with the used finite element code have been shown which are addressed in the following chapters and furthermore, possible solutions to overcome these issues will be presented.

6 Numerical back-calculation of Lysimeter-data

6.1 Introduction

When performing numerical analyses considering explicitly the unsaturated zone above the groundwater table, a linearly increasing negative pore water pressure above the groundwater-level will be the "default" condition due to equilibrium reasons. This may not be realistic to the condition in the field, especially if the initial groundwater-level is deep below the ground surface. In order to start the numerical analysis with reasonable initial suction or pore pressure profiles, continuously measured Lysimeter-data can be used to calibrate the initial suction profiles in the numerical model. Since the finite element (FE) program PLAXIS 2D allows the user to manually predefine suction values by means of pressure heads at any geometry line of the model, it is possible to implement measured field data of suction or pore water pressure (e.g. from the Lysimeter) directly into the model. Fig. 63 schematically indicates the differences between the manually user-defined ("model M") and automatically generated ("model A") initial pore water pressure profile. In order to study the effect of these initial conditions in boundary value problems, a preliminary study, back-calculating data from a Lysimeter-test, has been performed and is described in the following sections.

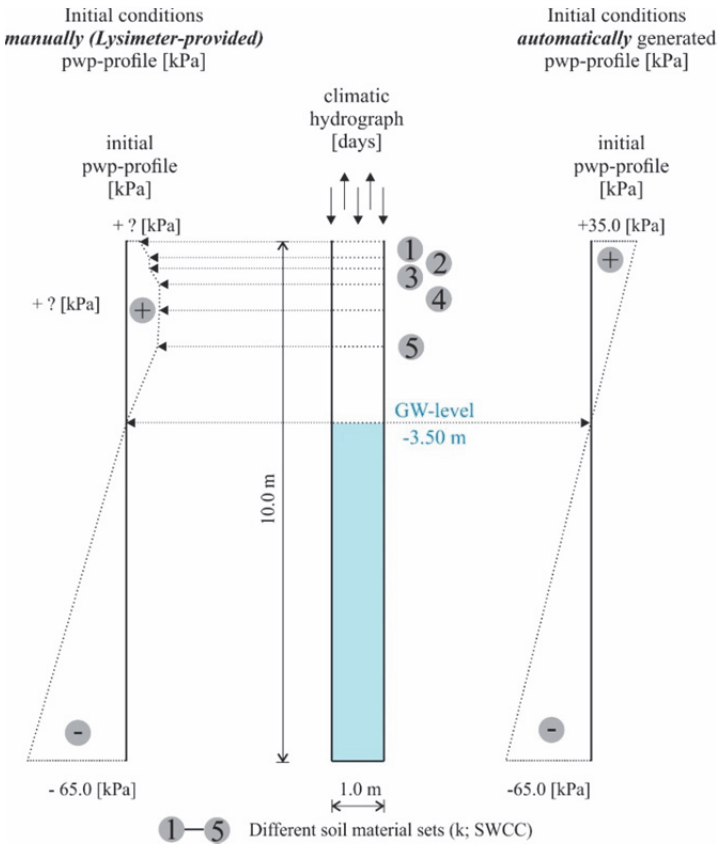

Fig. 63: Description of the initial pore water pressure profile - automatically generated vs. manually defined (schematic)

A grass-covered Lysimeter (provided by Joanneum Research), which is installed in a testfield in Wagna, Austria is illustrated in Fig. 64. The device has a height of 1.0 m and continuously measures suction-values in a depth of 20 cm and 50 cm. A local weather station gives information about precipitation, temperature, relative humidity and wind speed. Consequently, the actual evapotranspiration rate can also be determined. As indicated in the left hand side of Fig. 63, the Lysimeter-measured suction values can be directly used as user-defined pressure heads in the numerical model in order to reproduce the initial pore water pressure profile from the field.

Fig. 64: Grass-covered Lysimeter in the testfield "Wagna" in Austria (Fank & Unold 2007, adapted)

The direct use of Lysimeter-data into the model avoids the use of uncertain hydraulic input-parameters, which could affect the infiltration behaviour significantly. As it turns out, in order to reliably reproduce the Lysimeter field results, the Lysimeter suction measurements (plotted in Fig. 65 in 20 and 50 cm depths) turn out to be critical. However, there is the problem of possible dehydration of the tensiometers (the instrument used to measure suction) in dry periods (mainly in the summer). When the suction in the tensiometers reaches values of more than approximately 85 kPa, the cavitation point of the water inside the device is reached. Thus, there is a temporary failure of the measuring instrument, as indicated on the graphs by "zero-lines" with no suction at all. Fig. 65 additionally shows the climatic hydrograph (including precipitation "*P*", the evapotranspiration rate which was directly measured "*ETr*", and the calculated evapotranspiration rates "ET_0") at the test-field for a period of 4.5 years, starting in April 2013. In general, and if there is no Lysimeter available, it is very difficult and cost-intensive to measure evapotranspiration rates.

Many empirical and semi-empirical equations are available to calculate the evapotranspiration from weather data. The well-known and widely accepted FAO-Penman-Monteith (Allen et al. 1998) empirical method was used to calculate the ET_0 values, and are in good agreement with those directly measured at the Lysimeter (ET_r). As the Lysimeter device delivers reliable data for ET_r, these values are used in the presented analyses. Additionally, the careful determination of SWCCs (together with the saturated hydraulic permeability) in the laboratory is crucial for the numerical reproduction of Lysimeter-measured values.

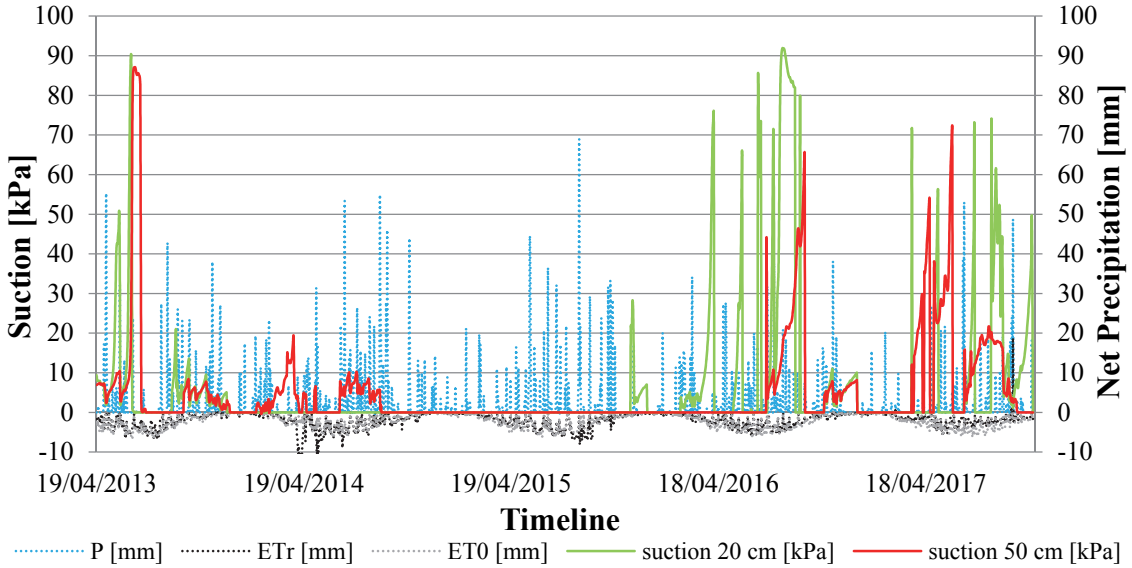

Fig. 65: Climatic hydrograph and suction measurements from the testfield "Wagna" in Austria (Klammler, personal communication)

6.2 Lysimeter - Hydraulic properties

In order to describe the relationship between water content and suction in the soil at the "Wagna" testfield, SWCCs for the soil at different depths (but right next to the Lysimeter) were determined from laboratory test results (Fank & Unold 2007). The depths are indicated and numbered 1-5 in Fig. 63. As previously mentioned, there are numerous models available to mathematically describe the SWCC, but in this study, only the commonly used and widely accepted van Genuchten model was used (Van Genuchten 1980). A general description of the van Genuchten function and its parameters is given in the earlier chapter 3.4.3. These curves, together with the data provided by the Lysimeter, enable the hydraulic behaviour in the unsaturated soil zone to be described with reasonably accuracy. Direct measurements of the unsaturated permeability as a function of the pressure head h are challenging, time consuming and cost intensive. As a commonly used alternative, the relative permeability $k_r = k/k_s$ can also be estimated directly from the corresponding SWCC model if the saturated hydraulic permeability k_s is known.

The SWCCs (both in terms of saturation and volumetric water content) and unsaturated permeability curves for soil depths of 0-30, 30-50, 50-80, 80-130 and > 130 cm, which were used in the numerical analysis and numbered by 1-5 in Fig. 63, are depicted in Fig. 66, Fig. 67 and Fig. 68.

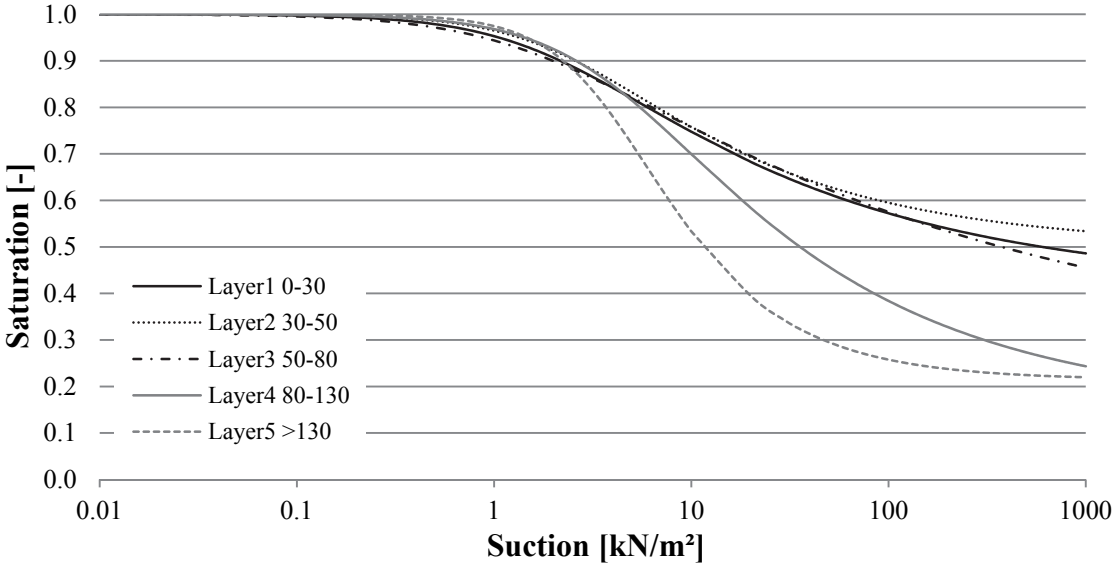

Fig. 66: SWCCs in terms of saturation for different soil depths next to the Lysimeter in the testfield "Wagna" in Austria (Schuhmann et al. 2015)

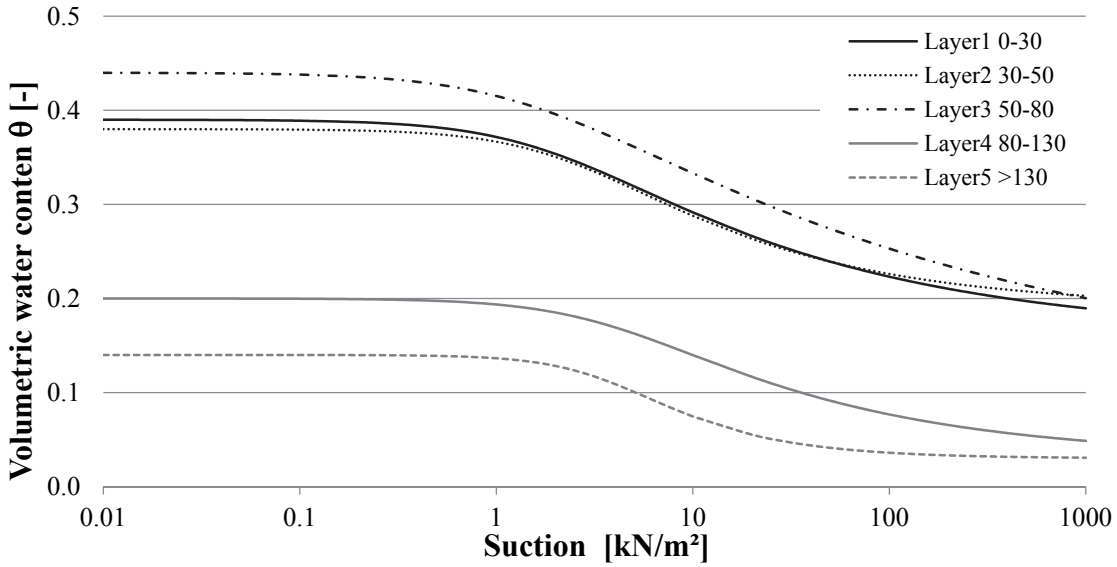

Fig. 67: SWCCs in terms of volumetric water content for different soil depths next to the Lysimeter in the testfield "Wagna" in Austria (Schuhmann et al. 2015)

The laboratory results show that the saturated hydraulic permeability increases with depth. This is also indicated by the sharper drop in the SWCC and unsaturated permeability curve for the soil clusters in a depth of 130 cm and below. The upper three soil layers (0-80 cm) show a similar behaviour, there are only slight differences in k_{sat} and in the shape of the curves.

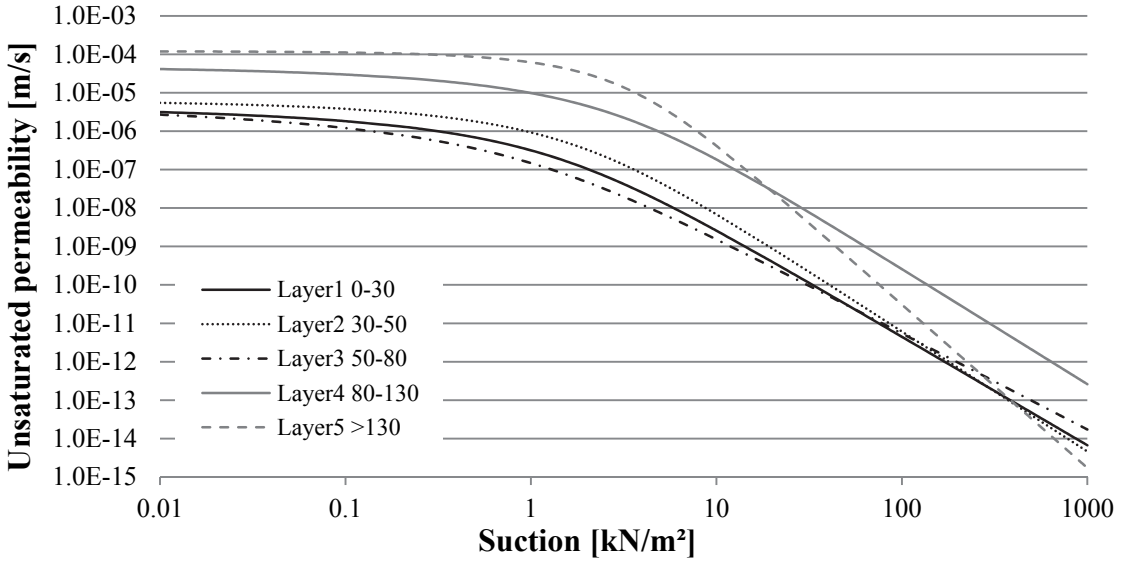

Fig. 68: Unsaturated permeability functions for different soil depths next to the Lysimeter in the testfield "Wagna" in Austria (Schuhmann et al. 2015)

The relationship between the water content and suction in the soil is hysteretic. This means that the SWCCs of the wetting- and drying paths are different and each equation that describes a SWCC can be best fitted to either the wetting (adsorption) or drying branch (desorption). In general, the drying path shows higher suction values at similar water content compared to the wetting path. Hence, an engineering judgement about which process (soil adsorption or desorption) is to be simulated is necessary in most geotechnical engineering problems. Within the framework of this study, only one average SWCC for both wetting and drying cycles was used for each soil layer (Fig. 66 and Fig. 67).

Since the focus of this study lies on the hydraulic behaviour only, the soil has been assumed to be a simple linear-elastic material with the same unit weight above and below the groundwater level, as given in Tab. 6.

Tab. 6: Soil parameters used for Lysimeter back-calculation

Description	**Symbol**	**Value**	**Unit**
Drainage type	drained		
Unsaturated unit weight	γ_{sat}	20	[kN/m³]
Saturated unit weight	γ_{unsat}	20	[kN/m³]
Elasticity modulus	E'	7500	[kPa]
Effective Poissons' ratio	ν'	0.35	[-]

6.3 Lysimeter - Back-calculation with FEM

The climatic hydrograph of a specific two-month period with reliable tensiometer data (01/10/2013-01/12/2013) was applied to a 1-D model (column) and is indicated by the dash-dotted line in Fig. 69. In this analysis, the "net-precipitation", which is defined as daily precipitation minus daily evapotranspiration (*P-ETr*), is the input dataset. The suction values at "day zero" (before the climatic hydrograph was applied) were taken directly from the Lysimeter measurements. Thus, the numerical analysis started with very low initial suction values at a depth of 0.2 m (1.27 kPa) and 0.5 m (2.42 kPa). The groundwater level was set to a depth of 3.5 m. The comparison of the numerically calculated suction values with time to the values delivered from the Lysimeter is given in Fig. 69 and shows a generally good agreement. Each drop in the suction-curve is induced by high daily rainfall rates, whereas drier periods lead to increasing suction values. The development of suction from both very low initial suction values, manually entered and shown as "model M" lines, and from higher initial suction values, automatically determined by the groundwater-level and subsequently designated as "model A" lines, are illustrated in the figure. As the groundwater level was given in 3.5 m below the surface, the automatically generated initial suction values are 33 kPa (20 cm depth) and 30 kPa (50cm depth) (see Fig. 63 for explanation). If the duration of the applied climatic hydrograph is long enough (in this specific case, greater than 35 days), the resulting suction values are not affected by the initially assumed starting values for this particular case. However, it should be mentioned, that this is the point where suction is equal to zero, both measured and calculated.

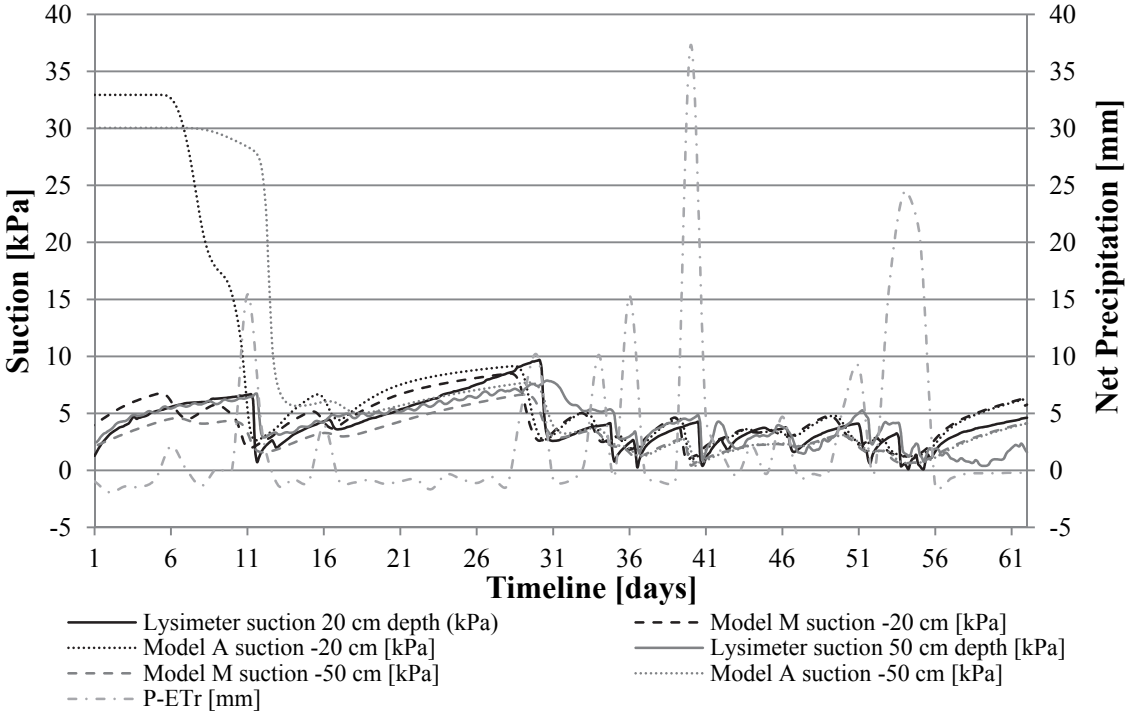

Fig. 69: Column test: Back-calculation of the suction development at certain depths

6.4 Numerical issues

The main goal of these column tests was to determine "realistic" initial suction profiles for subsequent studies with real slope geometries. With respect to the reproduction of in situ suction profiles in unsaturated soils, the back-calculation of Lysimeter data in a column-test with PLAXIS 2D delivers very satisfactory results. Nevertheless, this preliminary study pointed out that there could be a slight deviation of the calculated values to the measured values due to the predefinition of the initial pore water pressures. This is explained in the following chapter (6.4.1) in more detail. Additionally, chapter 6.4.2 presents the results of more general investigations concerning infiltration into unsaturated soils by means of numerical 1D-column tests.

6.4.1 Verification of user-defined model

"Model A", with automatically generated initial pore water pressures, is declared to be both, from the mechanical and the hydraulic points of view, in numerical equilibrium. In "model M", the initial pore water pressures are defined by means of pressure "heads" in order to reproduce the in-situ pressures measured by the Lysimeter. To reach steady-state conditions in the subsequent flow calculation of the user-defined "model M", an exact definition of the correct values of suction, saturation and SWCC would be necessary, but this is almost impossible. Thus, in order to numerically reach steady-state conditions and since the SWCC and the pore water pressures are inputs into the analysis, PLAXIS makes small adjustments in the saturation profile in the subsequent flow calculation in order to fulfil all numerical requirements for reaching this condition.

In order to quantify the influence on further results due to the deviation of the user-defined model ("model M") to the model with automatically generated initial pore water pressures ("model A"), a simple numerical column test has been performed (Fig. 70). The interaction of various boundary conditions (e.g. SWCCs and permeabilities of each soil layer) makes it impossible to start with the "model A" pressure profile, and numerically reach, with time, (e.g. by applying the climatic hydrograph) the exact suction-profile which occurs from in situ measurements.

To overcome this issue, the initial pore water pressure profile of "model A" was calculated with set boundary conditions and an initial gw-level (K_0-procedure; steady-state analysis) and then an arbitrary climatic hydrograph was applied. The resulting pore water pressure profile at the end of this fully-coupled flow-deformation analysis of "model A" was then used as the starting condition for the user-defined "model M" (where suction values at certain depths were manually predefined by means of heads). Subsequently, a steady-state flow analysis of the user-defined "model M" was performed.

This resulting calculated pore water pressure profile is then, as with "model A", in equilibrium from a mechanical and hydraulic point of view. Theoretically, both models should now deliver correct hydraulic starting conditions for further rainfall events. However, there are some slight differences in the pore water pressure profiles between both models due to the steady-state-analysis step required for "model M".

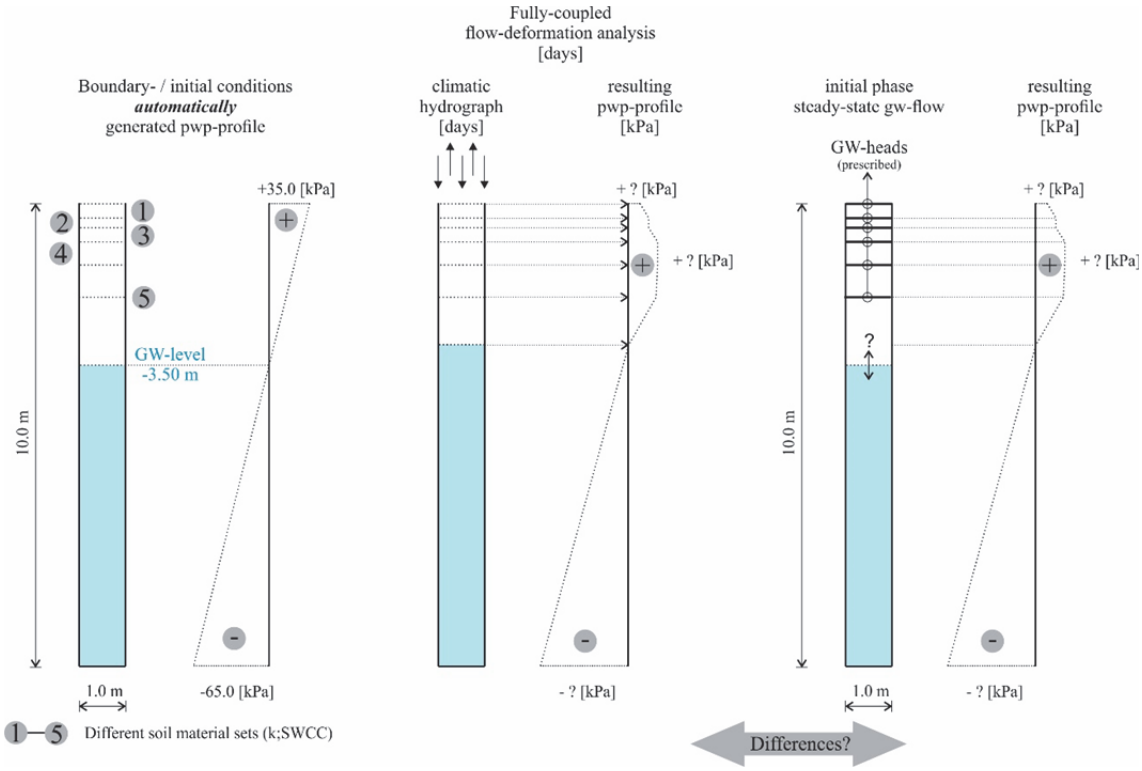

Fig. 70: Description of the column test verification

Fig. 71 shows the differences in the degree of saturation and pore water pressure p_{water} $(p_{steady}+p_{excess})$ between both models ("model M" and "model A") in a vertical cross section through the middle of the column, after the steady-state groundwater-flow calculation has been applied. The three black lines show the resulting degree of saturation S, and the three grey lines show the resulting pore water pressures p_{water}, over the depth of the 1-D column (10 m). The results where a prescribed head at the position of the initial gw-level of "model M" was used are indicated by the dash-dotted lines. When no "head" condition was defined at the position of the groundwater-level (solid line "Saturation_model M"), the numerical analysis leads to a higher gw-level (indicated by height at which 100 % saturation is reached), compared to "model A" and to the "model M" without prescribed "head" at this position.

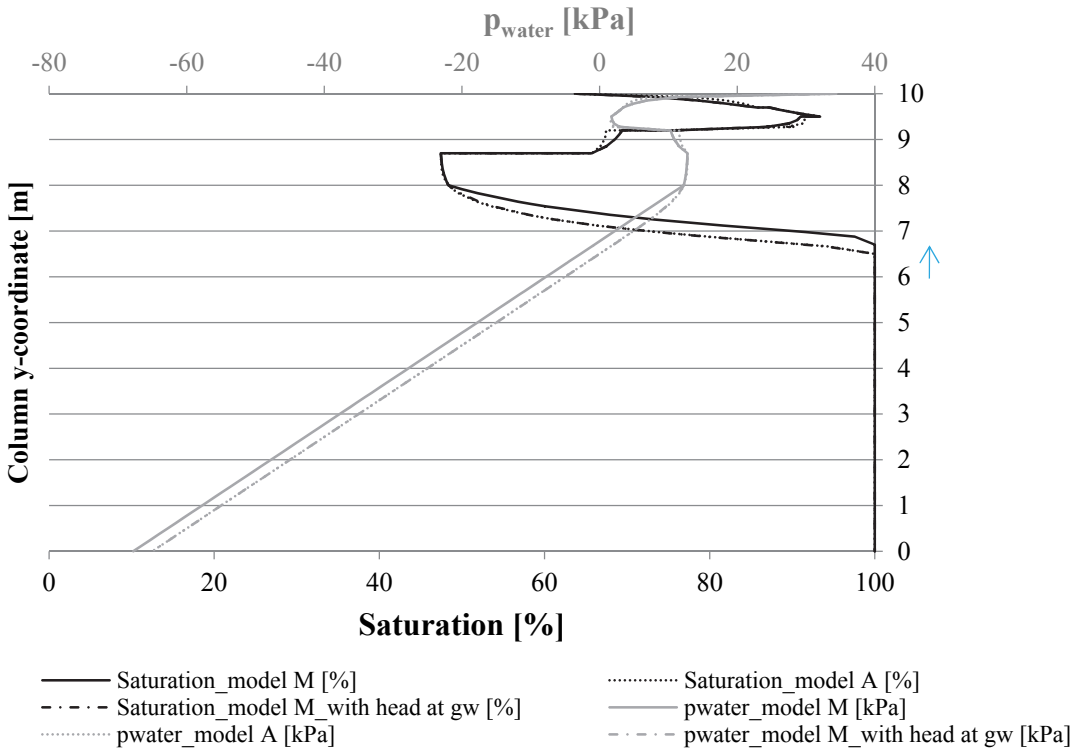

Fig. 71: Column test verification – results of p_{water} and saturation

The associated vertical groundwater-flow is constant between two levels of prescribed heads in the "model M" due to definitions in PLAXIS 2D. However, this is not the case in "model A", which leads to the slight differences in the overall results between the two models (Fig. 72). The kinks in saturation and pore water pressures (in Fig. 70), and the boxes in groundwater flow (in Fig. 71) in the upper two meters of the column demonstrate the changes between the soil layers modelled as single material sets (see 1-5 in Fig. 70) in "model M".

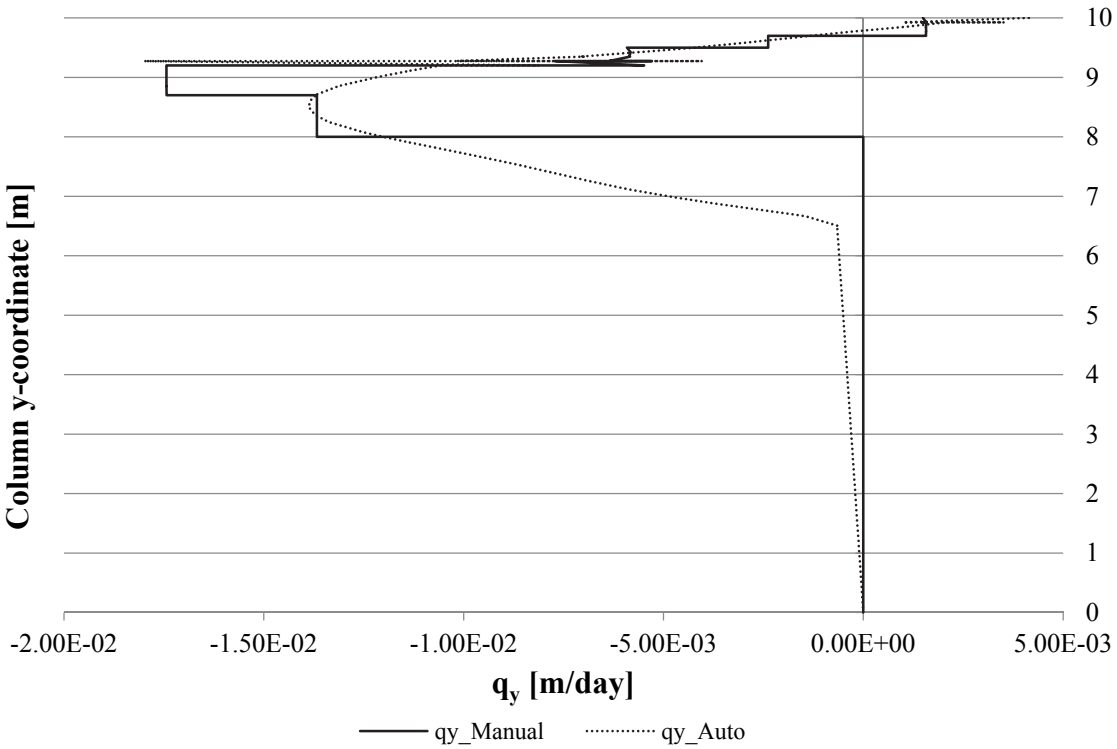

Fig. 72: Column test verification – vertical groundwater flow q_y

Since it is not possible to start with “model A” and numerically, (e.g. by applying climatic hydrographs) reach an exactly prescribed suction-profile, which is delivered from in situ measurements, this (numerical) problem was investigated. The next step would be to apply the climatic hydrograph of interest to the model and then to compare suction development at the end of the flow analysis. The better the discretization of the “model M” starting conditions in order to reproduce the “model A” results, the faster both stress curves match together and experience the same development of for example, suction, over time.

In contrast to the possible negative effects of unknown initial hydraulic conditions and hence simply using the automatically generated “model A”, the small deviations due to the aforementioned procedure are negligible and not further investigated.

6.4.2 Additional investigations and remarks on 1D column tests

In addition to the specific, and previously described Lysimeter-related numerical issues, more general investigations concerning water infiltration by means of simple numerical 1D- column tests have been performed and the results are presented in the following sections.

This section highlights the effects of an either opened or closed flow boundary condition at the bottom of the model, the differences between manually and automatically generated initial pore water pressure profiles and the influence of constant precipitation and using “flow only” phases without applying water from outside of the model, on the pore water pressure profile by means of simple 1D-column analyses.

The investigated column has a width of 1.0 m and a height of 10.0 m. The initial groundwater level was set at -3.5 m in all the analyses. The bottom model boundary was assumed to be either opened or closed, whereas the lateral model boundaries were closed in all analyses. The climatic hydrograph was defined as a constant precipitation of 0.5 mm per hour for 24 hours. In order to analyse the internal flow of the column only, a study without applying rainfall at the top of the model was also performed (see Fig. 76 and Fig. 77).

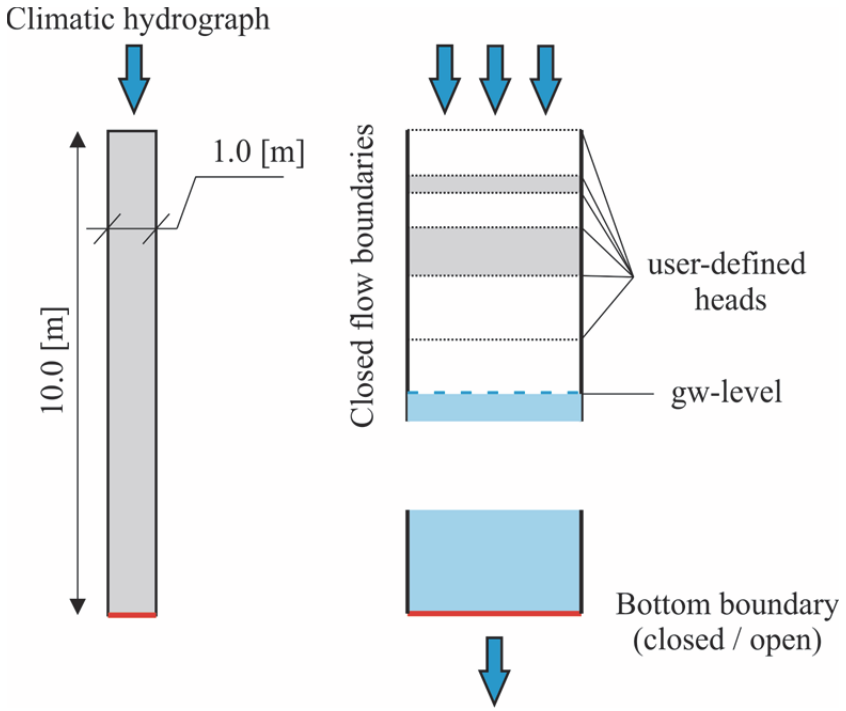

Fig. 73: General description of the 1D column test procedure

The darker shaded areas in the following results diagrams (Fig. 74 to Fig. 78) characterise changes in the SWCC at -0.5 / -0.8 / -1.3 / - 2.0 m. For better representation of the results, only the top 4.0 m of the 1D- column have been illustrated in the result diagrams (see ordinates in the corresponding diagrams). Suction is plotted at the upper abscissa whereas the lower abscissa provides information about the development of saturation. The differences in the SWCCs for the individual soil layers show up in the results by the kinks and jumps in the suction and saturation profiles. When a certain amount of water is allowed to infiltrate the column, a closed flow boundary at the bottom leads to a rising groundwater-level in the column. The following results figures (Fig. 74 to Fig. 78) show the development of suction and saturation over time.

The user-defined initial suction profile in combination with constant precipitation led to decreasing suction (indicated by a red arrow), and increasing saturation (indicated by a green arrow) in both the closed or open bottom boundary models (Fig. 74 and Fig. 75). Aside from the rising groundwater level accompanying the pore water pressure changes occurring predominantly at depths deeper than 1.3 m in the “closed” model (Fig 73), both open and closed models showed comparable results (Fig. 74 and Fig. 75).

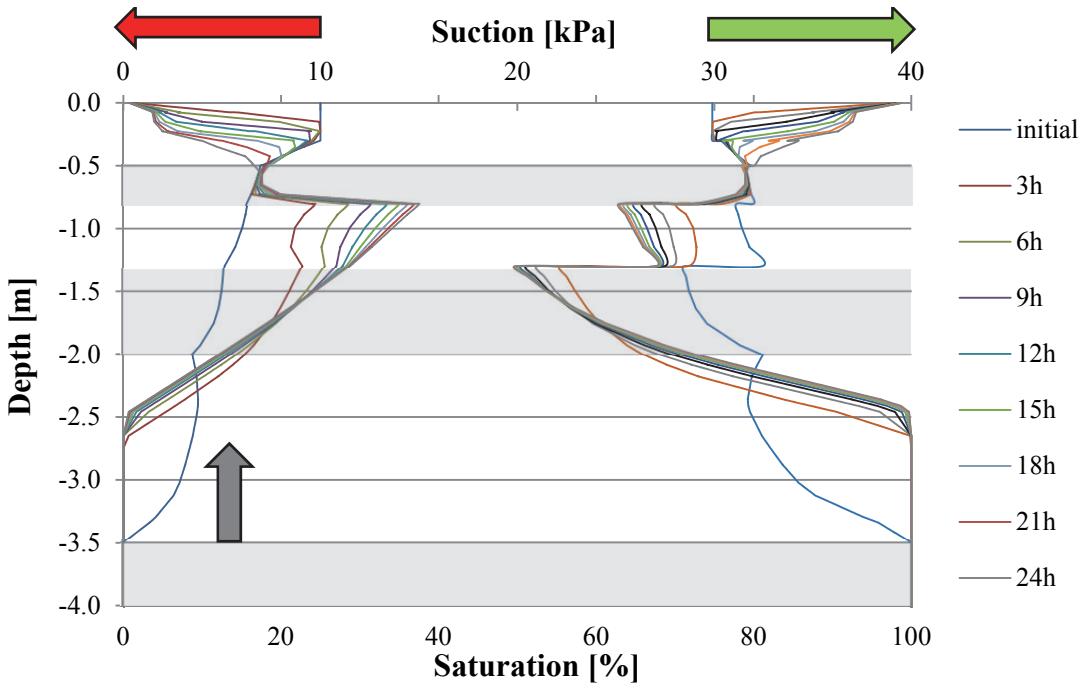

Fig. 74: Development over time of suction (lines on left) and saturation (lines on right) under constant precipitation for manually defined suction and a closed bottom boundary

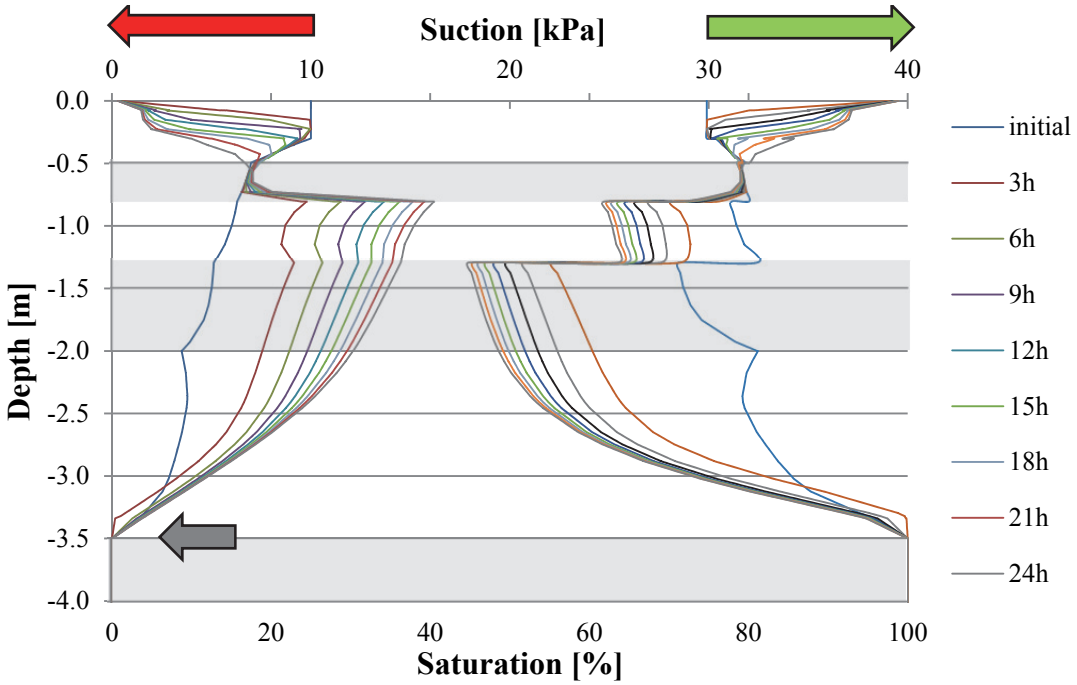

Fig. 75: Development over time of suction (lines on left) and saturation (lines on right) under constant precipitation for manually defined suction and an open bottom boundary

The option of modelling without assigning any precipitation at the top boundary was also investigated in this study. The flow-only calculation without any infiltration from external water (precipitation) led to a downwards water flow with increasing suction and decreasing saturation in the upper part of the column in both the closed and open bottom boundary models (Fig. 76 and Fig. 77). The closed flow bottom boundary led to a rising groundwater level when the water flow reached the deeper layers of the column (Fig. 76).

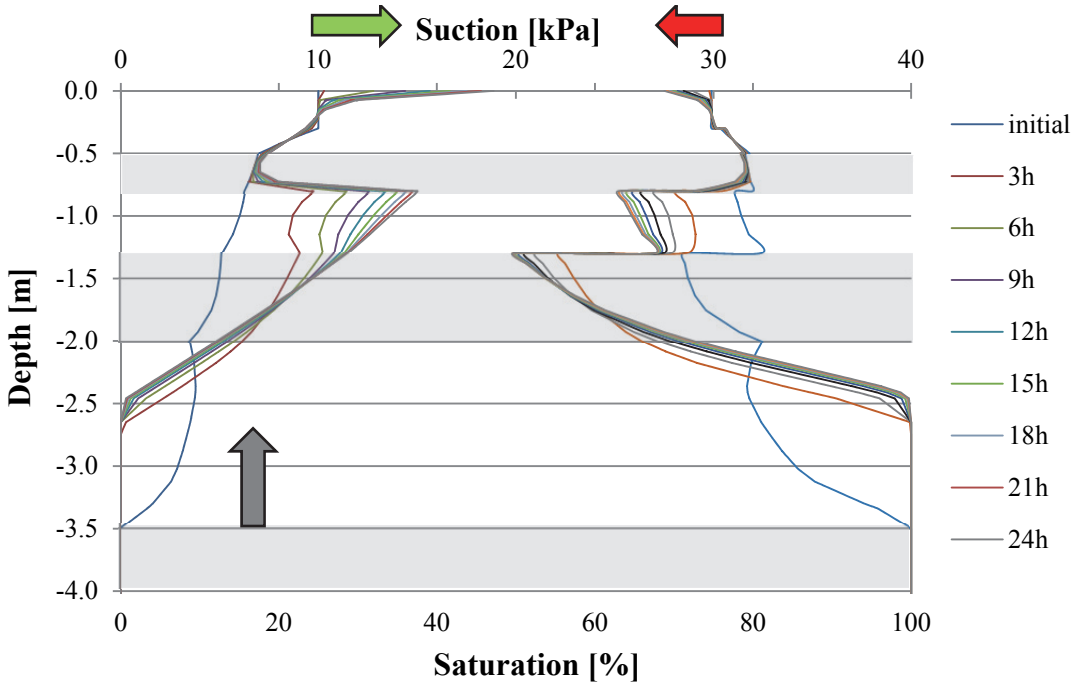

Fig. 76: Development over time of suction (lines on left) and saturation (lines on right) without any precipitation (flow only) for manually defined suction and a closed bottom boundary

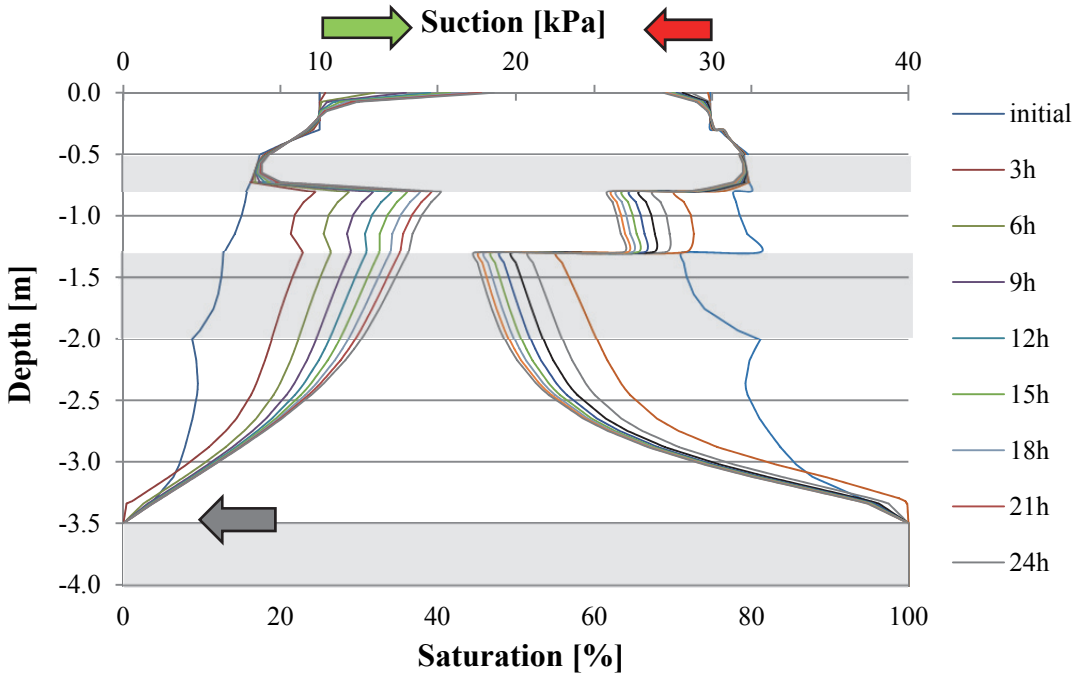

Fig. 77: Development over time of suction (lines on left) and saturation (lines on right) without any precipitation (flow only) for manually defined suction and an open bottom boundary

As a side note, there is theoretically no difference in the results, when the flow only calculation lasts long enough to reach steady state conditions, as to whether a user-defined or automatically generated initial suction profile would have been used in the calculation. In these analyses, only the automatically generated initial suction profile was used.

As the higher suction values at the top part of the model led to only small infiltration rates into the column, the resulting minor increase of saturation, in the uppermost part of the model only, means that the pore water profile was not affected by either the open or closed bottom boundary condition (Fig. 78).

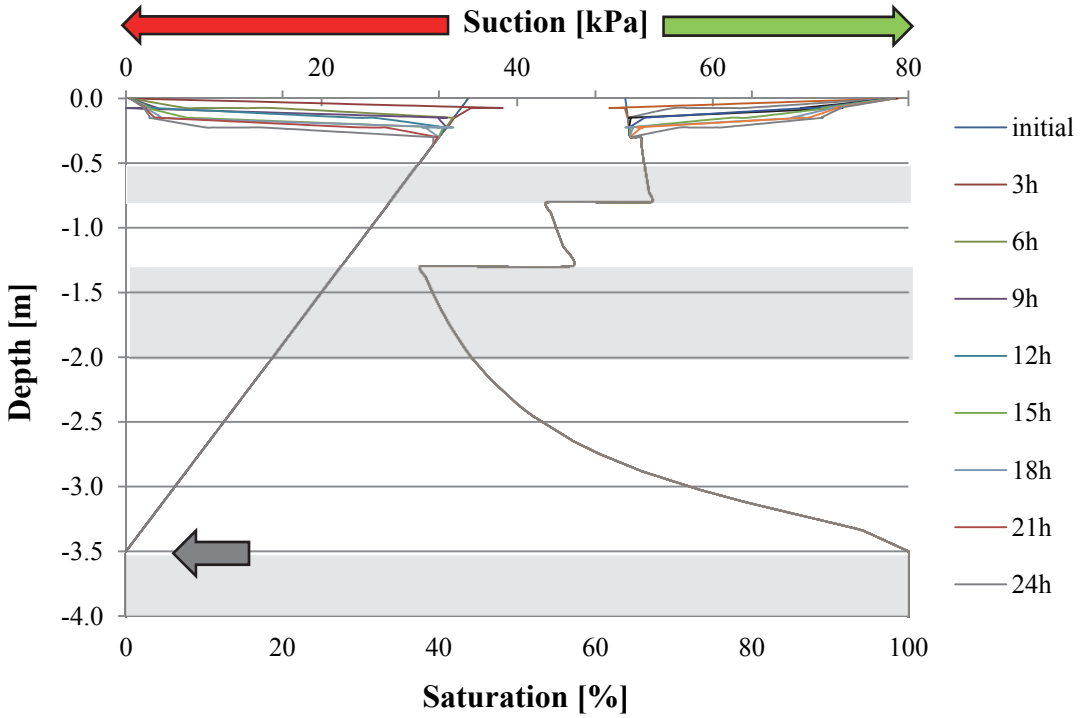

Fig. 78: Development over time of suction (lines on left) and saturation (lines on right) under constant precipitation for automatically defined suction (open and closed bottom boundary)

6.5 Conclusions and outcomes of numerical back-calculation of Lysimeter-data

With respect to the numerical replication of in situ measured suction profiles in unsaturated soils, the back-calculation of Lysimeter-data in a column-test with PLAXIS 2D deliveres very satisfactory results. The application of the described procedure avoids the use of uncertain hydraulic input-parameters, which can affect the infiltration behaviour siginificantly.

Further column tests were run to study the effects of various inputs. The main goal of these column tests was to determine “realistic” initial suction-profiles for subsequent studies with real slope geometries (in following chapters). Since the focus of this contribution was to quantify the influences of hydraulic parameters and boundary conditions, the impacts of hydraulic conditions on the results have been highlighted.

7 Benchmark slope analyses

In the previous chapter it was shown, through a preliminary study, that the numerical procedure adopted can replicate (to quite a satisfactory level) the change in suction profiles due to infiltration found in real in-situ measurements. The aim of this chapter is to investigate the infiltration behaviour due to rainfall on various slope geometries with variable boundary conditions. Specifically, the main goal is to predict and determine at what point the manually ("model M") and automatically ("model A") generated pore water pressures match in the climatic hydrograph. To answer this question, the use of linear-elastic analyses is sufficient, because the focus lies on the comparison of pore water pressure development over time. Generally, the determination of initial hydraulic boundary conditions within a slope is cost-intensive, hard to achieve or even impossible. Therefore, a further study to quantify the influence of the initial hydraulic conditions on numerical results was performed and is presented here. As the measurement data provided by the Lysimeter, as described and used in the preliminary study in chapter 6, is only available for depths until 0.5 m, it must be noted that the use of the Lysimeter dataset in the following calculations is for theoretical purposes only. It is meant to qualitatively highlight the differences between the ("model M") and ("model A") calculations.

7.1 Boundary conditions

There are many boundary conditions (BCs) which affect the stability of a slope in numerical calculations. One can divide these into geometrical and hydraulic boundary conditions. After the geometrical ones are briefly presented below, this study will focus on the influence of the hydraulic BCs and highlights the crucial parameters involved.

7.1.1 Geometrical boundary conditions

The geometry of the slope used in this study and its boundary conditions are illustrated in Fig. 79. The height of the slope is 10 m and the slope angle α was varied between 26.56°, 23.96° and 21.8° (equivalent to horizontal to vertical ratios of 2.00/2.25/2.50:1, respectively). The numbers 1 - 5 given (and for better representation highlighted by various colours) in Fig. 79 indicate the different soil layers used in the analyses, whereas the same properties as in the previous chapter 6 have been used. The initial groundwater level was set to be inclined to the same angle as the boundary between the different soil layers (~10.62°). The two-dimensional finite element mesh consists of 7278 15-noded elements. As the results showed that the slight changes in slope angle do not lead to significantly different values, only the results for the steepest slope (α = 26.56°) are presented. The development of pore water pressures over time is evaluated at a vertical cross-section through the center of the slope (see "axis of evaluation" in Fig. 79).

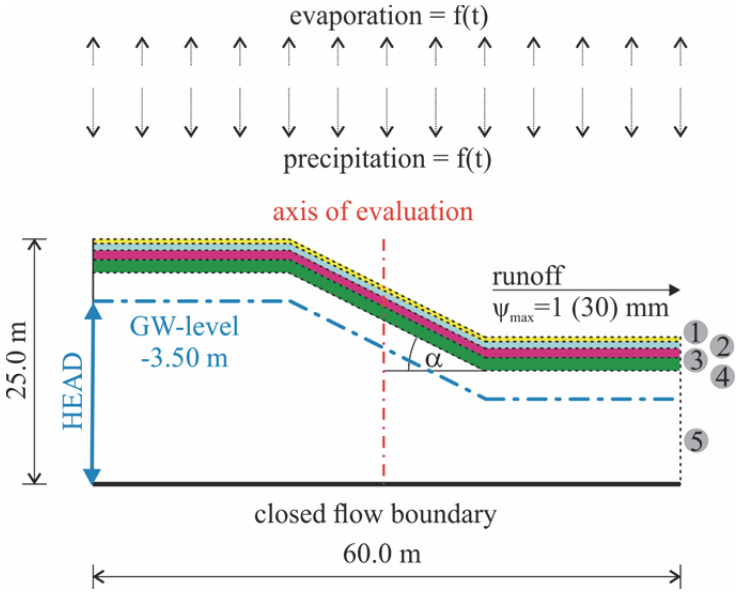

Fig. 79: Geometry and boundary conditions of the benchmark slope

7.1.2 Hydraulic properties

Local heterogeneities and preferential flow paths play a very significant role in a soil's permeability, even for the same general soil types, the permeability can vary significantly (Kawamoto et al. 2004). Due to preferential flow paths, rainwater can infiltrate into underlying, initially unsaturated soil layers which then leads to an increase in their degree of saturation and/or a rise of the groundwater table (Springman et al. 2013). Additionally, the relative density of the soil has an influence on its saturated permeability. Thus there is in general a high degree of uncertainty regarding the determination of the saturated hydraulic permeability. Therefore, in addition to the analyses with the original, right next to the Lysimeter measured values for the saturated hydraulic permeability, a study with changed values for k_{sat} $(= k_{ref})$ has been performed, in order to determine the influence of k_{sat} itself. This was done by reducing the hydraulic permeability by two orders of magnitude ("$k_{ref}/100$"), and the results are presented later in this chapter.

If a soil body is not able to take up the water from the applied precipitation, run-off will take place. In a numerical analysis, the ψ_{max} parameter (usually a positive number) controls the maximum allowable pore pressure head (relative to the elevation of the boundary to which it is applied). When the groundwater head rises above this user-defined level ($y+\psi_{max}$, thus above the ground level), the infiltration volume changes into that head level, and as that water level is then higher than the ground level, it must flow away, and thus run-off is simulated. In the course of this study, the ψ_{max} parameter was varied between 1 mm (to simulate that nearly all the water runs off if infiltration is not possible, e.g. if there is hardly any vegetation on the surface and it is very smooth) and 30 mm (to simulate almost no run off and a considerable amount of water acts as an additional surcharge on the upper model boundary).

The ψ_{min} parameter (usually a negative number) defines the minimum pore pressure head, relative to the elevation of the boundary to which it is applied, and is used where negative precipitation (evapotranspiration) should be allowed. Once the groundwater head falls below this user-defined level ($y+\psi_{min}$), the evaporation discharge (negative precipitation) stops and changes into that head level. Within the present slope analyses, this parameter was kept constant at -10.0 m. This means, that at each boundary to which it was applied, the increase of suction due to evaporation is limited to 100 kPa. It has to be mentioned, however, that suction is not influenced by this parameter at boundaries where the suction (before the fully-coupled flow-deformation analysis) was initially higher (e.g. due to steady state groundwater-flow analysis). Nevertheless, low to no precipitation phases within a climatic hydrograph could create such dry conditions which could lead to suction values below this limitation. From that moment on, suction is, as with the previously higher initial positive pore pressures, now limited by the ψ_{min} parameter.

In the present study, several different groundwater-flow boundary conditions have been used. As illustrated in Fig. 79, the closed flow boundary is assigned to the bottom boundary of the model in all the presented analyses, and consequently no water can pass through it. This refers not only to groundwater flow, but also to the dissipation of excess pore pressure. The constant “head” on the left indicates permanent natural groundwater flow into the left hand side of the numerical model. In order to ensure free water in- or outflow at the right hand side model boundary, a so called “seepage” boundary is assigned to it. In order to guarantee possible in- or exfiltration of water due to the assigned climatic hydrograph, a “seepage” condition is assigned to the upper model boundary.

7.1.3 Influence of the climatic hydrograph

The effects of different climatic hydrographs are analysed in this study. The weather station right next to the Lysimeter mentioned in chapter 5 provides real-time information about precipitation and evapotranspiration rates which can be directly implemented as a reliable dataset in the numerical analyses. Although no real slope exists near the Lysimeter, the weather and Lysimeter data are still used for the purpose of this study of a theoretical slope. The longest “continuous” dataset, where at least one tensiometer was working, had a duration of 192 days (*01/10/2013-10/04/2014).* In order to check the impact of the rainfall-dataset itself, additional studies with artificial, theoretical hydrographs (e.g. cutting out certain rainfall peaks or using average annual precipitation sums) have also been performed.

It is well known that antecedent rainfall has an influence on the current pore water pressure distribution in the soil before the rainfall event of interest takes place. To take this into account, the first 120 days of the longest related rainfall period (*01/10/2013-28/01/2014)* were applied twice, one after another.

The climatic hydrographs used in the analyses are indicated in their corresponding results graphs (Fig. 81 to Fig. 87, Fig. 89, Fig. 90). It is obvious, that this assumption of repeating a real dataset is purely hypothetical, but it allows for the possible effects of previous climatic conditions. Generally, the better the resolution of the provided data, the better the possibility to match the predicted (by the FE method) pore water pressure development. However, due to the necessity of the analyses to use very fine meshes and to perform fully-coupled flow-deformation calculations, a high resolution of input, by means of minute by minute or hourly data, would lead to a much too high calculation effort. As the observation periods of the measured data are quite long (192 to 240 days), the daily sum data was chosen as input data and considered to be of sufficient resolution.

Fig. 80 shows two options of applying a climatic hydrograph in PLAXIS 2D. The variant at the top of Fig. 80 is schematically describing the "stepwise" application of rainfall, which best represents daily sum data (which is either positive for precipitation, or negative for evapotranspiration). The second option, illustrated at the bottom of Fig. 80, shows the application of rainfall by means of "Δdischarge", applying an increase or decrease of rainfall with time which may not represent real conditions. As the net precipitation is not the same between these two options, in order to correctly model the environmental conditions, a careful shape definition of the climatic hydrograph dataset is necessary. It must be noted, however, that operators of weather stations usually provide rainfall data in terms of measured rainfall within a defined period, which fits better to the stepwise application of climatic hydrograph, and it is the stepwise application that has been used here.

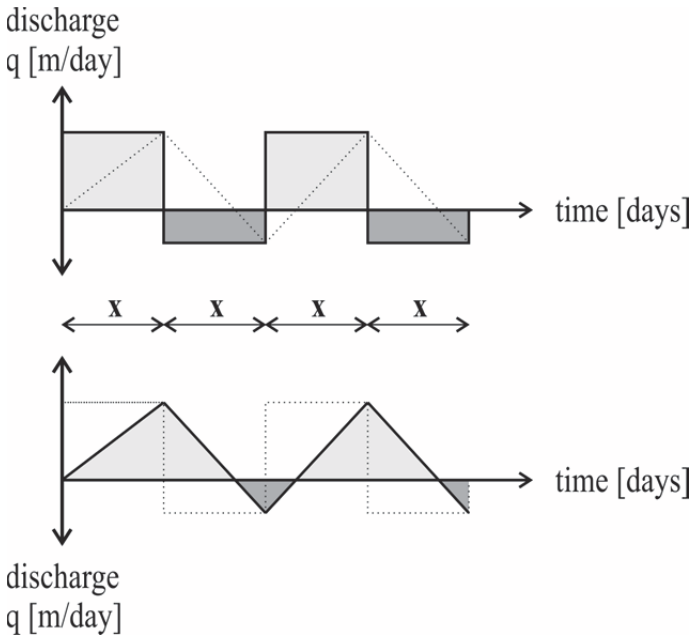

Fig. 80: Schematic description of two options of climatic hydrograph application in PLAXIS 2D

7.2 Results of the benchmark slope analyses

In this section, the results of the calculations considering various boundary conditions are presented. Crucial model boundary conditions and parameter values for worst-case scenarios could be identified. An explanation of the abbreviations used in naming the various calculations is given in Tab. 7.

Tab. 7: Abbreviations for the benchmark slope analyses

M	***192***	***20***	***k_{ref}/100***	***psi_1***
Initial suction	Climatic hydrograph	Depth	Permeability	Run-off
model M	192 days	20 cm	k_{ref}; k_{ref}/10; k_{ref}/100	1 mm
model A	120 + 120 days	50 cm		30 mm

The example given in the top line of Tab. 7 represents the name of the result for the calculation done by using the manually ("model M") generated initial suction, by applying the "climatic hydrograph" which lasts 192 days, for the evaluation which took place at the "20 cm" depth, by using the reduced saturated hydraulic permeability "*k_{ref}/100*" (see 7.1.2) and by setting the run-off criteria ψ_{max} to 1 mm.

7.2.1 Results of k_{ref}

The following Fig. 81 shows the results, when the original values for saturated hydraulic permeability (k_{ref}) have been used in the calculations. Although in these analyses the in-situ measurement data from the Lysimeter with respect to initial conditions and the climatic hydrograph are used, the change in suction cannot be compared to the field data anymore because the problem is no longer one-dimensional, even though the differences in the middle of the slope turned out to be not significant.

The numerical results are evaluated at stress points at 20 and 50 cm depth on the vertical cross section through the middle of the slope (see Fig. 79).

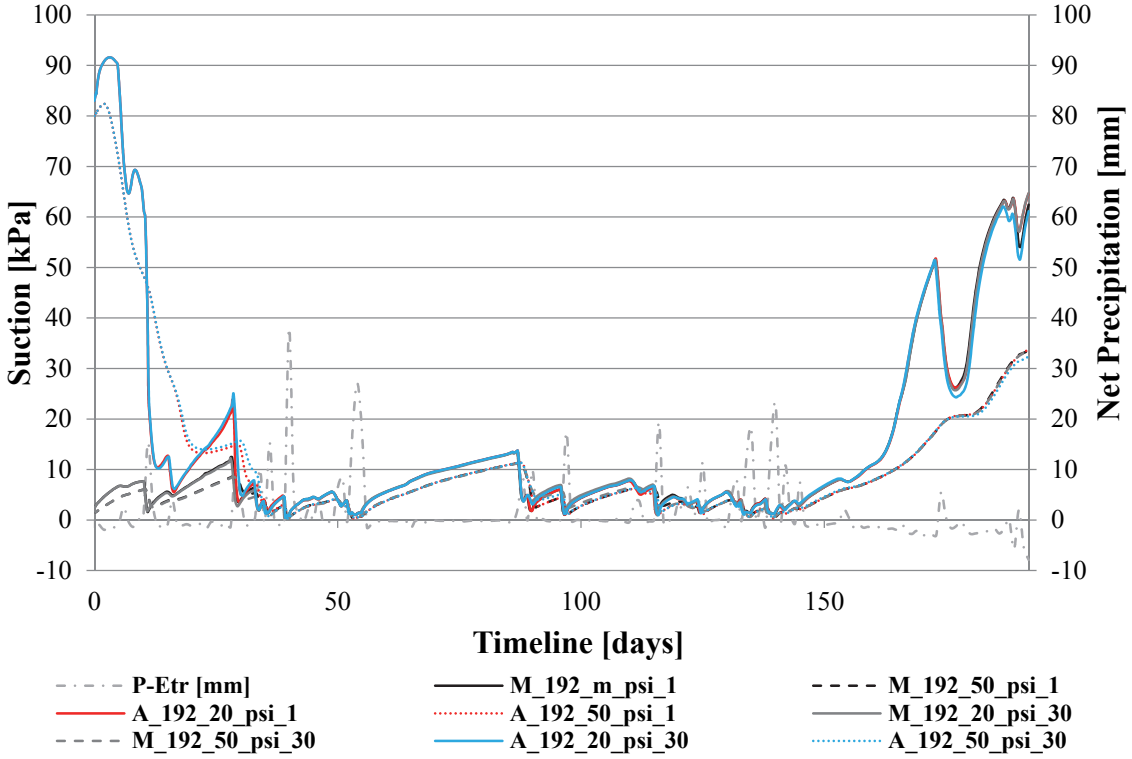

Fig. 81: ψ_{max} – k_{ref}: Results of suction development over time (192 days)

The grey dash-dotted line ($P\text{-}ET_r$) indicates the applied climatic hydrograph in Fig 80 and in the following figures of this chapter. Due to high suction values and, in drier periods, the accompanying temporary breakdown of the tensiometers, due to cavitation, in near surface areas, there are only a few measured data points at 20 cm depths available.

As rainfall events lead to decreasing, and drier periods to increasing, suction values, the "model M" results show the expected suction reaction to the applied climatic hydrograph. Due to the location of the groundwater-level and as a result of the steady-state analysis in the initial phase, the "model A" curves start with much higher suction values in the corresponding depths at a vertical cross-section through the middle of the slope. The red full line represents the results at the 20 cm depth and the red-dashed line at the 50 cm depth.

As previously mentioned, the focus of the present studies lies on the quantification of the influence of initial conditions on further results. The application of this specific climatic hydrograph, in combination with the relatively high saturated permeability of the upper soil layers, leads to sharp drops in suction under stronger rainfalls, especially in the first 40 days of the analysis. After this period, both the "M" and "A" model curves match for the first time (see Fig. 81). Since, except of the initial pore-water-pressure-profile, both models use identical SWCC boundary conditions, their suction development has to also be identical. This explains to multiple overlaps in the lines of Figure 80.

The variation of ψ_{max} from 1 mm to 30 mm, which is used to link possible vegetation and the smoothness of the surface to run-off (see chapter 7.1.2), was analysed. Under the circumstances shown in Fig. 81, the calculations results showed no significantly different results due to this parameter variation.

Due to the sharp drops noticed in the suction at days with high rainfall rates, an investigation was done into the effect on suction of an adapted climatic hydrograph. An artificial climatic hydrograph was created based on the one used in Fig. 81, by cutting away the "rainfall peaks" (larger 15 mm/day) and limiting the daily sum to 15mm/day. This change led to negligible changes in the results and is therefore not discussed in detail here.

An additional analysis was executed to highlight the importance of knowing where the initial groundwater level is located. The initial groundwater-level was positioned to 7.0 m below the surface of the slope, which is 3.5 m lower than in the previous analyses. Comparable to the results of the previously described procedure of "cutting of rainfall peaks", this procedure led to marginal changes in the results (see Fig. 82). It is obvious, that the deeper groundwater-level leads to higher initial suction values, but both "model A" curves show a generally comparable behaviour (and when compared to Fig. 81, the suction curves are simply shifted by the difference in initial suction at the beginning). However, under these given boundary conditions, all curves follow virtually the same line after approximately 40 days, which is the point in time where suction is zero for all assumptions of initial conditions.

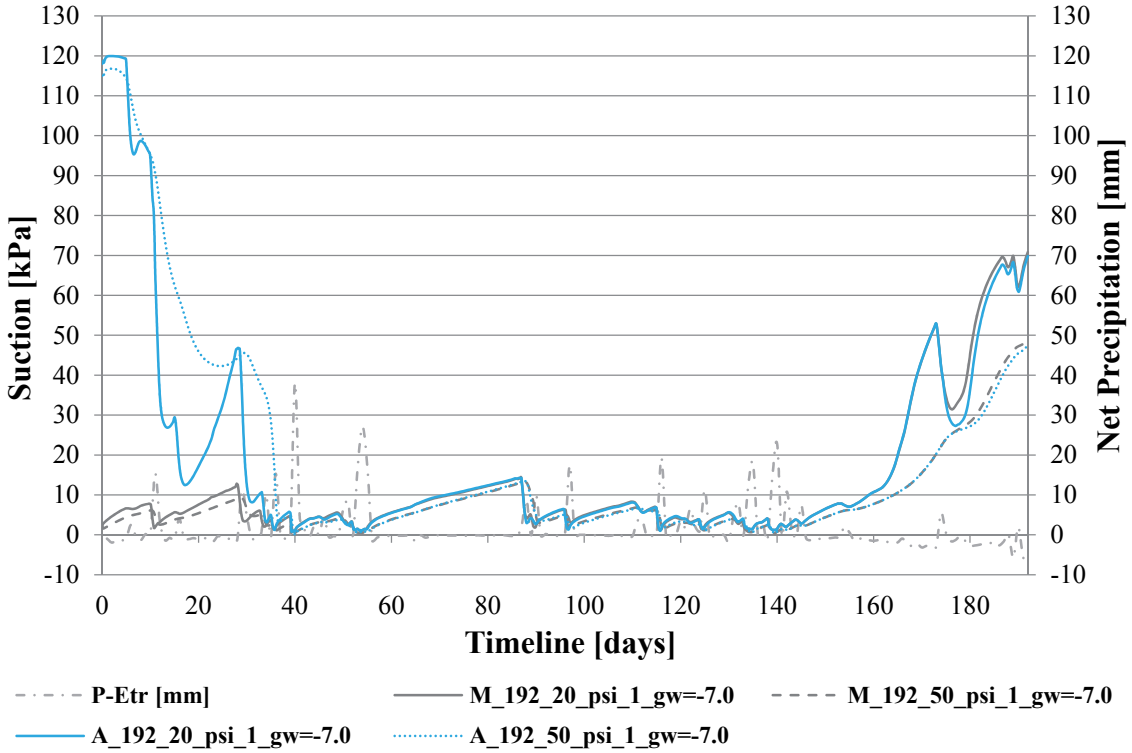

Fig. 82: gw = -7.0 m – k_{ref}: Results suction over time (192 days)

7.2.2 Results of $k_{ref}/100$

In this chapter it is assumed that the saturated permeability of each layer is divided by 100 (see Chapter 7.1.2). In comparison to the calculations with the original saturated hydraulic permeability k_{sat} (=k_{ref}), the results on suction change significantly.

As in the previous chapter 7.2.1, Fig. 83 shows the difference in results between "model A" and "model M" and the variation of ψ_{max} from 1 mm to 30 mm. As depicted in Fig. 83, even by assuming these low permeabilities ($k_{ref}/100$), all the "model M" curves, with their low initial suction values, show comparable results regardless if the runoff criteria ψ_{max} was set to 1 mm or to 30 mm.

Under these circumstances, none of the "model A" curves even reach the low suction levels, unlike the "model M" results; the evaluation of suction in the stress points in 50 cm depth (for "model A" curves) did not even show any significant suction changes within the 192 days modelled. For "model A", the near surface area (20 cm depths) experienced a continuous decrease in suction throughout this analysis. The calculations with higher ψ_{max} boundary condition (30 mm) showed this behaviour even more clearly, but did not come close to the results from the equivalent "model M" line within the 192 days.

Although a reduction in k_{sat} by a factor of 100 (=$k_{ref}/100$) is an extreme case, it is chosen here to emphasize the importance of having an appropriate estimate of k_{sat}.

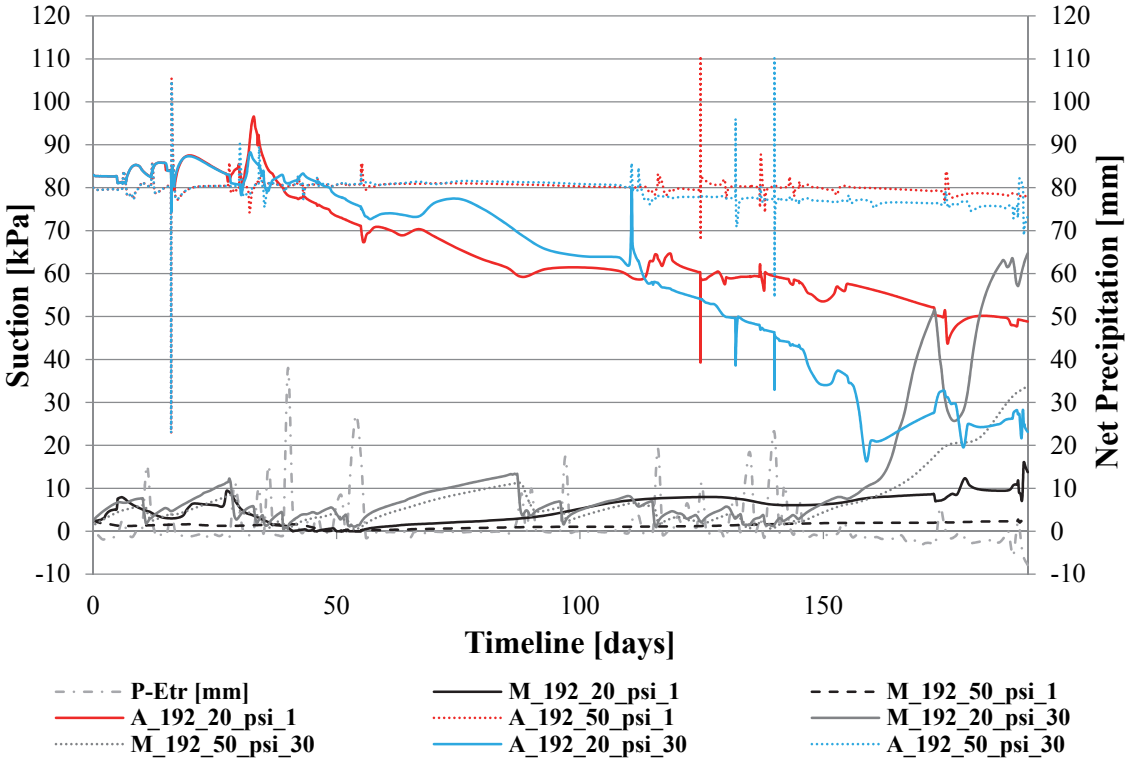

Fig. 83: $\psi_{max} - k_{ref}/100$: Results suction over time (192 days)

As with the calculations with higher saturated permeabilities presented in the last section, also here, with these lower saturated permeabilities, the effects of an adapted climatic hydrograph (where rainfall peaks larger than 15 mm/ day have been cut out) was investigated. For all the "model M" and the "model A" calculations, this modified precipitation input had no effect on the results evaluated in 50 cm depth. At the 20 cm depth in "model A" calculation, there are only marginal changes in the results due to this procedure. Due to these outcomes, the results are not further presented in this contribution.

The investigation into the effect of a lowered initial groundwater-level (-7.0 m) was also done here for the lower saturated permeability ($k_{ref}/100$) scenario. As depicted in Fig. 84, this procedure hardly had any influence on any of the "model M" results. However, at the higher suction ranges of the "model A" results, the results are significantly affected by the location of the groundwater-level. After the intense rainfall events at around day 40, the trend of decreasing suction of the "model A" variations (see Fig. 83) splits up in this case, the suction at 20 cm depth continuing to decrease, while the suction values remain similar at 50 cm depth.

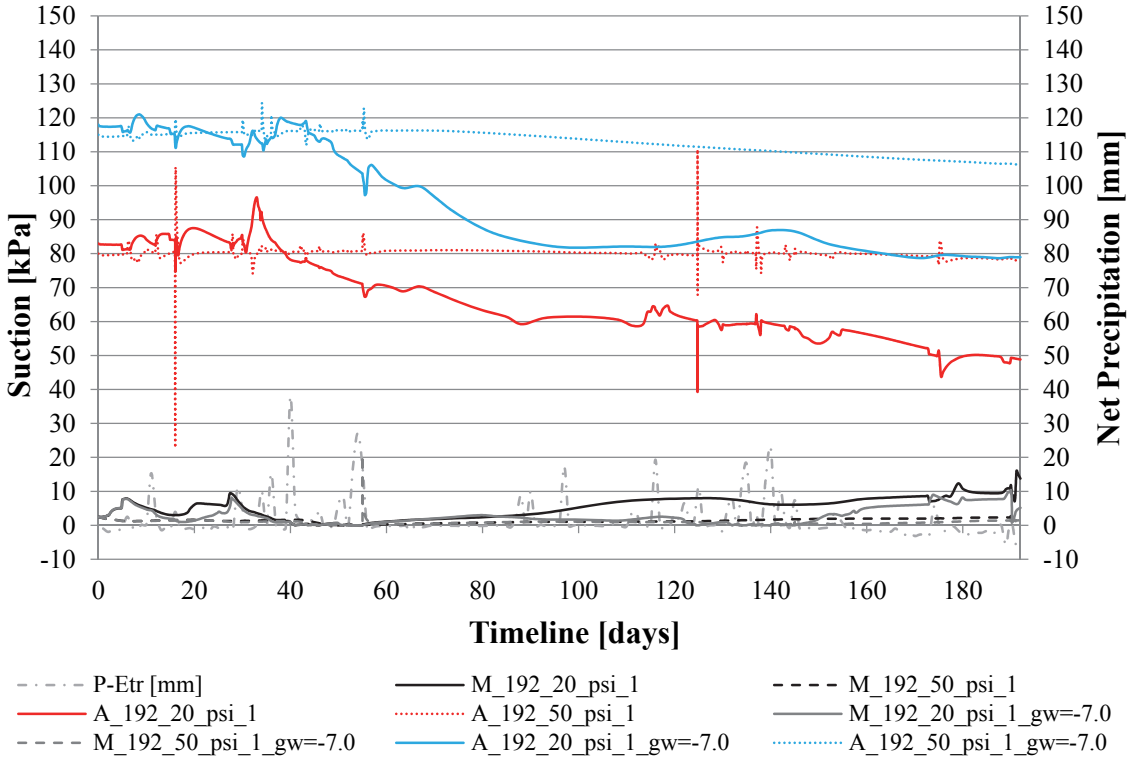

Fig. 84: gw = -7.0 m – k_{ref}/100: Results suction over time (192 days)

As there are still differences in the resulting pore water pressure profile between both variants ("model M" and "model A") at the end of the modelled 192 days in most of the analyses, the influence of repeating the first 120 days of the rainfall dataset was analysed in order to quantify the importance of antecedent rainfall events. Fig. 85 depicts the results for different run-off criteria (ψ_{max} = 1 or 30 mm) and the adapted 240 days ("120-120") climatic hydrograph. The "model A" results at 50 cm depth did not show any suction decrease by applying the first 120 days twice in a row. At 20 cm depth, there is a difference between the two "model A" results, with the higher ψ_{max} parameter (ψ_{max} =30 mm) line showing a sharp drop, followed shortly after by a significant increase in suction the end of the applied dataset. The "model M" calculations start with low initial suction values and the results show the expected behaviour of only minor differences in the suction developments with time.

For the sake of completeness, the influence of "cutting out rainfall peaks" was also analysed for this 240 days climatic hydrograph. Except for slight changes in the "model A" results at 20 cm depth, the results are similar to those illustrated in Fig. 85 and are therefore not separately illustrated.

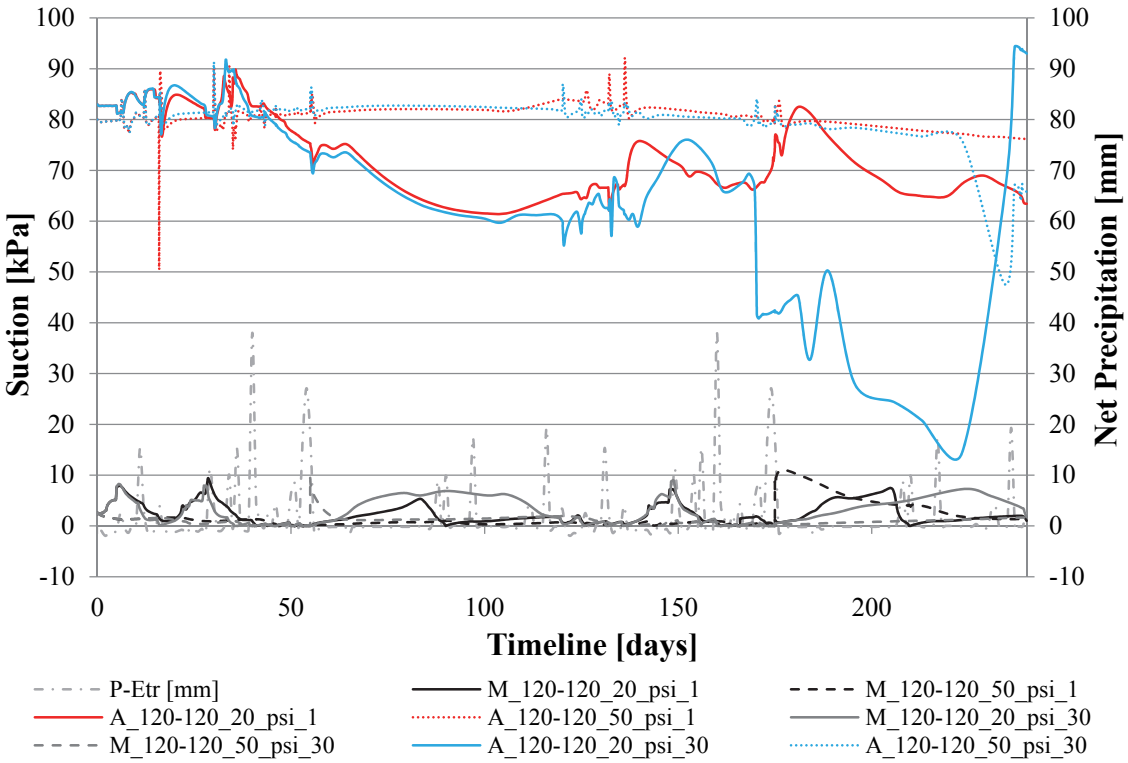

Fig. 85: ψ_{max} – k_{ref}/100: Results suction over time (240 days)

7.2.3 Variation of k_{ref}

In order to better highlight the influence of the saturated permeability used in the calculations, Fig. 86 shows the development in suction of "model A" calculations at depths of 20 cm and 50 cm, for three saturated permeability variants (k_{ref}, $k_{ref}/10$ and $k_{ref}/100$). The 192 day climatic hydrograph is applied and the run-off criterion ψ_{max} = 30 mm is kept fixed.

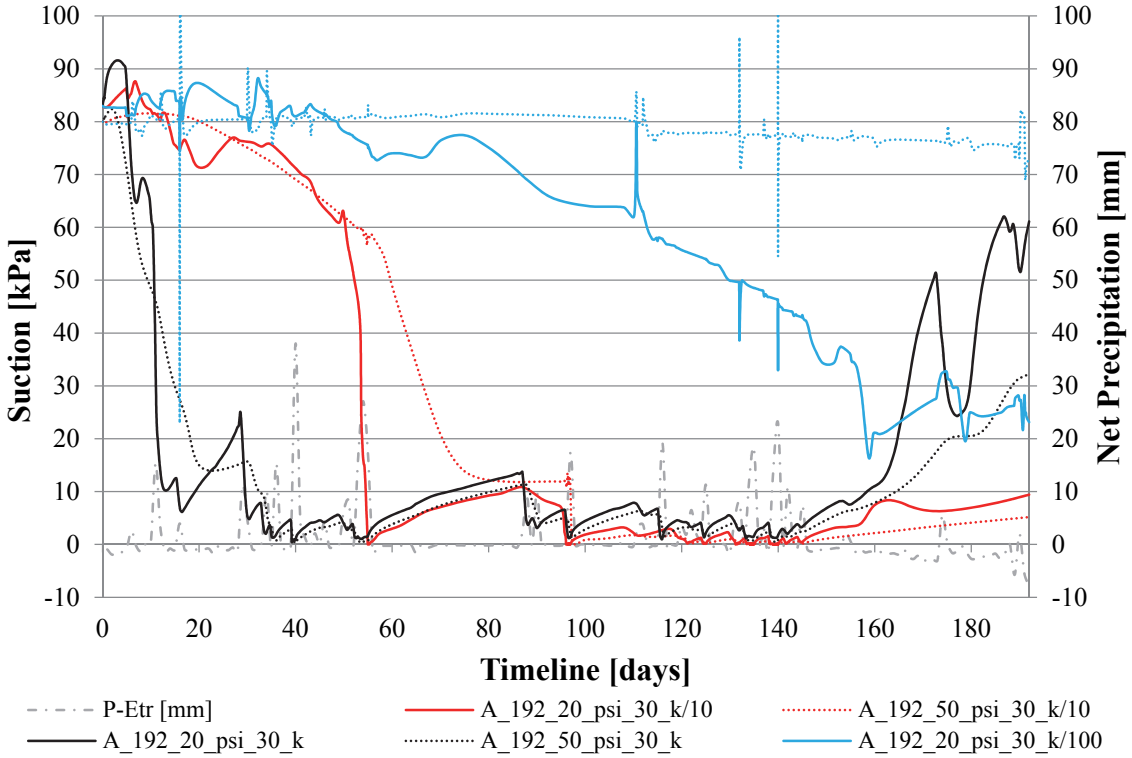

Fig. 86: Development of suction; k_{ref} vs. $k_{ref}/10$ vs. $k_{ref}/100$; model A; ψ_{max}= 30 mm

Generally, the results show the expected behaviour of earlier drops in suction when using k_{ref} and later and slighter decreases in suction when using $k_{ref}/100$ as the saturated hydraulic permeability. Under application of $k_{ref}/100$, suction did not decrease to zero in either depth considered. The stress point at 50 cm depth (dotted blue line) did not even undergo any significant change in suction during the 192 days.

The analysis using an intermediate $k_{ref}/10$ delivered results in between the two variations mentioned above. It stands out, however, that once suction reaches zero in both depths in the calculation using $k_{ref}/10$, the suction values stay lower compared to the equivalent analysis using k_{ref}. As it is generally expected that a lower saturated permeability would lead to higher suction levels, rather than lower ones, the following chapter 7.2.4 discusses the reasons for this kind of behaviour.

7.2.4 Discussion on $k_{ref}/10$

In order to clarify the relatively low suction values of the case of the $k_{ref}/10$ analysis as indicated in Fig. 86, Fig. 87 illustrates the development of the effective degree of saturation S_{eff} (see Equation 35) over time when using either k_{ref} or $k_{ref}/10$ in the numerical analyses.

$$S_{eff} = \frac{(S - S_{res})}{(S_{sat} - S_{res})} \tag{35}$$

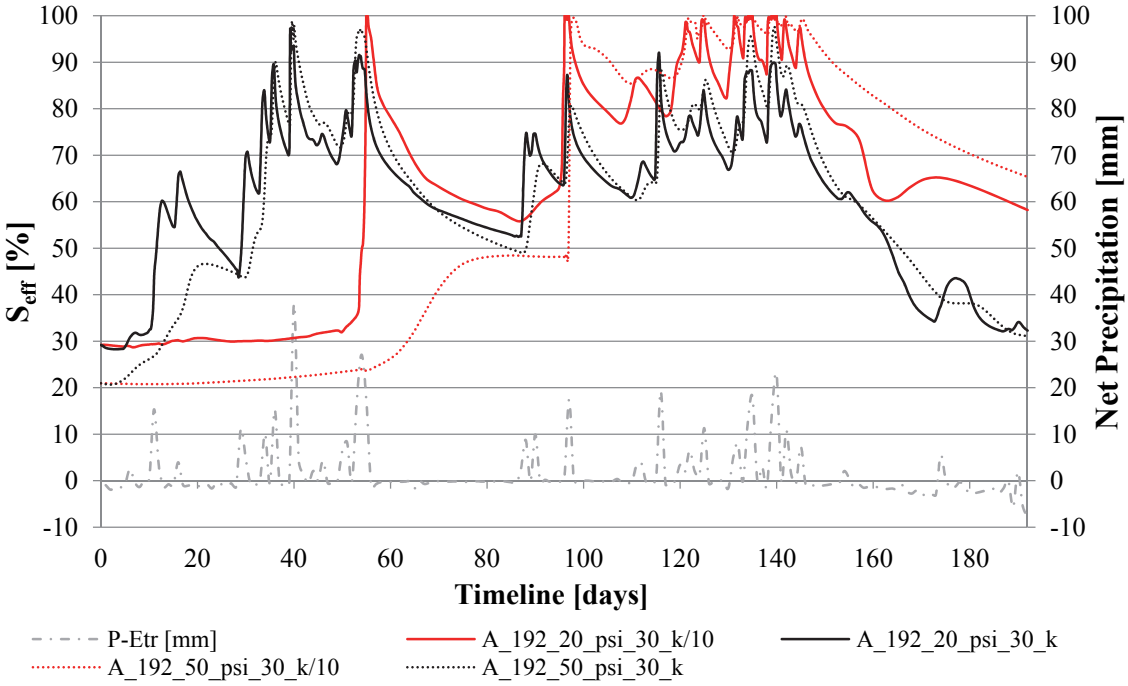

Fig. 87: Development of S_{eff}; k_{ref} vs. $k_{ref}/10$; model A; ψ_{max}= 30 mm

The point when suction equalled zero in Fig. 86 was around day 40 when using k_{ref} and approximately day 55 when using $k_{ref}/10$ in the numerical analyses. The higher permeability (k_{ref}) led to a higher infiltration rate at the high saturation ranges, but also led to a faster decrease in saturation after heavy rainfall events have been over. At 20 cm depth, the effective degree of saturation remains relatively high for a longer time after full saturation is reached in the $k_{ref}/10$ calculation, as compared to the calculations using k_{ref} after the rainfall event stopped. As the SWCC relates the degree of saturation to suction, the lower suction values which developed are a logical outcome of higher saturation. The generally higher level of saturation throughout the $k_{ref}/10$ variation makes it more sensitive to erratic and fast rises in saturation when heavy rainfall events take place.

From another perspective, Fig. 88 shows the corresponding (absolute) groundwater flow $|q|$ in stress points at 20 and 50 cm depths. Each peak in groundwater flow is attributed to heavy rainfall events with an associated increase in the effective degree of saturation.

It must be noted, however, that the saturated permeability also influences the development of suction in periods where no external water is applied to the system and solely the current degree of saturation defines the water flow rate inside the slope.

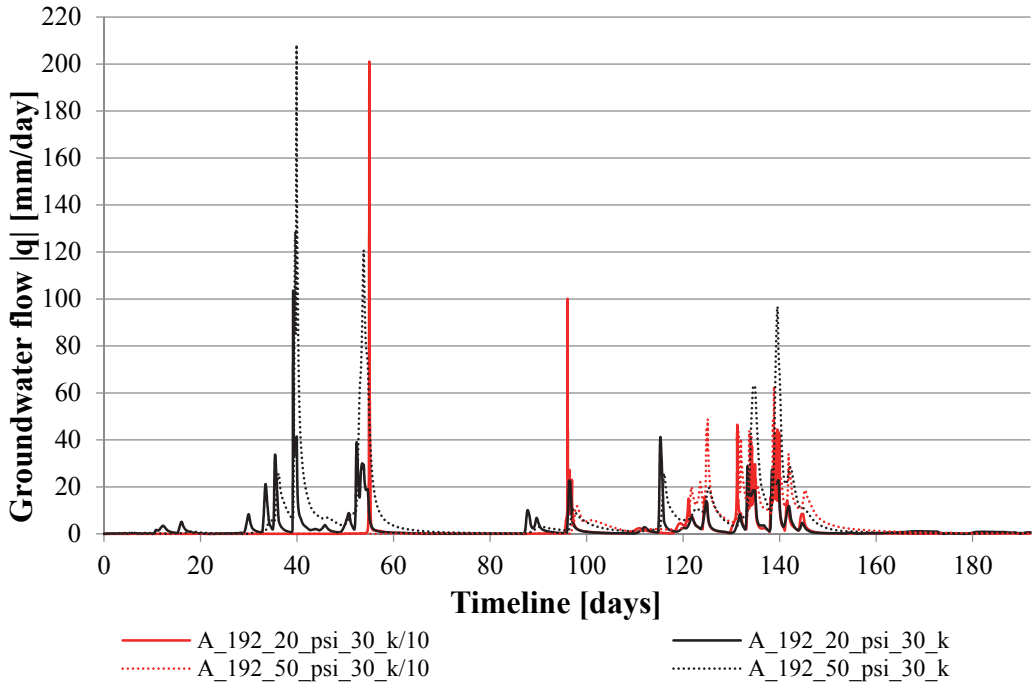

Fig. 88: Groundwater flow q; k_{ref} vs. $k_{ref}/10$; model A; ψ_{max}= 30 mm

7.2.5 Results using average constant precipitation

As a matter of interest, the influence of constant precipitation was investigated. To do so, the total rainfall sum of the 192 day climatic hydrograph, used in the calculations previously described in this chapter, was divided by 192 in order to get an average and constant precipitation rate. It is obvious that this procedure is purely theoretical, but could represent a worst case scenario, as there is then never any break in rainfall. Even though the total amount of applied rainfall remains unchanged, the continuous application of rainfall with a very low rate of approximately 1.38 mm /day led to a strong decrease in suction with time when the initial pore water pressures have been generated automatically. Fig. 89 illustrates the development of suction under the constant averaged climatic hydrograph and using the originally measured saturated hydraulic permeability (k_{ref}).

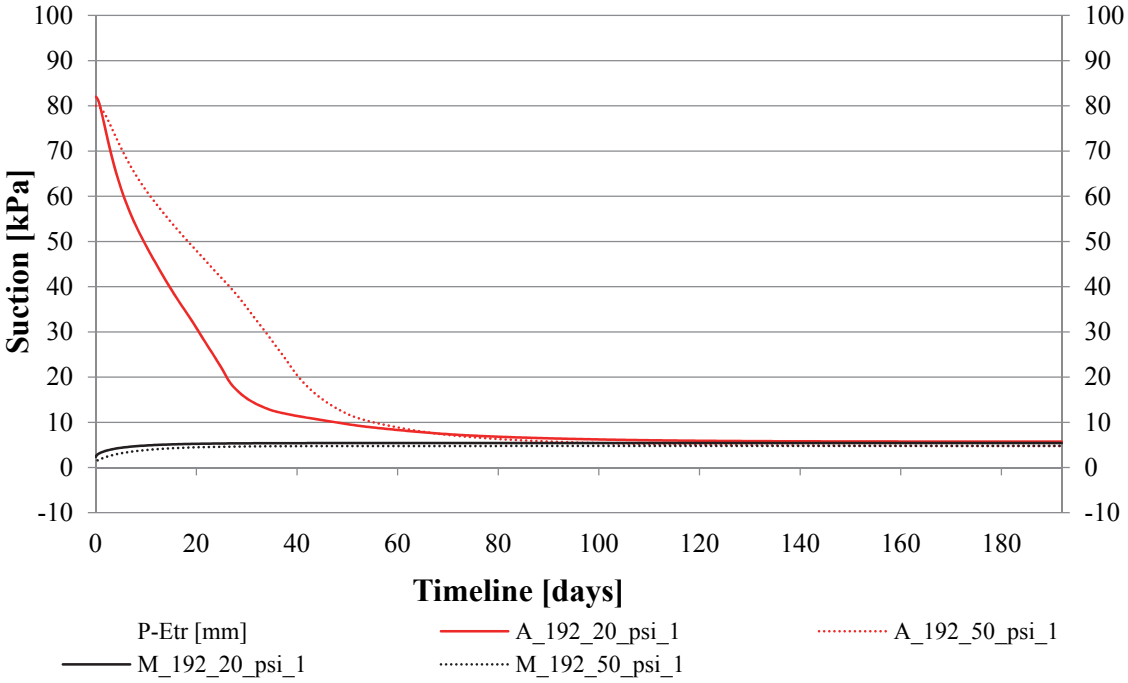

Fig. 89: Suction development under constant averaged climatic hydrograph; 1.38 mm/day; 192 days; k_{ref}

Because the applied precipitation rate is smaller than the (saturated) permeability of the soil, there is always, in both investigated variants, some suction remaining in the soil. It stays almost constant at about 5 kPa at all depths for all the investigated options during the 192 days considered.

Fig. 90 shows the suction development under constant averaged climatic hydrograph using the lower saturated permeability of $k_{ref}/100$. In this case, the average constant rainfall rate is larger than the upper soil layers permeability.

As expected, in the calculations starting with low manually defined suction values ("model M"), suction disappeared within the first couple of days, whereas the calculations with the significantly higher automatically generated initial suction values ("model A") experienced no suction reduction within the first ~ 40 (at 20 cm depth) or ~140 days (at 50 cm depth) of the applied climatic hydrograph.

For the calculation with automatically generated initial suction values, the lower suction decrease in the near surface stress point at 20 cm depth is (most likely) due to a continuous increase in saturation as a consequence of the applied climatic hydrograph. The sharp drop in suction at 50 cm depth (red dotted line) is due to a very fast rise of the groundwater table in the area of the corresponding stress point. As this fully saturated water front reaches this area, the degree of saturation increases rapidly to fully saturated conditions, whereas suction drops to zero.

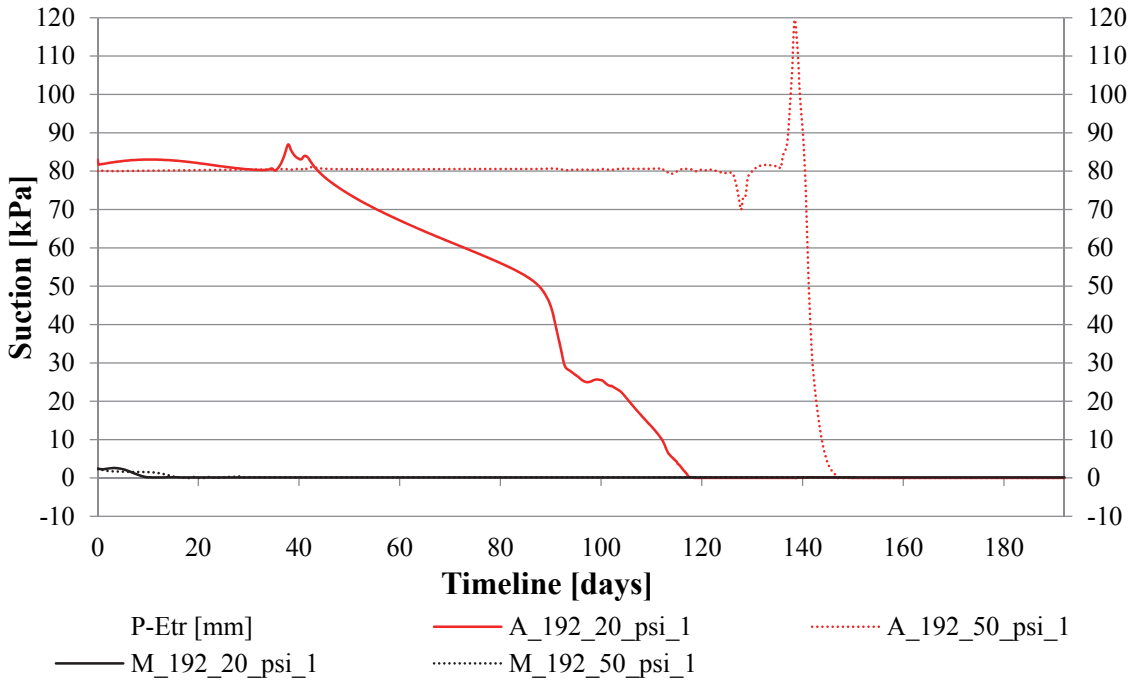

Fig. 90: Suction development under constant averaged climatic hydrograph; 1.38 mm/day; 192 days; $k_{ref}/100$

7.3 Safety calculations on benchmark slope

This chapter presents the results of safety calculations on the benchmark slope and discusses the effects of different assumptions concerning the role of suction within the phi-c-reductions used to determine FoS, which have been investigated in this numerical study.

The finite element code PLAXIS 2D (Brinkgreve et al. 2017) allows the user to take into account suction in either all or only selected calculation phases. In this study, three different options have been investigated:

- Suction in all phases
- Suction in all phases except of the “Safety”- phase
- No suction in any phase

It must be noted that the “ignore suction” option is always activated in the initial phase when using PLAXIS 2D. Furthermore, changing from a situation with suction to a situation without suction is physically not realistic and creates a numerical imbalance and is therefore not recommended. When the software code tries to solve this imbalance, it can lead to unrealistic additional deformations, excess pore pressures and stresses. To counter this, the user has to add a plastic nil step (phase), where large out-of-balance forces are solved and equilibrium is restored.

Since it is such a common situation for users to run a safety phase without suction following some calculation phases that included suction, PLAXIS has automatically build in a solution: any imbalance created due to changing from phases with suction to no suction is first solved before the factor of safety is determined in the factor of safety analysis phase. Consequently, it is not necessary for the user to implement a plastic nil step in the safety calculations as it is already part of the safety analysis (Brinkgreve et al. 2017).

As suction is an insoluble part of the coupling between deformations, pore pressure and groundwater flow, a fully coupled flow-deformation analysis will always take suction into account. Thus when using fully coupled flow-deformation analysis as part of a model, it is best practice to take suction into account for all calculation phases.

In order to calculate the factors of safety and to keep the calculation effort to a reasonable level, the following two options have been investigated:

- Determination of the FoS after "day 40" of the 192 day climatic hydrograph, taking all the previous 39 days of precipitation and numerical calculations into account (results in 6.3.1)

- Determination of the FoS after a direct application of the heavy rainfall event of "day 40", without taking into account the previous 39 days of the climatic hydrograph and thus also no previous numerical calculations (results in 7.3.2)

The climatic hydrograph with the aforementioned options highlighted is illustrated in Fig. 91.

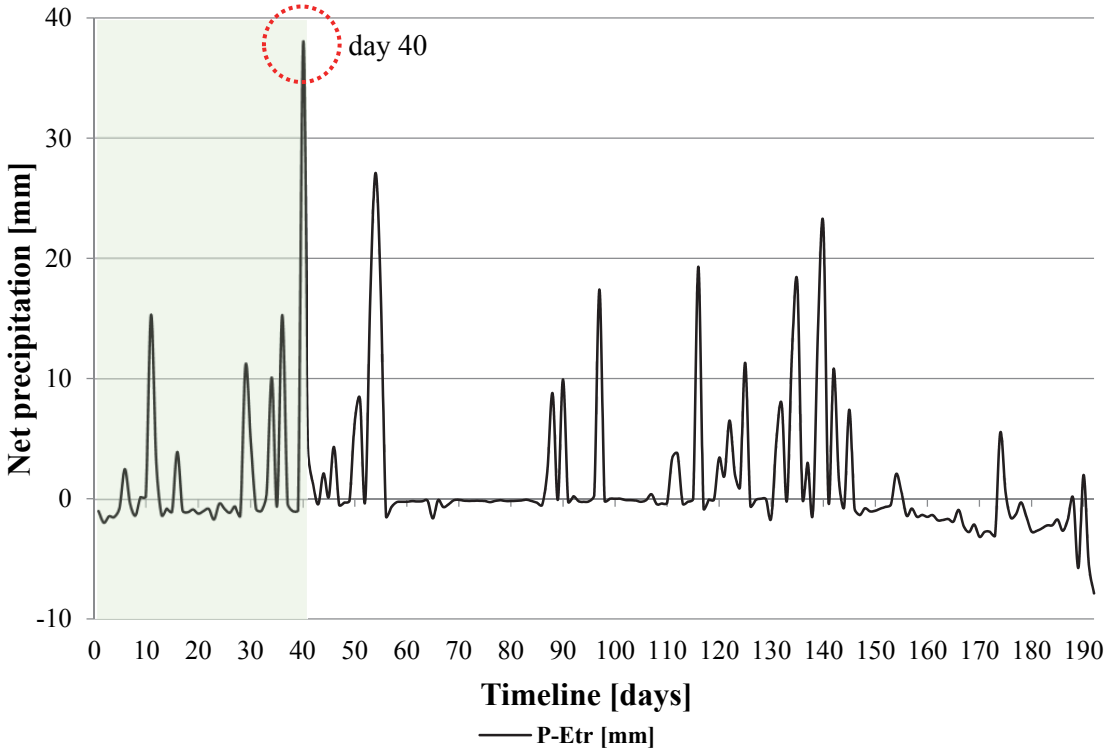

Fig. 91: Applied climatic hydrograph for the safety analysis investigation highlighting 1 day of heavy rainfall or the first 40 days of precipitation

The results show that executing a phi-c-reduction to determine the FoS (see 3.7.2), directly after the initial phase with the three suction options led to significant differences in the resulting factors of safety. The comparison between the option “suction in all phases” and the option “no suction in any phase” shows the expected: a higher FoS when suction was taken into account. However, neglecting suction only in the safety phase (the “suction in all phases except the safety phase” option) delivers an unrealistically high factor of safety. The failure mechanisms by means of incremental deviatoric strains for the three options are plotted in Fig. 92.

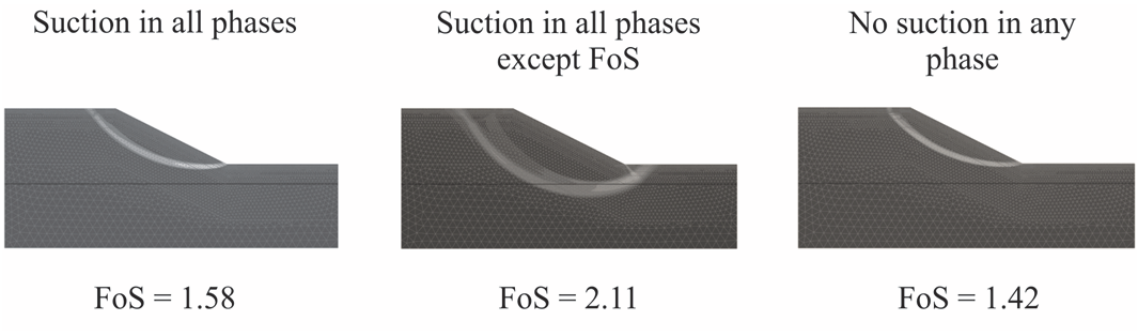

Fig. 92: Incremental deviatoric strains as a result of phi-c-reduction directly after initial phase as failure mechanism to show FoS

In order to investigate the general behaviour of the stresses during the calculations, stresses have been evaluated at certain stress points right before and after the numerical phi-c-reduction. To make this assessment of stresses more meaningful, two independent stress points ("Stress point A" and "Stress point B") are located in completely different areas of the slope as schematically indicated in Fig. 93. The results for "Stress point A" and "Stress point B" are given in Tab. 8 and Tab. 9, respectively.

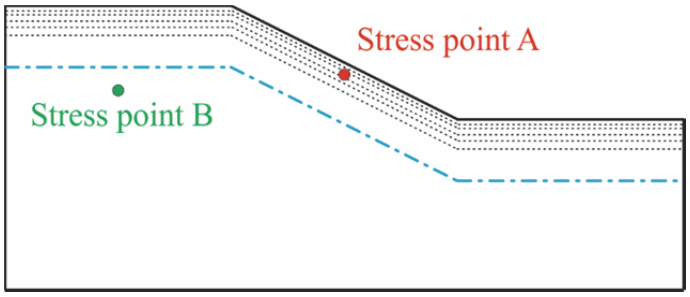

Fig. 93: Location of independent stress points used in comparative investigations

The resulting stresses indicate that the initial suction in the option "Suction in all phases except of FoS" is directly transferred into volumetric stresses *p'* (see Equation 36 for definition) during the safety calculation. This means an increase of *p'* and the Mohr's circle shifts to the right side during the execution of a numerical phi-c-reduction with PLAXIS 2D. Thus, a deeper slip surface failure mechanism, which is no longer comparable to the other two options, develops (see Fig. 92, centre).

$$p' = \frac{(\sigma_1' + \sigma_2' + \sigma_3')}{3} \tag{36}$$

Tab. 8: "Stress point A" – comparison of stresses before and after the phi-c-reduction for various suction options

Suction option	Suction in all phases		Suction in all phases except of FoS		No suction in any phase		[Unit]
FoS initial	**1.584**		**2.11**		**1.423**		[-]
	Initial phase	After safety phase	Initial phase	After safety phase	Initial phase	After safety phase	
Suction	76.235	76.235	76.235	0	0	0	[kPa]
σ_1'	-46.183	-35.587	-46.183	-133.34	-32.247	-14.883	[kPa]
σ_2'	-32.548	-32.622	-32.548	-86.68	-14.843	-6.689	[kPa]
σ_3'	-27.556	-23.873	-27.556	-86.613	-10.160	-4.228	[kPa]
p'	-35.429	-30.694	-35.429	-102.211	-19.083	-8.600	[kPa]
q	16.700	10.549	16.700	46.694	20.158	9.663	[kPa]

Tab. 9: "Stress point B" – comparison of stresses before and after the phi-c-reduction for various suction options

Suction option	Suction in all phases		Suction in all phases except of FoS		No suction in any phase		[Unit]
FoS initial	**1.584**		**2.11**		**1.423**		[-]
	Initial phase	After safety phase	Initial phase	After safety phase	Initial phase	After safety phase	
Suction	89.372	89.372	89.372	0	0	0	[kPa]
σ_1'	-81.930	-80.907	-81.930	-178.577	-76.559	-75.807	[kPa]
σ_2'	-40.276	-42.94	-40.276	-120.781	-36.800	-38.844	[kPa]
σ_3'	-33.143	-41.780	-33.143	-118.777	-28.585	-35.175	[kPa]
p'	-51.783	-55.209	-51.783	-139.379	-47.315	-49.942	[kPa]
q	45.641	38.560	45.641	58.823	44.44	38.927	[kPa]

7.3.1 FoS after a heavy rainfall event taking previous precipitation into account

The quantification of the influence and development of suction under various precipitation datasets was declared to be a major aim of this contribution. As precipitation is numerically applied to a fully coupled flow-deformation analysis which always takes suction into account, the suction option "no suction in any phase" has no longer been investigated.

Tab. 10 presents the FoS calculated after "day 40" of the 192 days climatic hydrograph, based on automatically generated initial pore water pressures ("model A") and taking the previous 39 days into account. The FoS are significantly reduced after 39 days of the applied precipitation, when compared to the initial FoS, for all the three saturated permeabilites (k_{ref}, $k_{ref}/10$, $k_{ref}/100$) conditions analysed. The application of the heavy rainfall of "day 40" led to a further, but moderate, decrease in the factor of safety in all the analyses. Neglecting suction in the safety phases led to considerably higher initial FoS but qualitatively showed the same behaviour, with a strong drop in FoS after the application of the 39 days of the climatic hydrograph. By neglecting suction in safety phases, the FoS are generally lower as compared to the calculations taking into account suction in all phases. As indicated in Tab. 10, the use of different run-off criteria ψ_{max} of either 1 or 30 mm had hardly any effect on the results.

Tab. 10: FoS after "day 40" of the 192 day climatic hydrograph, taking the previous 39 days into account; for "model A" with varying saturated permeabilities and run-off criteria ψ_{max}

k_{ref}	**suction in all phases**		**suction in all phases except FoS**	
	ψ_{max}= 1 mm	ψ_{max}= 30 mm	ψ_{max}= 1 mm	ψ_{max}= 30 mm
initial	1.58	1.58	2.11	2.11
after day 39	1.17	1.18	1.15	1.16
after day 40	1.15	1.16	1.13	1.14
$k_{ref}/10$	**suction in all phases**		**suction in all phases except FoS**	
	ψ_{max}= 1 mm	ψ_{max}= 30 mm	ψ_{max}= 1 mm	ψ_{max}= 30 mm
initial	1.58	1.58	2.11	2.11
after day 39	1.19	1.19	1.15	1.15
after day 40	1.18	1.17	1.14	1.14
$k_{ref}/100$	**suction in all phases**		**suction in all phases except FoS**	
	ψ_{max}= 1 mm	ψ_{max}= 30 mm	ψ_{max}= 1 mm	ψ_{max}= 30 mm
initial	1.58	1.58	2.11	2.11
after day 39	1.39	1.39	1.33	1.33
after day 40	1.39	1.39	1.32	1.33

Tab. 11 presents the FoS after "day 40" of the 192 day climatic hydrograph, based on manually defined initial pore water pressures ("model M") and taking into account the previous 39 days. The application of the 40 days lasting hydrograph led to only slight decreases in the FoS in all the analyses.

Tab. 11: FoS after "day 40" of the 192 day climatic hydrograph, taking the previous 39 days into account; for model M with varying saturated permeabilities and run-off criteria ψ_{max}

k_{ref}	suction in all phases		suction in all phases except FoS	
	ψ_{max}= 1 mm	ψ_{max}= 30 mm	ψ_{max}= 1 mm	ψ_{max}= 30 mm
initial	1.16	1.16	1.16	1.16
after day 39	1.15	1.15	1.14	1.15
after day 40	1.15	1.15	1.13	1.14
$k_{ref}/10$	suction in all phases		suction in all phases except FoS	
	ψ_{max}= 1 mm	ψ_{max}= 30 mm	ψ_{max}= 1 mm	ψ_{max}= 30 mm
initial	1.16	1.16	1.16	1.16
after day 39	1.16	1.17	1.16	1.16
after day 40	1.14	1.15	1.13	1.14
$k_{ref}/100$	suction in all phases		suction in all phases except FoS	
	ψ_{max}= 1 mm	ψ_{max}= 30 mm	ψ_{max}= 1 mm	ψ_{max}= 30 mm
initial	1.16	1.16	1.16	1.16
after day 39	1.15	1.16	1.14	1.13
after day 40	1.12	1.13	1.12	1.12

7.3.2 FoS after a heavy rainfall event without taking previous precipitation into account

It is well accepted that previous rainfall events before a major rainfall event takes place affect the pore water pressure profile and consequently, the soil's water infiltration capability. This leads to a higher sensitivity of the factor of safety of a slope to changes in the pore water pressure profile. In order to highlight the importance of taking antecedent rainfall events into account, calculations have been performed with the direct application of the heavy rainfall event of day 40, without taking the previous 39 days of the climatic hydrograph into account. The heavy rainfall event on day 40 is characterised by a constant discharge rate of 38 mm/day.

Tab. 12 shows the FoS after the direct application of "day 40" only from the 192 day climatic hydrograph, based on automatically generated initial pore water pressures ("model A") without taking previous rainfall into account. When assuming suction in all phases, this high rainfall led to almost no changes in the factor of safety, except for the calculation with the highest saturated permeability

k_{ref} that had a drop in FoS from 1.584 to 1.214. Neglecting suction in the safety phases led to considerably higher initial factors of safety but qualitatively showed the same behaviour with a strong drop in FoS due to the application of the heavy rainfall of "day 40". As with the results presented in the last section, by neglecting suction in the safety phases, the FoS are generally lower compared to the calculations taking into account suction in all phases.

Tab. 12: FoS after direct application of "day 40" of the 192 day climatic hydrograph, without taking the previous 39 days into account; for model A with varying saturated permeabilities and ψ_{max}

k_{ref}	**suction in all phases**		**suction in all phases except FoS**	
	ψ_{max}= 1 mm	ψ_{max}= 30 mm	ψ_{max}= 1 mm	ψ_{max}= 30 mm
initial	1.58	1.58	2.11	2.11
after day 40 only	1.21	1.22	1.17	1.17
$k_{ref}/10$	**suction in all phases**		**suction in all phases except FoS**	
	ψ_{max}= 1 mm	ψ_{max}= 30 mm	ψ_{max}= 1 mm	ψ_{max}= 30 mm
initial	1.58	1.58	2.11	2.11
after day 40 only	1.58	1.58	1.42	1.43
$k_{ref}/100$	**suction in all phases**		**suction in all phases except FoS**	
	ψ_{max}= 1 mm	ψ_{max}= 30 mm	ψ_{max}= 1 mm	ψ_{max}= 30 mm
initial	1.58	1.58	2.11	2.11
after day 40 only	1.57	1.58	1.42	1.43

A comparison of the results plotted in Tab. 10 and Tab. 12 clearly demonstrates that the direct application (without taking into account the previous 39 days of precipitation dataset) of a heavy rainfall event, such as "day 40" in the present analysis, led to noticeably higher factors of safety compared to the analyses which consider the whole climatic hydrograph (up to and including day 40). Therefore, antecedent rainfall events, as far back in time as available, should always be considered to avoid overestimating slope stabilities, as previous precipitation is the realistic scenario.

For theoretical purposes, the direct application of "day 40" precipitation has also been performed for the "model M" scenario (by utilizing manually defined initial pore water pressures which equal the values that have been used in the Lysimeter studies (see chapter 6). Tab. 13 shows that for this particular case, there are almost no differences in the initial and final (after the high rainfall event is applied) FoS, whether suction was considered in all phases or not. For the three saturated hydraulic permeabilities considered, the application of rainfall from "day 40" led to a decreasing FoS, and the calculation with $k_{ref}/10$ experienced the largest drop in the factor of safety.

Tab. 13: FoS after direct application of "day 40" of the 192 day climatic hydrograph, without taking the previous 39 days into account; for model M with varying saturated permeabilities and ψ_{max}

k_{ref}	**suction in all phases**		**suction in all phases except FoS**	
	ψ_{max}= 1 mm	ψ_{max}= 30 mm	ψ_{max}= 1 mm	ψ_{max}= 30 mm
initial	1.16	1.16	1.16	1.16
after day 40 only	1.15	1.15	1.13	1.14
$k_{ref}/10$	**suction in all phases**		**suction in all phases except FoS**	
	ψ_{max}= 1 mm	ψ_{max}= 30 mm	ψ_{max}= 1 mm	ψ_{max}= 30 mm
initial	1.16	1.16	1.16	1.16
after day 40 only	1.05	1.05	1.04	1.04
$k_{ref}/100$	**suction in all phases**		**suction in all phases except FoS**	
	ψ_{max}= 1 mm	ψ_{max}= 30 mm	ψ_{max}= 1 mm	ψ_{max}= 30 mm
initial	1.16	1.16	1.16	1.16
after day 40 only	1.09	1.09	1.08	1.08

Additionally, the results presented in this chapter clearly show that the run-off criterion (ψ_{max}) has, in all calculations of this particular study, only marginal effects on the factors of safety.

For clarification and better representation, Tab. 14 summarises the results previously presented in this chapter (only ψ_{max}*= 1 mm*; k_{ref}).

Tab. 14: Representative summary of the results; model A vs. model M, either taking previous 39 days of rainfall into account or not, equal k_{ref} and ψ_{max}

k_{ref} ψ_{max} **= 1 mm**	**suction in all phases**		**suction in all phases except FoS**	
	Model A	Model M	Model A	Model M
initial	1.58	1.16	2.11	1.16
after day 39	1.17	1.15	1.15	1.15
after day 40	1.15	1.15	1.13	1.14
k_{ref} ψ_{max} **= 1 mm**	**suction in all phases**		**suction in all phases except FoS**	
	Model A	Model M	Model A	Model M
initial	1.58	1.16	2.11	1.16
after day 40 only	1.21	1.15	1.17	1.13

7.3.3 Comments on the ignore undrained behaviour option

In addition to previous analyses concerning PLAXIS' "ignore suction" option, also the effects of the so-called "ignore undrained behaviour" option have been investigated. This option temporarily excludes the effects of undrained behaviour in conditions where undrained material sets are used. By applying this option, the stiffness of water is not taken into account and all undrained materials become temporarily drained. It must be noted that with this option, previously generated excess pore water pressures remain, but no new excess pore water pressures are generated in the specific calculation phase where the option is applied.

The ignore undrained behaviour option is not available for a consolidation analysis and a fully coupled flow-deformation analysis, since these calculation types do not consider the drainage type (drained or undrained) of the material sets, but rather use the material's permeability instead (Brinkgreve et al. 2017).

Thus there is also no difference between "drained" and "undrained" numerical analyses when these kind of calculations ("consolidation" or "fully coupled flow-deformation") are performed with PLAXIS 2D. Furthermore, the "ignore undrained behaviour" option needs to be activated in the initial phase. Therefore, in order to quantify the influence of this option and to make the results somewhat comparable to previous results of this chapter, the use of the "plastic" calculation type was necessary. As with the previous chapter 7.3.2, the influence of this option has been investigated by only applying the heavy rainfall event of day 40, without taking into account the previous 39 days of the climatic hydrograph.

Tab. 15 illustrates the effects on the FoS of using the PLAXIS' "ignore undrained behaviour" option or not when the heavy rainfall is applied directly after the initial phase for the three suction options. In order to limit the influencing parameters, the same k_{ref} and ψ_{max} (1 mm) were used within the framework of these analyses.

Tab. 15: Effects of PLAXIS' "ignore undrained behaviour" option on FoS – Direct application of day 40 after initial phase; "model A"; Plastic calculation

Plastic calculation with undrained behaviour			
k_{ref}	Suction in all phases	Suction in all phases except of FoS	No suction in any phase
initial	1.58	1.49	1,37
after day 40	1.50	1.40	1.36
Plastic calculation with ignored undrained behaviour			
k_{ref}	Suction in all phases	Suction in all phases except of FoS	No suction in any phase
initial	1.58	2.11	1.42
after day 40	1.16	1.17	1.13

Ignoring undrained behaviour in combination with neglecting suction only in the safety phases led to the highest, whereas the option of neglecting suction but allowing undrained behaviour led to the lowest initial FoS. When suction is activated in all phases, there is no influence of the PLAXIS' "ignore undrained behaviour" option on the initial FoS, whereas neglecting suction either in all or only in the safety calculation phases led to differences both in initial and safety factors after heavy rainfall events (see Tab. 15). The activation of the "ignore undrained behaviour" option led to significantly lower FoS after the heavy rainfall event on day 40, as compared to when it was not activated.

The FoS presented in the top half of Tab. 15 (when the "ignore undrained behaviour" option has not been activated), are also shown in Fig. 94 as plots of the incremental deviatoric strains as a result of phi-c-reduction, done either directly after initial phase (top row) or after 'day 40' (bottom row). The plots of the incremental deviatoric strains as a result of phi-c-reduction, done either directly after the initial phase (top row) or after 'day 40' (bottom row) when the ignore undrained behaviour ("IUB") option was switched on, are shown in Fig. 95.

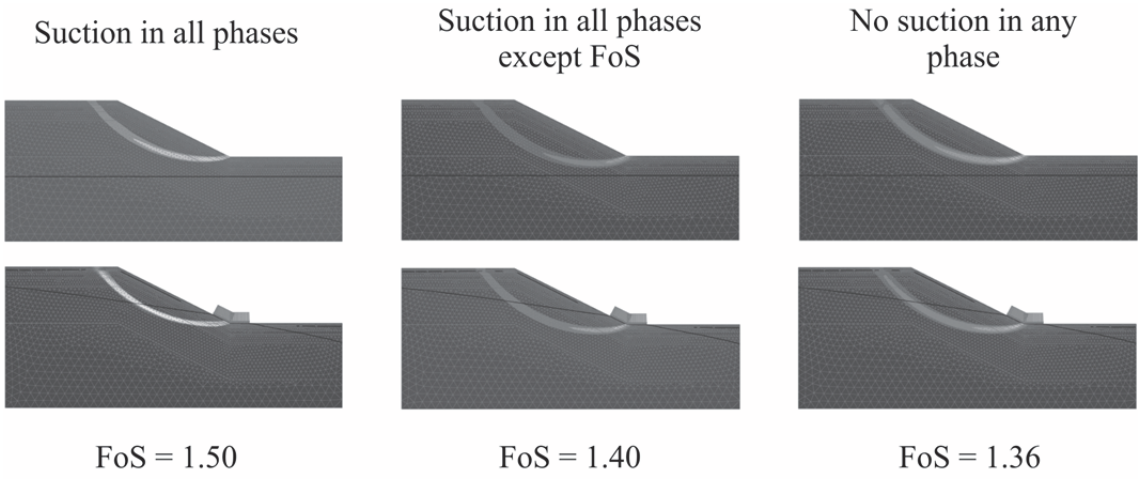

Fig. 94: Incremental deviatoric strains as a result of phi-c-reduction directly after initial phase (top) and day 40 (bottom); model A; Plastic calculation

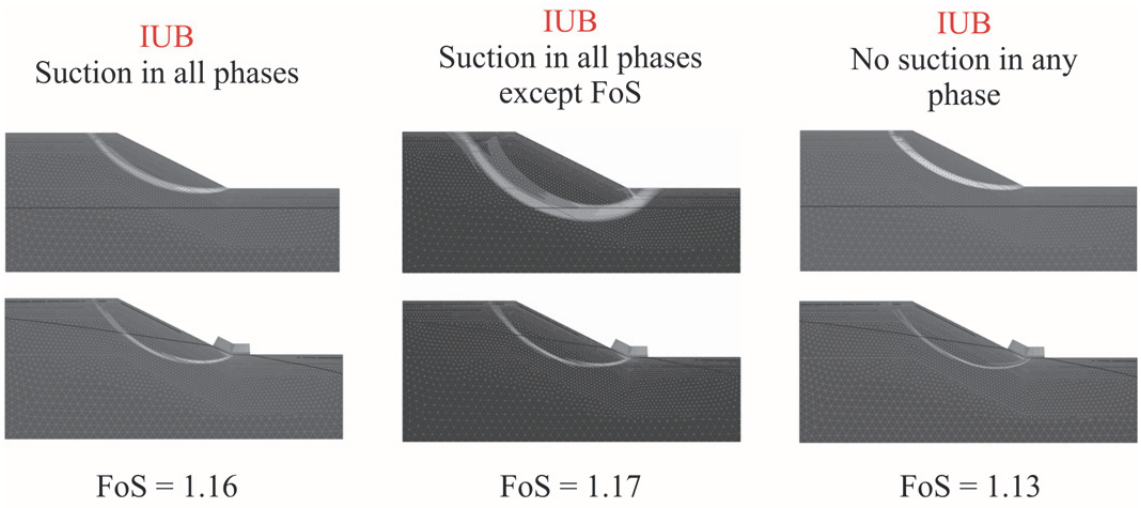

Fig. 95: Incremental deviatoric strains as a result of phi-c-reduction directly after initial phase; model A; Plastic calculation utilizing PLAXIS "Ignore undrained behaviour" (IUB) option

7.4 Conclusions and outcomes of the benchmark slope analyses

In chapter 6, it was shown that the numerical procedure adopted is capable of replicating the change of suction profiles due to infiltration as measured in the field. The same procedure was then utilized to investigate the infiltration behaviour of rainfall on slopes with variable boundary conditions. It should be mentioned that the investigations which were presented here are only relevant for very shallow slope failures and not for deep seated slope instabilities.

Besides the initial suction profile, of which the influence is investigated by the "model M" and "model A", further parameters which could affect the results significantly have been presented. The key parameter in both initial suction profile variants ("model M" and "model A") which affects all further results is the initial location of the groundwater-level. A deeper groundwater-level resulted in very high and unrealistic suction values at the surface. To quantify this significance, calculations with a changed, lowered groundwater level (-7.0 m instead of -3.5 m) have been performed.

Also in this chapter, the results of using three different values for the saturated hydraulic permeability have been presented. The application of the originally determined, relatively high permeability (k_{ref}) led to a fast reduction of suction in all the analyses. As a result of the 192 day climatic hydrograph (first presented in Chapter 5), in combination with the utilized internal and external boundary conditions in this study, all the curves fitted together after approximately 40 days. After this period (the first 40 days), suction reached zero for the first time and then any further climatic influences affected all the variants in the same way.

Contrary to that, the (hypothetical) analyses with a lowered saturated permeability, where the original one was divided by 100 ($k_{ref}/100$), generated large differences in the results.

Independently of the applied hydraulic boundary conditions (e.g. ψ_{max}, "cut rainfall peaks", groundwater-lowering to -7.0 m) the "model A" suction curves never matched the "model M" curves within the timeframe of the climatic hydrograph used here. This means that the starting condition (initial pore water pressure profile) significantly affects the development of suction and that previous rainfall events have to be taken into account whenever available.

In terms of suction develops over time, the type of climatic hydrograph plays a major role. Once the saturation of the soil reaches up to a certain level due to infiltration, an intense rainfall event can lead to significant drops in suction. A constant and low precipitation rate brings about the strongest decrease in suction, which is accompanied by reduced effective stresses which can lead to instability of a slope.

This (expected) behaviour clarifies the significance of having dryer periods or at least, of alternating, erratic weather conditions so as to regenerate suction, predominantly in near surface areas, in order to make the slope "safe" again.

The variation of hydraulic boundary conditions, such as increasing the ψ_{max} parameter, also affects the development of suction over time as a result of the fully-coupled flow-deformation analyses. On the one hand, a higher value of ψ_{max} can increase the stability of a slope because a head, which acts like an additional surcharge, would be able to build up and additionally, the possible presence of roots, which is normally the case if there is vegetation attracting water (soil-hydrological effect), has stabilizing effects on slopes' stability (e.g. Chirico et al. 2013). On the other hand, the higher elevation of the groundwater head would enlarge the hydraulic gradient and therefore increase the infiltration rate into the soil, which could lead to destabilization effects.

8 Influence of heavy rainfall events on variable slope geometries

Chapter 7 describes the study of a high intensity rainfall event, with a discharge of 300 mm/day, being constantly applied for 72 hours onto a slope. The slope is modelled with simple, homogeneous or inhomogeneous, slope geometries. The varied slope geometries with associated relevant boundary conditions are depicted and described in the corresponding chapters 8.1 and 8.2. The effects of varying run-off conditions (ψ_{max} = 1mm or 30 mm) and the influence of an either open or closed flow boundary on the right side of the numerical model on the FoS of the slope are presented. In order to simulate a constant and continuous groundwater level at the left boundary, a head boundary condition was applied to the left side of the model. The in all the analyses initially inclined groundwater level (~10.62°) is illustrated in Fig. 96 and Fig. 104, respectively. The SWCCs used in these calculations were taken from the HYPRES database (Wösten et al. 1999) and are described in chapter 3.4.4 in more detail.

In order to investigate the influence of all the various factors used in the calculations, the development of the FoS (how FoS changes with time) during periods of heavy rainfall was used. The FoS were determined by applying a phi-c-reduction phase after every 6 hours of constant precipitation (applied by means of fully-coupled flow deformation analyses).

As the purpose of this study is to evaluate solely the influence of hydraulic properties on the FoS of the slope, the strength and stiffness parameters are assumed to be the same for all soil layers (Tab. 16). Only the hydraulic properties (SWCCs, k_{sat}), differ for the various layers.

Tab. 16: Soil parameters for Mohr-Coloumb model

Description	**Symbol**	**Value**	**Unit**
Unit weight	γ	20	[kN/m³]
Elasticity modulus	E’	7500	[kPa]
Effective Poissons’ ratio	ν’	0.35	[-]
Effective cohesion	c’	10	[kPa]
Effective friction angle	φ’	20	[°]

After a short description of the examined hydraulic boundary conditions (see 8.1 and 8.2) the results, by means of changing FoS, are illustrated and discussed in the associated subchapters (8.1.x and 8.2.x).

8.1 Homogeneous slope geometry

This chapter presents the development of the FoS when the soil of entire model is assumed to be a homogeneous soil, meaning that only one material set with one SWCC and saturated hydraulic permeability is used for all soil layers of the model. Although only one material set was used, suction was defined manually at certain depths of the slope model (8.1.1). Same as in the previous chapters 6 and 7, the measurement data provided by the Lysimeter is used to define the initial suction values of the slope. It must be noted that the use of the Lysimeter dataset in the numerical calculations presented in the following chapter is for theoretical purposes only and meant to qualitatively highlight the differences between the ("model M") and ("model A") calculations.

The slope geometry, with a slope angle α of 26.56°, an either open or closed flow boundary on the right side of the model and near-surface heads in order to manually define suction, is illustrated in Fig. 96.

For the calculations using automatically generated initial pore water pressures, there are no manually defined heads in the model and the suction profile is solely determined by the location of the groundwater level (8.1.2.)

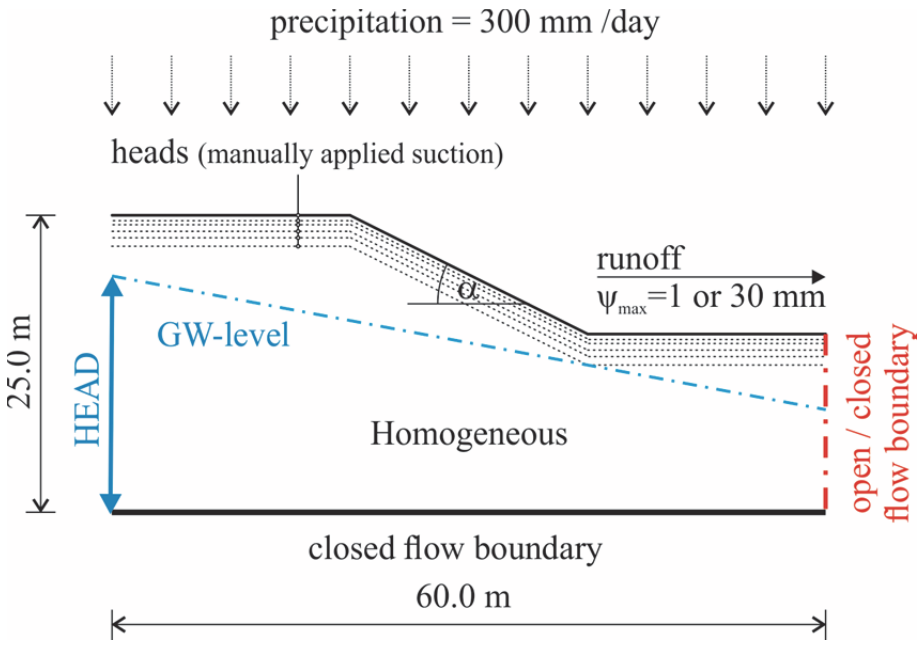

Fig. 96: Slope geometry and relevant boundary conditions

8.1.1 Results – suction manually defined (model M)

This section presents the results when suction was defined manually at certain depths of the slope model ("model M").

Fig. 97 shows the FoS curves (how FoS changes with time) when the right model boundary was closed. Independently of the SWCC used, the constant rainfall application in combination with a saturated hydraulic permeability of $k_{sat} = 10^{-3}$ m/s led to a strong decrease in FoS within the first 6 hours of the calculation, followed by constant FoS because water flows out of the model and no changes in the pore water pressure profile occurs. When using a lower permeability of $k_{sat} = 10^{-6}$ m/s, the usage of the HYPRES "coarse" SWCC even showed no change in the FoS during rainfall application. This behaviour is due to the presence of a very low permeability at the surface even under very low suction values (SWCC related), which led to nearly no infiltration with accompanying high run-off rates and therefore no change in the FoS. The use of finer grained SWCCs in combination with the lower permeability led to a continuous decrease in the FoS.

Under the before mentioned circumstances, the run-off criterion ψ_{max} had generally no impact on the results. Consequently, Fig. 98 shows only the results for $\psi_{max} = 30\ mm$ in combination with a closed flow boundary on the right side of the model. Again, the use of a high permeability of $k_{sat} = 10^{-3}$ m/s led to a significant drop in FoS for all the individual curves. The calculations assuming lower permeabilities resulted in slightly and continuous decreases of FoS when the HYPRES "MediumFine" or "VeryFine" SWCC was used respectively, whereas the SWCC "Coarse" showed negligible changes in the FoS.

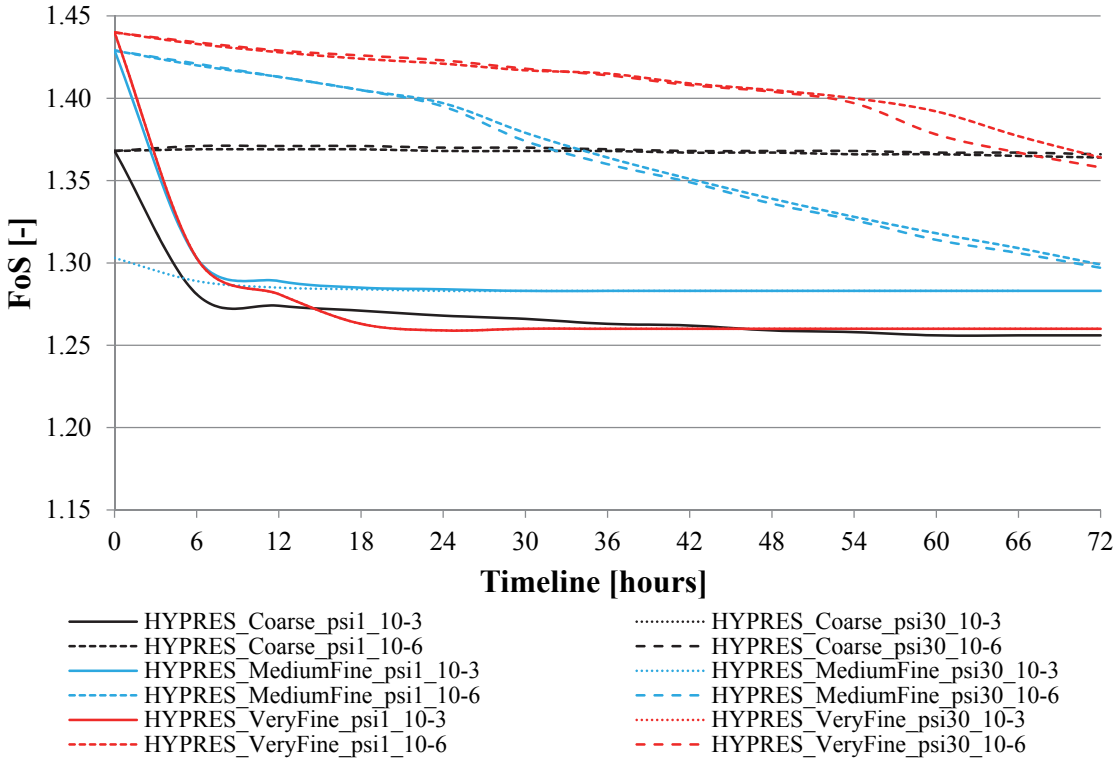

Fig. 97: FoS homogeneous slope, manual suction and open flow boundary

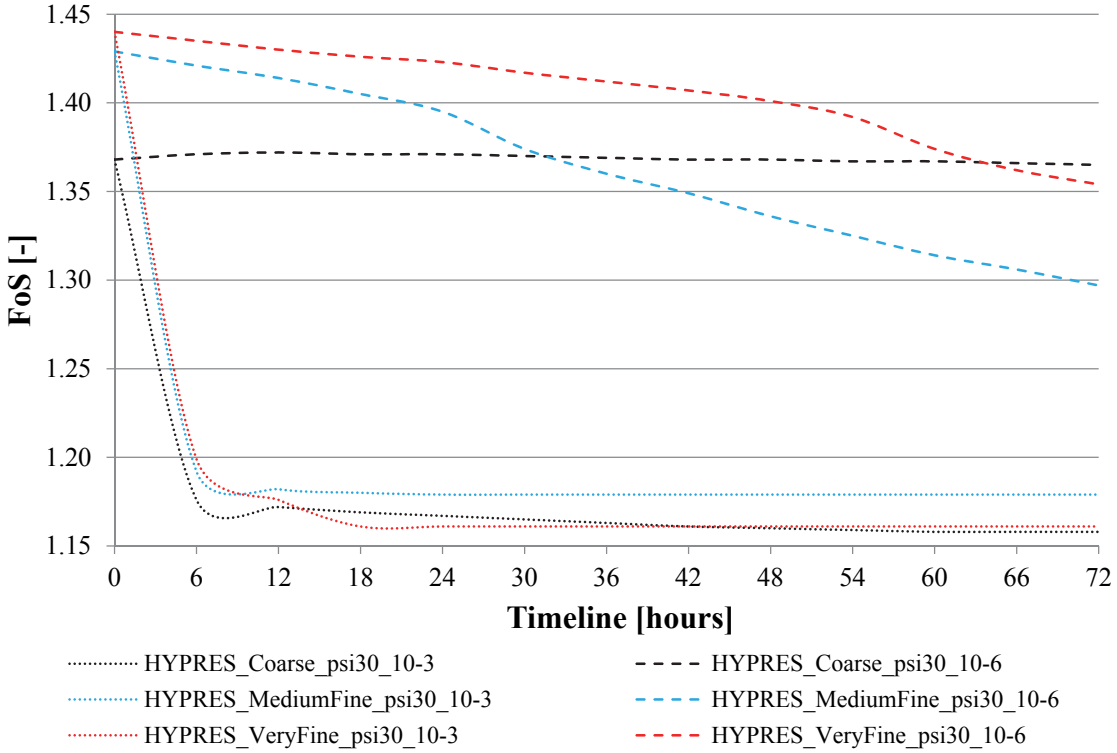

Fig. 98: FoS homogeneous slope, manual suction and closed flow boundary

For clarification and representative for the results given in the diagrams previously presented in this chapter, Fig. 99 shows the differences in suction development when k_{sat} was either assumed to be 10^{-3} or 10^{-6} m/s in the calculations with HYPRES "MediumFine" SWCC in combination with an open flow boundary on the right side and ψ_{max} = 30 mm.

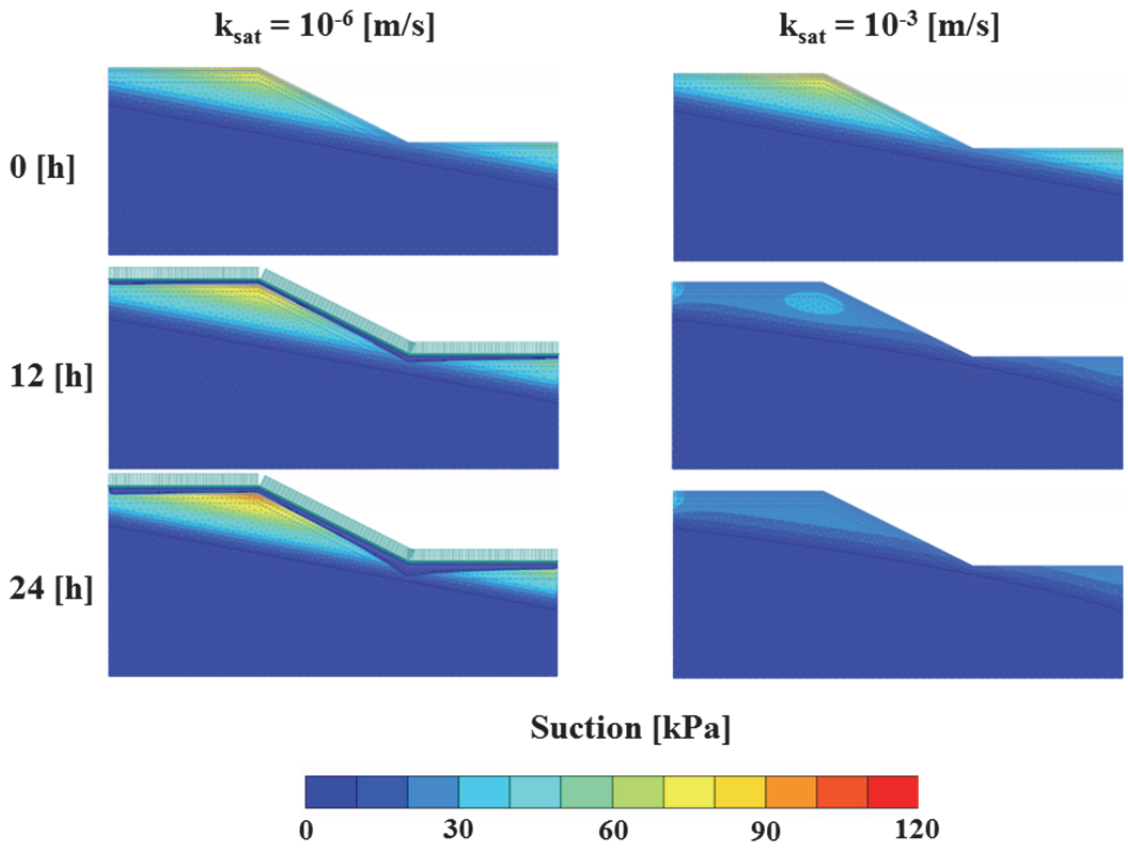

Fig. 99: Comparison of suction development; HYPRES MediumFine; ψ_{max}= 30 mm; open flow boundaries; $k_{sat} = 10^{-6}$ vs. $k_{sat} = 10^{-3}$ m/s

As clearly illustrated in Fig. 99, the first hours of heavy rainfall application led to a strong reduction in suction when $k_{sat} = 10^{-3}$ m/s have been used in the calculations, accompanied with a sharp and fast decrease in the FoS (see blue dotted line in Fig. 97). In contrast, by assuming $k_{sat} = 10^{-6}$ m/s in the analyses (see blue dashed line in Fig. 99) the applied rainfall rate is larger compared to the current permeability of the soil, which led to runoff conditions (indicated by downward arrows on top of the surface in the suction plots after 12 and 24 hours).As there has been less water infiltrating into the slope, the FoS stays higher, especially in the first hours of rainfall, compared to the calculations with higher permeable soils.

For clarification, Fig. 100 shows of the effects of and differences between either opened or closed flow boundaries on the right side of the model (also compare diagrams in Fig. 97 and Fig. 98). In the present case, the intermediate HYPRES SWCC "MediumFine" in combination with k_{sat} = 10^{-3} m/s and ψ_{max} = 30 mm was used to represent the general influence of this certain boundary condition.

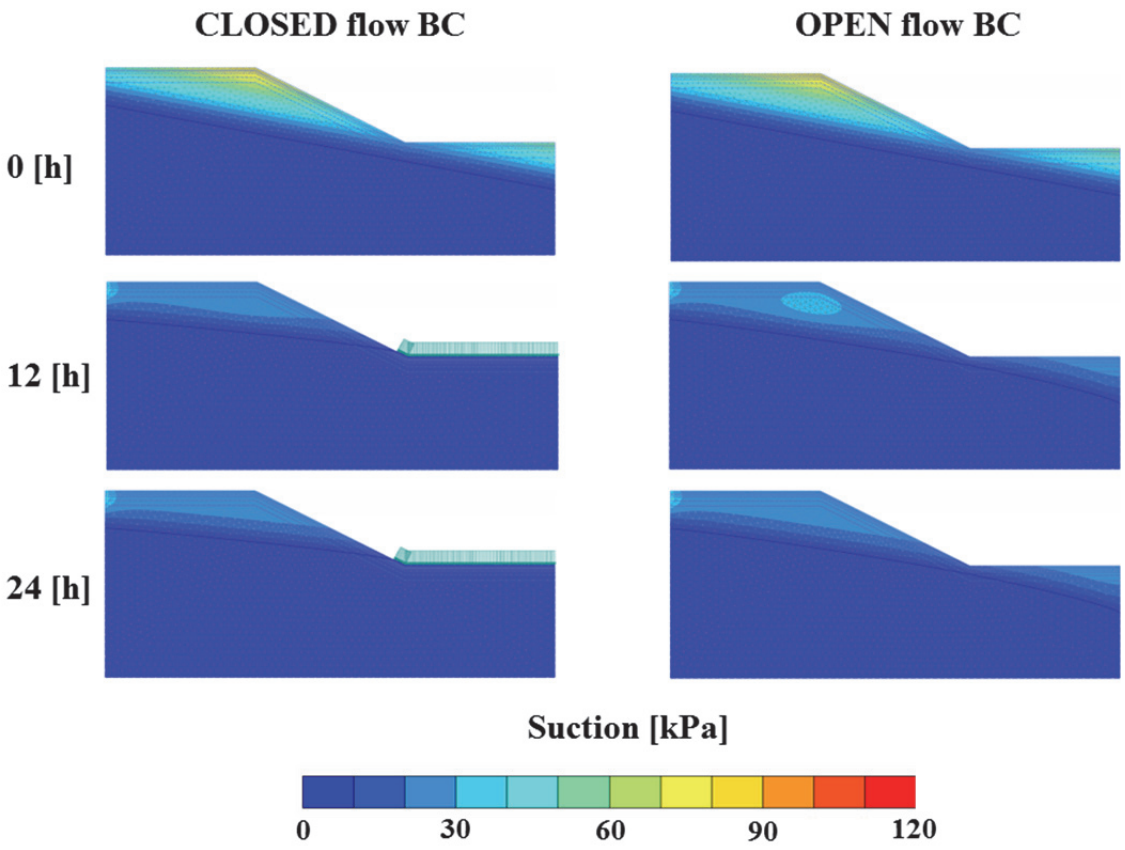

Fig. 100: Comparison of suction development; HYPRES MediumFine; ψ_{max}= 30 mm; k_{sat} = 10^{-3} m/s; OPEN vs. CLOSED flow boundary

The flow boundary condition on the right side of the model affects the pore water pressure distribution of the whole slope geometry, especially the area around the slopes' toe. As a consequence of the applied climatic hydrograph, a closed flow boundary generally leads to an increase in saturation, as the infiltrated water has to "stay" in the slope. This behaviour, which is comparable to filling a closed bucket with water, is associated with lower suction values and therefore leads to smaller FoS. As water continuously flows out of the model, as it is the case when an opened flow boundary has been assumed, there always remains suction in the slope model. Consequently, by assuming an opened flow boundary, the FoS has to be substantially higher compared to calculations assuming a closed flow boundary.

8.1.2 Results – suction automatically generated (model A)

This section presents the results when the initial suction profile of the slope was generated automatically and solely given by the location of the initial groundwater-level ("model A").

The results with an either open (Fig. 101) or closed (Fig. 102) flow boundary on the right side of the model are given in the following diagrams. Due to the (deep) location of the groundwater-level, the initial suction values at the surface have been higher than in the user-defined calculations as presented in the previous chapter 8.1.1. The development of the FoS for all SWCCs of the HYPRES database assuming a ψ_{max} criterion of 1 mm are given in Fig. 101. The results for $k_{sat} = 10^{-3}$ m/s showed a strong decrease in the first 6 hours of rainfall application, whereas the safety factors stayed almost constant after approximately 30 hours, independently of the used SWCC (water flows out of the model). The lower permeability calculations led to continuous decrease in the FoS, whereas the SWCC "MediumFine" showed the strongest, and the SWCC "Coarse" almost no decrease in FoS with time. Fig. 102 illustrates the results when the run-off criteria ψ_{max} was increased to 30 mm, which led to nearly identical results as indicated in Fig. 101.

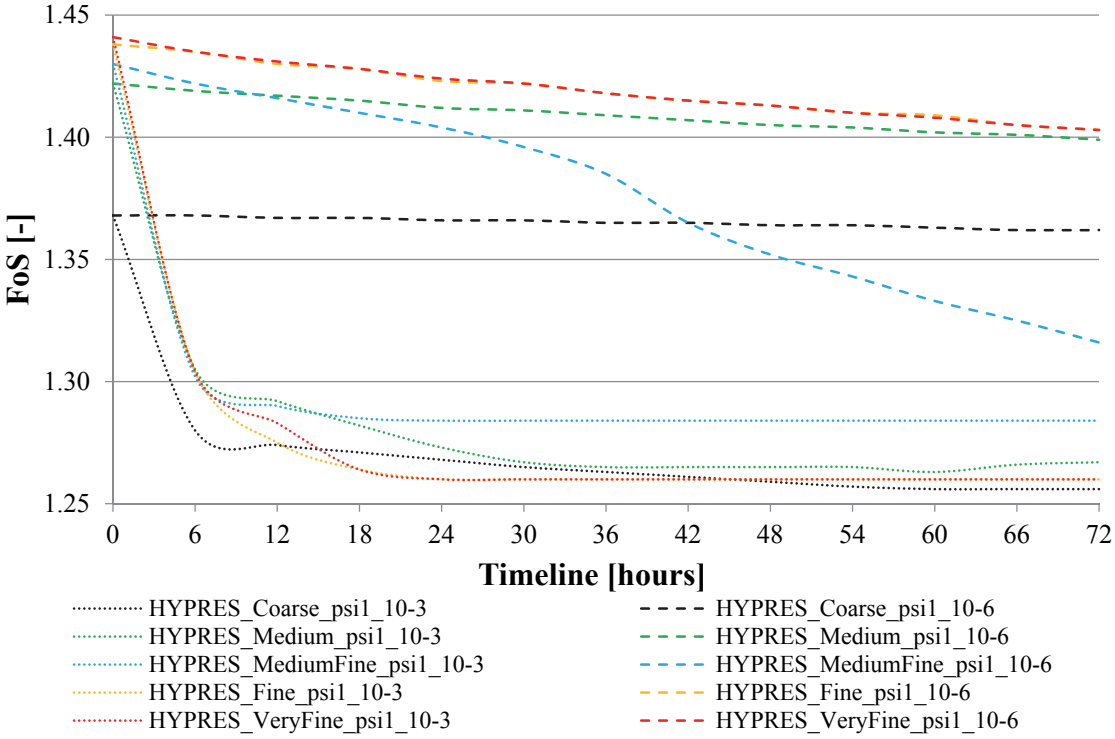

Fig. 101: FoS homogeneous slope, automatic suction and open flow boundary, ψ= 1 mm

The results when the right model boundary was assumed to be closed are given in Fig. 103. The results are comparable to those presented in Fig. 98, where the

initial suction profile has been manually defined. A sharp drop in the first hours is followed by constant factors of safety under high permeable conditions (k_{sat} = 10^{-3} m/s), whereas the calculations with lower permeability (k_{sat} = 10^{-6} m/s) showed only a moderately decrease in FoS with time.

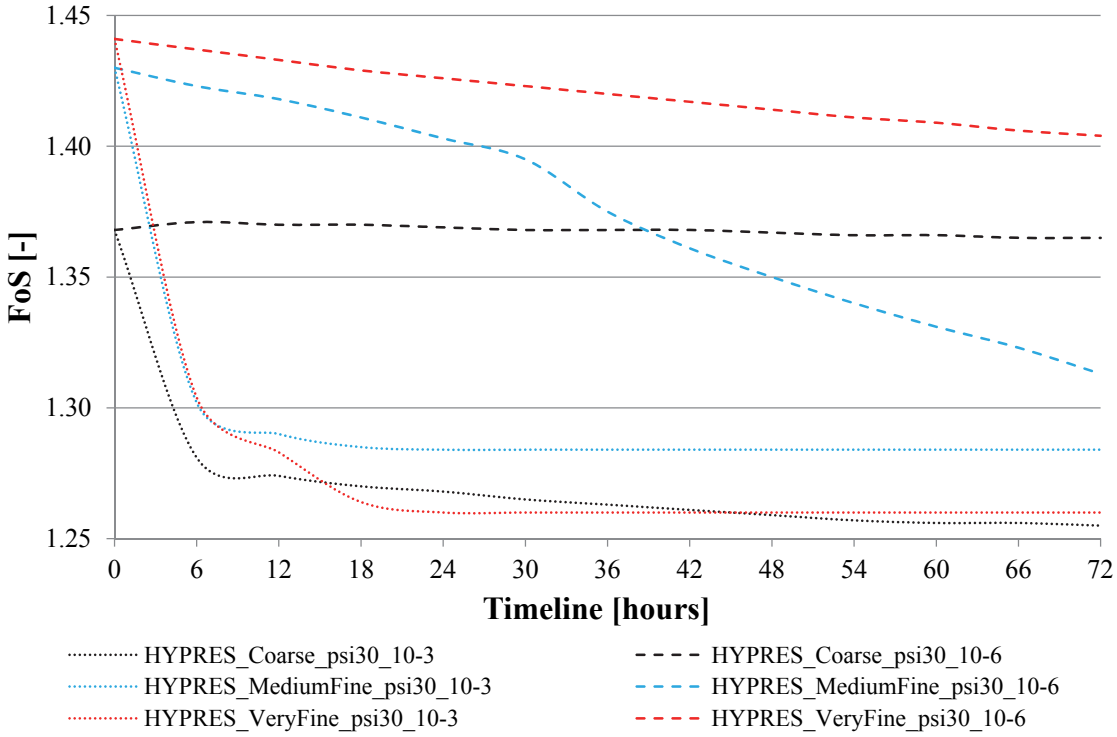

Fig. 102: FoS homogeneous slope, automatic suction and open flow boundary, ψ= 30 mm

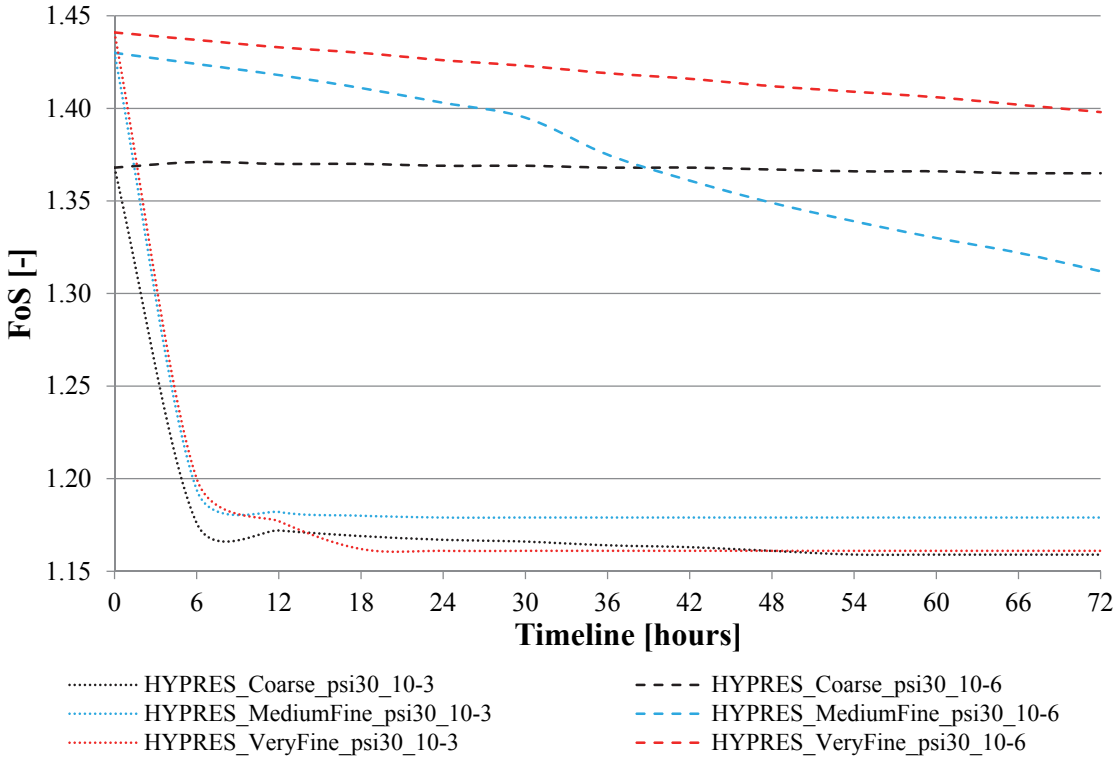

Fig. 103: FoS homogeneous slope, automatic suction and closed flow boundary, ψ= 30 mm

In order to quantify the differences between "model A" and "model M" calculations, Tab. 17 compares the development of the FoS during the 72 hours lasting heavy rainfall event in tabular form. For better representation, only the results using HYPRES MediumFine SWCC and ψ_{max} = 30 mm are given in Tab. 17.

Tab. 17: Homogeneous slope geometry: representative summary of the results, Model A vs. Model M, open vs. closed flow boundary, $k_{sat} = 10^{-3}$ m/s vs. $k_{sat} = 10^{-6}$ m/s; equal ψ_{max}

MediumFine ; ψ_{max} = 30 mm								
	Model M				**Model A**			
k_{sat}	**$k_{sat} = 10^{-3}$ [m/s]**		**$k_{sat} = 10^{-6}$ [m/s]**		**$k_{sat} = 10^{-3}$ [m/s]**		**$k_{sat} = 10^{-6}$ [m/s]**	
	open	**closed**	**open**	**closed**	**open**	**closed**	**open**	**closed**
0	1.43	1.43	1.43	1.43	1.43	1.43	1.43	1.43
6	1.30	1.19	1.42	1.42	1.30	1.19	1.42	1.42
12	1.29	1.18	1.41	1.41	1.29	1.18	1.42	1.42
18	1.29	1.18	1.41	1.41	1.29	1.18	1.41	1.41
24	1.28	1.18	1.40	1.40	1.28	1.18	1.40	1.40
30	1.28	1.18	1.37	1.37	1.28	1.18	1.40	1.40
36	1.28	1.18	1.36	1.36	1.28	1.18	1.38	1.38
42	1.28	1.18	1.35	1.35	1.28	1.18	1.36	1.36
48	1.28	1.18	1.34	1.34	1.28	1.18	1.35	1.35
54	1.28	1.18	1.33	1.33	1.28	1.18	1.34	1.34
60	1.28	1.18	1.31	1.31	1.28	1.18	1.33	1.33
66	1.28	1.18	1.31	1.31	1.28	1.18	1.32	1.32
72	1.28	1.18	1.30	1.30	1.28	1.18	1.31	1.31

When using a high saturated permeability (k_{sat} = 10^{-3} m/s), a closed-flow boundary at the right side of the model in combination with a heavy rainfall event with 300 mm per day led to the strongest (and between "model A" and "model M" equivalent) decrease in the FoS. Utilizing a lower saturated permeability (k_{sat} = 10^{-6} m/s) in the analyses led to a comparatively moderate decreases in FoS showing no influence of the either opened or closed flow boundary at the right side of the model.

8.2 Inhomogeneous slope geometry

This chapter presents the development of the factor of safety when the slope model was assumed to be inhomogeneous. This means that either two different SWCCs with two different saturated hydraulic permeabilities were used, or that the same SWCC was used twice and only the saturated permeability was assumed to be different between upper and lower layer. The inhomogeneous slope geometry with a slope angle α of 26.56°, an either opened or closed flow boundary on the right side of the model is shown in Fig. 104. The initial groundwater level was assumed to be inclined with the same angle as the boundary between the different soil layers (~10.62°).

In the present analyses considering inhomogeneous slope geometries, and contrary to the calculations assuming the slope to be homogeneous (see chapter 8.1), the initial pore water pressures are from now on solely given by the location of the groundwater level and automatically generated ("model A").

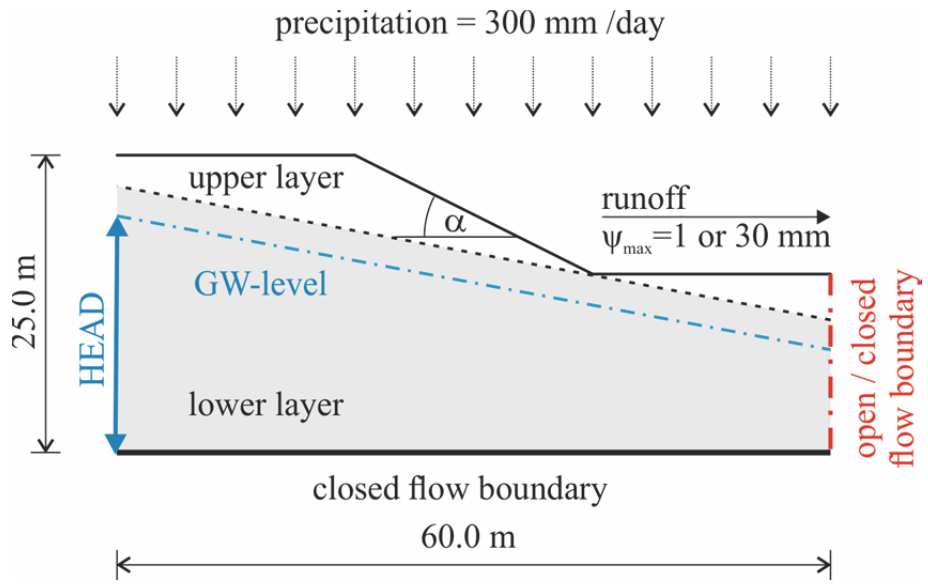

Fig. 104: Inhomogeneous slope geometry; automatically applied suction

8.2.1 Results – Equal SWCC & different permeabilities

The effects of using two different values for the saturated permeability of the upper and lower soil layer, respectively, are presented in the following diagrams (Fig. 105 and Fig. 106).

The calculation using HYPRES' "VeryFine" SWCC and the higher permeability k_{sat}= 10^{-3} m/s as upper soil layer ("H-L") led to numerical problems and stopped after generating the initial pore water pressure profile when the right model boundary was assumed to be open. The same SWCC in combination with the lower permeability k_{sat} = 10^{-6} m/s as upper soil layer ("L-H") was numerically possible and delivered, after a strong decrease in the first 6 hours, an almost constant FoS of around 1.31 after 12 hours of rainfall application.

The use of HYPRES' "Coarse" SWCC showed qualitatively the same behaviour, with an aborted calculation after 18 hours of rainfall application when utilizing the higher permeability on top and numerically calculated FoS of around 1.28 reached after 12 hours of infiltration.

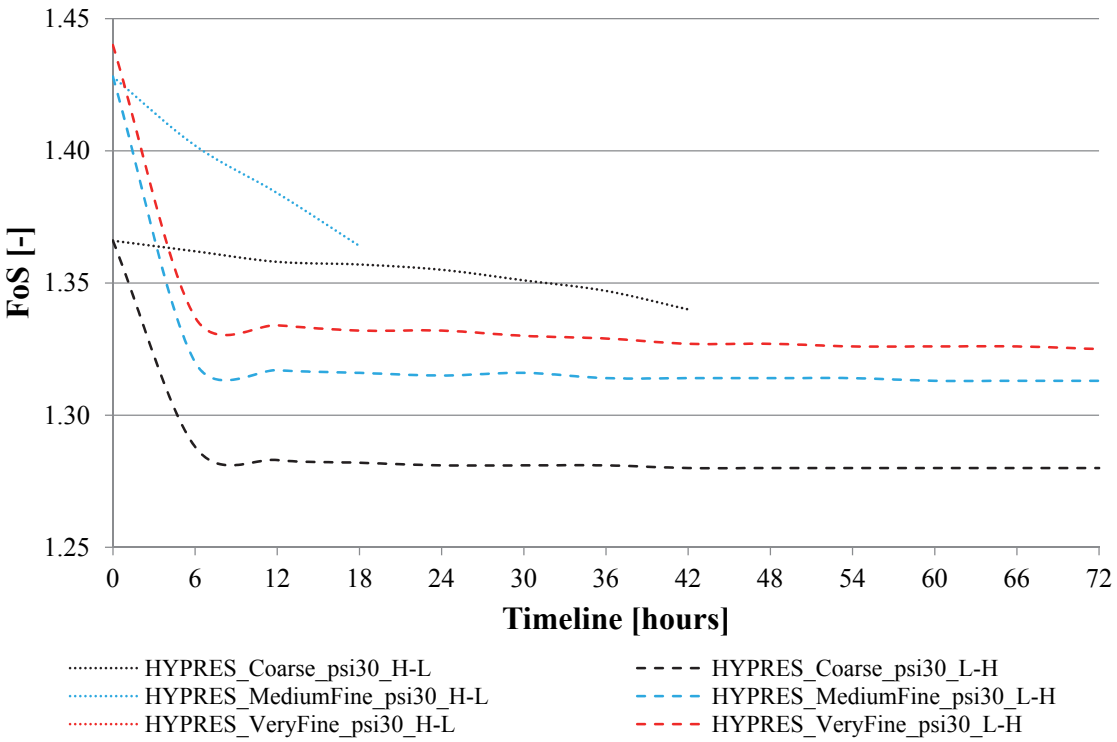

Fig. 105: FoS inhomogeneous slope, equal SWCCs, automatic suction and open flow boundary, ψ= 30 mm

A closed-flow boundary on the right model side led to a sharp drop in the FoS for all investigated HYPRES' SWCCs within the first 6 hours of constant rainfall application, whereas in this study, only the option with lower permeable upper soil layer has been investigated.

The numerical procedures utilizing HYPRES' "MediumFine" and "Coarse" (reached FoS of 1.14) SWCC (reached FoS of 1.19) stopped after 12 and 48 hours respectively. After a sharp drop in the first 6 hours of rainfall, the use of the "MediumFine" SWCC ended with a FoS of 1.19 after 12 hours.

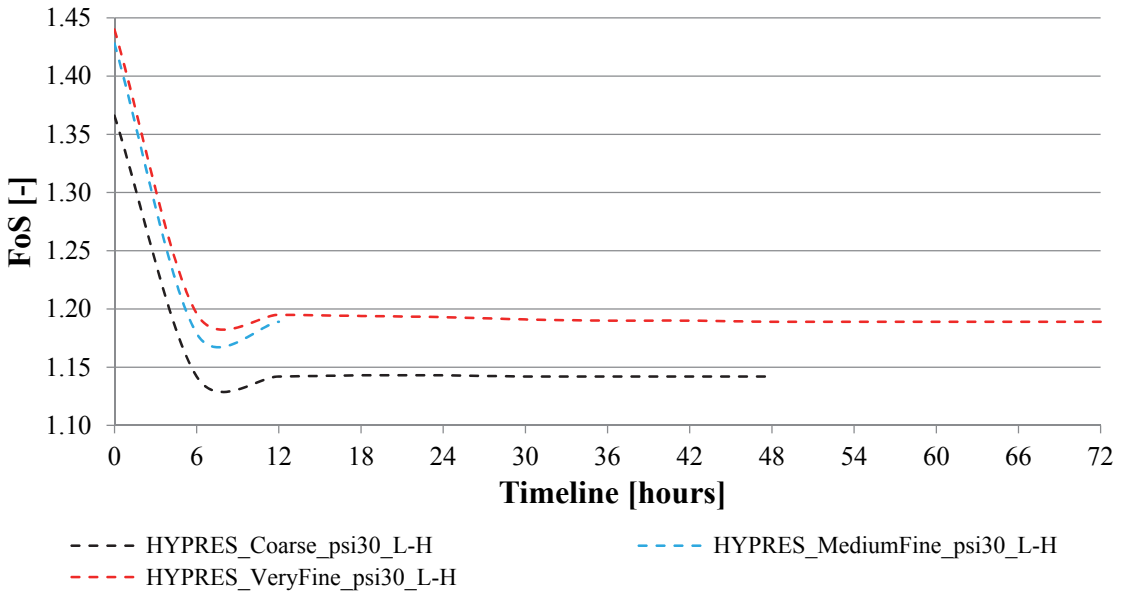

Fig. 106: FoS inhomogeneous slope, equal SWCC's, automatic suction and closed flow boundary, ψ= 30 mm

8.2.2 Results – Different SWCCs & different permeabilities

Within the framework of this study, also the option of using two different kinds of HYPRES' SWCCs in combination with two different hydraulic permeabilities has been investigated. The combination of using HYPRES' "Coarse" SWCC with k_{sat} = 10^{-3} m/s on top and HYPRES' "MediumFine" with k_{sat} =10^{-6} at the bottom, led to a continuous decrease in FoS until the calculation stopped after 54 hours. The "Coarse" (with k_{sat} = 10^{-3} m/s) and "VeryFine" (with k_{sat} = 10^{-6} m/s) combination aborted after the initial phase, reaching a FoS of around 1.39. The calculation with the "MediumFine" (with k_{sat} = 10^{-3} m/s) and "VeryFine" (with k_{sat} = 10^{-6} m/s) combination stopped after 18 hours reaching a FoS of 1.36. All other combinations (see Fig. 107) led to sharp drops in FoS within the first 6 hours, ending up with safety factors between 1.31 and 1.33.

The results assuming a closed-flow boundary on the right side of the model and inhomogeneous slopes are given in Fig. 108. In both calculations, the upper layer

was assumed to be less permeable (k_{sat} =10^{-6} m/s). The numerical procedure delivered comparable results for both investigated combinations reaching, after a sharp decrease within the first 6 hours, a FoS of about 1.17.

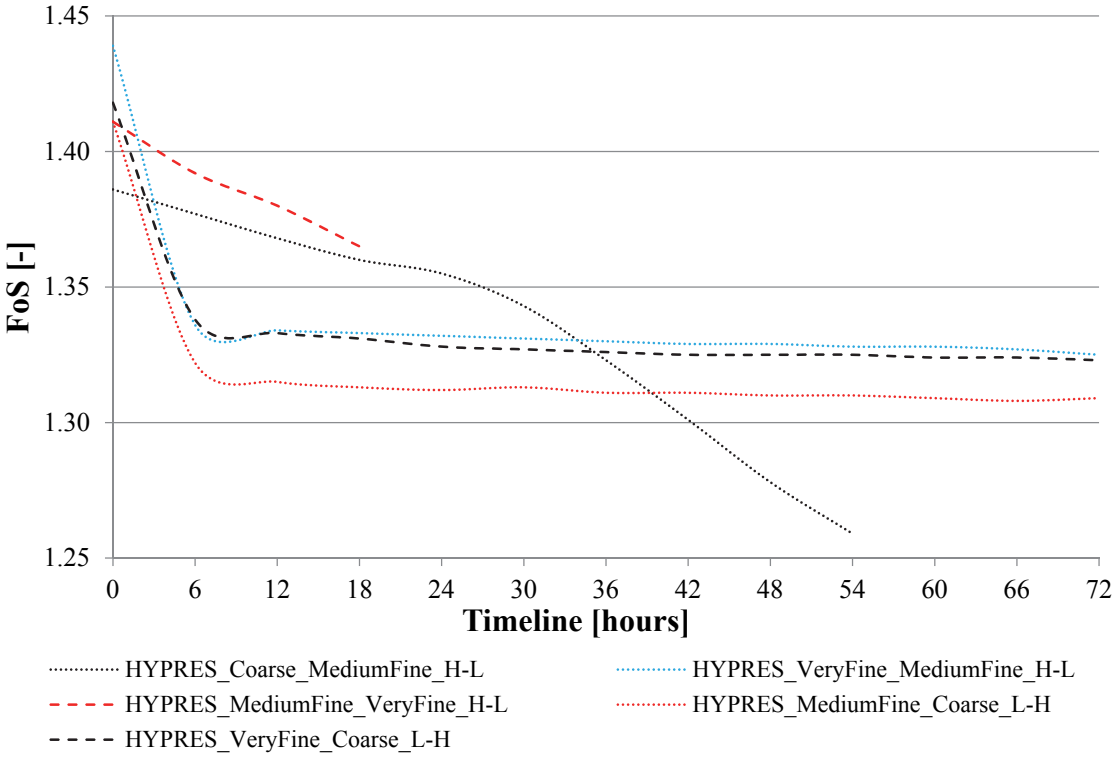

Fig. 107: FoS inhomogeneous slope, 2 SWCCs, automatic suction and open flow boundary, ψ= 30 mm

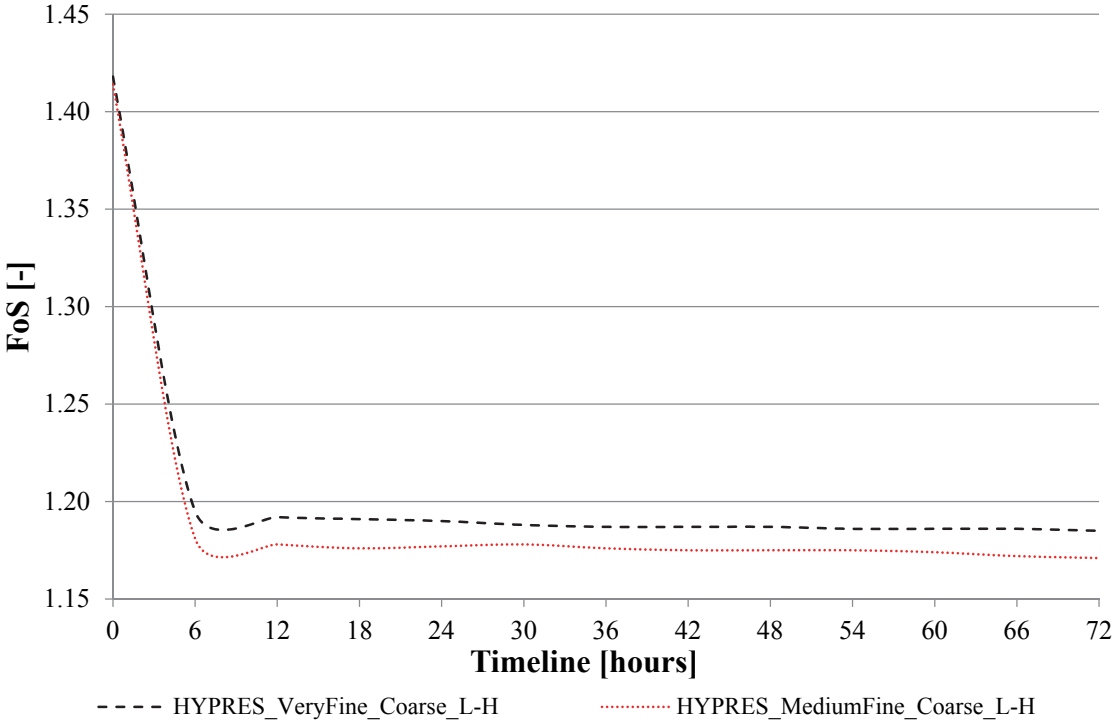

Fig. 108: FoS inhomogeneous slope, 2 SWCCs, automatic suction and closed flow boundary, ψ= 30 mm

8.3 Conclusions and outcomes heavy rainfall events on inhomogeneous slope geometries

Since heavy rainfall events with precipitation rates of up to 300 mm per day are occurring more frequently in Austria, a numerical study to investigate possible consequences of this intense precipitation on soil slopes was deemed to be of interest. This numerical investigation was done by quantifying the influence of an either open or closed flow boundary on the right side of the model, and various run-off conditions on the FoS of a simple slope geometry, with either homogeneous or inhomogeneous soil, and under simulation of heavy rainfall events.

The results of this numerical investigation have been presented by means of changing FoS due to the application of the rainfall event. It could be shown that the run-off criterion ψ_{max} had generally no impact on the FoS results for the assumptions taken in this study. As expected, a closed-flow boundary at the right side of the model led to a rising groundwater level within the slope with an accompanying increase of pore water pressures, resulting in a decrease of the FoS. When the slope was modelled with a homogeneous soil (consisting of only one material, one SWCC and one saturated permeability) and using a high saturated permeability ($k_{sat} = 10^{-3}$ m/s), the application of heavy rainfall led to a sharp and fast (within the first 6 to 12 hours) decrease of the FoS, independently of the (automatically generated or manually defined) initial pore water pressure condition. The similar analysis with lower saturated permeability ($k_{sat} = 10^{-6}$ m/s) led to a comparatively moderate decrease in FoS. Utilizing the HYPRES' "Coarse" SWCC showed the smallest and the HYPRES' "Medium Fine" SWCC the largest, reduction in FoS throughout all the analyses. The results showed that the initial pore water pressures and the SWCC used significantly influence the stability of the slope.

In the second part of this chapter, the slope was made inhomogeneous and was modelled with two soil layers so that either two different SWCCs with two different saturated hydraulic permeabilities could be used or that the same SWCC was used but with a different saturated permeability for the upper and lower layer. It must be noted, however, that some combinations (for example, if a higher permeability was used for the upper layer) led to problems in the numerical procedure, and it was not possible to apply the entire precipitation period. Generally, the use of a lower saturated permeability in the top layer led compared to the calculations using higher saturated permeabilities to a comparatively larger decrease in FoS, within the investigated period. The investigated option of using two different kinds of HYPRES' SWCCs in combination with two different hydraulic permeabilities led to varying reductions in the FoS depending on the combination of SWCCs.

9 Numerical investigation of rainfall infiltration into a real slope

9.1 Introduction

During extension works at a water storage basin for a pumped-storage power plant located in the Hohen Tauern, a region in the Central Eastern Alps, slope movements of an adjacent slope with an average inclination of 30° were observed. The influence of water level changes in this water storage basin and further influences from precipitation and the creep behaviour of the lacustrine fine sediments on the movement behaviour of this slow moving landside was numerically investigated by Ausweger (2018).

Within the framework of this thesis, the focus lies solely on the quantification of the influence of changing hydraulic boundary conditions within the numerical model, on the FoS of the slope. The finite element model with a total length of 380 m and a total height of 256 m, as well as all the soil stiffness and strength parameters of individual soil clusters have been taken directly from Ausweger (2018).

Fig. 109 gives an overview of the storage basin and the slow moving landslide, with a rough indication of the area undergoing slope movements. Additionally, the installed measurement devices are indicated.

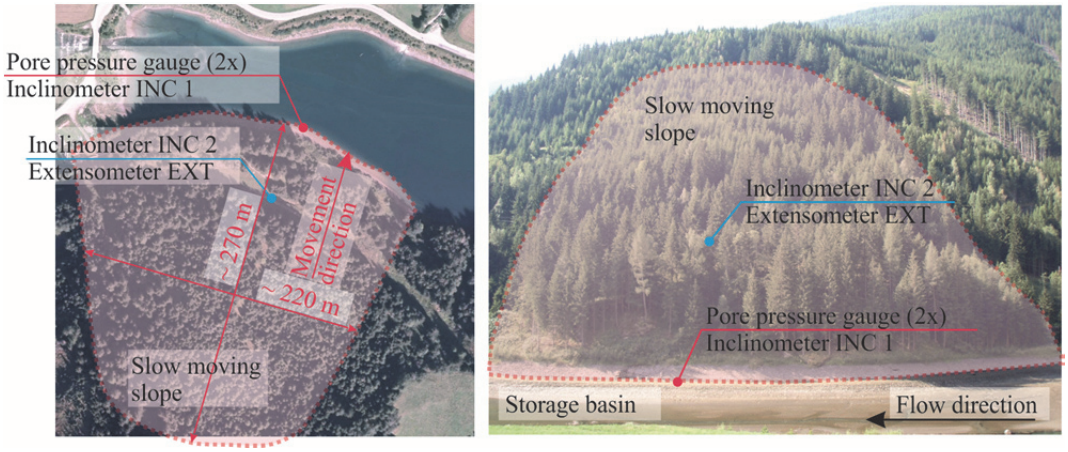

Fig. 109: Plan view and side view of the water storage basin and slowly moving slope (Ausweger 2018)

The dimensions of the water storage basin are roughly 400 x 100 m, amounting to a volume of roughly 300,000 m³. The operation of the pumped-storage power plant leads to maximum changes in the water level of ~7.5 m in the storage basin

up to three times a day. The slow moving landslide has a horizontal length of approximately 270 m, and movements were detected across a width of 220 m with an associated sliding surface, detected by inclinometer measurements, between 20 and 40 m below ground surface in the lower part of the slope. As the sliding surface becomes shallower in the upper part of the slope, the average depth of the sliding mass can be considered to be 20 m, and the resulting volume of the slow moving slope is roughly 1.2 million m³.

The discretised finite element model consisting of 5,287 6-noded elements is illustrated in Fig. 110. The zones where higher deformations are expected, such as the "Transition zone" and the lacustrine sediments at the slope toe, are more finely discretised, whereas the "Intact rock" is discretised very coarsely as there are no results extracted from this part of the model. At the bottom edge of the model, the displacements are fixed in both horizontal and vertical direction, whereas the displacements at the left and right boundaries of the model are fixed in horizontal direction only. A closed flow boundary condition is applied at the left, right and lower boundary of the model.

The mechanisms and the challenges with regard to the modelling of the slow moving landslide and the water storage basin, as well as an overview about the applied material parameters and constitutive models used, are discussed in detail in (Ausweger 2018).

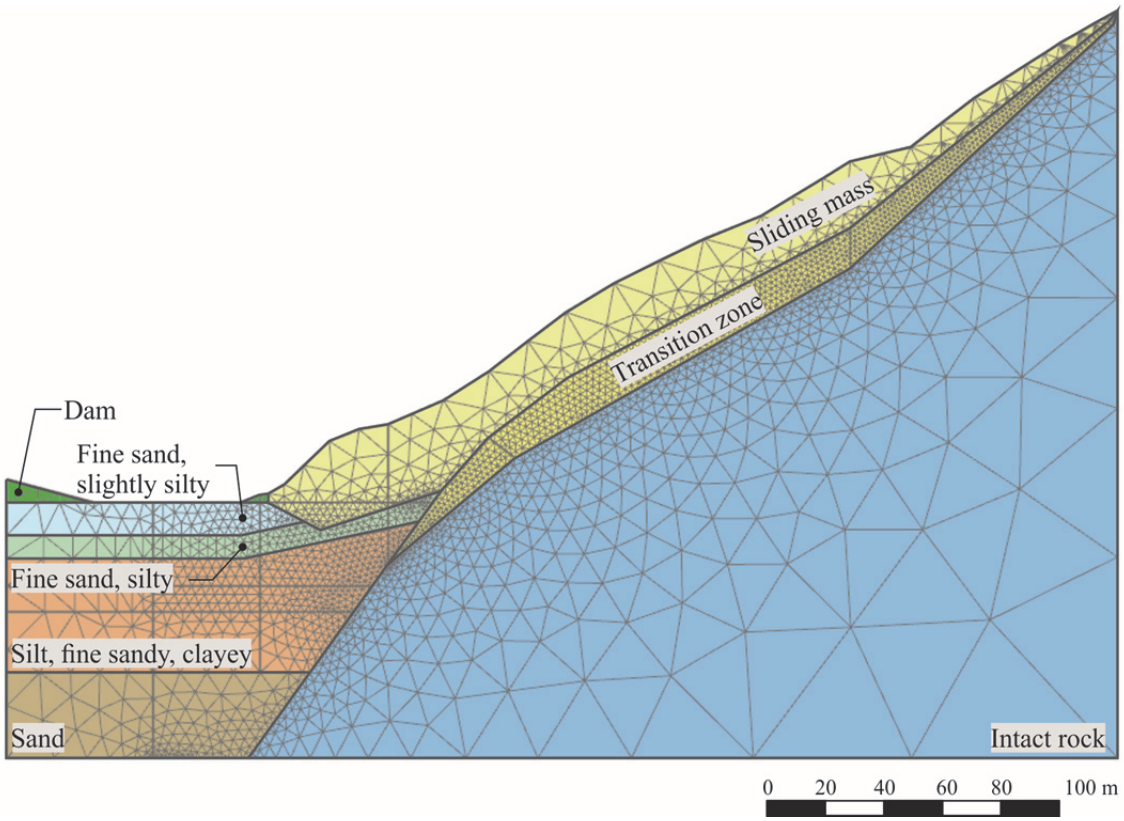

Fig. 110: FE-model for slow moving landslide and water storage basin (Ausweger 2018)

In this chapter, the influence of varying hydraulic characteristics of the "Sliding mass" and the "Transition zone" on the factor of safety of the slope are analysed under different climatic conditions.

The material of both these soil layers is characterized as a sheared and weathered rock with many joints filled with gravel, sand and silt. As the determination of material parameters in the laboratory is very challenging and difficult for this type of soil, the strength parameters were determined by means of back-calculations in order to reach a stress state which is close the ultimate limit state of the slope, and the stiffness parameters were estimated from engineering judgement. Based on the observations during drilling works at the site (see (Ausweger 2018), the saturated hydraulic permeability of both layers was predicted to be $k_{sat} = 10^{-3}$ m/s, a relatively high value. Tab. 18 summarizes the parameters for the "Sliding mass" and the "Transition zone" materials used in the numerical analysis.

Tab. 18: Soil parameters for the "Sliding mass" and "Transition zone" materials

Parameter	**Unit**	**Sliding mass**	**Transition zone**
Model	-	Mohr-Coulomb	Mohr-Coulomb
γ_{unsat}	kN/m³	20.0	20.0
γ_{sat}	kN/m³	22.0	22.0
E_{oed}	kPa	200,000	200,000
ν'	-	0.3	0.3
φ'	°	40.0	33.0 (39.0)
c'	kPa	10.0	1.0
ψ'	°	0.0	0.0
k_x / k_y	m/sec	10^{-3} / 10^{-3}	10^{-3} / 10^{-3}

It must be noted, however, that the lower friction angle φ' of 33° for the "Transition zone" led to numerical problems, therefore the friction angle was increased to 39° in selected calculations to ensure comparability of the results. As the originally used strength parameters were determined by means of back-calculations in order to reach a stress state which is close the ultimate limit state of the slope, this procedure seems to be justifiable.

9.2 Initial conditions

The simplified simulation of the geological history and the procedure used in order to reach the “initial condition” before the application of various rainfall events is illustrated in Fig. 111, and was originally used by Ausweger (2018).

As schematically shown in Fig. 111, the finite element simulation starts with the activation of the intact rock (in phase 1), followed by the activation of the sediments beneath the water storage basin under undrained conditions (phase 2), which leads to the generation of high excess pore water pressures. Subsequently, a consolidation phase for the dissipation of the excess pore water pressures (phase 3) follows, in which the overconsolidation ratio is increased and the lacustrine fine sediments are allowed to creep. The next phase (phase 4) is characterized by the activation of the “Transition zone” and the “Sliding mass”.

However, in order to reduce the calculation effort, already large in the original model and as the investigation of numerous variations of climatic conditions would enlarge it, the at this stage originally applied and 5 years lasting “Creep phase” (between phase 4 and 5 in Fig. 111) was not executed within the framework of this thesis.

Accordingly, the moment when the “Sliding mass” and the “Transition zone” have been activated represents the initial hydraulic condition with regards to saturation, suction and permeability for the entire subsoil before the rainfall event of interest is applied.

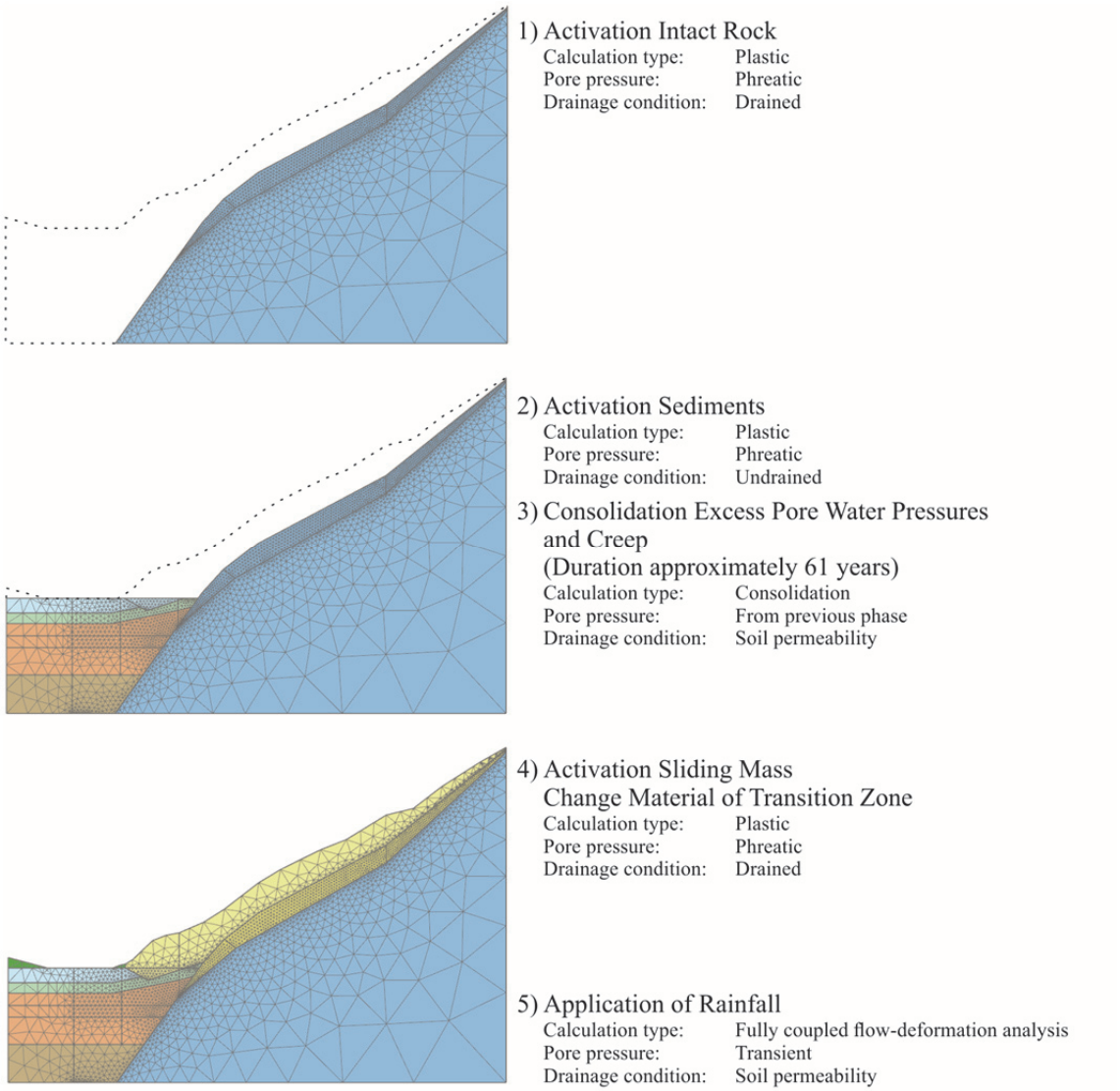

Fig. 111: Simplified simulation procedure (phase description) of geological history (Ausweger 2018, adapted)

9.3 Application of various climatic conditions

In addition to daily precipitation measurements, there were only monthly averages available for air temperature, sunshine hours and snow-covered days close to the project site. The very limited measurement data made it nearly impossible to determine a detailed modelling of water infiltration at the ground surface due to precipitation, evaporation and transpiration. Therefore, the net-precipitation into the numerical model in Ausweger (2018) is based on the available monthly averaged datasets and is modelled in a very simplified way.

Fredlund et al. (2012) described the infiltration at the ground surface by the following equation:

$$Net\ infiltration\ (I) = Precipitation\ (P) - Actual\ evaporation\ (AE) - Transpiration\ (T) - Runoff\ (R) \quad (37)$$

where precipitation is obtained from data recordings next to the project site, the actual evaporation is calculated from potential evaporation, transpiration is neglected and run-off is determined automatically during the finite element analysis by defining a maximum water height that is allowed at the soil surface (as described in previous chapters).

In order to determine the monthly average for daily potential evaporation, Ausweger (2018) utilized an empirical equation according to Thornthwaite (1948). The actual evaporation takes the suction acting in the subsoil into consideration and is determined from the potential evaporation, which describes evaporation from an open water surface. Thus, actual evaporation rates can be considerably lower than potential evaporation rates. The required coupling between evaporation and suction in the subsoil is not provided in the finite element software PLAXIS 2D, therefore the influence of suction on the evaporation is neglected. The effects of transpiration are also neglected in the following analysis. As the influence of suction on evaporation would increase infiltration rates, and the influence of transpiration would decrease infiltration rates into the slope, it is reasonable to assume that their combined effect likely compensates each other and is negligible in the context of this study.

However, for the purpose of the study in Ausweger (2018), the modelling of these environmental influences is considered as sufficient for his qualitative discussion of the changes in the subsoil due to the infiltration and a quantitative estimation of their influence on the total displacements.

In order to model the rainfall infiltration into this slope, a scenario associated with water flow in unsaturated soil conditions, definition of the unsaturated characteristics of the slope material is necessary. This chapter summarizes the differences in FoS results when alternative SWCCs and saturated hydraulic permeabilities k_{sat} are used in the numerical analysis.

The saturated hydraulic permeability of the "Sliding mass" and "Transition zone" was either kept to the originally used $k_{sat} = 10^{-3}$ m/s or decreased to $k_{sat} = 10^{-6}$ m/s in order to investigate the effects of a less permeable covering layer under real slope geometry conditions.

SWCCs from the HYPRES dataset have been used to specify the SWCC in this analysis. The originally used SWCC for both relevant soil clusters ("Sliding mass" and "Transition zone") corresponds to a "Coarse" soil of the HYPRES data set (Wösten et al. 1999) and is based on the van Genuchten model (van Genuchten 1980). As there were no laboratory tests available to determine the SWCC, they have been estimated from the material description in the available borehole logs.

As it would had not been appropriate to use the HYPRES "Coarse" SWCC when decreasing the saturated hydraulic permeability to $k_{sat} = 10^{-6}$ m/s, the more suitable HYPRES "Very Fine" SWCC has been used in the numerical analysis. Additionally, the intermediate "Medium Fine" SWCC was used within the framework of this comparative study. Fig. 112 illustrates the different SWCCs utilized in this study, and which have been taken from the HYPRES database.

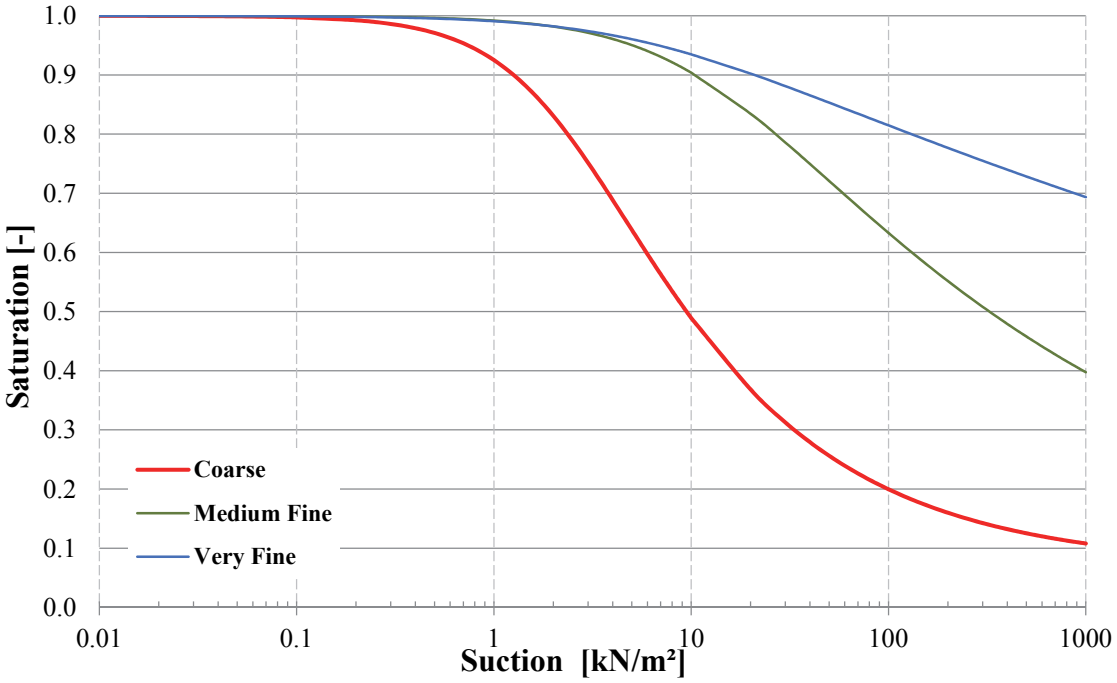

Fig. 112: The "Coarse", "Medium Fine" and "Very Fine" SWCCs of the HYPRES series

The associated relative permeability curves for the “Coarse”, “Medium Fine” and “Very Fine” HYPRES materials are given in Fig. 113.

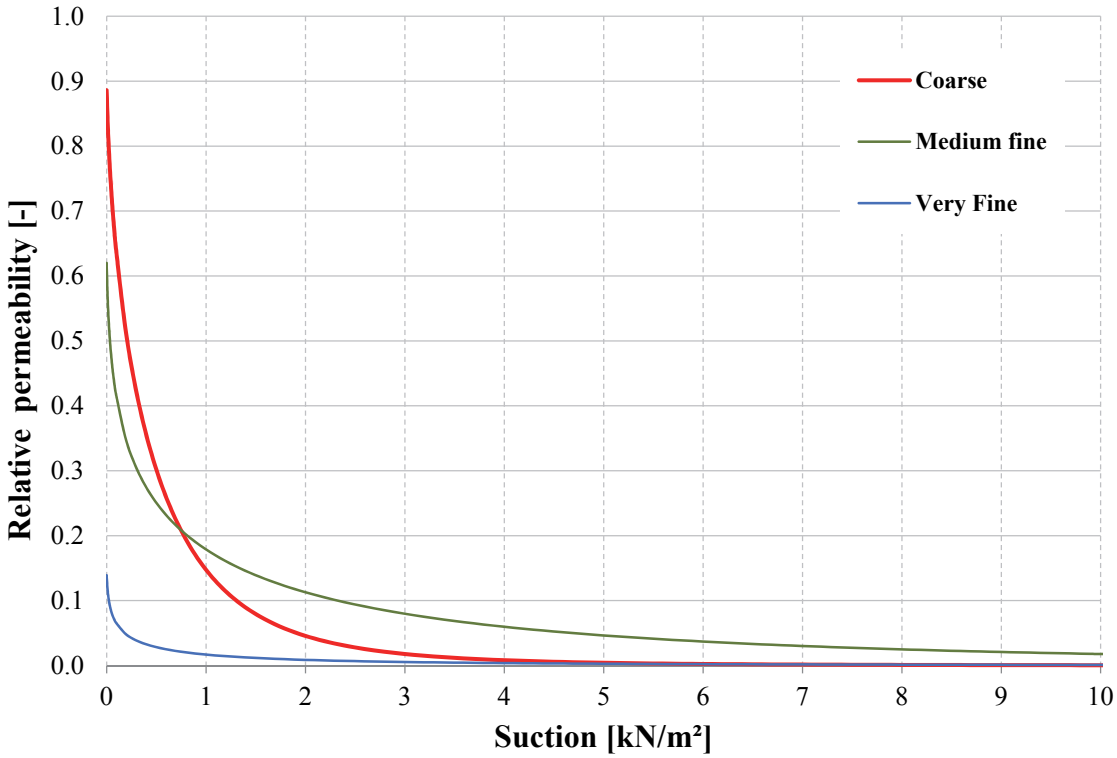

Fig. 113: Relationship between relative permeability and suction for the “Coarse”, Medium Fine’ and “Very Fine” materials of the HYPRES series

The applied net-precipitation was either kept to the original one based on monthly averages and rainfall measurements from weather stations close to the project site (“measurement point A”) as used in Ausweger (2018) or changed to data delivered from a measurement site nearby (“measurement point B”). Both measurements show, that during periods with snow-cover, as was the case in January and February 2015, almost no infiltration occurred. However, to take account of the recorded precipitation during this period, the precipitation was added to the rates of the two subsequent months March and April. Fig. 114 shows the monthly infiltration volumes composed of precipitation, potential evaporation and infiltration delivered by measurement points “A” and “B”. In the 1 year period considered, the total sum of precipitation was 1059 mm (“measurement point A”) or 1064 mm (“measurement point B”), and the evaporation considered at both measurement points was calculated as 231 mm. Therefore, the (net-) infiltration was 827 mm (“measurement point A”) or 820 mm (“measurement point B”).

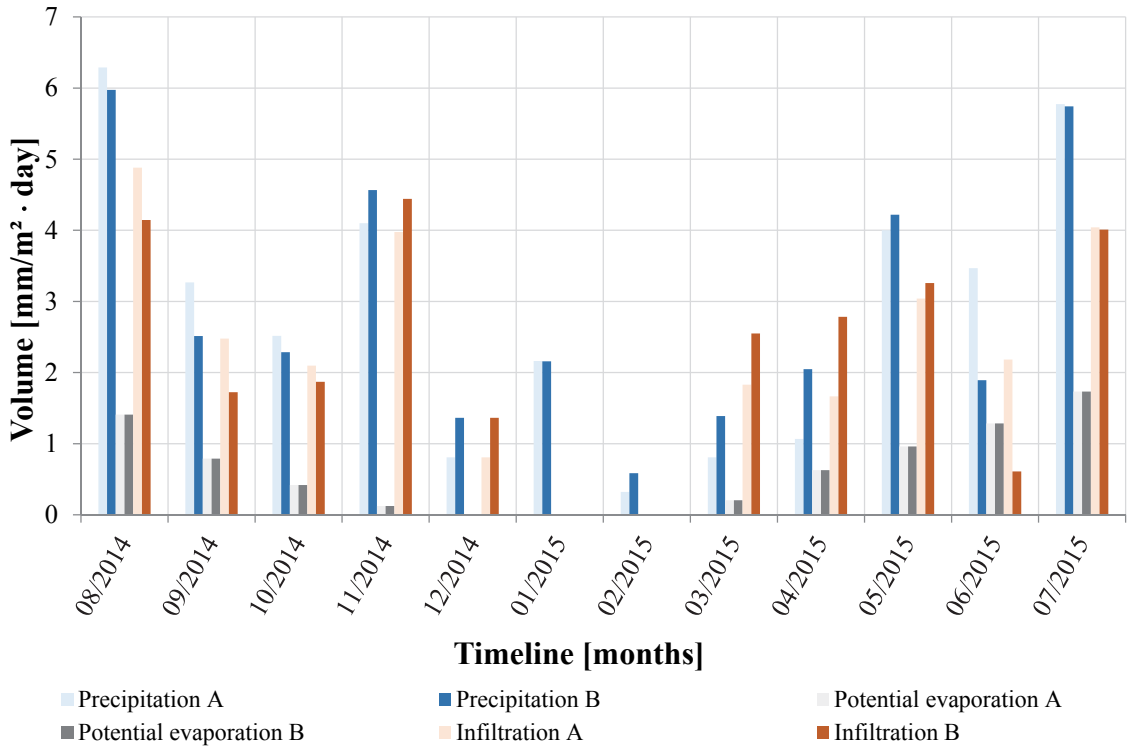

Fig. 114: Applied datasets ‘A’ and ‘B’ with precipitation, potential evaporation and the resulting infiltration

In order to determine the differences in resulting factors of safety by using a more discretized precipitation dataset, daily input compared to the simplified monthly rainfall application, a comparative study has been performed. As daily rainfall sums were only available at “measurement point B” and the data necessary for the calculation of evaporation was only provided at “measurement point A”, the average monthly evaporation was divided by the numbers of days per month to get daily values which were then considered with the daily rainfall dataset from “measurement point B”. As there was not any significant difference in precipitation rates between the two measurement points (which lie not far apart), this procedure is reasonable for the purpose of this study. As was done for the monthly data, the precipitation measured in the winter months with snow cover were shifted to the subsequent two months. Fig. 115 illustrates the climatic hydrograph based on daily precipitation rates which has been used in the comparative study.

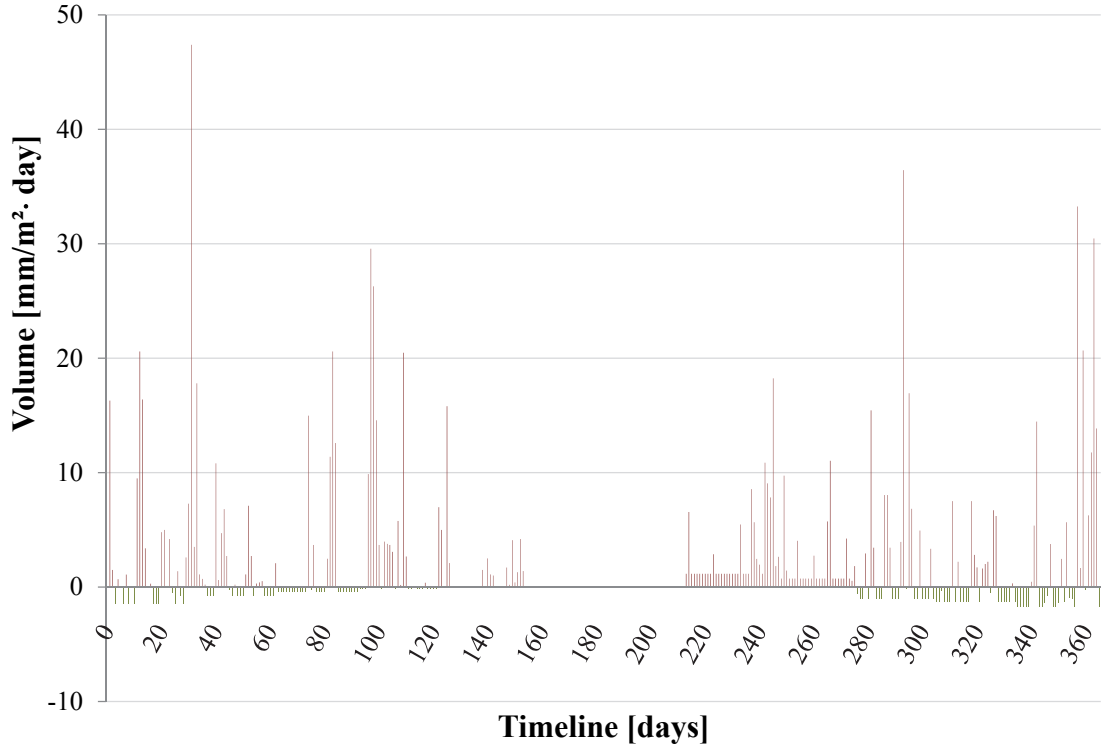

Fig. 115: Alternate net-infiltration dataset based on daily rainfall of "measurement point B" and evaporation from "measurement point A"

As described in previous chapters, heavy rainfall events, with precipitation rates up to 300 mm/day are happening more frequently in recent times in Austria, and this study also investigated their effects on the stability of this slope. This has been performed by applying constant precipitation of 300 mm/day to the slope for a period of 10 days or until failure occurred in the numerical analysis.

As discussed in previous chapters, the initial condition of the soil before a heavy rainfall event takes place plays a significant role in the instability of soil slopes. To analyse this effect, the aforementioned constant, high precipitation rate was either applied instead of, or directly after the climatic hydrograph presented in Fig. 114. This procedure allows for a quantification of antecedent rainfall effects on the FoS of this slope.

9.4 Results

The factors of safety of the slope were determined by the phi-c-reduction method. Tab. 19 presents the varying parameters and results (FoS) for the case of using the monthly precipitation dataset and either taking the previous 1-year precipitation dataset into account (Fig. 114) or not ("-1 year" in Tab. 19).

As a reminder, the originally back-calculated strength parameters for the "Transition zone" are a cohesion c'= 1 kPa and friction angle φ'= 33° and are referred to as "1-33" in the following Tab. 19. The SWCCs used in the following Tab. 19 to Tab. 22 have been abbreviated to "C" ("Coarse"), "MF" ("Medium Fine") and "VF" (Very Fine).

Tab. 19: Results of using the monthly precipitation dataset while varying SWCCs and saturated permeabilities and either considering the antecedent on year of precipitation or not

Type	Sliding mass		Transition zone		Original data		Additional rainfall		
	SWCC	k_{sat} [m/s]	SWCC	k_{sat} [m/s]	FoS before	FoS after	q [m/day]	duration [days]	FoS
1-33	C	1.0 e-3	C	1.0 e-3	1.28	1.14	0.3	2	**1.13**
- 1 year	C	1.0 e-3	C	1.0 e-3	1.28	-	0.3	5	**1.20**
1-33	C	1.0 e-6	C	1.0 e-6	1.28	1.26	0.3	10	**1.24**
- 1 year	C	1.0 e-6	C	1.0 e-6	1.28	-	0.3	10	**1.28**
1-33	MF	1.0 e-3	MF	1.0 e-3	1.49	**x**			
- 1 year	MF	1.0 e-3	MF	1.0 e-3	1.48	-	0.3	5	**1.37**
1-33	MF	1.0 e-6	MF	1.0 e-6	1.48	1.44	0.3	2	**1.45**
- 1 year	MF	1.0 e-6	MF	1.0 e-6	1.48	-	0.3	5	**1.45**

The results show that the application of the originally used monthly precipitation dataset and the use of the high permeabilities in combination with the "Coarse" ("C") SWCC in both soil layers led to a significant decrease in the FoS (1.28 to 1.14). When a constant heavy rainfall event, with 300 mm/day over a two-day period, is additionally applied, the FoS experiences a further reduction of roughly 1.5 percent (1.14 to 1.13). Neglecting antecedent rainfall and directly applying the heavy rainfall event for a five-day period ("-1 year"), causes a smaller decrease in the overall FoS. This again clearly indicates that the "initial" hydraulic condition, before a heavy rainfall event is applied, affects the FoS of a slope significantly. By changing the saturated permeability of both layers to k_{sat} = 10^{-6} m/s, these effects are not that strong but still recognizable. Employing the HYPRES "Medium Fine" SWCC ("MF") in combination with the high permeability of k_{sat} = 10^{-3} m/s causes the calculation to stop (indicated by "x" in the table) when applying the monthly dataset, and can therefore not be compared with the case variation where the previous rainfall dataset was neglected.

The calculation, for this material, with the lower saturated permeability of k_{sat} = 10^{-6} m/s was possible and led to only slight decreases in the FoS and there were no differences in the results whether the monthly dataset had been applied or not.

The application of the daily precipitation dataset, portrayed in Fig. 115 and discussed with Tab. 22, led to numerical problems when using it on soil characterised by the "Coarse" SWCC in combination with high saturated permeabilities (k_{sat} = 10^{-3} m/s). Thus, in order to compare the effects of either using the monthly or the daily precipitation datasets, the friction angle for the "Transition zone" was increased to 39° (cohesion was kept to 1 kPa) to solve the numerical problem, and used in all cases, for both those applying the monthly or the daily precipitation. The results for cases using the monthly precipitation dataset and the increased friction angle are given in Tab. 20.

Tab. 20: Results of using the monthly precipitation dataset under increased friction angle φ' for transition zone, while varying SWCCs and saturated permeabilities and either considering the antecedent one year of precipitation or not

Type	Sliding mass		Transition zone		Original data		Additional rainfall		
	SWCC	k_{sat} [m/s]	SWCC	k_{sat} [m/s]	FoS before	FoS after	q [m/day]	duration [days]	FoS
1-39	C	1.0 e-3	C	1.0 e-3	1.44	1.31	0.3	5	**1.30**
- 1 year	C	1.0 e-3	C	1.0 e-3	1.44	-	0.3	5	**1.41**
1-39	C	1.0 e-6	C	1.0 e-6	1.44	1.43	0.3	10	**1.41**
- 1 year	C	1.0 e-6	C	1.0 e-6	1.44	-	0.3	10	**1.43**
1-39	MF	1.0 e-3	MF	1.0 e-3	1.64	1.47	0.3	5	**1.42**
- 1 year	MF	1.0 e-3	MF	1.0 e-3	1.64	-	0.3	5	**1.51**
1-39	MF	1.0 e-6	MF	1.0 e-6	1.64	1.59	0.3	10	**1.59**
- 1 year	MF	1.0 e-6	MF	1.0 e-6	1.64	-	0.3	10	**1.59**

The adaptation of the friction angle made the numerical calculation of all investigated combinations of SWCCs and saturated permeabilites k_{sat} possible. The results presented in Tab. 20 show the same qualitative behaviour as by using the originally determined strength parameter (results in Tab. 19). It is obvious, that due to the increased strength parameter, the initial FoS before the first rainfall dataset was applied is significantly higher compared to the previous study using the original friction angle for the "Transition zone". Within the results of this change, the application of the heavy rainfall event once again resulted in higher safety factors when applied to the slope that had not experienced any previous rainfall, as opposed to the slope which had experienced a year's worth of precipitation. This again undoubtedly shows that previous rainfall should be taken into account whenever available to avoid overestimating the safety of the slope. Within the following two tables (Tab. 21 and Tab. 22), the influence of the discretisation of the rainfall dataset, into monthly or daily input, has been

investigated. Tab. 21 presents the results utilizing the rainfall dataset discretised into monthly input, whereas Tab. 22 presents the effects of applying the rainfall dataset which is discretised into daily precipitation. The two applied precipitation datasets led to comparable results with generally only marginal deviations in FoS, except for the anomaly (clear difference in FoS) when using the HYPRES' "Medium Fine" SWCC ("MF") with a more impermeable "Sliding mass" material and highly permeable "Transition zone" material. Thus, the discretization of the rainfall dataset did not affect the factor of safety of the slope, under the assumptions and tested circumstances of this study.

Tab. 21: Results of using the monthly precipitation dataset under increased friction angle φ' for transition zone, while varying SWCCs and saturated permeabilities

Type	Sliding mass		Transition zone		Original data		Additional rainfall		
	SWCC	k_{sat} [m/s]	SWCC	k_{sat} [m/s]	FoS before	FoS after	q [m/day]	duration [days]	FoS
1-39	C	1.0 e-3	C	1.0 e-3	1.44	1.31	0.3	5	**1.30**
1-39	MF	1.0 e-3	MF	1.0 e-3	1.64	1.47	0.3	5	**1.42**
1-39	VF	1.0 e-3	VF	1.0 e-3	1.76	**x**			
1-39	C	1.0 e-6	C	1.0 e-6	1.44	1.43	0.3	10	**1.41**
1-39	MF	1.0 e-6	MF	1.0 e-6	1.64	1.59	0.3	10	**1.59**
1-39	VF	1.0 e-6	VF	1.0 e-6	1.77	1.71	0.3	10	**1.74**
1-39	C	1.0 e-6	C	1.0 e-3	1.44	1.44	0.3	10	**1.41**
1-39	MF	1.0 e-6	MF	1.0 e-3	1.63	1.59	0.3	10	**1.32**
1-39	VF	1.0 e-6	VF	1.0 e-3	1.76	1.70	0.3	10	**1.69**
1-39	VF	1.0 e-6	C	1.0 e-3	1.52	1.49	0.3	10	**1.48**
1-39	MF	1.0 e-6	C	1.0 e-3	1.51	1.47	0.3	10	**1.32**

Tab. 22: Results of using the daily precipitation dataset under increased friction angle φ' for transition zone, while varying SWCCs and saturated permeabilities

Type	Sliding mass		Transition zone		Original data		Additional rainfall		
	SWCC	k_{sat} [m/s]	SWCC	k_{sat} [m/s]	FoS before	FoS after	q [m/day]	duration [days]	FoS
1-39	C	1.0 e-3	C	1.0 e-3	1.44	1.31	0.3	5	**1.30**
1-39	MF	1.0 e-3	MF	1.0 e-3	1.64	**x**			
1-39	VF	1.0 e-3	VF	1.0 e-3	1.76	**x**			
1-39	C	1.0 e-6	C	1.0 e-6	1.44	1.43	0.3	10	**1.42**
1-39	MF	1.0 e-6	MF	1.0 e-6	1.64	1.59	0.3	10	**1.59**
1-39	VF	1.0 e-6	VF	1.0 e-6	1.77	1.71	0.3	10	**1.71**
1-39	C	1.0 e-6	C	1.0 e-3	1.44	1.44	0.3	10	**x**
1-39	MF	1.0 e-6	MF	1.0 e-3	1.63	1.59	0.3	10	**1.60**
1-39	VF	1.0 e-6	VF	1.0 e-3	1.76	1.70	0.3	10	**1.70**
1-39	VF	1.0 e-6	C	1.0 e-3	1.52	1.49	0.3	10	**1.48**
1-39	MF	1.0 e-6	C	1.0 e-3	1.51	1.46	0.3	10	**1.32**

9.5 Conclusions and outcomes investigation on a real slope geometry

Based on the work of Ausweger (2018), who thoroughly investigated the influence of water level changes in a water storage basin and further influences from precipitation and the creep behaviour of the lacustrine fine sediments on the movement behaviour of a slow moving landside, additional numerical studies in order to quantify the influence of changing hydraulic boundary conditions (SWCCs, k_{sat} and climatic hydrograph) on the factor of safety of this slope (landslide) have been performed and presented in this chapter.

The results clearly indicate that they are sensitive to changes in the SWCCs of both considered soil layers ("Sliding mass" and "Transition zone"), as different SWCCs resulted in distinct differences in the factors of safety after rainfall application. This highlights the need of carefully selecting the SWCC from available curves databases (HYPRES, USDA), if the determination of the SWCC in the laboratory is not possible.

Compared to the calculations utilizing the higher, original saturated hydraulic permeabilities ($k_{sat} = 10^{-3}$ m/s), the calculations with lower permeabilities ($k_{sat} = 10^{-6}$ m/s) showed only slight decreases of the FoS when the antecedent one year of precipitation was applied.

Under the assumptions and circumstances tested in this study, the discretization of the precipitation dataset, either into monthly or daily inputs, did not affect the factor of safety of the slope.

The effects of a heavy rainfall event on the stability of the slope was investigated by applying constant precipitation of 300 mm/day for a period of 10 days or until failure occurred in the numerical analysis. The results presented in this chapter again showed that the initial pore water pressure condition in the slope, before a heavy rainfall event is applied, plays a significant role in the stability of soil slopes and therefore that antecedent precipitation, which greatly influences the pore water pressure profile, should always be considered.

10 Conclusions and further research

10.1 Conclusions

Previous research has shown that the stability of unsaturated soil slopes may be affected by precipitation due to the accompanying changes in the pore water pressure profile. Throughout the execution of numerous numerical preliminary studies to investigate the general infiltration behaviour into unsaturated soils due to precipitation, several shortcomings were raised. A very important point that needed to be examined is the automatically generated linearly increasing initial negative pore water pressure (suction) above the initial groundwater-level to reach numerical equilibrium in numerical analyses. This leads to high suction values in the upper soil zone, especially if the starting groundwater-level is deep below the ground surface, and this causes very low hydraulic permeabilities, which may not be realistic. Thus, besides highlighting the influence of other (hydraulic) boundary conditions the stability of unsaturated soil slopes, finding an adequate solution to overcome this initial pressure issue forms the basis for this thesis. One possible solution of using continuously measured Lysimeter-data was found and it could be used for a reasonable calibration of the suction profiles in the numerical model.

After the detailed introduction to unsaturated soils, the significant influence of the degree of saturation, and associated suction, on the infiltration behaviour, defined by the Soil Water Characteristic Curve (SWCC), was shown by means of numerically modelling water flow into and through unsaturated soils (chapter 4). As particular types of unsaturated soils can be used as cover-layers for underground waste storage and containment and are regulated by limitations on the amount of water may reach the protected layer, this study was used to clearly show the sensitivity of numerically modelled water flow through unsaturated soil to even slight changes in the SWCC and the saturated hydraulic permeability used to define the material's hydraulic characteristics. Additionally, the effects of evapotranspiration, which decreases the amount of net-infiltration into the soil, were shown. In the particular case presented, the saturated permeability proved to be the critical parameter in order to fulfil the prescriptions of the authorities, while the SWCC showed a smaller impact on the results.

The influence of varying climatic hydrographs, its associated changes of pore water pressures and shear strength on the stability of simplified slope geometries with inhomogeneous soil was examined in chapter 5. The effects of different SWCCs on the FoS of the slope were evaluated by means of fully coupled flow-deformation analyses. The strength reduction method (explained in chapter 2) was used to determine the slopes' FoS after specific infiltration and evaporation were applied to the model according to a climatic hydrograph. As the initial pore water pressure distribution in the model is solely determined by the location of

the groundwater level, high suction values at the ground surface are the initial condition for the model and generally lead to very small infiltration rates into the unsaturated slope. Various climatic hydrographs were used in this study, with only slight differences between them. However, the largest decrease in slopes' stability was the result of constant precipitation being applied, without any intervening periods of evaporation. Even though the total amount of rainfall was kept the same across the hydrograph variations, a low precipitation rate over a longer period causes a greater reduction in FoS of the slope compared to a shorter more intense precipitation rate.

Within the boundary conditions investigated, a lower saturated permeability of the upper fine-grained soil layer led to an increase in the FoS if the applied precipitation was larger than the hydraulic permeability of the soil because the precipitation volume becomes a built up pressure head, which then flows off as run-off instead of infiltrating. Having an additional water load which acts like a "surcharge" of 10 cm (defined by ψ_{max} = 0.1 m in this preliminary study) is a situation which is unlikely to occur in practice, but it highlights the importance of careful selection of hydraulic boundary conditions. The factor of safety of the slope decreased when the upper soil layer had a higher saturated hydraulic conductivity because water was able to infiltrate in more easily.

The results of the preliminary studies described in this thesis clearly indicated that automatically generated initial pore water pressures based on the defined (deep-lying) groundwater level, led to unrealistically high suction values at the ground surface and do not represent the majority of naturally occurring matric suction profiles. However, is known and accepted that there exist natural mechanisms which add and remove water to or from the subsoil (see Fig. 1 in chapter 3 representing the natural hydrological cycle) and that therefore, the conditions at the natural boundary between soil and atmosphere, which the FE-code simulates and which results in the high suction values at the ground surface, are most likely not realistic. Besides the location of the groundwater-level, the drainage conditions, the saturated hydraulic permeability of the soil, the SWCC used for the soil and environmental conditions such as precipitation and evaporation also affect the shape of the matric suction profile near the ground surface.

Since PLAXIS 2D allows suction values to be manually predefined by means of heads at any geometry line of the model, it is possible to implement measured field data of suction directly into the model, overcoming the issue above. The Lysimeter, a device which is typically used for agricultural research purposes, is able to provide such data to calibrate the hydraulic conditions of soils in numerical analysis. This device is installed in the ground and continuously measures suction in certain depths of the soil. A nearby weather station gives information about the current precipitation and evapotranspiration. Within the framework of a numerical 1D-column test presented in chapter 6, these data were

used as input data to define the initial pore pressure profile. With respect to the replication of in situ measured suction profiles in unsaturated soils, the back-calculation of Lysimeter-data in a column-test delivered very satisfactory results. Each drop in the suction-curve was induced by high daily rainfall rates, whereas drier periods led to increased suction values. The development of suction over time were shown for both calculations that used the manually defined initial suction values ("model M"), and those that used the automatically generated initial suction values ("model A"). It was shown that if the duration of the applied climatic hydrograph was long enough (in this specific case >35 days), the resulting suction values were not affected by the initial starting values. From this point onwards, both calculation options ("model A" and model M") show the same suction development as a consequence of the applied climatic hydrograph. However, it should be mentioned, that this was the point where suction was equal to zero, both measured and calculated.

The application of the procedure described in chapter 6 avoids the use of uncertain hydraulic input-parameters, which can affect the infiltration behaviour siginificantly. In addition, numerically calculated suction development could also be used to predict suction for periods in which no measured values were available (e.g. temporary failure of the tensiometers) or to predict pore water pressure developments in the future.

Nevertheless, this preliminary study pointed out, that there could be a slight deviation to the measured values due to the predefinition of the initial pore water pressures. However, it could be proved that in contrast to the possible negative effects of unknown initial hydraulic conditions and hence simply using the automatically generated initial pore water pressures, the small deviations due to the before mentioned method are negligible and not further investigated.

Based on the outcomes of the preliminary study of chapter 6, the infiltration behaviour due to rainfall on slope geometries with variable boundary conditions was investigated in chapter 6. The main goal of this chapter was to predict and determine when the manually ("model M") and automatically ("model A") generated pore water pressures match in the climatic hydrograph. The determination of initial hydraulic boundary conditions within a slope is cost-intensive, hard to achieve or even impossible. Therefore, in order to quantify the influence of the initial hydraulic conditions on numerical results, a numerical study using the Lysimeter delivered suction values also for manually describing initial suctions in the benchmark slope, has been performed. The data delivered from the Lysimeter, as described and used in the preliminary study, is only available for depths until 0.5 m. Consequently, it must be noted that the use of the Lysimeter dataset in the benchmark slope calculations served only to qualitatively highlight the differences between ("model M") and ("model A") calculations. It should also be noted that these conclusions are only relevant for very shallow slope failures and not for deep seated instabilities.

The initial location of the groundwater-level turned out to be the key parameter in both variants ("model M" and "model A"), and affects all further results. Additionally, the results of using three different values for the saturated hydraulic permeability were presented. The application of the original, relatively high, permeability (k_{ref}) led to a fast reduction of suction in all the analyses. As a result of the application of 192 days climatic hydrograph and the given boundary conditions, all the curves fitted together after approximately 40 days. After this period (the first 40 days), suction reached zero for the first time and then any further climatic influences affected all the variants in the same way. Contrary to that, the (hypothetical) analyses with a lowered saturated permeability, where the original one was divided by 100 ($k_{ref}/100$), generated big differences in the results. As there always remains a high degree of uncertainty with regards to the determination of the saturated hydraulic permeability due to local heterogeneities and preferential flow paths of a soil body, this hypothetical assumption seems justified. Utilizing these lower permeabilities, the "model A" suction curves never matched the "model M" curves within the timeframe of the climatic hydrograph used (independently of the applied hydraulic boundary condition). This means that the starting condition (initial pore water pressure profile) significantly affects the development of suction and that previous rainfall events have to be taken into account whenever available.

Furthermore, the effects of different assumptions concerning the role of suction within phi-c-reductions were investigated. As suction is an indissoluble part of the coupling between deformations, pore pressure and groundwater flow, a fully coupled flow-deformation analysis will always take suction into account. Thus, when using fully coupled flow-deformation analysis as part of a model, it is best practice to take suction into account for all calculation phases. The significant influence on the FoS of a benchmark slope of taking previous precipitation into account was also demonstrated. Since heavy rainfall events, with precipitation rates up to 300 mm/day are happening more frequently in recent times in Austria, the effects of applying a constant precipitation rate of 300 mm/day was investigated. In order to simulate an extreme case, this high intensity rainfall has been applied for a period of 10 days or until failure occurs in the numerical analysis. Independently of the SWCCs used in the calculations, the results generally showed a strong decrease in the FoS within the first 6 to 12 hours for high saturated permeabilities ($k_{sat} = 10^{-3}$ m/s) of the soil.

Based on the work of Ausweger (2018), additional numerical studies in order to quantify the influence of changing hydraulic boundary conditions (SWCCs, k_{sat} and climatic hydrograph) on the factor of safety of a landslide slope were performed and presented.

The results clearly indicate that they are sensitive to changes in the SWCCs of both considered soil layers ("Sliding mass" and "Transition zone"), as different SWCCs resulted in distinct differences in the factors of safety after rainfall application. This highlights the need of carefully selecting the SWCC from available curves databases (HYPRES, USDA), if the determination of the SWCC in the laboratory is not possible.

As mentioned several times in previous chapters, the results presented in this thesis showed that the initial pore water pressure condition in the slope, before a heavy rainfall event is applied, plays a significant role in the stability of soil slopes and therefore that antecedent precipitation, which greatly influences the pore water pressure profile, should always be considered.

10.2 Further research

Recommendations for further research in the field of numerical modelling of the particular behaviour of unsaturated soils are given in the following bullets:

- With respect to commercial finite element codes, the development and / or implementation of more advanced constitutive models (e.g. Barcelona Basic model) in order to simulate the particular deviatoric and volumetric behaviour of unsaturated soils is recommended

- The hysteretic behaviour of the SWCC should be taken into account in numerical analyses

- The determination of Soil Water Characteristic Curves based on laboratory results should be standardized and performed for each specific project

- To make such measurements also possible on hard to reach slopes and landslides, easy to install devices for in-situ measurements of suction development should be developed

- To calibrate initial suction profiles in numerical models, continuously monitored investigations on suction profiles to deeper depths should be performed

11 Bibliography

Alonso, E., Gens, A. & Hight, D., 1987. Special problem soils. General report. In: *Proceedings of the Ninth European Conference on Soil Mechanics and Foundation Engineering.* Dublin, Ireland, Vol. 3, pp. 1087-1146.

Alonso, E., Gens, A. & Josa, A., 1990. A constitutive model for partially saturated soils.. *Géotechnique, 40(3)*, pp. 405-430..

Askarinejad, A., 2013. *Failure mechanisms in unsaturated silty sand slopes triggered by rainfall.* DISS. ETH NO. 21423 ed. ETH Zürich

Ausweger, G., 2018. *Influences of water level changes on the behaviour of a slow moving landslide - in-situ measurements, model tests and numerical analyses.* Graz: Dissertation Technische Universität Graz.

Barbour, S., 1998. The soil-water characteristic curve: a historical perspective. *Canadian Geotechnical Journal 35*, pp. 873-894.

Bishop, A., 1959. The principle of effective stress, Teknisk Ukeblad, 106 (39). pp. 859-863.

Bishop, A. & Blight, G., 1963. Some aspects of effective stress in saturated and partly saturated soils. *Géotechnique, 13(3)*, pp. 177-197.

BMLFUW, 2012. *Hydrographisches Jahrbuch in Österreich (120), Gitterpunkt 5214*

Boutonnier, L., 2010. Coefficient B, consolidation and swelling in fine soils near saturation in engineering practice. In: L. &. Hoboken, ed. *Mechanics of unsaturated geomaterials.* s.l.:ISTE Ltd and John Wiley & Sons, pp. 327-352.

Brinkgreve, R., Kumarswamy, S. & Swolfs, W., 2017. *PLAXIS 2D 2017 - User Manual.* Delft: Plaxis bv.

Burland, J., 1964. Effective stresses in partly saturated soils, Discussion of "Some aspects of effective stress in saturated and partly saturated soils," by G. E. Blight and A. W. Bishop.. *Géotechnique, 14*, pp. 65-68.

Cai, F. & Ugai, K., 2004. Numerical analysis of rainfall effects on slope stability. *ASCE International Journal of Geomechanics, Vol. 4 (2)*, pp. 69-78.

Casini, F., 2012. Deformation induced by wetting: a simple model. *Canadian Geotechnical Journal, 49*, pp. 954-960.

Childs, E., 1969. Soil Water Phenomena. *Wiley-Interscience, New York*.

Chirico, G. et al., 2013. Role of vegetation on slope stability under transient unsaturated conditions. *Procedia Environmental Sciences (19)*, pp. 932-941.

Chiu, C., Yan, W. & Yuen, K.-V., 2012. Reliability analysis of soil-water characteristic curve and its application to slope stability analysis. *Engineering Geology*, pp. 83-91.

Cho, S. & Lee, S., 2001. Instability of unsaturated soil slopes due to infiltration. *Computers and Geotechnics (28)*, pp. 185-208.

Delage, P., 2002. Experimental unsaturated soil mechanics. *Proceedings of the 3rd International Conference on Unsaturated Soils (3)*, pp. 973-996.

Delage, P., 2015. Water retention and transport properties of unsaturated materials. In: *7th Alert Olek Zienkiewicz course on unsaturated soil mechanics: From fundamentals to applications.* UPC Barcelona

Dorsey, N., 1940. Properties of Ordinary Water Substances. In: *American Chemical Society Monograph Series.* New York: Reinhold.

Edlefsen, N. & Anderson, A., 1943. Thermodynamics of soil moisture. *Hilgardia Vol. 15*, pp. 31-298.

Eijkelkamp, 2007. *User Manual - Sandbox for pf-determination.* s.l.:Eijkelkamp Soil & Water.

Eijkelkamp, 2009. *Operating instructions - 15 Bar Pressure Plate Extractor*

Escario, V., Juca, J. & Coppe, M., 1989. Strength and deformation of partly saturated soils. In: *Proceedings of the 12th International Conference on Soil Mechanics and Foundation Engineering, Vol. 3.* Rio de Janeiro, pp. 43-46.

Fank, J. & Unold, G., 2007. High precision weighable filed Lysimeter. A tool to measure water and solute balance parameters. *International Water & Irrigation, 27 (3)*, pp. 28-32.

Fourie, A., 1996. Predicting rainfall-induced slope instability. *Proceedings of the Institution of Civil Engineers: Geotechnical Engineering 119 (4)*, pp. 211-218.

Fredlund, D., 1976. Density and compressibility characteristics of air-water mixtures. *Canadian Geotechnical Journal, Vol. 13 (4)* , pp. 386-396.

Fredlund, D. G. & Xing, A., 1994. Equations for the soil-water characteristic curve. *Canadian Geotechnical Journal, Vol. 31, No. 3* , pp. 521-532.

Fredlund, D. & Morgenstern, N., 1977. Stress state variables for unsaturated soils. *ASCE Journal of the Geotechnical Engineering division, 107 (GT5)*, pp. 447-466.

Fredlund, D., Rahardjo, H. & Fredlund, M., 2012. *Unsaturated Soil Mechanics in Engineering Praxis.* New Jersey: John Wiley & Sons.

Fredlund, D., Sheng, D. & Zhao, J., 2011. Estimation of suction from the soil-water characteristic curve. *Canadian Geotechnical Journal, Vol. 48 (2)*, pp. 186-198.

Fredlund, D., Xing, A., Fredlund, M. & Barbour, S., 1995. The relationship of the unsaturated soil shear strength to the soil-water characteristic curve. *Canadian Geotechnical Journal, Vol. 33 (3)*, pp. 440-448.

Galavi, V., 2010. *Groundwater flow, fully coupled flow deformation and undrained analysis in PLAXIS 2D and 3D,* s.l.: Plaxis BV.

Gardner, W., 1956. Calculation of capillary conductivity from pressure plate outflow data. *Soil Science Society of America, Proceedings, 20*, pp. 317-320.

Gasmo, J., Rahardjo, H. & Leong, E., 2000. Infiltration effects on stability of a residual soil slope. *Computers and Geotechnics, Vol. 26 (2)*, pp. 145-165.

Griffiths, D. & Lane, P., 1999. Slope stability analysis by finite elements. *Geotechnique 49 (3)*, pp. 387-403.

Griffiths, D. & Lu, N., 2005. Unsaturated slope stability analysis with steady infiltration or evaporation using elasto-plastic finite elements. *International Journal of Numerical and Analytical Methods in Geomechanics, Vol. 29 (3)*, pp. 249-267.

Hillel, D., 1998. Environmental Soil Physics. *Academic Press, San Diego*.

Jommi, C., 2000. *Remarks on the constitutive modelling of unsaturated soils. In International Workshop on Experimental Evidence and Theoretical Approaches in Unsaturated Soils; 139-153.* Trento- Italy

Kawamoto, K., Kawamura, T., Kobayashi, T. & Oda, M., 2004. Soil water dynamics in a forested soil at a landslide site under natural precipitation. In: *Research report.* Saitama University, Tokio, Japan

Khalili, N. & Khabbaz, M., 1998. A unique relationship for χ for the determination of the shear strength of unsaturated soils. *Geotechnique 48,2*, pp. 1-7.

Köhler, H. & Montenegro, H., 2005. Investigations regarding soils below phreatic surface as unsaturated porous media. In: *Proc. International Conference "From Experimental Evidence towards Numerical Modeling of Unsaturated Soils".* Weimar, Germany, pp. 139-157.

Krahn, J. & Fredlund, D., 1972. On total matric and osmotic suction. *Journal of Soil Science, Vol. 114 (5)*, pp. 339-348.

Lu, N. & Griffiths, D., 2004. Profiles of steady-state suction stress in unsaturated soils. *Journal of Geotechnical and Geoenvironmental Engineering, Vol. 130 (10), ASCE*, pp. 1063-1076.

Lu, N. & Likos, W., 2004. *Unsaturated Soil Mechanics.* New Jersey: John Wiley & Sons.

Lu, N. & Likos, W., 2006. Suction stress characteristic curve for unsaturated soil. *Journal of Geotechnical and Geoenvironmental Engineering, Vol. 132 (2), ASCE*, pp. 131-142.

Mualem, Y., 1976. A new model for predicting the hydraulic conductivity of unsaturated porous media. *Water Resources Research (12)*, pp. 513-522.

Mualem, Y., 1984. A modified dependent domain theory of hysteresis. *Soil Science, 137*, pp. 283-291.

Murray, E. & Sivakumar, V., 2010. *Unsaturated Soils - A fundamental interpretation of soil behaviour.* UK: John Wiley & Sons.

Ng, C. & Shi, Q., 1998. A numerical investigation of the stability of unsaturated soil slopes subjected to transient seepage. *Computer and Geotechnics 22 (1)*, pp. 1-28.

Ni, P., Mei, G. & Zhao, Y., 2018. Influence of Raised Groundwater Level on the Stability of Unsaturated Soil Slopes. *ASCE International Journal of Geomechanics 18 (12)*.

Nuth, M. & Laloui, L., 2008. Effective stress concept in unsaturated soils: clarification and validation of a unified framework. *International Journal for Numerical and Analytical Methods in Geomechanics, 32*, pp. 771-801.

Öberg, A.-L. & Sällfors, G., 1997. Determination of shear strength parameters of unsaturated silts and sands based on the water retention curve. *Geotechnical Testing Journal, 20 (1)*, pp. 40-48.

Oh, W. & Vanapalli, S., 2010. Influence of rain infiltration on the stability of compacted soil slopes. *Computers and Geotechnics (37)*, pp. 649-657.

Peters, A. & Durner, W., 2008. Simplified evaporation method for determining soil hydraulic properties. *Journal of Hydrology (356)*, pp. 147-162.

Pham, H., Fredlund, D. & Barbour, S., 2003a. A practical hysteresis model for the soil-water characteristic curve for soils with negligible volume change. *Geotechnique, Vol. 53 (2)* , pp. 293-298.

Pham, H., Fredlund, D. & Barbour, S., 2003b. Estimation of the hysteretic soil-water characteristic curves from the drying boundary curve. In: *Proceedings of the Fifty-Sixth Canadian Geotechnical Conference.* Winnipeg, MB, Vol.2, pp. 115-121.

Rahardjo, H., Nio, A., Leong, E. & Song, N., 2010 . Effects of Groundwater Table Position and Soil Properties on Stability of Slope during Rainfall. *Journal of Geotechnical and Geoenvironmental Engineering (136)*, pp. 1555-1564.

Rahardjo, H., Ong, T., Rezaur, R. & Leong, E., 2007. Factors controlling instability of homogeneous soil slopes under rainfall. *ASCE Journal of Geotechnical and Geoenvironmental Engineering (12)*, pp. 1532-1543.

Rahimi, A., Rahardjo, H. & Leong, E., 2010. Effect of hydraulic properties of soil on rainfall-induced slope failure. *Engineering Geology 114 (3-4)*, pp. 135-143.

Reszler, C. & Fank, J., 2016. Unsaturated zone flow and solute transport modelling with MIKE SHE: model test and parameter sensitivity analysis using Lysimeter data. *Environmental Earth Sciences*, pp. 75-253.

Richards, B., 1965. Measurement of the free energy of soil moisture by the psychometric technique using thermistors. *Moisture Equilibria and Moisture Changes in Soils Beneath Covered Areas, A Symposium in Print, Buttersworth, Sidney*, pp. 39-46.

Richards, L., 1941. A pressure mebrane extraction apparatus for soil suction. *Soil Science 51 (5)*, pp. 377-386.

Robinson, J., Vahedifard, F. & Aghakouchak, A., 2017. Rainfall-triggered slope instabilities under a changing climate: comparative study using historical and projected precipitation extremes. *Canadian Geotechnical Journal (54)*, pp. 117-127.

Schaap, M. & Leij, F., 2000. Improved prediction of unsaturated hydraulic conductivity with the Mualem-van Genuchten model. *Soil Science Society of America Journal (64)*, pp. 843-851.

Schindler, U., 1980. Ein Schnellverfahren zur Messung der Wasserleitfähigkeit im teilgesättigten Boden an Stechzylinderproben. *Archiv für Äcker- und Pflanzenbau und Bodenkunde 24 (1)*, pp. 1-7.

Schindler, U. et al., 2010. The evaporation method: Extending the measurement range of soil hydraulic properties using the air-entry pressure of the ceramic cup. *Journal of Plant Nutrition and Soil Science (173)*, pp. 563-572.

Schindler, U. & Müller, L., 2006. Simplifying the evaporation method for quantifying soil hydraulic properties. *J. Plant Nutr. Soil Sci. 169*, pp. 623-629.

Schuhmann, A. et al., 2015. A long-term Lysimeter experiment to investigate the environmental dispersion of the herbicide chloridazon and its metabolies - comparison of Lysimeter types. *Journal of Soils and Sediments (16)*, pp. 1032-1045.

Schuurmann, I., 1966. The compressibility of an air/water mixture and a theoretical relation between the air and water pressures. *Geotechnique, Vo. 16 (4)*, pp. 269-281.

Senthilkumar, V., Chandrasekaran, S. & Maji, V., 2018. Rainfall-Induced Landslides: Case Study of the Marappalam Landslide, Nilgris District, Tamil Nadu, India. *International Journal of Geomechanics 18 (9)*.

Siemens, G., 2017. Thirty-Ninth Canadian Geotechnical Colloquium: Unsaturated soil mechanics - bridging the gap between research and practice. *Canadian Geotechnical Journal (55)*, pp. 909-927.

Springman, S., Thielen, A., Kienzler, P. & Friedel, S., 2013. A long-term field study for the investigation of rainfall-induced landslides. *Geotechnique 63 (14)*, pp. 1177-1193.

Tarantino, A. & Jommi, C., 2005. *Proceedings of the Hydraulic and Mechanical Behaviour of Unsaturated Soils - Experimental Evidence and Constitutive Modeling.* Trento, s.n.

Terzaghi, K., 1936. *The shear resistance of saturated soils and the angle between the planes of shear.* 1st International Conference on Soil Mechanics, 1; 54-56.

Thornthwaite, C., 1948. An Approach toward a Rational Classification of Climate Geographical. *Geographical Review, Vol. 38 (1)*, pp. 55-94.

Townsend, R. & Rice, S., 1991. Molecular dynamic studies of the liquid-vapour interface of water. *Journal of Chemical Physics Vol 94 (3)*, pp. 2207-2218.

Tsiampousi, A., Zdravkovic, L. & Potts, D., 2013. Variation with time of the factor of safety of slopes excavated in unsaturated soils. *Computers and Geotechnics 48 (2013)*, pp. 167-178.

UMS, 2015. *Operational manual HYPROP.* München, Germany: UMS GmbH.

Valentino, R., Montrasio, L., Losi, G. & Bitelli, M., 2011. An empirical model for the evaluation of the degree of saturation of shallow soils in relation to rainfalls. *Canadian Geotechnical Journal (48)*, pp. 795-809.

van Genuchten, M., 1980. A Closed-form Equation for Predicting the Hydraulic Conductivity of Unsaturated Soils. *Soil Science Society of America Journal, 44*, pp. 892-898.

van Mechelen, J., 2004. Strength of moist sand controlled by surface tension for tectonic analogue modelling. *Tectonophysics*, pp. 275-284.

Vanapalli, S. & Fredlund, D., 2000. Comparison of empirical procedures to predict the shear strength of unsaturated soils using the soil-water characteristic curve. In: C. Shackelford, S. Houston & N. Chang, eds. *Advances in Unsaturated Geotechnics.* ASCE, Reston, VA: GSP No. 99, pp. 195-209.

Vanapalli, S., Fredlund, D., Pufahl, D. & Clifton, A., 1996. Model for the presiction of shear strength with respect to soil suction. *Canadian Geotechnical Journal 33 (3)*, pp. 379-392.

Wang, C.-C.et al., 2018. Simplified monitoring and warning system against rainfall-induced shallow slope failures. *Canadian Geotechnical Journal (55)*, pp. 1421-1432.

Wind, G., 1966. Capillary conductivity data estimated by a simple method. *Proceedings UNESCO / IASH Symposium*, pp. 181-191.

Wösten, J., Lilly, A., Nemes, A. & Bas, C., 1999. Development and use of a database of hydraulic properties of european soils. *Geoderma, 90 (3)*, pp. 169-185.

Zhang, L., Zhang, J., Zhang, L. & Tang, W., 2011. Stability analysis of rainfall-induced slope failure: a review. In: *Proceedings of the institution of civil engineers - Geotechnical Engineering, 164, Issue GE5.* 299-316